R. & M. 2522
(Monograph)

MINISTRY OF SUPPLY

AERONAUTICAL RESEARCH COUNCIL

REPORTS AND MEMORANDA

Some Experiments on the Resistance of Metals to Fatigue under Combined Stresses

BY

H. J. GOUGH, C.B., M.B.E., D.Sc., M.I.Mech.E., F.R.S.

with

Part I: H. V. POLLARD, M.B.E., M.I.Mech.E.

and

Part II: W. J. CLENSHAW, B.Sc., A.M.I.Mech.E.

LONDON: HIS MAJESTY'S STATIONERY OFFICE

1951

PRICE £2 5*s* 0*d* NET

MINISTRY OF SUPPLY

AERONAUTICAL RESEARCH COUNCIL
REPORTS AND MEMORANDA

Some Experiments on the Resistance of Metals to Fatigue under Combined Stresses

BY

H. J. GOUGH, C.B., M.B.E., D.Sc., M.I.Mech.E., F.R.S.

with

Part I : H. V. POLLARD, A.M.I.Mech.E.

and

Part II : W. J. CLENSHAW, B.Sc.

LONDON: HIS MAJESTY'S STATIONERY OFFICE

1951

PRINTED AND PUBLISHED BY HIS MAJESTY'S STATIONERY OFFICE

To be purchased from

York House, Kingsway, LONDON, W.C.2 429 Oxford Street, LONDON, W.1

P.O. Box 569, LONDON, S.E.1

13a Castle Street, EDINBURGH, 2 1 St. Andrew's Crescent, CARDIFF

39 King Street, MANCHESTER, 2 Tower Lane, BRISTOL, 1

2 Edmund Street, BIRMINGHAM, 3 80 Chichester Street, BELFAST

or from any Bookseller

1951

Price £2 5*s* 0*d* net

PRINTED IN GREAT BRITAIN

S.O. Code No. 23-2522

CONTENTS

CONTENTS—*continued*

PART II. Fatigue Strength of a Nickel-Chromium-Vanadium-Molybdenum Steel under Combinations of Reversed Bending Stresses, Reversed Torsional Stresses, and Superimposed Static Bending and Torsional Stresses (Four Independent Variables).

SUMMARY*

OBJECTS, METHODS AND SCOPE OF INVESTIGATION

The basic object of the investigation was an experimental study of the fatigue resistance of metals to combined flexural and torsional stresses to which many engineering components, particularly crankshafts, are subjected in practice. Four independent variables have been employed; reversed bending stresses, reversed torsional stresses, static bending stresses and static torsional stresses superimposed on these cyclic stresses. Supplementary static, impact and simple fatigue tests, with chemical analysis and metallurgical examination, have been made on all the test materials. The investigation falls naturally into two parts, in which form it is reported.

Part I of the report describes a comprehensive research into the fatigue behaviour of a selection of engineering steels and two alloy cast irons under combined bending and torsional stresses alternating in phase, the mean stress of both types of stress cycle being zero in every case; thus, two cyclic variables only have been explored in this part of the investigation. A special form of high-speed testing machine, referred to as the No. 1 Combined Stress Fatigue Testing Machine, was developed for this part of the research and is described in detail.

The principal test materials were chosen to represent a range of the ductile steels employed in aircraft and automobile practice and covered a wide range of tensile strengths; some selected heat-treatments enabled an examination to be made of the influence on the fatigue properties of four types of microstructure :—(*a*) Ferrite and Pearlite, (*b*) Pearlitic, (*c*) Uniform matrix containing spheroidised Cementite, and (*d*) Hardened and Tempered. These ductile steels, with heat-treatments and tensile strengths, were :—(i) 0·1% C. (Normalised : 28 t/in.²); (ii) 0·4% C. (Normalised : 42 t/in.²); (iii) 0·4% C. (Spheroidised : 31 t/in.²); (iv) 0·9% C. (Pearlitic; 55 t/in.²); (v) 3% Ni. (H. & T.; 34 t/in.²); (vi) 3/3½% Ni. (H. & T.; 47 t/in.²); (vii) Cr. Va. (H. & T.; 49 t/in.²); (viii) 3½% Ni. Cr. (H. & T., quickly cooled; 58 t/in.²); (ix) 3½% Ni. Cr. (H. & T., slowly cooled; 58 t/in.²); (x) Ni. Cr. Mo. Va. (H. & T.; 65 t/in.²); (xi) Ni. Cr. Mo. (H. & T.; 81 t/in.²); (xii) Ni. Cr. (H. & T.; 108 t/in.²). The 3½% Ni. Cr. steel was tested both in the 'normalised' and 'embrittled' conditions, having the same tensile strength (58 t/in.²) but widely different notched bar impact values (76 and 5½ ft. lb. respectively); the 0·4% C. steel was also tested in two forms of heat-treatment: thus, steels of ten compositions afforded twelve materials for test. Two cast irons were also investigated; 'Silal', chosen as a near approach to a 'brittle' material, and 'Nicrosilal', as representing a comparatively ductile cast iron.

The main programme of tests has been carried out using solid specimens of 0·3 in. diameter at the test section; two steels, the 0·1% C. (Normalised) and the 3½% Ni. Cr. (Normal impact), have also been tested using both solid and hollow specimens. For each material and form of specimen investigated, seven fatigue ranges have been determined in which the ratio of the applied range of reversed bending stresses to the applied range of reversed torsional stresses ($\pm f/\pm q$), has been held constant at the values of (*a*) infinity (reversed bending stresses only), (*b*) 7·464, (*c*) 3·464, (*d*) 2·0, (*e*) 1·155, (*f*) 0·536 and (*g*) zero (reversed torsional stresses only). To obtain data on the resistance to combined stresses in the presence of a stress concentration due to a discontinuity of section, the same series of seven fatigue tests have also been made, on each of seven of the steels, using specimens containing a circumferential, and sharp, 55 deg. Vee-notch. The investigation described in Part I of the report has involved the determination of 161 separate fatigue ranges in the No. 1 type of combined stress fatigue testing machine.

Part II of the report describes a research into the resistance of a Ni. Cr. Mo. Va. aircraft steel to combined fatigue stresses in which the four independent variables (see above) have been investigated. A second new type of machine, referred to as the No. 2 Combined Stress Fatigue Testing Machine, was specially designed for this purpose and is described in detail. The test material, to British Standards Specification S.65A, was investigated in the hardened and tempered condition, having a tensile strength of 65 t/in.². The programme of combined stress fatigue tests consisted essentially of (*a*) tests on solid specimens of circular cross section, and (*b*) tests on three forms of hollow specimen each containing one type of discontinuity unavoidably associated with practical crankshafts; a radial oil-hole, a transition fillet of small radius, a splined shaft having six splines; the external diameters, at the test section, of the solid specimen, the specimen with an oil-hole and the specimen with small fillet, was 0·500 in. in each case; the splined-shaft specimens measured 0·4913 in. over the crest diameter.

In the tests made on solid specimens, three values of superimposed static bending stress, f_s, were investigated, 0, 17¼ and 34½ t/in.², also, three values, 0, 11 and 22¼ t/in.², of superimposed static torsional stress, q_s. This selection was chosen after preliminary tests had determined the safe ranges under repeated stresses (varying cyclically from zero to a maximum value), for this 65-ton steel, as 69 t/in.² (i.e. 34½ ± 34½) and 44½ t/in.² (i.e. 22¼ ± 22¼), for bending and torsion, respectively. Each of the three values of static bending stress was used in conjunction with each of the three values of static torsional stress, giving nine different conditions of superimposed static stress :—(1) $f_s = 0$, $q_s = 0$; (2)

* The Monograph as published, received 28th June, 1949. It embraces A.R.C. Reports Nos. 1397, 1873, 2575, 2684, 2685, 3168, 3703, 4041, 4270, 4585, 4755.

$f_s = 17\frac{1}{4}$, $q_s = 0$; (3) $f_s = 34\frac{1}{2}$, $q_s = 0$; (4) $f_s = 0$, $q_s = 11$; (5) $f_s = 17\frac{1}{4}$, $q_s = 11$; (6) $f_s = 34\frac{1}{2}$, $q_s = 11$; (7) $f_s = 0$, $q_s = 22\frac{1}{4}$; (8) $f_s = 17\frac{1}{4}$, $q_s = 22\frac{1}{4}$; (9) $f_s = 34\frac{1}{2}$, $q_s = 22\frac{1}{4}$. With each of the superimposed static stress conditions thus defined by (1), (5) and (9), five fatigue ranges have been determined in which the ratio of the range of reversed bending to the range of reversed torsional stress ($\pm f/\pm q$), has been held constant, respectively, at the values of (*a*) infinity (reversed bending stresses only), (*b*) $3\frac{1}{2}$, (*c*) $1\frac{1}{2}$, (*d*) $\frac{1}{2}$ and (*e*) zero (reversed torsional stresses only). With each of the superimposed static stress conditions defined by (2) and (4), three fatigue ranges have been determined, having the constant ratios of f/q, respectively, of (*a*) infinity, (*c*) $1\frac{1}{2}$ and (*e*) zero. With each of the remaining four static stress conditions, defined by (3), (6), (7) and (8), two fatigue ranges have been determined, in which the constant ratios employed of f/q were (*a*) infinity, and (*e*) zero. A total of twenty-nine separate fatigue ranges was thus obtained using solid specimens.

A more restricted programme was carried out on each of the three forms of hollow specimen containing a discontinuity, i.e. radial oil-hole, small transition fillet and six splines ; the highest values of the superimposed static stresses used for solid specimens were omitted as unlikely to be applied in practice to components containing such discontinuities. The remaining values of static bending and static torsional stress thus gave the following four superimposed static stress conditions :—(1) $f_s = 0$, $q_s = 0$; (2) $f_s = 17\frac{1}{4}$, $q_s = 0$; (3) $f_s = 0$, $q_s = 11$; (4) $f_s = 17\frac{1}{4}$, $q_s = 11$. With condition (1), five fatigue ranges were determined, in which the ratio of f/q was held constant at (*a*) infinity, (*b*) $3\frac{1}{2}$, (*c*) $1\frac{1}{2}$, (*d*) $\frac{1}{2}$ and (*e*) zero. For each of the remaining three conditions of superimposed static stress, three fatigue ranges were determined, in which f/q was held constant, respectively, at (*a*) infinity, (*c*) $1\frac{1}{2}$ and (*e*) zero. Thus fourteen separate fatigue ranges were determined for each form of discontinuity ; a total of seventy-one determinations for Part II of the investigations.

RESULTS AND CONCLUSIONS

Considering, firstly, Part I of the investigation in which two variables only were employed, i.e. cycles of reversed bending and reversed shearing stresses, the principal results and conclusions may be summarised as follows :—

The twelve ductile steels and two cast irons have been tested in the form of solid specimens under reversed bending stresses, reversed shearing stresses and five combinations of these ; two of the steels have also been tested in the form of hollow specimens. Allowing for some normal irregularities, the data plotted satisfactorily to give regular f/q curves between the test limits of $f/q = 0$ (reversed shearing stresses) and $f/q = \infty$ (reversed bending stresses). The f/q relation, found to apply to solid and hollow specimens alike of the ductile steels, was the ellipse quadrant expressed by

$$f^2/b^2 + q^2/t^2 = 1$$

where $\pm b$ is the fatigue limit under reversed bending stresses only, $\pm t$ is the fatigue limit under reversed torsional stresses only, and $\pm f$ and $\pm q$ are the ranges of the bending and torsional stress components at the fatigue limit of any combination. This relation was found to apply irrespective of the tensile strength, microstructure, heat treatment of the steel, or form (solid or hollow) of the specimen used. Equally definite was the different behaviour of the two cast irons, whose data plotted to give an f/q relation which was the ellipse arc represented by

$$\frac{q^2}{t^2} + \frac{f^2}{b^2}\left(\frac{b}{t} - 1\right) + \frac{f}{b}\left(2 - \frac{b}{t}\right) = 1$$

In another combined fatigue stress investigation, the f/q relations exhibited by solid specimens of four alloyed cast iron crankshaft materials were also accurately represented by ellipse arcs ; this may prove to be the general criterion for brittle—as compared with ductile materials, on whose mode of fracture principal stress or principal strain evidently exerts an important influence.

Thus, it is only necessary to determine experimentally the two ' end-point ' values of b and t ; the fatigue range for any combination of these two types of cyclic stresses can then be calculated using the ellipse quadrant or ellipse arc relation, whichever is appropriate. The maximum divergence between the quadrant and the arc depends on the ratio b/t, which varies with different materials : both curves are shown on the plot of each set of experimental data. The twelve ductile steels, tested in the form of solid specimens, gave values of b/t varying from 1·93 to 1·46; the two cast irons gave values of 1·2 and 1·1. Values ranging from 1·02 to 1·65 were obtained from the grooved specimens of the seven ductile steels.

Turning to the combined fatigue stress tests made on grooved specimens of seven steels, with the exception of a few irregular test points, the data yield regular f/q curves. These curves are represented closely by the ellipse arc, which affords a satisfactory and safe basis for design. The values of the Theoretical Stress Concentration Factor, K_t, for this form of groove have been estimated as $\left\{1 + 1{\cdot}7\left(\frac{d}{r}\right)^{1/2}\right\}$ for reversed bending stresses, and $\left\{1 + 0{\cdot}6\left(\frac{d}{r}\right)^{1/2}\right\}$ for reversed torsional stresses, where d is the notch depth and r its root radius : r was accurately measured on each specimen and varied somewhat according to the hardness of the material. The experimental values of the Fatigue Strength Reduction Factor, K_f (fatigue limit of solid specimen/fatigue limit of grooved specimen) varied widely from material to material. With every steel tested, the actual reduction in fatigue strength, in bending or torsion, was much less than the estimated theoretical value. Under reversed bending stresses, the highest value of K_f was 2·43, associated with an 80-ton Ni. Cr. Mo. steel, the lowest value was 1·47 obtained with a 47-ton 3/3½% Ni. Cr. steel : under reversed torsional stress, the highest value was 1·78, associated with a 58-ton 3½% Ni. Cr. steel (embrittled), a 42-ton 0·4% C. steel yielding the lowest value of 1·18. The values of the ratio K_t/K_f varied from 11·0 to 3·0, under reversed bending stresses, and fell steadily, if irregularly, with increase in tensile strength ; under reversed torsional stresses, the ratio varied from

5·9 to 2·1 and showed the same general trend in regard to tensile strength, although more irregularly. The curious variations in the values of K_f for each material, over the whole range of combinations of bending and torsional stresses, are displayed in a diagram.

A comparison of fatigue ranges of each material determined in both the combined stress machine and a rotating bar machine showed that the fatigue limit (solid or hollow specimens) under reversed plane bending stresses was always greater than the Wohler value, the amount of the excess varying with different materials. The results of the supplementary mechanical tests showed the usual complete absence of any correlation between the fatigue strengths of the materials and static and impact properties such as elastic limit, yield point, notched-bar value, etc. The values of the Endurance Ratio (fatigue limit under reversed plane bending stresses/ultimate tensile strength) showed, for the ductile steels, a very approximate correlation between these properties: the ratio values ranging between 0·42 and 0·65. The cast irons yielded the abnormally high Endurance Ratios of 1·15 (' Silal ') and 1·05 (' Nicrosilal ').

Turning to Part II of the investigation, in which the four independent variables were studied, using one material only, the 65-ton alloy steel, the principal results and conclusions are as follows :—

1. Solid Specimens. The effect on the fatigue strength under simple reversed stresses (bending or torsion) of superimposing static mean stresses of up to considerable amounts of either (i) a similar (bending or torsion) type of stressing alone, or, (ii) a dissimilar (torsion or bending) type alone, or (iii) a combination of similar and dissimilar types (bending and torsion) was to reduce the fatigue strength, but the amount of the reductions was relatively small. Under the most severe condition of static superimposed stresses ($34\frac{1}{2}$ t/in.^{2} bending stress plus $22\frac{1}{4}$ t/in.^{2} shear stress) the fatigue limit for reversed bending stresses ($\pm 37{\cdot}8$ t/in.^{2}) was reduced by 19% and the fatigue limit under reversed torsional stresses ($\pm 24{\cdot}0$ t/in.^{2}) by 23%.

In each of three series of tests, certain values of static bending and static torsional stresses (f_s and f_q) were imposed, singly and in combination, and the fatigue ranges determined for the complete series of five cyclic stress combinations represented by $f/q = \infty$, $3\frac{1}{2}$, $1\frac{1}{2}$, $\frac{1}{2}$ and 0. In each series, the data plotted regularly and consistently within the limits of accuracy of the experiment and have been compared both with the ellipse quadrant and the ellipse arc drawn through the two end-points ($f/q = \infty$ and 0). In the first series, no static stress is superimposed ($f_s = 0$, $q_s = 0$) and, as would be anticipated from the results of Part I of the investigation, the results are accurately represented by the ellipse quadrant. In the second ($f_s = 17\frac{1}{4}$, $q_s = 11$) and the third ($f_s = 34\frac{1}{2}$, $q_s = 22\frac{1}{4}$) series, the results are also represented by corresponding ellipse quadrants. The results are, therefore, represented by three ellipse quadrants successively displaced towards the origin; this lowering of the ' end-point ' values is the only effect of the applied mean stress, the form of the f/q relation being unchanged. For this material, the ratio of b/t is such that the divergence between each pair of curves, the quadrant and the arc, is small: the quadrant, however, definitely supplies the better fit to the data. On the remaining two series ($f_s = 17\frac{1}{4}$, $q_s = 0$) and ($f_s = 0$, $q_s = 11$), although only one point ($f/q = 1\frac{1}{2}$) intermediate between the two ' end-points ' has been determined, that point, in each series, falls satisfactorily near the corresponding ellipse quadrant, thus supporting the conclusion drawn from the more complete series. A most important general deduction and design rule can, therefore, be made: within the limits explored, whatever combination of static bending and/or torsional stress is imposed, the ' end-point ' cyclic fatigue limits having been determined, the fatigue limit of any combination of these cyclic stresses can be calculated using the ellipse quadrant relation.

In the following portion of the summary relating to the tests made on specimens containing discontinuities of form or section, the stresses quoted are nominal values, calculated on the moduli of section by the ordinary rules and neglecting the stress concentration effect.

2. Specimens containing a radial Oil Hole. The effect on the fatigue strength (bending or torsion) under simple reversed stresses of superimposing similar or dissimilar types of static stresses, singly or in combination, was perceptible but extremely small in amount. Under the most severe conditions ($f_s = 17\frac{1}{4}$, $q_s = 11$), the reversed bending fatigue limit ($\pm 16{\cdot}8$ t/in.^{2}) was reduced by $8\frac{1}{2}$% only, the reversed torsional fatigue limit ($\pm 11{\cdot}7$ t/in.^{2}) by 6% only.

The values of K_t, which have been taken as applicable, when compared with the experimentally-determined values of K_f, are in fairly close agreement. Under reversed torsional stresses, the full theoretical effect is realised: under reversed bending stresses, the actual reduction in strength is 10 to 16% less than that predicted by available theory; the S.65A steel is extremely sensitive to this form of discontinuity. The experimental values of K_f obtained over the complete series of combinations of reversed bending and reversed shearing stresses are :— $2{\cdot}2_5$ ($f/q = \infty$); 2·5 ($f/q = 3\frac{1}{2}$); 2·2 ($f/q = 1\frac{1}{2}$); 2·0 ($f/q = \frac{1}{2}$); 2·0 ($f/q = 0$). The values quoted refer to zero static mean stress ($f_s = 0$, $q_s = 0$) but superimposing any of the applied combinations of static stresses did not appreciably affect the K_f values; it is evident that the extent of the damage caused by the presence of the stress concentration is primarily determined by the applied cyclic stressing.

The results of the complete series of five tests in which no static stresses were superimposed fit satisfactorily the ellipse arc drawn through the end-points. In the series ($f_s = 0$, $q_s = 11$) and ($f_s = 17\frac{1}{4}$, $q_s = 0$), the result of each intermediate test made at $f/q = 1\frac{1}{2}$ is in close agreement with the corresponding ellipse arc: in the remaining series ($f_s = 17\frac{1}{4}$, $q_s = 11$) the result of the test made at $f/q = 1\frac{1}{2}$ gives a fatigue limit which is 14% lower than predicted by the corresponding ellipse arc.

3. Specimens containing a small Transition Fillet. The effect on the fatigue strength under simple reversed stresses (bending or torsion) of superimposing a static stress of the same kind was negligible: superimposing a static torsional stress of 11 t/in.^{2} did not reduce the

fatigue limit under reversed bending stresses ($\pm$22/23 t/in.^{2}) ; superimposing a static bending stress of $17\frac{1}{4}$ t/in.^{2} reduced the fatigue limit under reversed torsional stresses ($\pm$17·5 t/in.^{2}) by 10%. The addition of both static stresses operating simultaneously, produced a total reduction of $8\frac{1}{2}$% in the value of the reversed bending fatigue limit and a total reduction of 15% in the value of the reversed torsional fatigue limit.

The values of K_t, which are appropriate for this fillet are 2·1 when subjected to bending stresses and 1·6 when subjected to torsional stresses. Under cycles of simple reversed stresses ($f_s = 0$, $q_s = 0$), the experimental values of K_f were 1·68 for reversed bending stresses and 1·37 for reversed torsional stresses, giving values for the ratio of K_f/K_t of 80 and $85\frac{1}{2}$%, respectively. In all four series of tests, the values of K_f obtained at any constant combination of fatigue stresses, i.e. $f/q = \infty$, $1\frac{1}{2}$ or 0, were in extremely good agreement, showing that the value of K_f is determined primarily by the applied cyclic stresses and is not appreciably affected by the superimposed static bending and/or torsional stress.

The results of the series of five tests in which no static stresses were superimposed, fall on the appropriate ellipse arc or in the region enclosed by that curve and the corresponding ellipse quadrant ; it is concluded that the f/q relation is satisfactorily represented by the ellipse arc. The intermediate points ($f/q = 1\frac{1}{2}$) of the three remaining series of tests also fit satisfactorily the ellipse arcs passing through their respective end points.

4. Six-splined Shaft. The effect on the fatigue strength under simple reversed stresses (bending or torsion) of superimposing static bending and static torsional stresses, singly and in combination, was extremely small. Under the most severe conditions ($f_s = 17\frac{1}{4}$, $q_s = 11$) the fatigue limit under reversed bending stresses ($\pm$36·5 t/in.^{2}) was reduced by 4·7% only, the fatigue limit under reversed shearing stresses ($\pm$12 t/in.^{2}) by 6·2% only, the reductions being due entirely to the influence of the static torsional stresses.

When subjected to bending stresses, theoretically no stress concentration effect is produced in a splined shaft and $K_t = 1$; under torsional stresses, a marked stress concentration is set up at the bottom corners of each spline in the direction of its length and the estimated value of K_t is 2·1 for the dimensions of the specimen used. The experimental values of K_f under simple reversed bending stresses ($f/q = \infty$) were 1·04 ($f_s = 0$, $q_s = 0$), 1·03 ($f_s = 17\frac{1}{4}$, $q_s = 0$), 1·03 ($f_s = 0$, $q_s = 11$) and 1·03 ($f_s = 17\frac{1}{4}$, $q_s = 11$) ; thus confirming, within the limits of accuracy of the experiments, the absence of any appreciable stress concentration effect. Under simple reversed torsional stresses ($f/q = 0$), the corresponding values of K_f were 2·0, 1·7, 1·9 and 1·75, giving values of K_f/K_t between 95 and 83%. For the same four combinations of superimposed static stresses, the values of K_f obtained in the series in which f/q was held constant at $1\frac{1}{2}$, were 1·47, 1·57, 1·51 and 1·50. The small variations existing in each series show that with a splined shaft, as with the other two types of discontinuity, the reduction in fatigue strength, K_f, is primarily determined by the applied cyclic stressing, the effect of the superimposition of quite considerable static stresses being very small.

Two types of fracture occurred. Under the cyclic stress conditions, $f/q = \infty$ and $3\frac{1}{2}$, a 'bending stress' type of failure always occurred, originating at the crest of a spline ; under $f/q = 1\frac{1}{2}$, $\frac{1}{2}$ and 0, the shear stress concentration took charge and cracking always originated at and along the bottom corner of a spline. These two distinct types of cracking occurred irrespective of whether superimposed static stresses were absent or present and, also, irrespective of their amount ; they are reflected in the f/q relation. Where the stress concentration governs failure, the data fit satisfactorily the ellipse arc ; failures at the crest give the higher fatigue limit associated with solid specimens and conforming to an equivalent ellipse quadrant. Thus, the true f/q relation for this particularly interesting case is probably a curve containing a sharp discontinuity. But the ellipse arc drawn through the experimental end points provides a safe design basis over the whole range of combinations.

ILLUSTRATIONS

PART I

ILLUSTRATIONS—*continued*

ILLUSTRATIONS—*continued*

PART II

TABLES

PART I

PART II

Some Experiments on the Resistance of Metals to Fatigue under Combined Stresses

REPORTS AND MEMORANDA No. 2522

INTRODUCTION AND ACKNOWLEDGMENTS

Less than one hundred years have elapsed since it was established that metals could be fractured by repetitions of a cycle of stress of which the maximum stress of the cycle was less than the ultimate strength of the material ; Fairbairn's experiments, carried out in 1860/61 on a wrought iron girder, were one of the earliest investigations which conclusively demonstrated the general phenomena with which the term ' Fatigue of Metals ' has become universally associated. In 1870 were published the extensive investigations of Wohler which formed the first quantitative basis for the design of machines and structures subjected to cyclic stressing. Since then, increasing attention has been given to the study of fatigue by investigators in many countries, very largely stimulated by the rapid development of the steam and internal combustion engines, light-weight structures and high-speed machinery of every kind. At first, laboratory tests were principally made on plain specimens tested at normal air temperatures. Soon, however, it was recognised that a very large proportion of fatigue failures in service originated at discontinuities of section caused by grooves, screw-threads, oil holes, keyways, surface irregularities and imperfections, etc., and much experimental and analytical attention has been, and still is, devoted to the effect of such stress concentrations. The trend towards the use of increasingly high operating temperatures then opened up many experimental investigations into the influence of temperature on fatigue resistance. Similarly, the effect of corrosive environment on fatigue strength has received much attention and the literature on ' Corrosion-Fatigue ' is, in itself, very extensive.

As the result, a very large mass of published fatigue data is now available from many sources and covering a wide range of metals and alloys, yet it mainly relates to simple fatigue stressing systems ; the designer, faced with the problem of a component subjected to combinations of cyclic stresses or strains, is forced to rely mainly on his judgment and experience, with or without empirical design rules which have little, if any, experimental basis.

The failure which the designer seeks to avoid may be determined by one or more of three principal causes :— (*a*) the breakdown of primitive elasticity, (*b*) a condition of appreciable yielding, and (*c*) fracture. In regard to (*a*) and (*b*), the stress conditions governing failure of metals under combined static stressing has received much attention, both analytical and experimental ; in regard to ductile metals, although no single theory is generally accepted, yet the field appears to have narrowed down to a few criteria, notably those of Guest and of Misés-Hencky. In regard to the third type of failure, by fracture, this may be due to one of two causes ; by exceeding the statical ultimate strength of the metal—the avoidance of which usually presents no real problem—or failure by combined fatigue stresses. It is in regard to the latter that available experimental data is so extremely scanty.

For each of the simple stressing systems—direct, bending or torsional stresses—any applied cycle can be expressed by $M \pm R/2$, where R is the cyclic range of stress and M is the mean stress of that cycle. If R is the limiting range of stress, or fatigue limit, then R is dependent, to some extent, on M. The M/R relation has been determined for a few metals and alloys : its form varies with the material and, also, with the type of applied stressing. Broadly speaking, under cycles of bending and torsional stresses, R diminishes with increases in M. With cycles of direct stress, R diminishes with increasing tensile values of M ; with some materials, R increases as M assumes increasing values of compressive stress.

Consider some combination of the static and cyclic direct, bending and torsional stresses

$$D \pm d/2, \quad B \pm b/2 \text{ and } T \pm t/2$$

To avoid fatigue fracture, it might appear to be sufficient to consider only the combined effect of the cyclic components, $\pm d/2$, $\pm b/2$ and $\pm t/2$. But, as the limiting values of each of these cyclic components is dependent,

to some extent, on its own type of mean stress, and also on the mean stress of the other types of stress cycles, one is not justified in regarding the total damage as due to merely the sum of the additive effects of the cyclic components (considered together) and of the static mean stresses (considered together). Thus, with such a mixed combination of static stresses and cyclic ranges of stress, each term must be considered as a variable in an experimental investigation of combined stresses.

In 1932, when the present investigation was planned as a long-range research, the existing position was, roughly, as follows :—

STATIC STRESS SUPERIMPOSED ON CYCLIC STRESSES OF THE SAME TYPE

This is merely the effect of the mean stress of the cycle on the safe range. A very considerable volume of experimental data has been published, relating to direct, bending and torsional stresses ; no single M/R relation applied to ductile metals as a group.

STATIC STRESS SUPERIMPOSED ON CYCLIC STRESSES OF A DIFFERENT TYPE

Ono[1] had made a few experiments on the effect of a static torsional stress superimposed on cycles of alternating bending stresses. With Ingot Iron and a 0·3% C. Steel, the bending fatigue limit was slightly raised by the superimposition of moderate shearing forces but these had no effect on a 0·25% C. Steel. Similar experiments were made by Lea and Budgeon[2], who reported that, using one low carbon and one high carbon steel, the effect of adding a moderate static shear stress increased the bending fatigue limit. Hohenemser and Prager[3] investigated the effect of static tensile stress superimposed on alternating torsional stresses : the material was a dead-mild steel. Up to the point where yielding occurred, the superimposed stress caused an increasing drop in the torsional fatigue limit, according to the ellipse quadrant relation :—

$$S^2/q^2 + p^2/f^2 = 1$$

where f is the ultimate tensile strength, p is the superimposed static tensile stress, $\pm q$ is the range of shear stress at the fatigue limit under reversed torsional stresses, and $\pm S$ is the range of shear stress at the fatigue limit under combined stresses. [Note.—In 1935, in discussing some preliminary results of the present investigation, Davies[9] gave results of tests on a 3% Nickel Steel and a Ni. Cr. Steel, in which static torsional stresses were superimposed on cycles of reversed bending stresses. The bending fatigue limit was reduced by the static torsional stress according to the relation

$$p^2/P^2 + q/Q = 1$$

where $\pm P$ is the fatigue limit under reversed bending stresses only, Q is the static ultimate shear strength of the material, $\pm p$ is the reversed bending fatigue limit when the superimposed static shear stress is q.]

Combinations of cyclic stresses of different types

A search through the literature indicated that only one series of such combined fatigue stress tests had been published. This was due to Stanton and Batson[4] who devised a modified form of rotating bar machine for applying cycles of reversed bending stresses, reversed torsional stresses and combinations of these stresses. Tests were made on a dead-mild steel (U.T.S. = $22\frac{1}{2}$ t/in.^{2}) using six combinations of cyclic bending and torsional stresses. The results were in very good agreement with a constant value of Maximum Shear Stress.

In view of the extremely limited knowledge of the resistance of metals to combined fatigue stresses, it was concluded that the proposed investigation might usefully be directed to a study of the effect of the four variables :— B, ($\pm b/2$), T, ($\pm t/2$), in which the cyclic components were in phase ; such combinations of bending and torsional stresses are commonly encountered in engineering practice, especially in connection with crankshaft design. An estimate of the number of experiments involved in exploring the effect of all four variables even on a single material, led to the decision to divide the research into two stages. First, a study of the effect of the two cyclic components only, on a fairly wide range of engineering materials ; secondly, a study of all four variables on a few selected materials of special interest. No testing machines existed for either type of investigation and special apparatus had to be designed ; a smaller and less complicated type of machine would be sufficient for the simpler type of test and thus considerable economy would result from the proposed step-by-step procedure, as it was recognised that a number of machines of each type would be required if a worthwhile rate of progress was to be achieved.

In regard to a suitable cyclic frequency to be employed in the research, much reliable information existed regarding speed effect, although all the work had been carried out on small specimens. It may be briefly summarised thus :—In general, the fatigue limit increases with cyclic frequency to an extent dependent on the material under test. With many metals, the increase is appreciable when frequencies of the order of 10,000 cycles per minute are reached and, in some cases, at lower frequencies. At very high frequencies, marked increases in the fatigue limit have been recorded. It can be concluded that, at frequencies between 150 and 5,000 cycles per minute, the effect of frequency may be neglected. It was decided to design the required testing machines to operate at about 2,000 cycles per minute.

The determination of the size of specimen to be used was much more difficult. As far as testing only is concerned, the smallest practicable specimen size is to be preferred. Increases in size entail rapidly mounting increases in the applied loading forces, in the size and cost of the testing machine, in the weights of materials required and in the difficulties of ensuring uniformity in heat-treated materials. But, having in mind the subsequent application of the results to the design of

full-sized engineering components, the consequences of 'size-effect' in fatigue must be recognised. It is an aspect of the fatigue of metals which has very great practical importance: unfortunately, it is one of the least understood. It is a very difficult matter to ensure, in the first place, that a series of specimens of the same material, covering a range of sizes, have initially identical physical properties; any such series of specimens should, also, be geometrically similar in form and be similarly loaded; some investigations which have been made have not conformed to these primary requirements and the results may, in consequence, have been misleading. However, at the time of the review of the literature made when planning this investigation, there were distinct indications that, with solid specimens of diameters up to about two inches, no marked scale effect was established; where any difference was found, the fatigue resistance always diminished as the specimen size was increased. In the presence of a stress concentration, however, the size effect was much more marked, the fatigue resistance again diminishing with increase in size. But it was quite impracticable to consider carrying out the proposed lengthy programme of combined fatigue stresses entirely on specimens of dimensions equal to that of full-sized components. It was decided to employ specimens not exceeding half an inch in diameter and to make the study of size effect the subject of a subsequent and separate research, in which it would probably be sufficient to investigate a few materials only.

Since the present research was commenced, the results of several important investigations into size effect under fatigue stressing, have been published. Peterson[5, 6] carried out a careful series of rotating bar tests on five sizes of geometrically similar solid specimens, having diameters of 0·05, 0·273, 0·469, 1·00 and 2·00 in. Four carbon steels and two cast irons were tested. Allowing for small variations in the results, Peterson concluded that no important size effect was exhibited for solid specimens of these materials and within this range of sizes. Mailander and Bauersfeld[7] investigated geometrically similar specimens of a Cr. Ni. W. steel under reversed torsional stresses: the specimen sizes were 0·55, 1·18 and 1·77 in. They found a decrease of 28% in fatigue strength with this increase in size for solid cylindrical specimens and 21% with hollow cylindrical specimens. Horger[8], using geometrically similar specimens of a 0·47% C. Steel under reversed bending stresses, reported that increasing the diameter from 0·3 to 2·0 in. produced a drop in fatigue strength of 14%. These and other investigations show that the size effect of solid specimens in fatigue, requires much further investigation; larger sizes should also be explored. But, uncertain as may be the existence of size effect on the fatigue strength of specimens free from stress concentration, the results of a number of independent investigations all indicate unmistakably that the effect is real when discontinuities of section are present; reference to a typical experiment of the investigations of Peterson[5, 6], who carried out notable pioneer work in this field, will be sufficient for the present purpose. Rotating bar fatigue tests were carried out on a 0·45% C. Steel, using a geometrically similar series of specimens having diameters of $\frac{1}{4}$, $\frac{1}{2}$, 1 and 3 in.: each specimen was pierced transversely by a small hole, the ratio of whose diameter to that of the test piece was 0·063. The values of the ratio of the fatigue strength of the solid specimen to that of the corresponding size of specimen containing the hole for the $\frac{1}{4}$, $\frac{1}{2}$, 1 and 3 in. sizes were, respectively, 1·1, 1·33, 1·56 and 1·84. Thus, with increase in size, the reduction in fatigue strength increased, although at a decreasing rate. The estimated stress concentration factor due to the presence of the hole was about 2·41.

The investigation to be described divides naturally into two parts. Part I deals with two independent variables, i.e. reversed bending and reversed torsional stresses and various combinations of these.

Part I. Several possible types of testing machine were considered and worked out in detail, final choice being given to a machine employing the inertia forces of revolving out-of-balance wheels, the inertia of the remaining vibrating and rotating parts being eliminated from the specimen by a suspensory spring system whose natural frequency was in tune with that of the working speed of the machine; the use of synchronous A.C. motors removed the difficulty of maintaining accurate speed control which used to render necessary constant supervision of testing machines of the inertia type. A prototype was constructed and thoroughly tested: it gave excellent results, could be accurately calibrated and maintained its accuracy for long periods. The tests showed, however, that the prototype was unnecessarily bulky and complicated: it was redesigned and two machines were constructed, which, retaining exactly the essential principle of operation of the prototype, were simpler in detail and much less costly. The redesigned machine has required no further modification and a number have been produced. In what follows, it will be referred to as the 'No. 1 Combined Stress Fatigue Machine' to distinguish it from the machine designed later for the study of the four independent variables. The No. 1 Combined Stress Machine was first publicly exhibited, in September 1933, at the Shipping Engineering and Machinery Exhibition held at Olympia.

In the meantime, very careful consideration had been given to a suitable choice of materials for test. The general plan for this stage of the work, the study of two variables only, was to make a survey of a widely-representative series of steels used in the design of engineering components subjected to these combined stresses but, by suitable choice of representative compositions and heat-treatments, to keep the actual number of steels tested within practicable limits. In determining this choice, I was indeed fortunate in obtaining the keen interest, helpful advice and generous co-operation of the late Dr. W. H. Hatfield, F.R.S. Ten compositions of steel were finally decided on: two of these to be tested

each in two different forms of heat-treatment, thus providing twelve materials. The quantities required were very liberally estimated. The complete series was specially made, rolled and heat-treated at the Sheffield works of Messrs. Thomas Firth and John Brown, Ltd. and were presented, free of charge, by the Directors of that Company, for the purposes of the research. This group of steels represented ductile engineering materials. By contrast, as representing a class of material normally weaker in tension than in shear, two cast irons were added to the programme ; for the selection, preparation and presentation of these irons, I am indebted to Mr. J. G. Pearce, Director of the British Cast Iron Research Association.

The initial stages of the development and testing of the No. 1 Combined Stress Machine were carried out as an item of general research under the auspices of the Executive Committee of the National Physical Laboratory. In 1933, work commenced on the main programme which was approved and financed throughout by funds provided by the Department of Scientific and Industrial Research. A preliminary report[9] has been published on the results of the tests on two steels and one cast iron. A second preliminary report[10] described the results of comparative tests of hollow and solid specimens of two steels. For completeness, these results are included in this report on the whole investigation.

Part I of the present report describes the results of the investigation into the effect of the two variables, cyclic reversed bending and torsional stresses. For the convenience of the reader, the detailed results—which are very extensive—are recorded in three Appendices, dealing with ' Chemical Analysis and Metallurgical Examination of Materials ' (Part I, Appendix No. 1) ; ' Supplementary Mechanical Tests ' (Part I, Appendix No. 2) ; ' Combined Fatigue Stress Tests ' (Part I, Appendix No. 3). The six sections forming the main body of Part I contain a description of the machine and details of the test programme, followed by a summarised presentation and discussion of the results obtained.

Passing reference only will be made in Part I to a separate investigation[11] on cast materials which was also carried out using the No. 1 Combined Stress Fatigue Testing Machine developed for the present research.

Recognising the need for an intensive attack on the combined fatigue stress problem and experience having developed complete confidence in the accuracy and reliability of the No. 1 Type Combined Stress Machine, drawings and notes on its calibration and operation were issued, without charge, to many applicants in the United Kingdom and overseas. The Bristol Aeroplane Co., in particular, have constructed a battery of these machines and have recently published[12] a report on some very interesting tests. It is understood that machines have also been constructed in the U.S.A., Switzerland, France and Poland.

The combination of cyclic bending and cyclic torsional moments produces a condition of stress in which one of the three principal stresses has zero value throughout. Sufficient as this bi-axial stress system may be for many design purposes, the extension of the research to an investigation of the effect of variation of all three principal stresses is very attractive, from the theoretical aspect. Work was planned in which this could be done by using a thin tubular specimen and subjecting this to an internal cyclic pressure in phase with the applied bending and torsional moments ; a method was worked out but the outbreak of war stopped all work on the project. A research of this type will, it is hoped, receive the attention of future investigators.

Part II. The investigation of the four independent variables—reversed bending stresses, reversed torsional stresses, superimposed static bending moments and static torsional couples—is the subject of Part II of the present report. By 1935/36, the investigation which forms the subject of Part I of this report was in full swing while some thought had been given to a suitable form of moderately high-speed combined fatigue stress testing machine for determining the effect of static bending and/or static torsion superimposed on cycles of reversed bending and/or cycles of reversed torsional stresses. Several types of machine had been considered and carried to the preliminary design stage ; finally, it was decided to develop a machine based on the ' No. 1 Combined Stress Fatigue Machine ' whose performance had proved entirely satisfactory in every way and whose basic simple principles could be adapted, by modification of design, to provide for an experimental study of the required four independent variables in place of the two used in Part I of the investigation. The design, construction and method of operation of the ' No. 2 Combined Stress Fatigue Machine ' will be fully described later ; for the present purpose, it is sufficient to record that the essential modification to the earlier machine, in order to obtain any required combination of superimposed static bending and/or torsional moments, was by making use of the suspensory spring system ; each pair of springs was mounted so as to be separately adjustable in regard to each other and to the specimen. Such a machine, necessarily larger and more complicated in detail than its predecessor, was constructed and subjected to searching tests under which it behaved in an entirely satisfactory manner. That this machine was successfully developed straight from the drawing board was, of course, primarily made possible by the experience already gained with the earlier type. The construction of three further machines was put in hand ; these differed from the prototype only in small details of design. All four machines have been employed continuously on the test programme.

The proposed study of the four variables offered promise of useful experimental data, in particular regard to the problem of the aero-engine crankshaft ; the research obtained the interest of the Air Ministry who generously undertook to bear the whole cost of the investigation and the work to be described has been carried out on their behalf to an approved programme.

This report covers the work carried out on one material, a Nickel-Chromium-Molybdeum-Vanadium Steel to Specification S.65 of the British Standards Institution. The basic fatigue properties of this material, under various applied combinations of static and cyclic loadings, have been determined using solid specimens of 0·5 in. diameter. To obtain data relating to the influence of practical forms of discontinuity of section, it was decided, after consultation with the aircraft industry, to include tests on specimens containing oil holes, small transition fillets and splines. At a later stage, it was hoped to carry out a selected series of tests on large specimens of $2\frac{1}{2}$ in. diameter to obtain information on size effect. The required amount of material sufficient for both investigations was very liberally estimated and, by arrangement with the late Dr. W. H. Hatfield, F.R.S., Messrs. Thomas Firth and John Brown, Ltd. made a special cast of steel for the investigation. This $32\frac{1}{2}$-ton cast produced forty-seven ingots : a very interesting metallurgical study of one of these ingots has been published[13].

The investigations described in Parts I and II of this report had just been completed when the outbreak of war in 1939 stopped work on this research. Brief statements of the results obtained, in the form of confidential reports, had been rendered to the Department of Scientific and Industrial Research (Part I) and the Air Ministry (Part II), who gave permission for the full report on the work to be prepared and published after the conclusion of hostilities.

ACKNOWLEDGMENTS

The combined fatigue stress experiments of Part I were made in collaboration with Mr. H. V. Pollard, of the Engineering Division, National Physical Laboratory.

The combined fatigue stress experiments of Part II were made in collaboration with Mr. W. J. Clenshaw, also of the Engineering Division, National Physical Laboratory.

The chemical analyses and metallurgical examinations were undertaken by the Metallurgical Department of the N.P.L. under the direction of Dr. C. H. Desch, F.R.S. Valuable assistance was afforded by Miss Burns and Messrs. Fenner, Forrest and Mills of the N.P.L. Engineering Department, in connection with some of the supplementary mechanical tests. The testing machines were constructed in the workshops of the Engineering Department and it is desired to pay special acknowledgment in this matter to the skill and care of Mr. A Eaton.

The late Dr. W. H. Hatfield, F.R.S., advised on the choice and personally supervised the manufacture and heat-treatment of all the steels. Mr. J. G. Pearce, Director of the British Cast Iron Research Association, kindly arranged for the preparation and supply of the cast irons. Messrs. Thomas Firth and John Brown, Ltd. generously presented all the steels used in the first part of the research. The machining of the specimens containing stress concentrations used in the second part of the research was kindly undertaken by the Bristol Aeroplane Co., Ltd., under the direction of Mr. N. Rowbotham.

I am greatly indebted to my colleague, Mr. H. L. Cox, for most helpful advice and discussion in regard to the sections of this monograph dealing with stress concentration effects.

The work described above was carried out in the Engineering Division, National Physical Laboratory, Part I as part of the general research programme of the laboratory and Part II on behalf of the Air Ministry. This monograph is published on the recommendation of the Aeronautical Research Council and by permission of the Director of the National Physical Laboratory.

I desire to make grateful acknowledgments to the above named individuals and bodies for the invaluable assistance rendered, and to record my very special thanks to the Department of Scientific and Industrial Research and to the Air Ministry for the constant encouragement and support I received in pursuing this line of investigation, for the generous grants they made over a number of years and for their permission to publish a full account of the researches.

H. J. GOUGH.

PART I

Fatigue under Combinations of Reversed Bending and Reversed Torsional Stresses (Two Independent Variables)

by

H. J. GOUGH, F.R.S. and H. V. POLLARD, M.I.Mech.E.

I. THE No. 1 COMBINED STRESS FATIGUE TESTING MACHINE

Description of Machine

Fig. 1 shows the general arrangement of the machine. One end of the specimen S is rigidly clamped in a movable bracket K bolted to the casting G which is attached to the baseplate B. The other end of the specimen is held in the collar C to which the arm A is pivoted about a vertical axis passing through the centre of the specimen. The disk D carrying the out-of-balance weights W is supported upon an axle and bracket housing F suitably clamped to the ends of the springs E, the other ends of which are rigidly clamped to a bracket carried by the baseplate. The disk D is driven through a belt drive by the synchronous motor M, running at 1,500 r.p.m. The bracket F is connected by links L to the centre of percussion of the arm A ; a rubber bush is inserted between the ends of the links L and the arm A, so that the deformation of the specimen shall not be seriously constrained.

Thus the general principle of the machine is that the vertical component of the out-of-balance forces, developed at the axle of the disk, is transmitted as an alternating moment to the specimen through the arm A.

The speed of the disk is adjusted—by varying the ratio of the pulley diameters—to the resonant frequency of all the moving parts vibrating on the outer ends of the springs E ; this adjustment is effected by the use of a very flexible specimen in the form of a thin strip. This is an important feature of the machine, as all inertia forces, other than those due to the out-of-balance weights, are thereby eliminated. The resonant speed of the machine shown is 2,130 r.p.m.

In the position shown in Fig. 1, cycles of reversed plane bending are imposed on the specimen. The bracket K and collar C can be rotated and clamped to any other position, so that the arm A makes an angle θ with the longitudinal axis of the specimen ; the bending moment applied to the specimen is then proportional to cos θ and the torque to sin θ ; it will be noted that the bending moment and torque are in phase so that they reach their maximum or minimum values simultaneously. Thus, when θ is 0 deg., cycles of reversed plane bending are applied to the specimen and, when θ is 90 deg., cycles of reversed torsion are applied, while any desired combination of bending and torsion is available by an appropriate choice of an intermediate value of θ. Fig. 2 shows the machine adjusted to apply alternating cycles intermediate between those of plane bending and pure torsion.

As shown in Fig. 2 the out-of-balance weights which generate the alternating stresses are attached at two diametrically opposite positions on the disk ; any weights not in use are housed on the arm A over the centre-line of the links L, the mean weight distribution of the moving parts being thereby maintained constant in all tests. By a suitable choice of out-of-balance weights, ranges of bending stress (on a standard specimen of 0·3 in. diameter) varying from ± 5 to ± 60 tons per sq. in., with intermediate steps of $\pm \frac{1}{2}$ ton per sq. in., can be obtained using six weights only. When required, finer adjustment of the applied stress range is obtained by small alterations to the standard diameter of the test portion of the specimen.

For calibration of the machine, the accurate measurement of the masses of the out-of-balance weights was all that was really necessary, as the only forces applied to the specimen under test are the inertia forces due to these masses ; these forces can, of course, be estimated directly from the respective masses and the observed speed of rotation, provided that the machine is correctly tuned. However, it was considered desirable to make an independent static calibration. For this purpose, the links L were removed, thus disconnecting the loading arm A from the springs, etc. A specimen, reserved for calibration purposes, was placed in the machine and loaded by applying a series of weights to a scale pan suspended from the loading arm A at the points at which the links L are normally connected. The deflection of the specimen was then determined by measuring, by means of a measuring microscope, the vertical distance traversed by a fine line scribed on the end of the lever A (see Fig. 1) ; a static load/deflection curve was thus obtained. The required masses of the out-of-balance weights to produce the designed ranges of loading, were estimated from the known speed and effective diameter of the driving disk D. The machine was then re-assembled and a second load/deflection curve obtained under

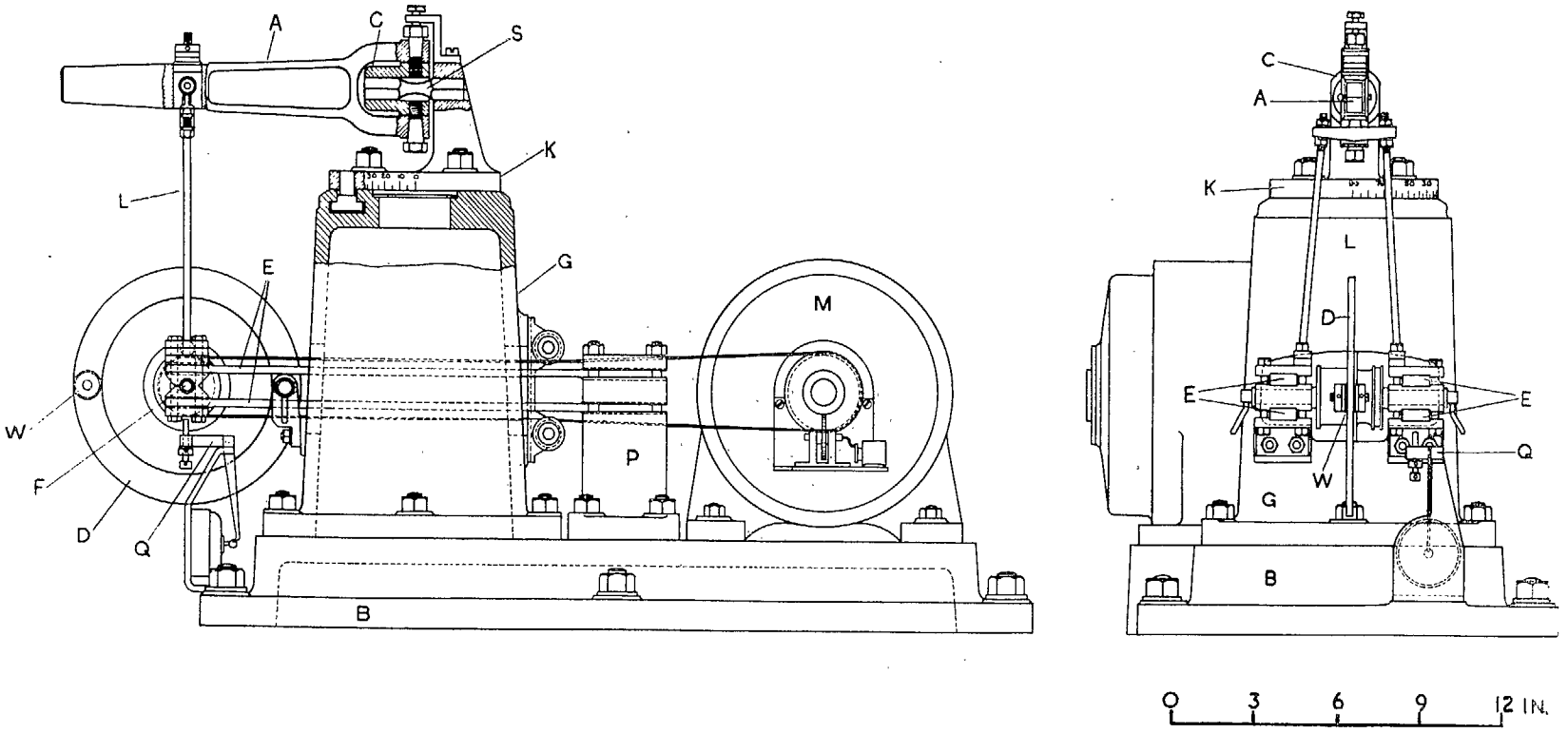

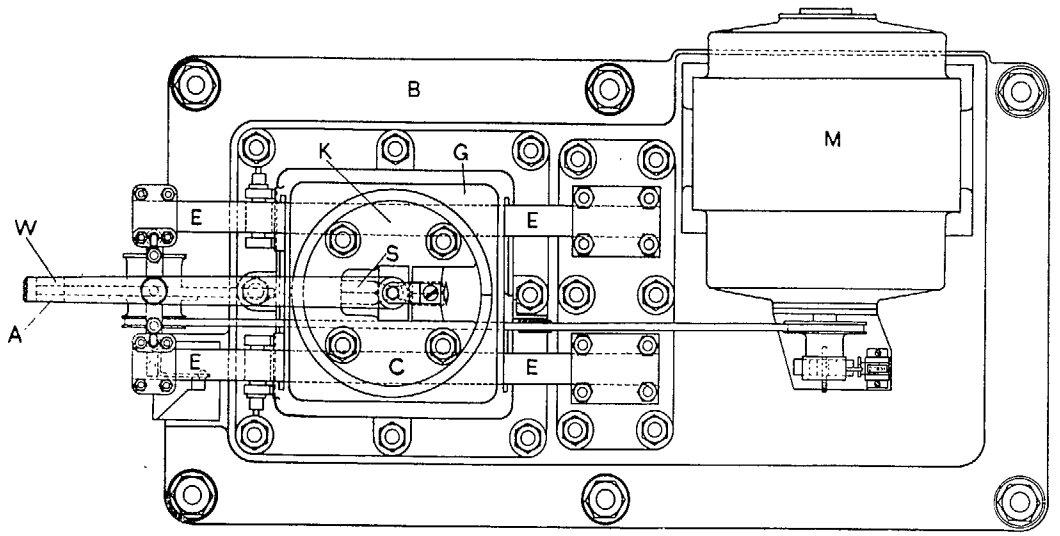

FIG. 1. General Arrangement of No. 1 Combined Stress Fatigue Testing Machine. Two variables :—Cycles of Reversed Bending and Reversed Torsional Couples.

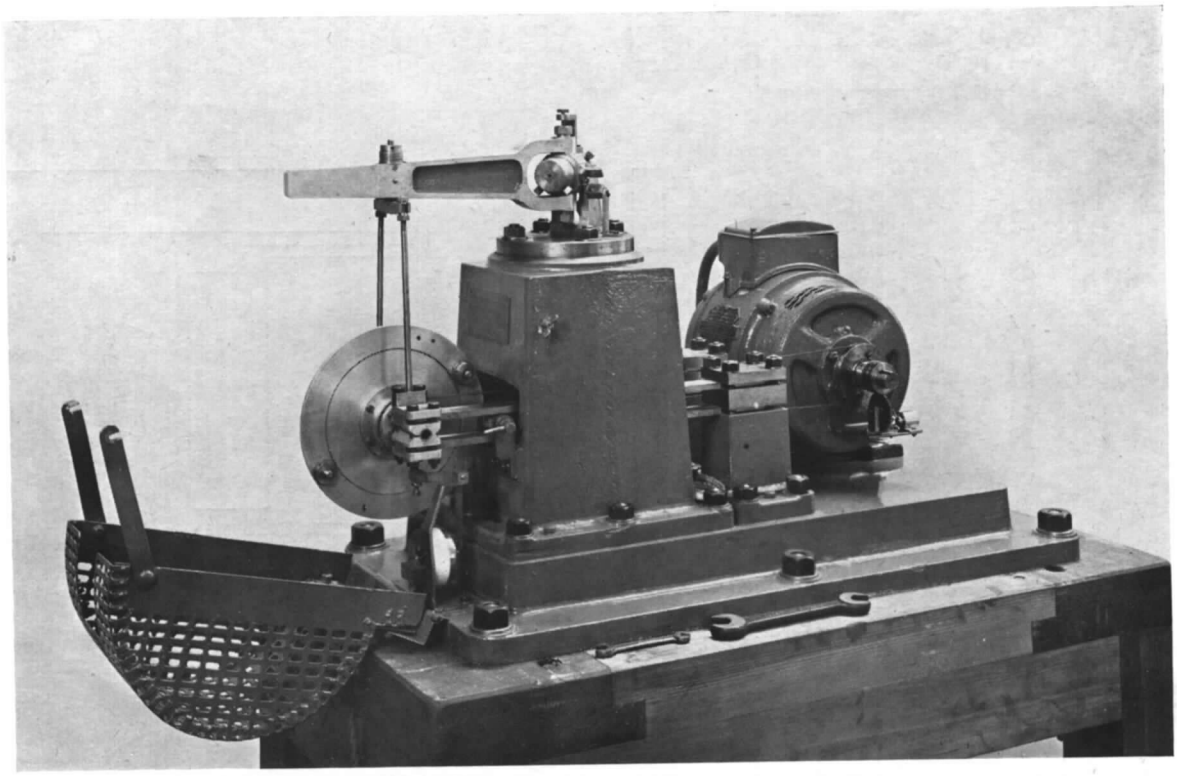

FIG. 2. No. 1 Combined Stress Fatigue Testing Machine.

running conditions. The two curves were found to be in excellent agreement. From time to time during the course of the research, repeat static calibrations were made to ensure that the accuracy of the machines had suffered no deterioration.

In view of the extent of the programme, a battery of four machines of this type was constructed and used continuously throughout the research.

The Applied Stressing System

Fig. 3 shows, diagrammatically, a view in plan of the relationship of the loading forces applied by the combined stress machine to the specimen under test. Arising from the inertia forces of the unbalanced weights, a range of load $\pm P$ is applied, at a distance L from the centre of the specimen, in a vertical plane making an angle θ with the vertical plane containing the axis of the specimen; a moment PL equal, say, to M is thus imposed; the range of shearing force $\pm P$ is, relatively, very small and may be neglected.

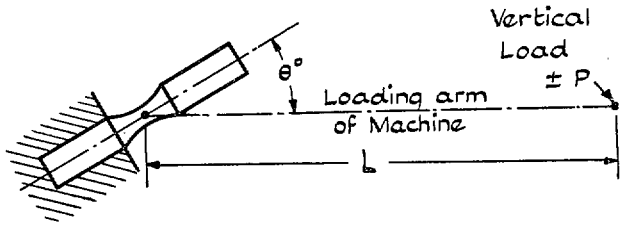

FIG. 3. Loading System applied to Specimen in the Combined Stress Machine.

The specimen is thus subjected to bending and twisting moments equal, respectively, to $M \cos \theta$ and $M \sin \theta$, which produce the following maximum flexural and shearing fibre stresses :—

Flexural stress f due to bending moment $= KM \cos \theta$

Shear stress q due to twisting moment $= \frac{1}{2}KM \sin \theta$

Here $K = d/2I$, where d is the diameter of specimen and I is the second plane moment of specimen section ($\pi d^4/64$ for solid circular specimen).

The stress system induced consists of two principal stresses, p_1 (tension), p_2 (compression), the third principal stress, p_3, having always zero value as it occurs at a free surface. Then

$$p_1 = \tfrac{1}{2}f + \sqrt{(\tfrac{1}{4}f^2 + q^2)} = \tfrac{1}{2}KM(\cos\theta + 1)$$
$$p_2 = \tfrac{1}{2}f - \sqrt{(\tfrac{1}{4}f^2 + q^2)} = \tfrac{1}{2}KM(\cos\theta - 1)$$
$$p_3 = 0.$$

while the normal of the plane of the principal stress p_1 is inclined to the axis of the specimen at an angle $\tan^{-1} q/p_1$, i.e. at an angle of $\frac{1}{2}\theta$.

The value of the maximum shear stress S induced (half the greatest difference of the principal stresses) is merely $\frac{1}{2}KM$* and occurs on planes inclined at 45 deg. to the planes of greatest principal stress. It will be found convenient to use the maximum shear stress value in expressing the results obtained in the combined fatigue stress experiments.

In the fatigue tests made using this machine, the normal practice throughout has been to determine the fatigue limit (by the usual endurance tests) of each material at each of seven values of θ, i.e. 0, 15, 30, 45, 60, 75 and 90 deg. These correspond to

(*a*) Reversed plane bending ($\theta = 0°$)

(*b*) Reversed torsion ($\theta = 90°$)

and (*c*) Five combinations of reversed plane bending and reversed torsion in which the ratios of the range of the applied twisting moment to the applied bending moment (represented by tan θ) have the values :—

0·268	($\theta = 15°$)
0·577	($\theta = 30°$)
1·0	($\theta = 45°$)
1·732	($\theta = 60°$)
3·732	($\theta = 75°$)

The 'end points' ($\theta = 0$ and 90 deg.) were, of course, essential values to which especial importance was attached (no economy in specimens was allowed to interfere with the closest possible determination of those 'key' values of the fatigue limits). The choice of the five selected intermediate combinations appears to have been justified by the results obtained, which it is considered sufficiently clearly indicate the relationship between the fatigue limits over the whole range.

* Thus a constant value of $\pm M$, at all angles of θ, induces the same value of range of maximum shear stress on specimens of the same diameter.

II. MATERIALS INVESTIGATED AND RESEARCH PROGRAMME

A. MATERIALS INVESTIGATED

In planning this research, one of the most difficult matters on which to make a decision was a suitable choice of materials; of a number sufficient to explore a wide field, yet keeping the amount of testing involved within practicable limits. A primary object of the research was to provide data of real practical value to those engaged in the design of engineering components subjected to combinations of cyclic bending and torsional stresses. The steels available in practice for these purposes cover an extensive range of tensile strengths and, clearly, the materials selected must equally be selected with that property in mind. But such tensile strengths can be obtained by a great variety of chemical compositions and heat-treatments. Again, in

the proposed exploration of what is practically a new field of research, the possibility existed that resistance to combined fatigue stresses might prove to be influenced, to a greater or lesser extent, by the form of microstructure ; in any case, this factor could not be overlooked. But these three factors—tensile strength, composition, microstructure—cannot, of course, be regarded as independent variables, if a range of practical engineering steels is to be used (and it was regarded as an essential that the final choice of materials would be steels used in actual design). It was decided to select the steels mainly from the aspects of Microstructure and Tensile Strength as more likely to afford data of an informative and practical nature than if attention were devoted to chemical composition and heat-treatment, of which there are endless combinations.

In arriving at the list of steels which have been used, the writers desire to make grateful acknowledgment of the valuable advice and assistance given by the late Dr. W. H. Hatfield, F.R.S., Director of Messrs. Thomas Firth and John Brown, Ltd. After considerable discussion and redrafting of possibilities, the following plan was agreed :—

Microstructure :—Four types of structure to be investigated.

(*a*) Ferrite and Pearlite, as in normalised carbon steels.

(*b*) Pearlitic.

(*c*) Uniform Matrix containing Spheroidised Cementite, as in fully annealed steels of moderate carbon content.

(*d*) Hardened and Tempered.

Under (*a*) two carbon contents, 0·1 and 0·4%, to be investigated, the remainder of the analysis to be that usual for Siemens O.H. quality. Under (*b*), the eutectic composition of 0·9% C. Under (*c*), the 0·4% C. steel used under (*a*) to be employed ; a critical annealing condition to be applied to give a relatively soft condition with the carbides well spheroidised. Under (*d*), a range of hardened and tempered alloy steels, so chosen as to provide a wide range of tensile strengths as follows :—

Tensile Strengths :—

30/35 t/in.² A low-carbon nickel steel (H. & T.)

45/50 t/in.² A Ni. Steel (H. & T.)

45/50 t/in.² A Cr. Va. Steel (H. & T.)

Note.—This strength value is duplicated to examine the effect of chemical composition on two steels having the same ultimate tensile stress.

55/60 t/in.² A Ni. Cr. Steel (H. & T. and quickly cooled).

55/60 t/in.² The same Ni. Cr. Steel (H. & T. but slowly cooled).

Note.—This apparent duplication to examine the effect of widely-differing impact strength but having the same tensile strength.

60/70 t/in.² A Ni. Cr. Mo. Steel (H. & T.)

75/80 t/in.² A higher Ni. Cr. Mo. Steel (H. & T.)

95/105 t/in.² An Air-Hardening Ni. Cr. Steel (H. & T.)

All the above steels to be in accordance with British Standards Institution (B.S.I.) or Air Ministry Specifications.

Such steels are essentially ductile materials. In contrast, it was felt that the addition of materials which are normally weaker in tension than in shear, would possess considerable interest. As a class of engineering material in common use, cast irons appeared very suitable. Mr. J. G. Pearce, Director of the British Cast Iron Research Association, was approached and took great interest in the matter. At his suggestion, the following two cast irons* were selected for the investigation :—

'Silal', chosen to represent a near approach to a brittle material, and

'Nicrosilal', chosen to represent a comparatively ductile cast iron, thus affording an interesting comparison in the same field of materials.

B. RESEARCH PROGRAMME

1. **Main Programme** (carried out on all materials) :—

(*a*) FATIGUE TESTS USING THE COMBINED STRESS FATIGUE TESTING MACHINE

The fatigue limit of each material has been determined, by the usual method of endurance tests, at a frequency of about 2,130 stress cycles per minute, under reversed plane bending stresses, reversed torsional stresses, also under each of five combinations of reversed plane bending and torsional stresses. Solid specimens, having a diameter of 0·3 in. at the test section, were employed.

(*b*) SUPPLEMENTARY MECHANICAL TESTS

(i) *Fatigue Tests* :—The fatigue limit of each material has been determined in a rotating bar machine of the Wohler type (operating at a frequency of 2,400 stress cycles per minute), also, the reversed torsional fatigue limit has been obtained using the Stromeyer fatigue testing machine (operating at 1,000 stress cycles per minute) installed at the National Physical Laboratory. These results are of interest, in comparison with the values obtained from the Combined Stress machine, in examining results from machines of essentially different design, imposing somewhat different test conditions.

* *Note* :—The results of a separate and special investigation into the resistance to combined fatigue stresses of another four cast-irons, as used for crankshafts, have been published by Gough and Pollard.[11]

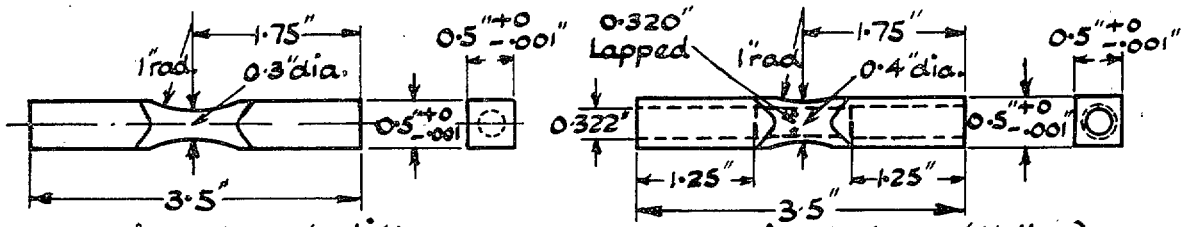

(a) Combined Stress (Solid)

(b) Combined Stress (Hollow)

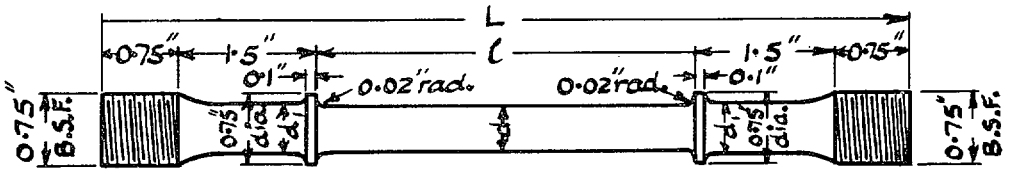

Stress tons	d	l	L	d_1	
30 - 60	0·50"	4"	8·5"	0·55"	c
60-120	0·375"	3"	7·5"	0·42"	d

(c & d) Dalby Tensile Stress

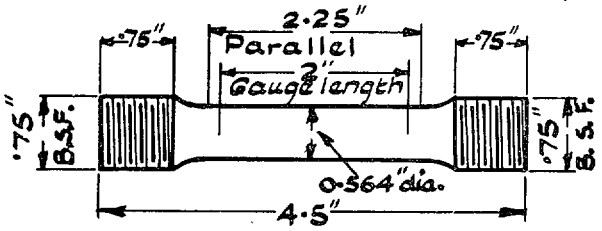

(e) Tensile Stress

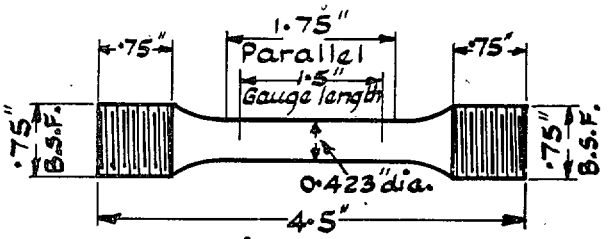

(l) Tensile Stress

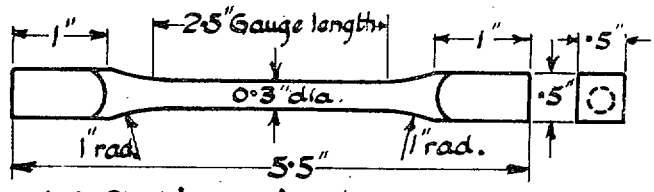

(g) Static Torsional Stress

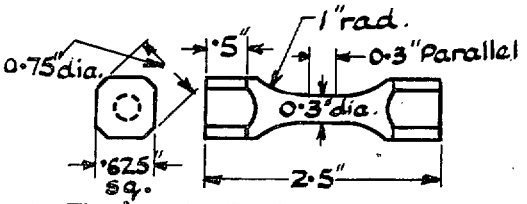

(j) Torsional Fatigue Stress

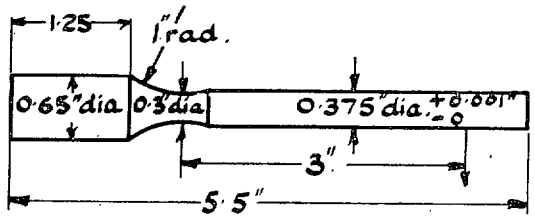

(f) Wöhler Rotating Bending Stress

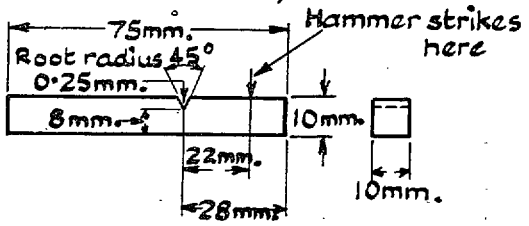

(h) Izod Impact Test

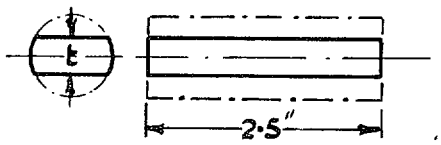

t = (I) 0·3" (II) 0·4" (III) 0·5" (IV) 0·6"

(K) Hardness determination

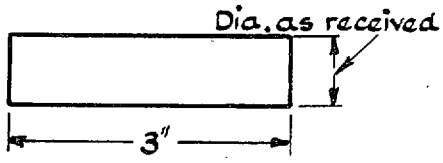

(m) Microstructure examination

FIG. 4. Test Specimens for Combined Stress Research.

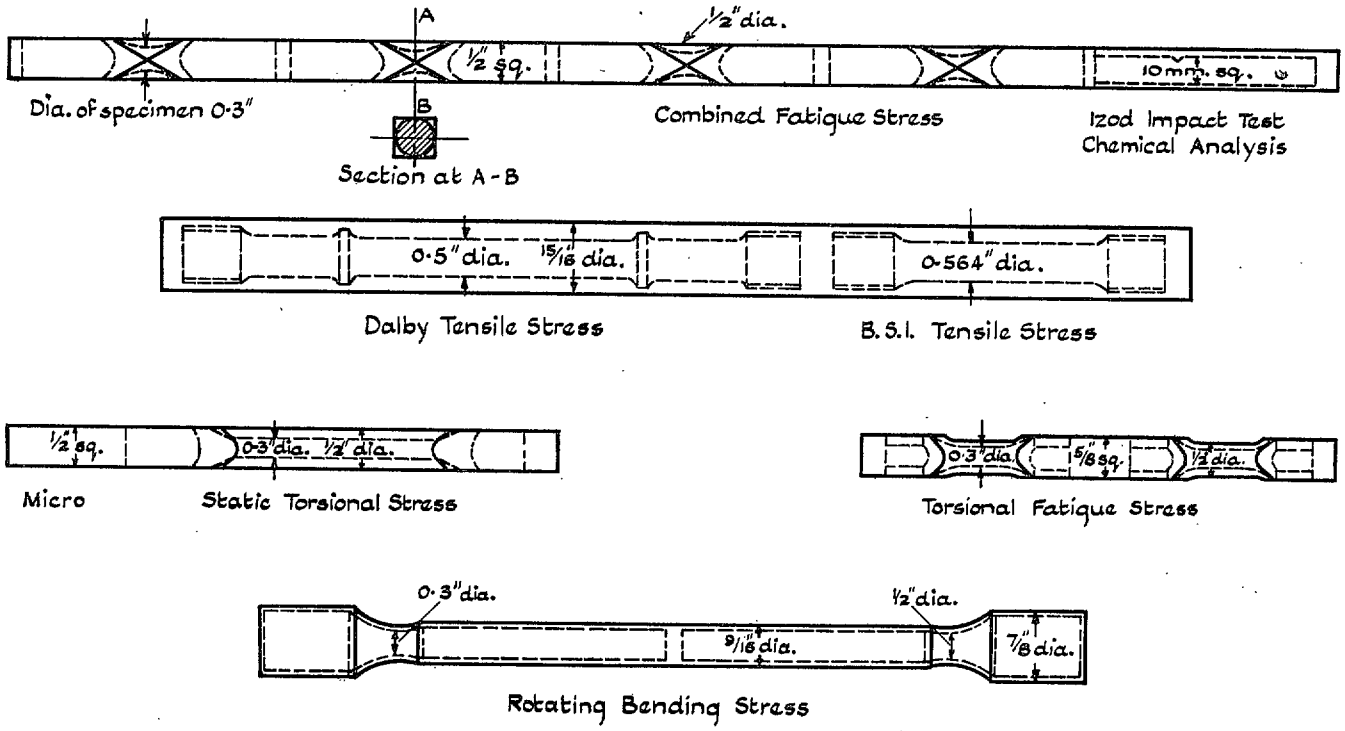

FIG. 5. Cast Irons. Forms of Cast Bars showing location of Specimens.

(ii) *Static Tests* :—Complete static tensile tests to destruction were made on two specimens of each material, the elastic limit, etc., being determined by using a mirror extensometer of the Martens type. Further, in order to obtain the true form of the load/elongation curve to fracture, two autographic load/elongation diagrams to fracture have also been obtained, using a Dalby optical load/extension recorder.

Two specimens of each material have been tested to destruction under statical torsional straining, the first portion of the torque/twist diagram being determined using a mirror extensometer.

With the exception of the cast irons, the materials were supplied in the form of $\frac{7}{8}$ in. dia. bar. To reveal any significant lack of uniformity in the bar, indentation tests have been made on specimens of four thicknesses ; these tests include ball and diamond pyramid indentations.

(iii) *Impact Tests* :—Notched bar impact tests have been made, on four specimens of each material, in an Izod machine of 120 ft.-lb. capacity.

Fig. 4 shows the forms of all the specimens used in the mechanical tests described above. For all the engineering steels, the specimens were machined, in the usual manner, from the solid $\frac{7}{8}$ in. dia. bars in which these steels were supplied.

In regard to the cast irons, Fig. 5 shows the relation of the positions of the final test pieces to the forms of the various shaped bars as cast ; these bars were cast from patterns representing the nearest practicable approach to the required finished shapes, plus an allowance for machining.

(*c*) CHEMICAL ANALYSIS AND METALLURGICAL EXAMINATION

A chemical analysis and microscopical examination was carried out, at the National Physical Laboratory, on each material investigated.

2. Additional Items of Investigation

As described above, the main programme of combined stress fatigue tests were made using solid specimens, having a test section of 0·3 in. diameter, the test section being smoothly joined to the remainder of the specimen by a transition radius of one inch ; the results to be obtained can be regarded as representing the intrinsic fatigue resistance of the materials under the applied test conditions and in the absence of appreciable stress concentration effects.

(*a*) SOLID AND HOLLOW SPECIMENS

In regard to the form of test section, experience of fatigue testing under simple cyclic bending, and simple cyclic torsional stresses has shown* that the substitution

* For some examples, with discussion, *see* paper by Gough and Tapsell[14].

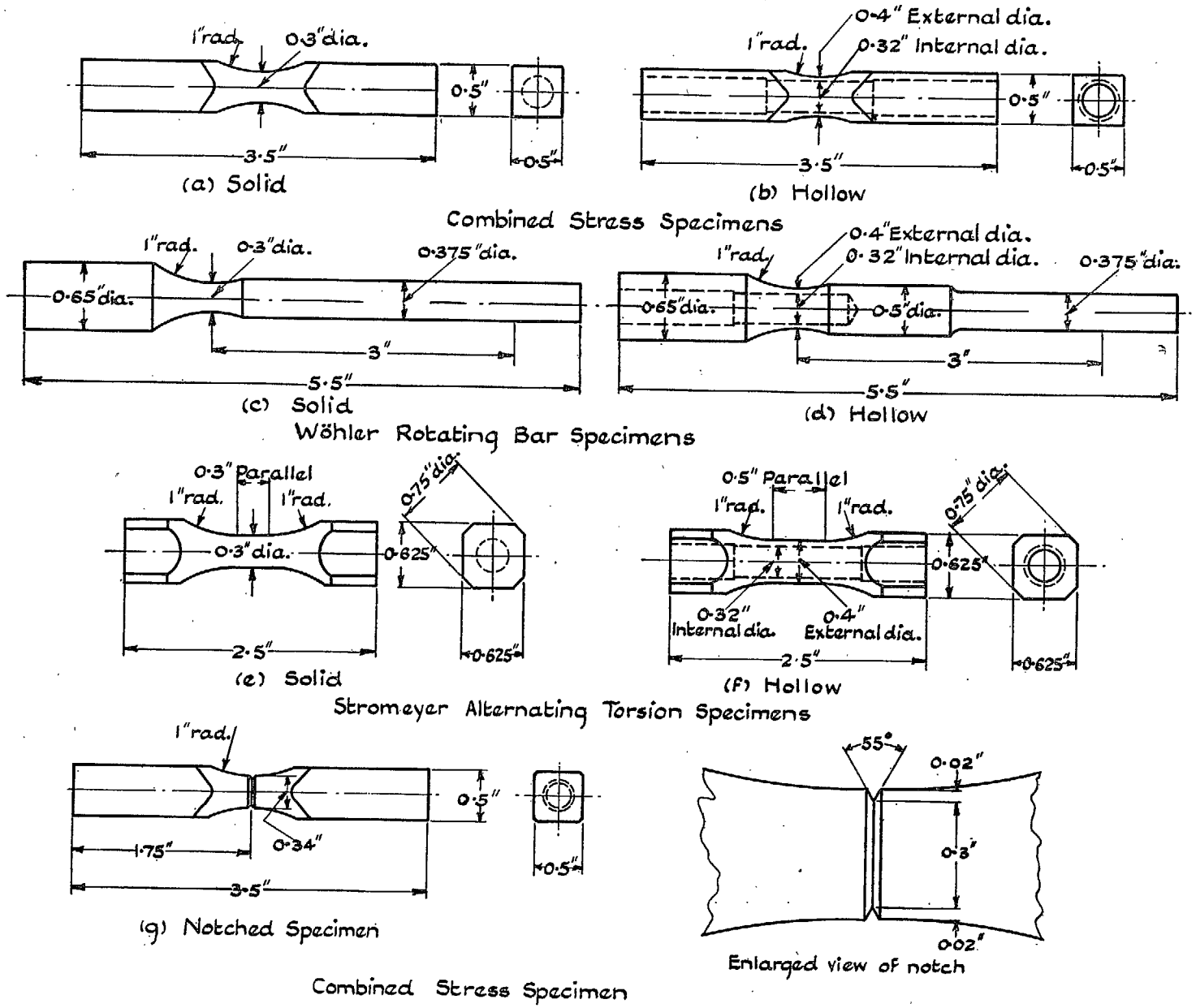

FIG. 6. Forms of Specimens used to investigate the effects of (*a*) Hollow and Solid section, and (*b*) Stress concentration due to a sharp Vee notch.

of a hollow for a solid cylindrical test section results, in general, in a reduction of endurance limit, usually of a small amount when bending fatigue stresses are applied and a larger amount under torsional fatigue stresses. It was a matter of interest and practical value, in studying the behaviour of metals under combined stresses, to examine if the general form of the relationship (to be determined)—as the applied stressing changed from cyclic bending to cyclic torsion throughout the intermediate combinations of these stresses—was also affected by the form of the test section. Two materials, used in the main investigation—the 0·1% C. Steel and the 3½% Ni. Cr. Steel—were selected for this purpose and the usual combined stress programme was repeated on each, using hollow specimens. To complete the comparison, the fatigue limit of each, again using hollow specimens, has been determined in (*a*) the rotating-bar machine, of the Wohler type, and (*b*) the Stromeyer alternating torsion machine. Fig. 6 shows the hollow specimens—and, for comparison—also the solid specimens used; each trio of specimens is similar in the test portions.

(*b*) EFFECT OF STRESS CONCENTRATION

The unavoidable inclusion in engineering design of changes in section, screwthreads, etc., indicated that the practical value of the proposed programme of tests on resistance of engineering steels to combined stresses would be greatly increased if it included some tests in which the effect of, at least, one form of stress concentration was studied. The form selected has been produced by machining a 55 deg. 'sharp' vee notch round the circumference of the test portion of the specimen, the depth of the groove being, approximately, 0·02 in. The form of the specimen used is shown in Fig. 6.

The nominal outside diameter was made 0·34 in., the root diameter at the base of the groove being 0·3 in., i.e. the same as the nominal diameter of the plain specimens used in the main investigation. Thus the difference between the values obtained in the tests made on the plain and notched specimens will give directly the decrease in the fatigue resistance due to the presence of the notch, as such.

In preparing the specimens, every effort was made to produce the bottom of the notch as sharp as possible; the cutting tool was carefully resharpened before the final cut, during which the specimen was turned by hand. Actually, of course, each notch had a transition curve at its root, approximating to a 'root radius'. This approximate radius was measured, on each specimen, using a very simple procedure which gave fairly accurate results. A thin sheet of white xylonite was drilled with holes having diameters of 0·02 to 0·14 in. in increments of 0·02 in. The holes were filled with black wax and the surface rubbed smooth, with pumice in water. The root of the notch of each specimen was projected optically on to a screen at a magnification of 50 and the radius determined by fitting the appropriate black spot into the projected image; by this means the root radius could be estimated to within 0·0001 in. All notch radii were measured and recorded; with any one steel, the variation was remarkably constant; it varied somewhat from steel to steel. With most steels, the notch radius was round about half a thousandth of an inch; with others it was round about one-thousandth.

In view of the importance of the subject, combined fatigue stress tests have been made, using notched specimens, on seven of the engineering steels, including the 3½% Ni. Cr. Steel in both the normal and embrittled conditions. In each case, the full seven determinations (pure bending, pure torsion and five combinations) have been made.

Note:—In endurance testing, the resulting data often plot regularly and consistently and the safe range of stress can be reliably estimated within close limits. In other cases, such a 'scatter' is obtained that much less reliance is placed on the estimated result; sometimes, the inconsistency is such that the fatigue limit can only be expressed by a 'bracket' of values; in extreme cases, even a bracket is hardly justified. Such scatter may be due to such factors as lack of uniformity of the material, presence of internal stresses varying from specimen to specimen, extreme sensitivity of the material to very small surface defects, etc. But, except where signs of unsoundness, surface defects, etc. are clearly visible on the original or fractured surfaces of the specimen, the cause is conjectural and rejection of the individual test is not strictly justified. When, as in the present series of tests, a very wide range of types and strengths of materials is investigated, one must, therefore, expect to find that a few of the estimated values of the fatigue limits cannot be assigned as good an accuracy as the majority; no doubt, a 'statistical' evaluation of the fatigue limits of those materials which behaved irregularly, by the use of a very large number of specimens, say fifty, would be an appropriate procedure to adopt, but it was not practicable to do so.

To facilitate balanced discussion, in assembling the results in the tables, an indication is given of the reliability placed on the quoted value of every fatigue limit by the use of one of three distinguishing marks:—'R' to indicate a clearly defined and apparently reliable value; 'LR' to indicate a result less reliable but probably not far from the correct value; 'U' to indicate a result in whose accuracy little confidence can be placed. Each assigned value of the 'reliability index' was, of course, made separately and independently for each *S/N* diagram, being determined, entirely and solely by inspection of the degree of consistency in which the experimental data plotted on that diagram and by consideration of the number of specimens tested. The fatigue history of every specimen used in the investigation is recorded in the *S/N* curves of Appendices 2 and 3; each assigned index can be compared by the reader with the corresponding curve.

TABLE 1

MATERIALS AND PROGRAMME

Identification Mark	Description of Material	Heat Treatment	Form of Microstructure	Tensile Strength t/in²	Izod value ft-lbs.	Remarks on Special Objects and Additional Tests (i.e. additional to normal full programme of combined stress tests on solid specimens, supplementary mechanical tests, chemical analysis and microscopical examination).
HEP	0·1% C. Steel (Normalised)	Normalised from 900°C.	Ferrite and Pearlite.	28	89	Fatigue tests on hollow specimens to determine effect of form of specimen (see also HGU).
JCA	0·4% C. Steel (Normalised)	Normalised from 850°C.	Ferrite and Pearlite.	42	30	A steel tested in each of two heat-treated conditions, to investigate effect of different forms of microstructure of the same chemical composition. The fatigue resistance of the normalised material using notched specimens was also determined.
JHM	0·4% C. Steel (Spheroidised)	Normalised from 900°C. Heated for six days at 650°C. and slowly cooled.	Uniform Matrix containing Spheroidised Cementite (as in fully annealed steels of moderate carbon content).	31	32	
JMV	0·9% C. Steel (Pearlitic)	Normalised from 820°C.	Pearlite.	55	3	—
JSL	3% Ni. Steel (30/35 ton)	O.H. from 850°C. Tempered 700°C. Air cooled.	Hardened and tempered.	34	100	Fatigue strength of notched specimens determined.
HNZ	3/3½% Ni. Steel (45/50 ton)	O.H. from 850°C. Tempered 610°C. Air cooled.	Hardened and tempered.	47	86	Two steels selected as having approximately the same tensile strength but differing chemical compositions. Fatigue strength of each determined using notched specimens.
JXN	Cr. Va. Steel (45/50 ton)	O.H. from 850°C. Tempered 700°C. Air cooled.	Hardened and tempered.	49	96	
HGU	3½% Ni. Cr. Steel (Normal Impact)	O.H. from 830°C. Tempered 620°C. and cooled in water.	Hardened and tempered (quickly cooled).	58	76	The same material in the normal and embrittled conditions; same tensile strength but widely different impact values. On the normal material fatigue tests made on hollow specimens (see also HEP). Fatigue strength of both materials determined using notched specimens.
HKN	3½% Ni. Cr. Steel (Low Impact)	O.H. from 830°C. Tempered 1¾ hours at 620°C. and cooled to 100°C. in 42 hrs.	Hardened and tempered (slowly cooled).	58	5½	
JZP	Ni. Cr. Mo. Steel (60/70 ton)	Normalised 900°C. O.H. from 850°C. Tempered 640°C. Air cooled.	Hardened and tempered.	65	90	—
KHC	Ni. Cr. Mo. Steel (75/80 ton)	O.H. from 850°C. Tempered 600°C. Air cooled.	Hardened and tempered.	81	55	Fatigue strength of notched specimens determined.
KBT	Ni. Cr. Steel (95/105 ton)	Air Hardened from 820°C. Tempered 200°C. Air cooled.	Hardened and tempered.	108	24	—
HHV	'Silal' Cast Iron	As Cast.	Cast.	15	½	Chosen as a near approach to a brittle material.
HMY	'Nicrosilal' Cast Iron	As Cast.	Cast.	14	1½	Chosen as representing a comparatively ductile cast iron.

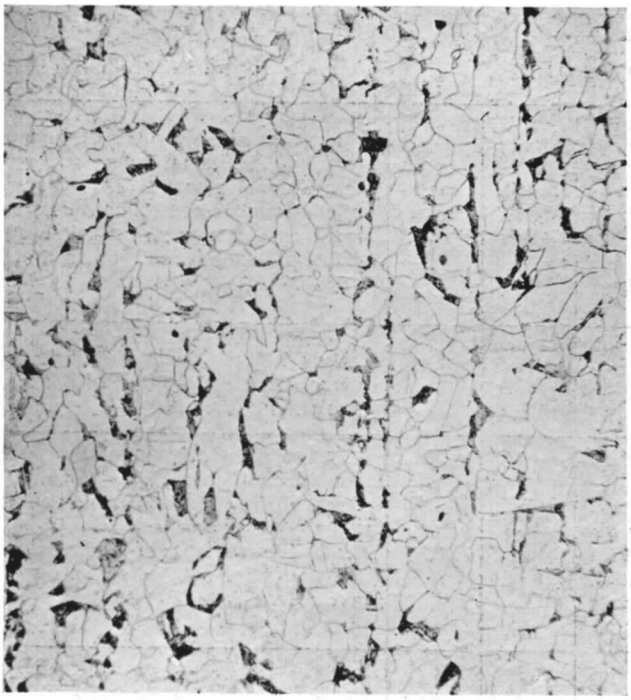

FIG. 7 (*a*). 0·1% C. Steel (Normalised). Longitudinal Section × 150.

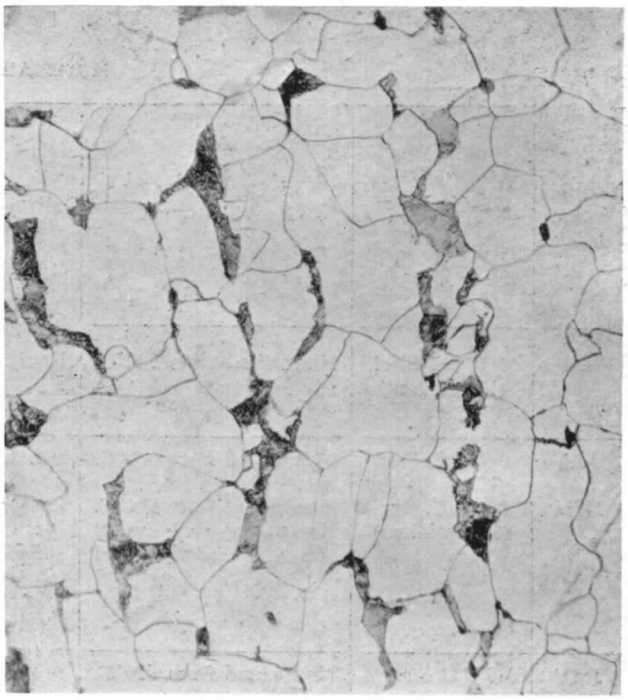

FIG. 7 (*b*). 0·1% C. Steel (Normalised). Longitudinal Section × 500.

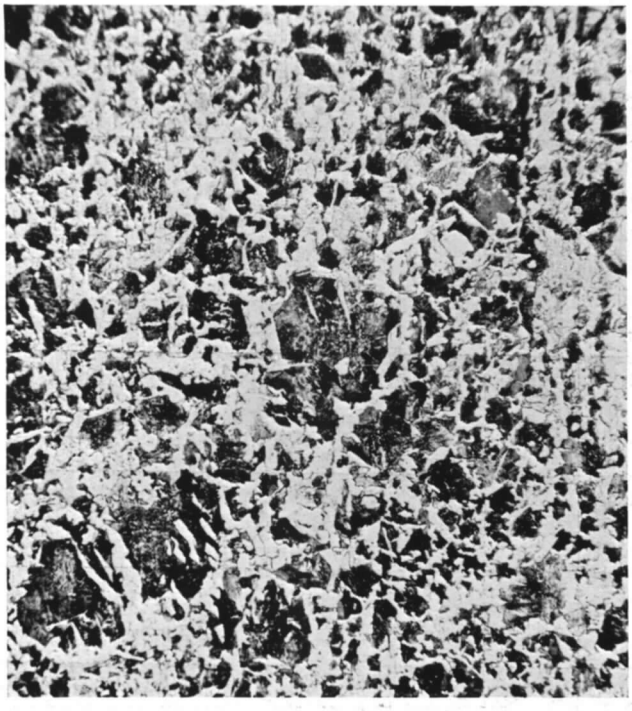

FIG. 7 (*c*). 0·4% C. Steel (Normalised). Representative Structure × 150.

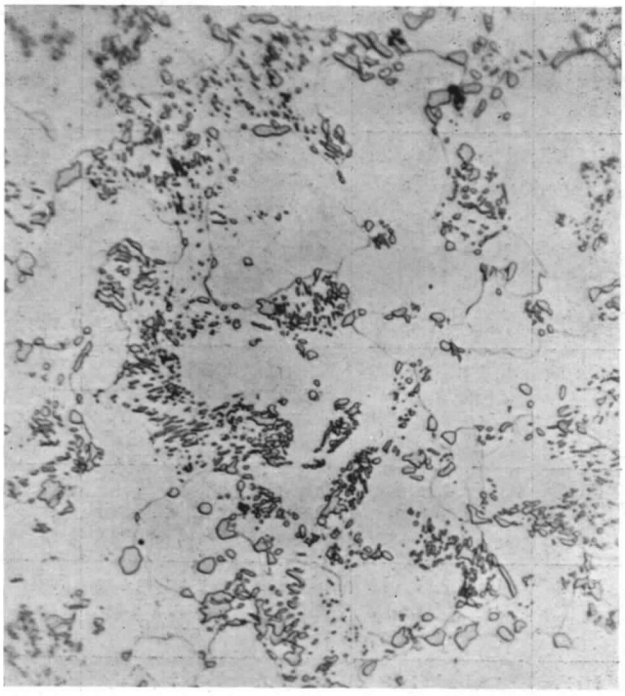

FIG. 7 (*d*). 0·4% C. Steel (Spheroidised). Longitudinal Section × 1500.

FIG. 7. Microphotographs.

FIG. 8 (*a*). 0·9% C. Steel (Pearlitic). Transverse Section, etched × 150.

FIG. 8 (*b*). 0·9% C. Steel (Pearlitic). Transverse Section, etched × 500.

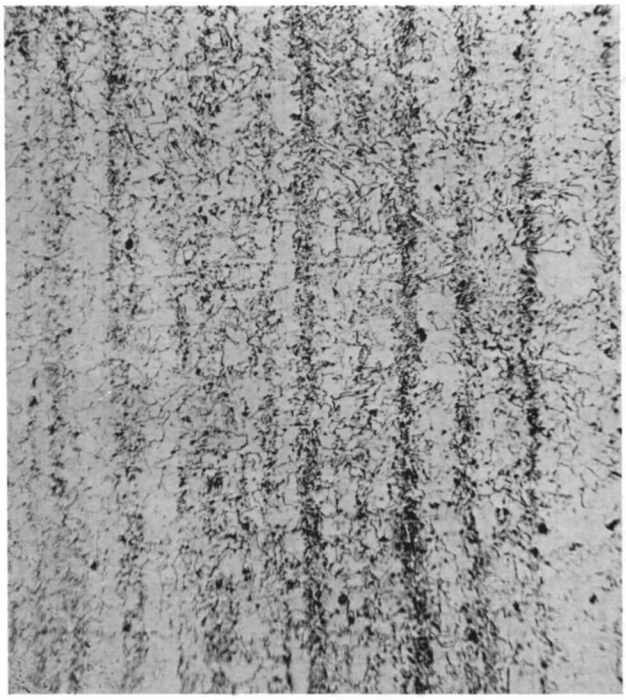

FIG. 8 (*c*). 3% Ni. Steel (O.H. & T.) (30/35 ton). Longitudinal Section, etched × 150.

FIG. 8 (*d*). 3% Ni. Steel (O.H. & T.) (30/35 ton). Longitudinal Section, etched × 500.

FIG. 8. Microphotographs.

FIG. 9 (*a*). 3/3½% Ni. Steel (O.H. & T.) (45/50 ton). Longitudinal Section, etched × 300.

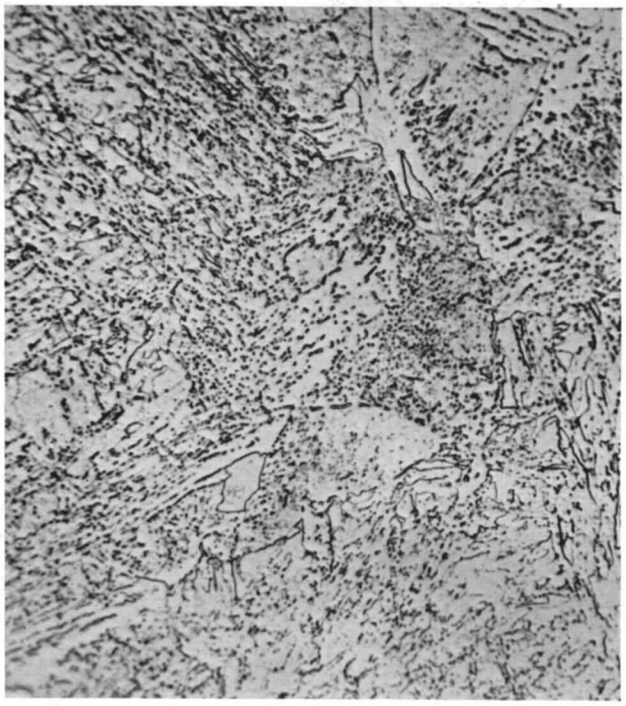

FIG. 9 (*b*). 3/3½% Ni. Steel (O.H. & T.) (45/50 ton). Longitudinal Section, etched × 1500.

FIG. 9 (*c*). Cr. Va. Steel (O.H. & T.) (45/50 ton). Longitudinal Section, etched × 500.

FIG. 9 (*d*). Ni. Cr. Steel (A.H. & T.) (95/105 ton). Longitudinal Section, etched × 500.

FIG. 9. Microphotographs.

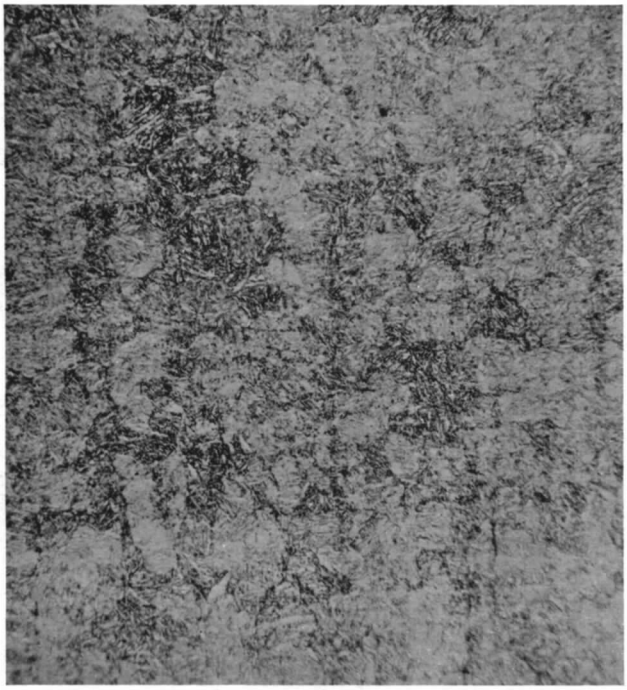

FIG. 10 (*a*). 3½% Ni. Cr. Steel (Normal Impact). Longitudinal Section, etched × 150.

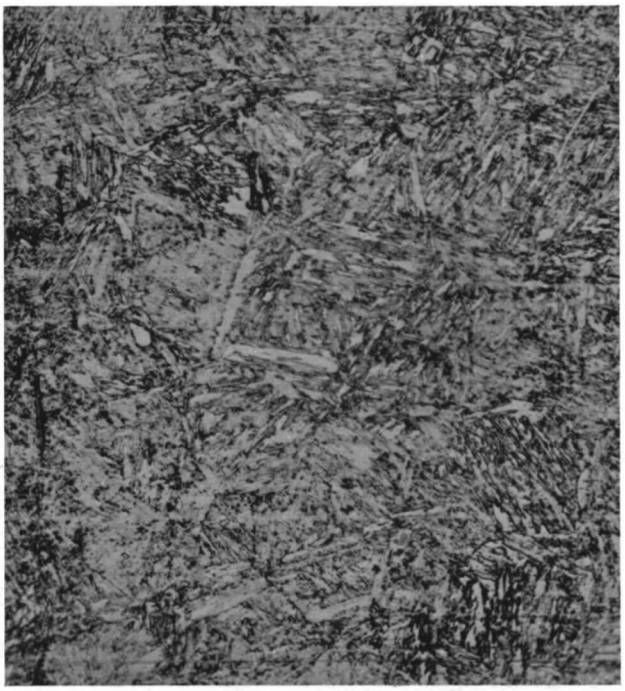

FIG. 10 (*b*). 3½% Ni. Cr. Steel (Normal Impact). Longitudinal Section, etched × 500.

FIG. 10 (*c*). 3½% Ni. Cr. Steel (Low Impact). Longitudinal Section, etched × 150.

FIG. 10 (*d*). 3½% Ni. Cr. Steel (Low Impact). Longitudinal Section, etched × 500.

FIG. 10. Microphotographs.

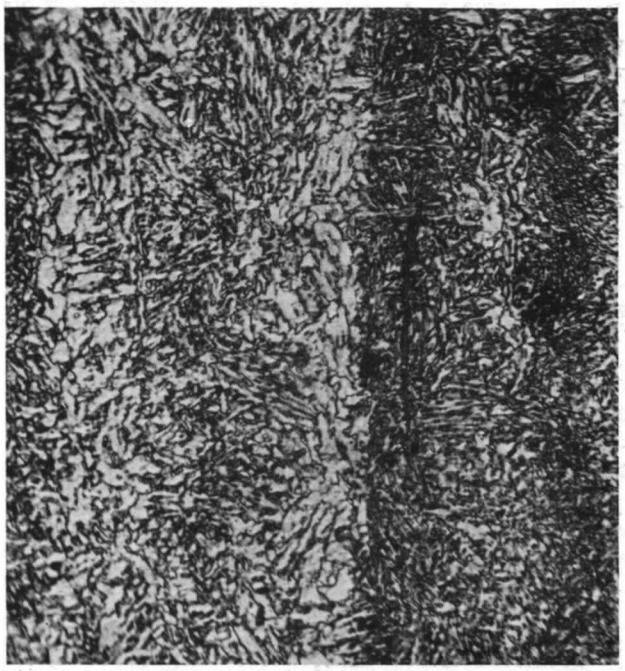

FIG. 11 (*a*). Ni. Cr. Mo. Steel (O.H. & T.) (60/70 ton). Longitudinal Section × 150 showing banding present.

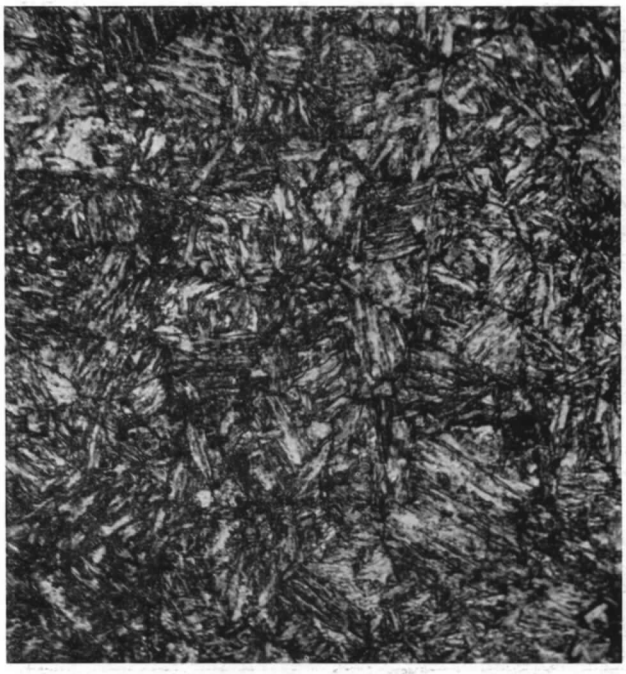

FIG. 11 (*b*). Ni. Cr. Mo. Steel (O.H. & T.) (60/70 ton). Longitudinal Section × 500. Uniform structure following heat-treatment above critical point.

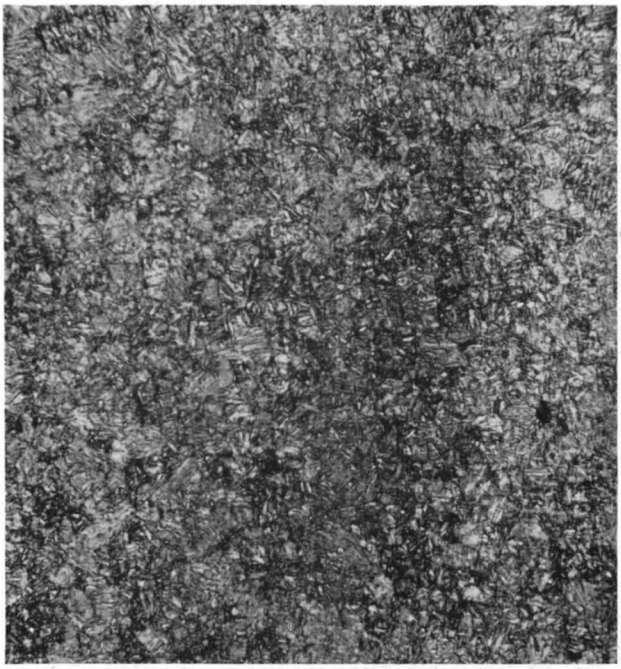

FIG. 11 (*c*). Ni. Cr. Mo. Steel (O.H. & T.) (75/80 ton). Longitudinal Section × 150.

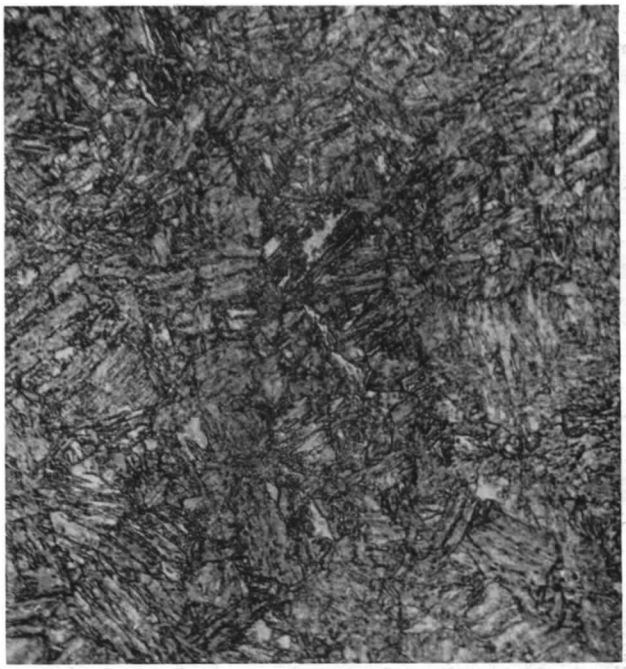

FIG. 11 (*d*). Ni. Cr. Mo. Steel (O.H. & T.) (75/80 ton). Longitudinal Section × 500.

FIG. 11. Microphotographs.

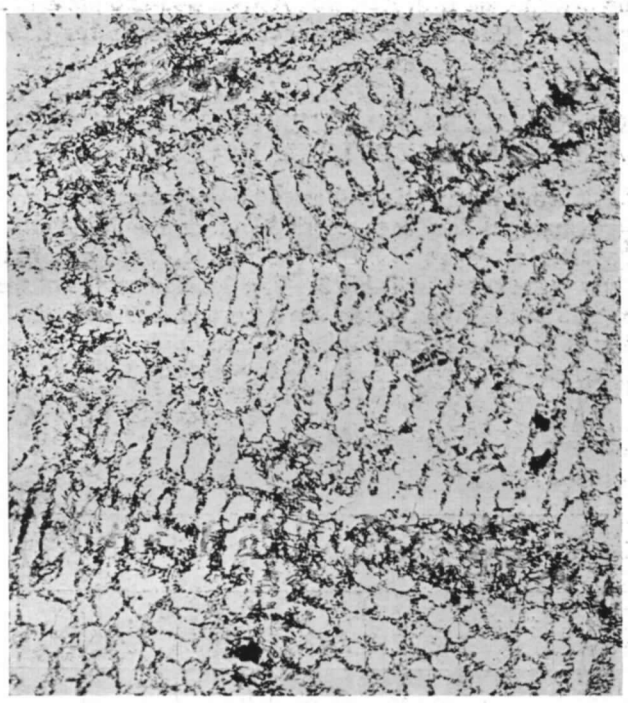

FIG. 12 (*a*). ' Silal ' Cast Iron. Longitudinal Section, etched × 150.

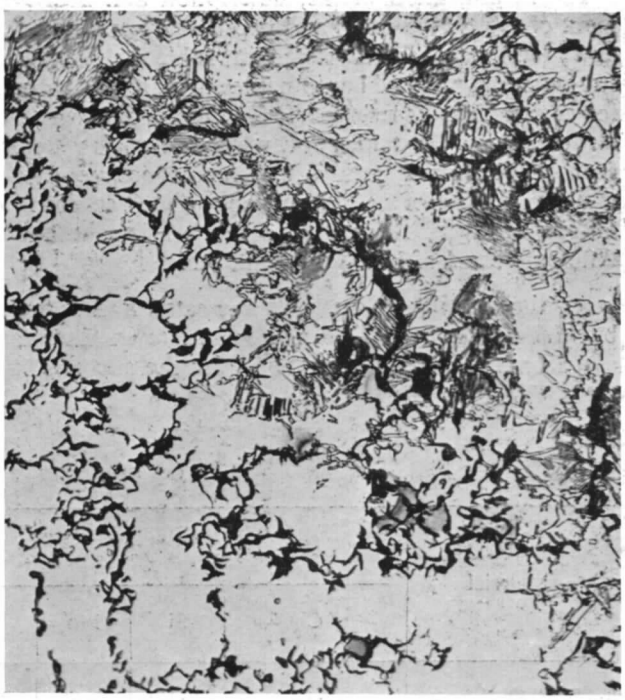

FIG. 12 (*b*). ' Silal ' Cast Iron. Longitudinal Section, etched × 500.

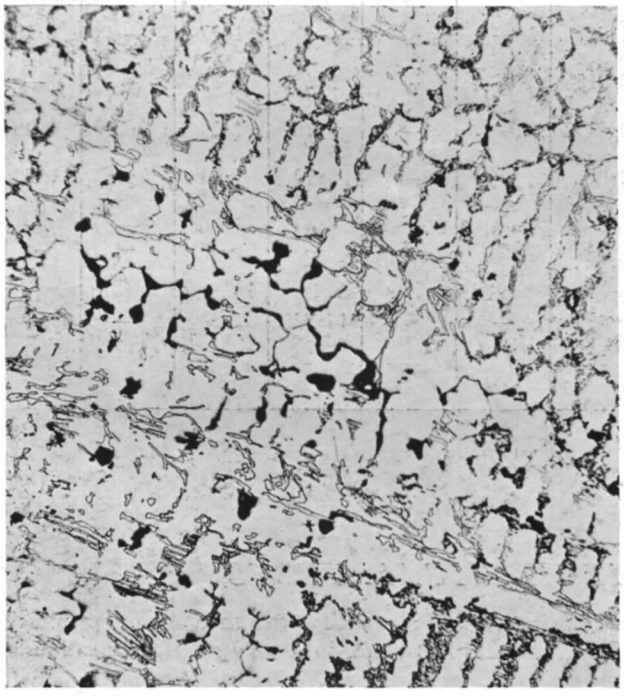

FIG. 12 (*c*). ' Nicrosilal ' Cast Iron. Transverse Section, etched × 150.

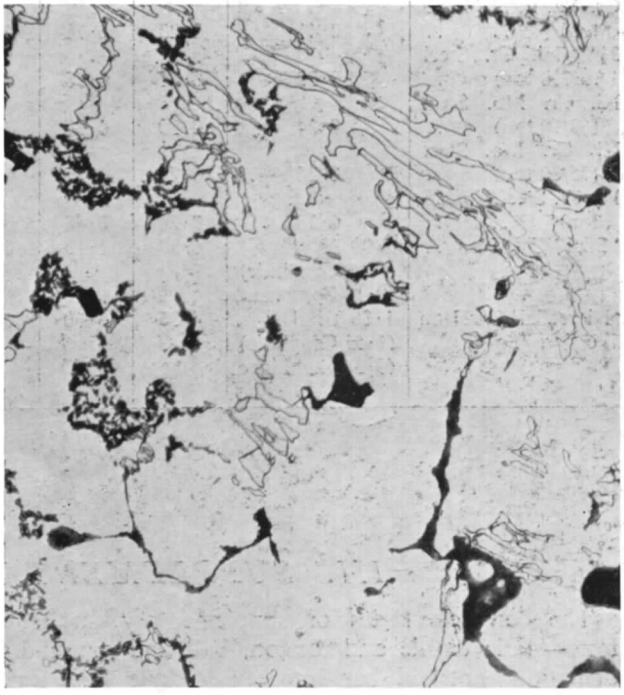

FIG. 12 (*d*). ' Nicrosilal ' Cast Iron. Transverse Section, etched × 500.

FIG. 12. Microphotographs.

The identification marks, description and heat-treatment of the twelve steels and two cast irons as supplied and investigated are as stated in Table 1 ; the tensile strengths and notched bar impact values are also included for convenience of reference. The remarks given in the last column of the table show which materials were used for the special investigations into form of specimen (hollow and solid), effect of a stress concentration (Vee-notch) on fatigue strength, the effects of embrittlement and of different forms of heat-treatment, etc.

All the steels were made, heat-treated and presented by Messrs. Thomas Firth and John Brown, Ltd. ; the cast irons were specially made under the supervision of the British Cast Iron Research Association and presented by them. Grateful acknowledgment is made for these valuable contributions to the research.

C. RESULTS OF CHEMICAL ANALYSES AND MICROSCOPICAL INVESTIGATION

A chemical analysis and metallurgical examination of each material has been carried out in the Metallurgy Department of the N.P.L. The results of the chemical analysis are given in Table 2. The detailed results of the metallurgical examination are recorded in Appendix I, Part I ; representative photo-micrographs are reproduced as Figs. 7 to 12 inclusive.

TABLE 2

CHEMICAL ANALYSES OF MATERIALS

Material	Chemical Composition, per cent.										
	C	Si	Mn	S	P	Al.	Cu	Ni	Cr	Mo	Va
0·1% C. Steel ..	0·12	0·185	0·61	0·012	0·016	—	0·075	0·06	Trace	—	—
0·4% C. Steel ..	0·39	0·23	0·65	0·017	0·02	—	—	0·12	—	—	—
0·9% C. Steel ..	0·86	0·05	0·13	0·026	0·02	—	—	—	—	—	—
3% Ni. Steel (30/35 ton)	0·11	0·22	0·42	0·011	0·011	—	—	3·18	Trace	—	—
3/3½% Ni. Steel (45/50 ton)	0·34	0·17	0·57	0·007	0·011	—	—	3·25	0·06	—	—
Cr. Va. Steel (45/50 ton)	0·41	0·23	0·71	0·006	0·017	—	—	—	1·27	—	0·28
3½% Ni. Cr. Steel (55/60 ton) ..	0·30	0·21	0·58	0·006	0·018	—	—	3·62	0·85	—	—
Ni. Cr. Mo. Steel (60/70 ton) ..	0·24	0·20	0·57	0·004	0·015	—	—	3·06	1·29	0·54	0·25
Ni. Cr. Mo. Steel (75/80 ton) ..	0·24	0·27	0·57	0·007	0·011	—	—	3·10	1·33	0·41	0·25
Ni. Cr. Steel (95/105 ton)	0·28	0·23	0·48	0·004	0·018	—	—	4·42	1·36	—	—
'Silal' Cast Iron ..	2·09 Total (1·99 Graphitic) (0·10 Combined)	6·39	1·13	0·031	0·047	0·08	—	—	—	—	—
'Nicrosilal' Cast Iron	1·88 Total (1·51 Graphitic) (0·37 Combined)	4·25	0·60	0·039	0·033	—	—	17·74	2·39	—	—

III. SUPPLEMENTARY MECHANICAL TESTS

The complete series of supplementary mechanical tests—static tensile and torsion, ball and pyramid indentation, notched bar impact ; fatigue limit under reversed bending (Wohler machine) stresses and reversed torsional (Stromeyer machine) stresses—have been made on each of the fourteen materials. The methods of tests, detailed results, observations, etc., are fully recorded in Appendix 2 of Part I. For ease of reference, the principal data are summarised in Table 3.

The test results show that the mechanical properties of all the materials meet, in a very satisfactory manner, the planned requirements of this selected range of materials. The alloy steels, chosen primarily in regard to a range of tensile strengths, give the expected values. The 3½% Ni. Cr. Steel, in two forms of heat-treatment gives the required wide variation in notched-bar values (76 ft. lb., 5½ ft. lb.) but the same tensile strength (58 t/in.²). The air-hardening Ni. Cr. Steel exhibits the required high

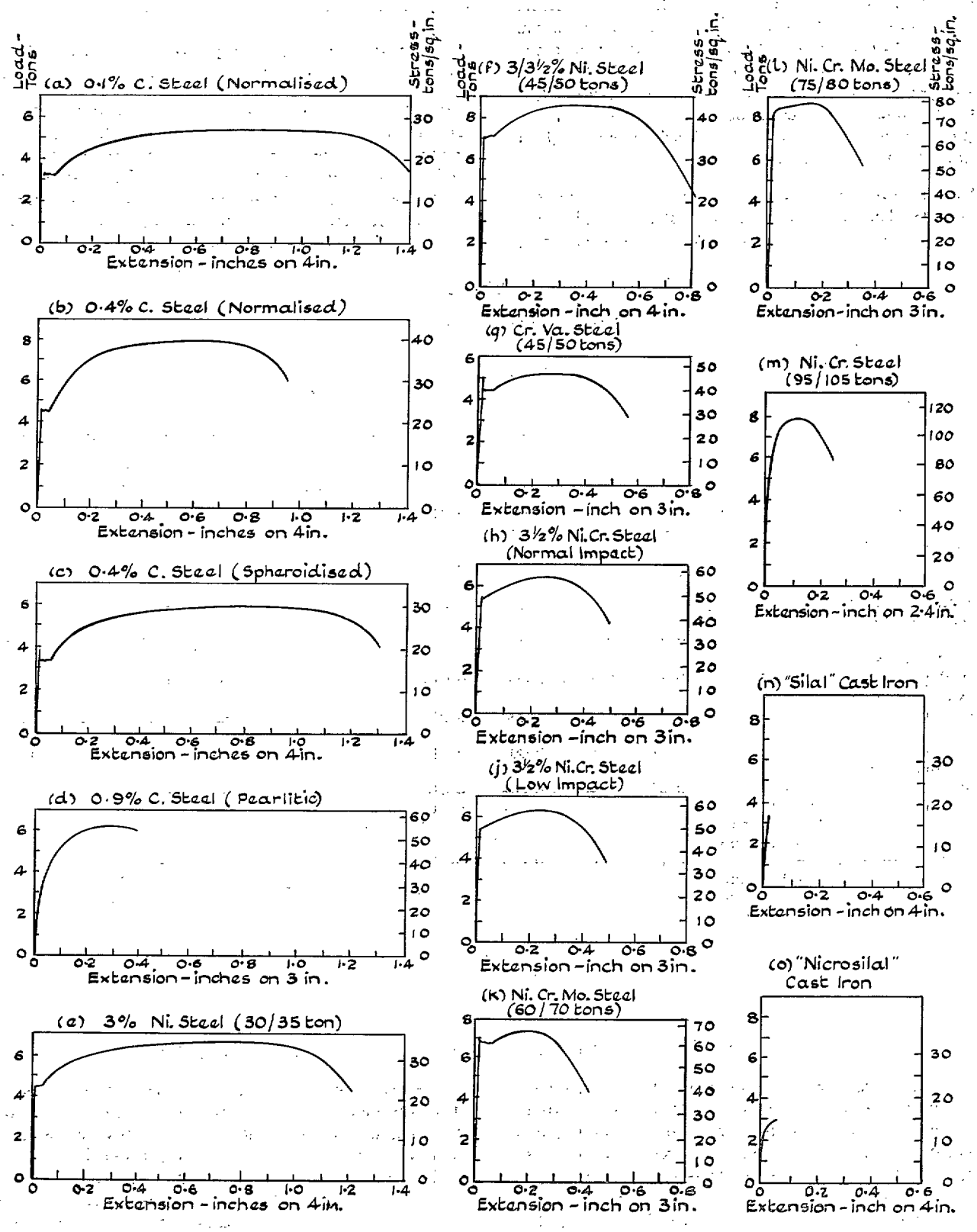

FIG. 13. Tensile Load/Elongation Diagrams to Fracture from Dalby Autographic Records.

TABLE 3

SUMMARY OF PRINCIPAL DATA OBTAINED FROM THE SUPPLEMENTARY STATIC, IMPACT AND FATIGUE TESTS

Principal Data	Materials													
	0·1% C. Steel (Normalised)	0·4% C. Steel (Normalised)	0·4% C. Steel (Spheroidised)	0·9% C. Steel (Pearlitic)	3% Ni. Steel (30/35 ton)	3/3½% Ni. Steel (45/50 ton)	Cr. Va. Steel (45/50 ton)	3½% Ni. Cr. Steel (Normal Impact)	3½% Ni. Cr. Steel (Low Impact)	Ni. Cr. Mo. Steel (60/70 ton)	Ni. Cr. Mo. Steel (75/80 ton)	Ni. Cr. Steel (95/105 ton)	'Silal' Cast Iron	'Nicrosilal' Cast Iron
Tensile Limit of Proportionality, t/in²	12·5	14·5	14·9	7·7	15·8	26·0	31·5	18·3	13·5	47·0	21	24	1·9	1·9
Upper Yield Point in Tension,* t/in²	16·6	23·4	18·6	N.D.	N.D.	38·0	44·1	49·2	48·9	61·3	N.D.	N.D.	N.D.	N.D.
Ultimate Tensile Strength, t/in²	27·9	42·0	30·9	54·9	34·1	46·8	48·7	58·0	58·1	64·8	80·5	108	14·9	14·2
Elongation at fracture ($l = 4\sqrt{A}$), per cent.	40¼	31	39½	13¾	40½	26½	26½	25	24	23½	20½	16	½	1
Reduction of Area at fracture, per cent.	70	58¼	67	18	72½	67½	66	65	60½	67	60	52	0	1·3
Young's Modulus, E, lb/in² × 10^{-6}	28·8	30·0	30·1	29·3	29·2	29·2	30·3	29·0	28·9	29·1	29·2	30·0	17·5	19·6
Brinell Hardness Number (2 mm. ball, 120 kg load)	127	195	144	248	163	237	229	282	278	325	394	479	322	182
Torsional Limit of Proportionality, t/in²	8·5	10·5	5·2	7·5	9·0	19·0	24·5	23·7	18·3	31·4	26·6	28·8	4·4	2·3
Yield Point in Torsion,* t/in²	11·7	16·8	11·7	N.D.	N.D.	27·8	30·8	37·8	N.D.	46·3	59·1	N.D.	N.D.	N.D.
Torsional Modulus of Rupture, t/in²	32·7	41·7	36·3	48·9	38·0	44·3	46·2	52·3	51·2	57·3	67·5	89·2	23·8	32·5
Total Twist at fracture ($L/d = 8\frac{1}{3}$), degrees	2859	1600	2190	552	2014	1991	1402	1230	1150	2085	1066	630	8	170
Modulus of Rigidity, G, lb/in² × 10^{-6}	11·5	11·8	11·8	11·4	11·5	11·4	12·1	11·4	11·5	11·5	11·6	11·3	7·6	8·6
Izod Notched Bar Value, ft-lb	89	30	32	3½	100	86	96	76	5½	90	55	24	½	1½
Fatigue Limit (Reversed Bending Stresses) t/in² (Wohler machine)														
(*a*) Solid Specimens	±17·0 (R)	±20·8 (R)	±15·9 to ±17·4 (U)	±22·2 (R)	±20·3 (R)	±26·5 (R)	±26·5 (R)	±33·7 (R)	±31·9 (R)	±37·5 (R)	±39·0 (U)	±45 (LR)	±14·9 (R)	±14·0 (R)
(*b*) Hollow Specimens	±16·5 (R)	—	—	—	—	—	—	±33·4 (R)	—	—	—	—	—	—
Fatigue Ratio (Fatigue Limit/Ultimate T.S.)														
(*a*) Solid Specimens	0·61	0·50	0·51 to 0·56	0·40	0·60	0·57	0·54	0·58	0·55	0·58	0·49	0·42	1·00	0·98
(*b*) Hollow Specimens	0·59	—	—	—	—	—	—	0·58	—	—	—	—	—	—
Fatigue Limit (Reversed Torsional Stress) t/in² (Stromeyer Machine)														
(*a*) Solid Specimens	±9·6 (R)	±13·5 (R)	±9·6 (R)	±16·3 (R)	±12·7 (R)	±18·0 (R)	±17·5 (LR)	±22·6 (R)	±21·7 (R)	±21·5 (U)(Est.)	±23·8 (R)	±28·5 (R)	±12·9 (R)	±11·8 (R)
(*b*) Hollow Specimens	±8·7 (R)	—	—	—	—	—	—	±21·5 (R)	—	—	—	—	—	—
Fatigue Ratio (Fatigue Limit/Ultimate T.S.)														
(*a*) Solid Specimens	0·34	0·32	0·31	0·30	0·37	$0·38_5$	0·36	0·39	0·37	0·33 (Est.)	0·30	0·26	0·87	0·83
(*b*) Hollow Specimens	0·31	—	—	—	—	—	—	0·37	—	—	—	—	—	—

Notes.—* N.D. Denotes 'No definite yield point.'

tensile strength (108) but can definitely be classed as ductile (16% elongation, 52% reduction of area) and provides, therefore, a suitable ' end-point ' to a series of ductile engineering steels. In Fig. 13 have been assembled one of the pair of autographic static tensile load/elongation diagrams to fracture which were obtained from each of the materials tested: these show at a glance the differences in ductility and yield-point characteristics. The careful exploration, by three types of indentation test, of the hardness of the steels at a series of distances from the bar axis, show that, although some small variations consistently occur in the hardness at these various depths, the heat-treatments applied have been successful in producing a very satisfactory degree of uniformity in all cases. Under each form of test, the two cast irons exhibit ' brittleness ' in contrast to the steels.

In the static torsion tests, the two cast irons were the only materials to give a helicoidal type of fracture. Under reversed torsional fatigue, the cast irons again fractured spirally; so, also, did seven of the ten ductile steels. But, whereas the values of the ' fatigue ratio ' of these seven steels are quite normal (0·37 to 0·26) for shear failure, ' Silal ' and ' Nicrosilal ' give results for this ratio of 87% and 83%, respectively. These abnormally high values, taken in conjunction with their helicoidal type of fracture, give a strong indication that they are behaving as brittle materials whose fracture may be largely controlled by principal stress or principal strain. In the detailed discussion of these results, in Appendix 3, Part I, reference is made to an earlier research, by Southwell and Gough,[20] which discusses this fracture problem analytically and shows experimentally that the path of fracture of an essentially ductile steel can be changed, from the normal fracture occurring on planes of maximum shear stress, to planes of principal stress (or strain) by the presence of a very small surface flaw.

Attention may also be drawn to the results in Table 4 of the fatigue tests made on solid and hollow specimens of two materials, as determined using the Wohler and the Stromeyer fatigue machines.

With both materials and under each of the two types of stressing, the fatigue limit determined using hollow specimens is lower than that when solid specimens are used. But under reversed bending stresses, the difference is small, 3% with the softer steel, 1% with the harder. Under reversed torsional stresses, however, the difference is much larger, 9% with the softer steel, 5% with the harder steel. These results are in accordance with our general experience. The explanation lies in the difference in the ' impressed conditions ' of test, i.e. the effect of modifications in the conditions of stress and strain caused by super-elastic straining within the fatigue range. The subject has been discussed in a paper by Gough and Tapsell[14]. The ductility of the material is the essential factor. Once a departure from truly elastic conditions obtains within the test section as a whole, or in parts of the test section, then this effect may exert a degree of influence upon the calculated result (as determined using the usual formulae which assume elasticity) which will vary with the type of machine used and/or the type of test piece employed. But the effect is not, in itself, truly a ' machine ' effect nor a ' shape of specimen ' effect; these are secondary effects, not primary causes. If a material was initially elastic and remained so until fracture, no ' impressed conditions ' effect could occur. But, as far as is known, such a truly elastic material would not be subject to fatigue; no material used in engineering, certainly no ferrous metal or alloy, is of such a truly elastic nature. This interesting aspect will be again referred to, when the results are available of tests on solid and hollow specimens, made on the same machine—the No. 1 Combined Stress Machine—and covering not only the cases of cycles of reversed bending and reversed torsional stresses but various combinations of these.

One further point of interest, in connection with Table 3, is the comparison of the values of the ratio, for solid specimens, of the fatigue limit under reversed torsional stresses to the fatigue limit under reversed bending stresses for the whole series of the materials tested. Taking the materials in the sequence (left to

TABLE 4

EFFECT OF SPECIMEN FORM ON FATIGUE LIMITS UNDER REVERSED BENDING AND REVERSED TORISONAL STRESSES

Material	Form of Specimen	Fatigue Limit		Ratio, b/a	
		Reversed Bending	Reversed Torsion	Reversed Bending	Reversed Torsion
0·1% C. Steel (Normalised) U.T.S. = 27·9 t/in²	Solid	(*a*) ±17·0	(*a*) ±9·6	0·97	0·91
	Hollow	(*b*) ±16·5	(*b*) ±8·7		
3½% Ni. Cr. Steel (Normal Impact) U.T.S. = 58 t/in²	Solid	(*a*) ±33·7	(*a*) ±22·6	0·99	0·95
	Hollow	(*b*) ±33·4	(*b*) ±21·5		

right) as set out in that Table, and omitting the unreliable values for the 0·4% C. Steel (Spheroidised) and the Ni. Cr. Mo. (60/70 ton), these values are :—0·56, 0·65, 0·74, 0·63, 0·68, 0·66, 0·67, 0·68, 0·61, 0·63, 0·86, 0·84. The values for the ten steels quoted thus show the wide variation from 0·56 to 0·74. No constant ratio obtains, such as would be expected, for example, if certain well-known theories which have been advanced to account for elastic failure also applied to fatigue failure. The values of the ratio for the cast irons are abnormally high—0·86 and 0·84—but yet not high enough to be quite consistent with failure by principal stress, for which the ratio value would, of course, be unity. The Guest criterion for elastic failure, when adjusted to cover failure by fatigue, takes care of this lack of constancy of ratio value and will be discussed later.

IV. RESULTS OF THE COMBINED STRESS FATIGUE TESTS

These tests were all made using the No. 1 type of Combined Stress Fatigue Testing Machine, previously described. All fatigue limits were determined by the usual method of endurance testing, on a minimum ' reversals ' basis of 10^7. For each material and form of specimen, fatigue limits were determined at each of seven ' settings ' of the machine, i.e. at $\theta = 0$, 15, 30, 45, 60, 75 and 90 deg.

The programme falls naturally into three series of tests. Firstly, that in which all fourteen materials were investigated using specimens having a solid cylindrical form at the test section, to yield what may be termed the basic fatigue strengths of those materials under the applied test conditions ; secondly, the series in which two of the steels were also tested using specimens having a hollow cylindrical form of test section, to obtain some information regarding the effect of this change of form on the basic fatigue resistance ; thirdly, the series made on a selected seven of the steels using solid cylindrical specimens containing a circumferential sharp Vee groove, to determine the effect of a simple type of stress concentration often encountered in engineering practice. It will be convenient to present separately the results of each of these three series of tests.

The detailed results and observations of all the tests, together with the plotted data in the form of S/N diagrams, are reported fully in Appendix 3 of Part I of this paper. For the convenience of the general reader, the essential data only will be brought forward in this section, summarised in a form suitable for subsequent discussion.

In recording and plotting the fatigue data in Appendix 3, it was sufficient to express the applied stress system in terms of the induced (actual or nominal) Maximum Shear Stress, S. In the summary tables which follow, the values have also been inserted of f (direct stress due to the applied bending moment) and q (shear stress due to the applied twisting moment), also, of the ratio S/S_0 ; these data are required subsequently for collective comparison and discussion of the results. It appears unnecessary also to tabulate, for all materials, the calculated values of the induced Principal Stress, p_1 and p_2 ; if required, they can be directly estimated from the tabulated data, using the usual formulae quoted in Part I, Section 1 of the paper.

A. SUMMARY OF RESULTS OF TESTS MADE ON SOLID SPECIMENS OF CIRCULAR SECTION

The form and dimensions of the specimens are shown in Fig. 4 ; the diameter of the test section is 0·3 in. On every specimen which failed in an endurance test, measurements were made of the orientation of the trace of the fatigue crack, at and near to the apparent origin of the crack.

The summarised results of the tests are as stated in Table 5.

The critical examination and discussion of the variation of the fatigue limits of each material, as the applied stress system changed from bending to torsional stresses through the five intermediate combinations of these stresses, is reserved for a later section of the paper.

The broad results of the measurements made of the orientation of the fatigue cracks and fracture planes may be summarised as follows. With seven of the steels, the orientation of the cracks, both at their origin and in the early stages of their development, were random and irregular and showed no consistent tendency to coincide with the trace of any identifiable plane associated with the regular change in applied stress conditions. In the case of the 0·9% C. Steel, the traces of the fatigue cracks were in fair general agreement with the trace of Maximum Principal Stress ; to a lesser extent, this was also true of the Ni. Cr. Mo. Steel (75/80 ton), but many cracks in this material were indefinite or irregular in this respect. With the remaining three steels, although the cracks at their origin were apparently random in orientation, there was some indication that they tended to develop in directions across which Maximum Principal Stress was operating. In general, therefore, the measurements made on the fractures of the steels were inconclusive, except for an indication that the direction of propagation of the cracks is assisted in directions across which the Maximum Principal Stress is acting.

TABLE 5

SUMMARY OF RESULTS OF COMBINED STRESS FATIGUE TESTS (SOLID SPECIMENS)

Material	Value of θ deg.	Fatigue Limits, tons per sq. in.				Reliability Index	Remarks on measurements of orientation of traces of fatigue cracks
		Range of Direct Stress due to Bending, f	Range of Shear Stress due to Torsion, q	Range of Maximum Shear Stress, S			
				Value	Ratio S/S_0		
0·1% C. Steel (Normalised) ..	0	±17·4	0	± 8·7	1·00	R	Irregular paths showing no consistent tendency to change with change in applied stress conditions.
	15	±17·0	± 2·3	± 8·8	1·01	R	
	30	±15·7	± $4·5_5$	± 9·1	$1·04_5$	R	
	45	±13·3	± 6·7	± $9·4_5$	$1·08_5$	R	
	60	± $9·5_5$	± 8·3	± $9·5_5$	1·10	R	
	75	± $5·1_5$	± $9·5_5$	± 9·9	1·14	R	
	90	0	± $9·8_5$	± $9·8_5$	1·13	R	
0·4% C. Steel (Normalised) ..	0	±21·5	0	±$10·7_5$	1·00	R	Irregular and ragged at origin. As cracks developed and branched, some measure of agreement with corresponding planes of Max. Principal Stress.
	15	±21·3	± $2·8_5$	±11·0	1·02	R	
	30	±19·2	± $5·5_5$	±11·1	1·03	R	
	45	±16·4	± 8·2	±11·6	1·08	R	
	60	±12·3	±10·6	±$12·2_5$	1·14	R	
	75	± 6·6	±12·2	±12·7	1·18	LR	
	90	0	±13·4	±13·4	1·25	R	
0·4% C. Steel (Spheroidised)	0	±17·8	0	± 8·9	1·00	R	Some specimens fractured transversely in an irregular manner; the traces of the cracks of others were in fair agreement with traces of Max. Principal Stress planes.
	15	±17·8	± 2·4	± 9·2	$1·03_5$	R	
	30	±16·1	± $4·6_5$	± 9·3	$1·04_5$	R	
	45	±13·5	± 6·8	± 9·6	1·08	R	
	60	±10·0	± $8·6_5$	±10·0	1·12	R	
	75	± 5·1	± 9·5	± 9·8	1·10	R	
	90	0	±10·1	±10·1	$1·13_5$	R	
0·9% C. Steel (Pearlitic) ..	0	±22·8	0	±11·4	1·00	R	Traces of cracks consistently in fair general agreement with those of corresponding planes of Max. Principal Stress.
	15	±22·8	± $3·0_5$	±11·8	$1·03_5$	R	
	30	±20·8	± 6·0	±12·0	1·05	R	
	45	±18·2	± 9·1	±12·9	1·13	LR	
	60	±13·8	±11·9	±13·8	1·21	R	
	75	± 7·3	±13·5	±14·0	1·23	R	
	90	0	±15·6	±15·6	1·37	R	
3% Ni. Steel (30/35 ton) ..	0	±22·2	0	±11·1	1·00	R	Traces irregular and inconsistent.
	15	±21·2	± $2·8_5$	±11·0	0·99	R	
	30	±19·7	± 5·7	±11·4	1·03	R	
	45	±17·2	± 8·6	±12·2	1·10	R	
	60	±12·3	±10·7	±12·3	1·11	R	
	75	± $6·7_5$	±12·6	±13·0	1·17	R	
	90	0	±13·3	±13·3	1·20	R	
3/3½% Ni. Steel (45/50 ton) ..	0	±28·8	0	±14·4	1·00	R	Wide variation in directions of traces at origin; some rather uncertain indication that development of cracks appear to follow trace of plane of Max. Principal Stress.
	15	±27·2	$3·6_5$	±14·1	0·98	R	
	30	±25·4	± $7·3_5$	±14·7	1·02	R	
	45	±21·5	±10·8	±$15·2_5$	1·06	LR	
	60	±15·9	±13·8	±15·9	1·10	R	
	75	± 8·6	±16·0	±16·6	1·15	R	
	90	0	±17·3	±17·3	1·20	R	
Cr. Va. Steel (45/50 ton) ..	0	±27·8	0	±13·9	1·00	R	Slopes of traces widely irregular.
	15	±26·6	± 3·6	±$13·7_5$	0·99	R	
	30	±24·6	± 7·1	±$14·2_5$	1·02	LR	
	45	±21·4	±10·7	±15·2	1·09	R	
	60	±15·9	±13·8	±15·9	1·14	LR	
	75	± 8·6	±15·9	±16·5	1·19	R	
	90	0	±16·7	±16·7	1·20	R	

TABLE 5—*continued*

Material	Value of θ deg.	Fatigue Limits, tons per sq. in.				Reliability Index	Remarks on measurements of orientation of traces of fatigue cracks
		Range of Direct Stress due to Bending, f	Range of Shear Stress due to Torsion, q	Range of Maximum Shear Stress, S			
				Value	Ratio S/S_0		
3½% Ni. Cr. Steel (Normal Impact).	0	±35·0	0	±17·5	1·00	R	All cracks showed merely slight and irregular deviations from transverse direction.
	15	±35·0	± 4·7	±18·1	$1·03_5$	R	
	30	±31·8	± 9·2	±18·4	1·05	R	
	45	±26·5	±13·3	±18·8	$1·07_5$	R	
	60	±21·3	±18·4	±21·3	1·22	R	
	75	±11·6	±21·6	±22·4	1·28	R	
	90	0	±22·8	±22·8	$1·30_5$	R	
3½% Ni. Cr. Steel (Low Impact)	0	±33·0	0	±16·5	1·00	R	Traces irregular and incapable of correlation.
	15	±33·4	± 4·5	±17·3	1·05	R	
	30	±30·5	± 8·8	±17·6	1·07	LR	
	45	±25·8	±12·9	±18·3	1·11	R	
	60	±20·4	±17·7	±20·4	$1·23_5$	R	
	75	±10·9	±20·2	±21·0	1·27	R	
	90	0	±21·0	±21·0	1·27	R	
Ni. Cr. Mo. Steel† (60/70 ton)	0	±39·0	0	±19½	1·00	LR	Orientation of cracks, many of which 'branched,' were most irregular and apparently random.
	15	±36·3	± 4·9	±18¾	0·96	U	
	30	±34·6	±10·0	±20	1·03	LR	
	45	±30·4	±15·2	±21½	1·10	LR	
	60	±22·0	±19·1	±22	1·13	LR	
	75	±11·5	±21·4	±22¼	1·15	LR	
	90	0	±21 to ±22¾	±21/±22¾	1·08/1·17	U	
Ni. Cr. Mo. Steel (75/80 ton)	0	±42·8	0	±21·4	1·00	LR	Direction of cracks bore some signs of following traces of Max. Principal Stress plane but many were indefinite or irregular.
	15	±40·5	± 5·4	±21·0	0·98	LR	
	30	±35·4	±10·2	±20·4	$0·95_5$	R	
	45	±32·8	±16·4	±23·2	$1·08_5$	R	
	60	±23·0	±19·9	±23·0	1·08	R	
	75	±11·9	±22·2	±23·0	1·08	R	
	90	0	±22·2	±22·2	1·04	R	
Ni. Cr. Steel (95/105 ton) ..	0	±50·0	0	±25·0	1·00	LR	Direction of cracks showed no consistent tendency.
	15	±51·2	± 6·9	±26·5	1·06	R	
	30	±47·6	±13·7	±27·5	1·10	R	
	45	±39·4	±19·6	±27·8	1·11	U	
	60	±27·8	±24·1	±27·8	1·11	U	
	75	±14·6	±27·1	±28·1	1·13	R	
	90	0	±29·3	±29·3	$1·17_5$	R	
'Silal' Cast Iron	0	±15·6	0	± 7·8	1·00	R*	Every specimen fractured completely; the fracture face being a close approach to a plane, in very good agreement with the plane of Max. Principal Stress.
	15	±15·3	$\pm 2·0_5$	± 7·9	$1·01_5$	R	
	30	±13·6	± 3·9	$\pm 7·8_5$	$1·00_5$	R	
	45	±12·6	± 6·3	± 8·9	1·14	R	
	60	± 9·9	± 8·6	± 9·9	1·27	R	
	75	± 5·8	±10·8	±11·2	$1·43_5$	R	
	90	0	±14·2	±14·2	1·82	R*	
'Nicrosilal' Cast Iron ..	0	±16·4	0	± 8·2	1·00	R	Fractures more ragged than those of "Silal" but traces of cracks near origin in consistent good agreement with those of planes of Max. Principal Stress.
	15	±15·8	± 2·1	± 8·2	1·00	LR	
	30	±14·9	± 4·3	± 8·6	1·05	R	
	45	±12·4	± 6·2	± 8·8	$1·07_5$	R	
	60	±11·0	± 9·5	±11·0	1·34	R	
	75	$\pm 5·9_5$	±11·1	±11·5	1·40	R	
	90	0	±13·7	±13·7	1·67	R	

Notes.—* Having rejected a single specimen only, in each case, as inconsistent.

† Owing to exceptional scatter, little reliance can be placed on the accuracy of these values.

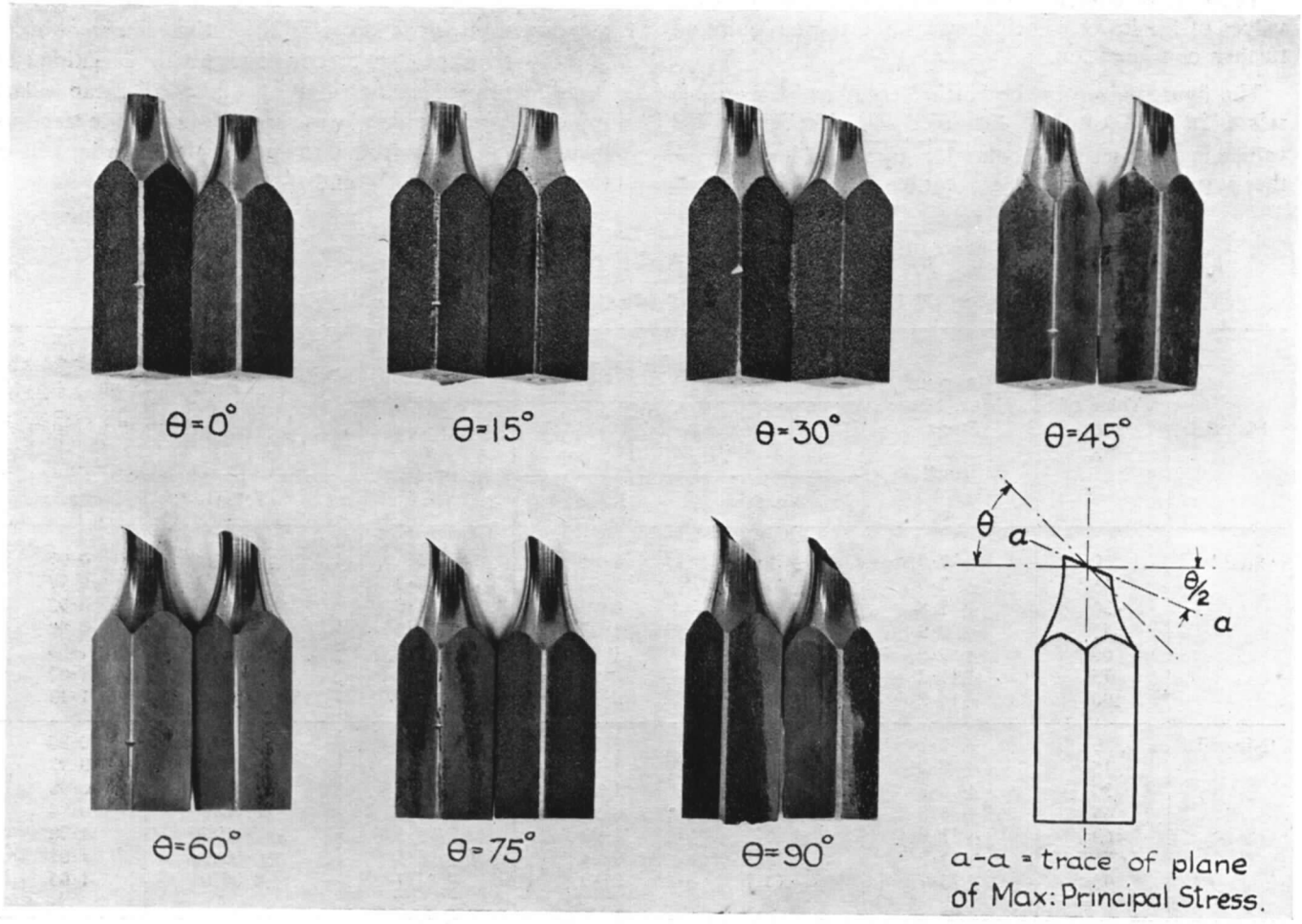

FIG. 14. Typical Fractured Specimens of ' Silal ' Cast Iron.

Note :—θ = Angle of Setting of Testing Machine : $\tan\theta = \dfrac{\text{Twisting Moment}}{\text{Bending Moment}}$

With ' Silal ' cast iron, however, a very definite result emerged. Every fatigued specimen fractured completely, the face of the fracture having an essentially brittle appearance. Moreover, every fracture face was a very close approach to a single plane, whose orientation agreed very closely indeed (see the readings given in Appendix 3) with the plane of Maximum Principal Stress for every applied stress system. This regular correspondence is also brought out by the photographs which have been assembled in Fig. 14. The fracture surfaces of ' Nicrosilal ' were more ragged than those of ' Silal ' ; nevertheless, the average values of their slopes show good general agreement with the corresponding plane of Maximum Principal Stress. Both cast irons are therefore sharply distinct from all the steels in that the fracture planes of the former agree very closely throughout with one identical set of planes, determined by the stress or strain conditions, as these conditions change from reversed plane bending to reversed shear through the five intermediate stress combinations. In view of this constancy of fracture plane, it is worth while examining the magnitude of the ranges of principal stresses and principal strains at the fatigue limits of the two cast materials.

The values of the ranges of the two principal stresses, p_1 and p_2, are directly calculable from the values of f and q, or of S, as tabulated in Table 5. The value of the range of maximum principal strain is $\pm(p_1 + \sigma p_2)/E$ as, at any instant, p_1 and p_2 are of opposite sign. The values of E (Young's Modulus) have been determined experimentally as 7,810 t/in.^{2} and 8,750 t/in.^{2} for Silal and Nicrosilal respectively. The value of 0·284 will be assumed for σ (Poisson's ratio) ; it represents a value for steels which was most carefully determined by Smith and Cox[15] and is also an average of the considerable range of values for cast irons which are reported in the literature.

The calculated values, at the fatigue limits, of the ranges of the two principal stresses and of the maximum principal strain are given in Table 6.

There is, of course, no approach to constancy in the values of the lower principal stress and these require no further consideration.

The figures given in the ' ratio ' columns of the table relate, in each case, to the arithmetical mean of the values in the preceding column : these are inserted for the purpose of approximate comparison.

In regard to ' Silal ', the values of the ranges of maximum principal stress at the fatigue limits show a fairly good approach to constancy, with deviations of $\pm 5\%$ from the value of the arithmetical mean. The principal strain values, however, show a definite trend to increase as θ varies from 0 to 90 deg., the deviations from the mean being -8% and $+13\%$.

TABLE 6

RANGES OF PRINCIPAL STRESS AND STRAIN : ' SILAL ' AND ' NICROSILAL '

Material	Value of θ deg.	Range of Max. Shear Stress, S t/in²	Ranges of Principal Stresses, t/in²			Ranges of Maximum Principal Strain $\frac{1}{E}(p_1 + \sigma p_2)$	
			p_1 (tension)		p_2 (compression)		
			Value	Ratio		Value	Ratio
' Silal '	0	± 7·8	±15·6	1·05	0	±0·00200	0·97
	15	± 7·9	±15·5	1·04	± 0·3	±0·00200	0·97
	30	± $7·8_5$	±$14·6_5$	0·98	± $1·0_5$	±0·00191	0·92
	45	± 8·9	±15·2	1·02	± 2·6	±0·00204	0·99
	60	± 9·9	±$14·8_5$	1·00	± $4·9_5$	±0·00208	1·00
	75	±11·2	±14·1	0·95	± 8·3	±0·00211	1·02
	90	±14·2	±14·2	0·95	±14·2	±0·00233	1·13
'Nicrosilal'	0	± 8·2	±16·4	1·07	0	±0·00187	0·98
	15	± 8·2	±16·1	1·05	± 0·3	±0·00185	0·97
	30	± 8·6	±$16·0_5$	1·04	± $1·1_5$	±0·00187	0·98
	45	± 8·8	±15·0	0·97	± 2·6	±0·00180	0·94
	60	±11·0	±16·5	1·07	± 5·5	±0·00206	1·08
	75	±11·5	±14·5	0·94	± 8·5	±0·00193	1·01
	90	±13·7	±13·7	0·89	±13·7	±0·00201	1·05

TABLE 7

SUMMARY OF RESULTS OF COMBINED STRESS FATIGUE TESTS (HOLLOW SPECIMENS)

Material	Value of θ, deg.	Fatigue Limits, t/in²				Reliability Index
		Range of Direct Stress due to Bending, f	Range of Shear Stress due to Torsion, q	Range of Maximum Shear Stress, S		
				Value	Ratio S/S_0	
0·1% C. Steel (Normalised)	0	±17·5	0	± $8·7_5$	1·00	R
	15	±16·8	± $2·2_5$	± 8·7	$0·99_5$	R
	30	±$15·7_5$	± $4·5_5$	± 9·1	1·04	R
	45	±13·2	± 6·6	± $9·3_5$	1·07	R
	60	± 9·1	± 7·9	± 9·1	1·04	R
	75	± $4·7_5$	± $8·8_5$	± $9·1_5$	$1·04_5$	R
	90	0	± $9·1_5$	± $9·1_5$	$1·04_5$	R
3½% Ni. Cr. Steel (Normal Impact)	0	±33·6	0	±16·8	1·00	R
	15	±32·4	± $4·3_5$	±16·8	1·00	R
	30	±29·5	± 8·5	±17·0	1·01	R
	45	±26·5	±$13·2_5$	±$18·7_5$	$1·11_5$	R
	60	±19·3	±16·7	±19·3	1·15	R
	75	±$10·6_5$	±19·9	±20·6	$1·22_5$	R
	90	0	±20·5	±20·5	1·22	R

With ' Nicrosilal ', the trend of the maximum principal stress values is to diminish as θ increases, the deviations from the mean being from + 7 to − 11%. The maximum principal strain values, however, although showing a slight trend to increase with θ, indicate a fairly good approach to constancy, the extreme variations from the mean being − 6 and + 8%.

Taken in conjunction with the identity of the fracture planes with those of maximum principal stress or strain, the combined stress results thus indicate that the fatigue failure of ' Silal ' may have been largely influenced by maximum principal stress and the fatigue failure of ' Nicrosilal ' by maximum principal strain. In the absence of experiments in which the effect of the third principal stress could be studied, this is as far as the present experiments warrant speculation as to the determining stress condition.

B. SUMMARY OF RESULTS OF TESTS MADE ON HOLLOW SPECIMENS OF CIRCULAR SECTION

The form and dimensions of the test specimens are shown in Fig. 6, the external and bore diameters were 0·4 in. and 0·32 in., respectively. Two ductile steels were tested, the 0·1% C. Steel (Normalised) and the 3½% Ni. Cr. Steel (Normal Impact) ; the former material exhibits a definite drop of stress at the static tensile yield point, the latter does not.

The summarised results of the tests are as stated in Table 7.

The examination and discussion of the variation of the fatigue limits of each material, as the applied stress system changes from bending to torsional stresses through the five intermediate combinations of these stresses, is reserved for a later section of the paper.

The effect on the fatigue limit, under each stressing condition, of the substitution of the hollow for the solid section is brought out by a comparison of the following key data drawn from Tables 5 and 7 :—

Material	*Value of θ deg.*	*Fatigue Limits in terms of S* — *Solid Specimens (a)*	*Hollow Specimens (b)*	*Ratio b/a*
0·1% C. Steel (Normalised)	0	± 8·7	± $8·7_5$	1·00
	15	± 8·8	± 8·7	0·99
	30	± 9·1	± 9·1	1·00
	45	± $9·4_5$	± $9·3_5$	0·99
	60	± $9·5_5$	± 9·1	0·95
	75	± 9·9	± $9·1_5$	0·92
	90	± $9·8_5$	± $9·1_5$	0·93
3½% Ni. Cr. Steel (Normal Impact)	0	±17·5	±16·8	0·96
	15	±18·1	±16·8	0·93
	30	±18·4	±17·0	0·92
	45	±18·8	±$18·7_5$	$0·99_5$
	60	±21·3	±19·3	0·91
	75	±22·4	±20·6	0·92
	90	±22·8	±20·5	0·90

Considering only, for the present, the end points, i.e. reversed plane bending stresses (θ = 0 deg.) and reversed torsional stresses (θ = 90 deg.), we observe confirmation of former general experience, mentioned earlier in the paper, that the substitution of a hollow for a solid cylindrical test section usually results in a reduction of the fatigue limit, of a negligible or small amount under bending stresses and a larger amount under torsional stresses. With the mild steel, the reductions are zero and 7%, respectively : with the harder steel, the reduction is 4% in reversed bending and 10% in reversed torsion. The corresponding fatigue limits for the same two materials, but determined in a Wohler machine and the Stromeyer alternating torsion machine, are given in Table 4 and all the results obtained are assembled in Table 8 for comparison :—

TABLE 8

FATIGUE LIMITS OBTAINED WITH SOLID AND HOLLOW SPECIMENS USING THREE TYPES OF TESTING MACHINE

Material	Tensile Strength t/in²	Fatigue Limits, t/in²							
		Cycles of Reversed Flexural Stress				Cycles of Reversed Shear Stress			
		Combined Stress Machine (plane bending)		Wohler Machine (Rotating Bar)		Combined Stress Machine		Stromeyer Machine	
		Solid (a)	Hollow (b)	Solid (c)	Hollow (d)	Solid (e)	Hollow (f)	Solid (g)	Hollow (h)
0·1% C. Steel (Normalised)	27·9	±17·4	±17·5	±17·0	±16·5	± $9·8_5$	± $9·1_5$	± 9·6	± 8·7
		b/a = 1·00		d/c = 0·97		f/e = 0·93		h/g = 0·91	
3½% Ni. Cr. Steel (Normal Impact)	58·0	±35·0	±33·6	±33·7	±33·4	±22·8	±20·5	±22·6	±21·5
		b/a = 0·96		d/c = 0·99		f/e = 0·90		h/g = 0·95	

The main conclusion of the experiments—the effect of form of the specimen on the fatigue limit—is clearly brought out irrespective of the machine used. The reason for this effect—the modifications in the conditions of stress and strain caused by super-elastic straining within the safe range of stress—has been sufficiently discussed earlier (Part I, Section 3) in the paper.

C. SUMMARY OF RESULTS OF TESTS MADE ON SOLID SPECIMENS CONTAINING A CIRCUMFERENTIAL 55 DEG. SHARP VEE NOTCH

The form and dimensions of the specimens used are shown in Fig. 6. The depth of the notch is 0·02 in. The diameter of the specimen at the bottom of the notch is 0·3 in., equal to the diameter of the solid circular specimens used in the main series of tests. A comparison of the results of the two series of tests should thus give directly the decrease in fatigue resistance due to the presence of the notch, as such. The nominal fatigue ranges summarised below are calculated, in the ordinary way, on the diameter at the root of the notch and take no account of the stress concentration due to the presence of the notch.

The experiments were made on seven steels selected from the twelve steels used in the main investigation.

The specimens were most carefully machined to produce the nearest practicable approach to a sharp vee notch ; in fact, of course, the bottom of the profile of each notch, examined under high magnification, was blunted. As recorded in Part I, Appendix 3 (where the results are fully reported), measurements of the apparent 'root radius' showed that these varied slightly from material to material ; also, but to a lesser extent, from specimen to specimen of a material, but that these differences did not appear to affect the fatigue resistance appreciably or consistently.

The results of the tests are summarised in Table 9 : for purposes of comparison, the corresponding fatigue limits obtained with solid specimens have been inserted to indicate the reduction in strength due to the presence of the discontinuity.

Inspection of the results given in the last column of Table 9—the percentage reduction in fatigue strength caused by the presence of the Vee groove—suggests that the materials are affected by widely varying amounts. But these variations cannot be ascribed directly to varying sensitivities in fatigue resistance of these materials in the presence of one strictly common form of stress concentration for, as recorded in Part I, Appendix 3, the average value of root radius of the notch varied from material to material. It is, therefore, necessary to use existing theory as far as that is available to eliminate or reduce the effect of the 'shape difference' and thus, to place, on a more satisfactory basis, the comparison of the fatigue resistances of the materials.

No exact analytical solution of the problem of the theoretical stress concentration due to the presence of a small Vee-shaped circumferential groove subjected to bending or torsion appears yet to have been published. Employing the soap-bubble analogy, Griffith[16] determined, experimentally, the stress concentration factors of circular shafts, containing Vee grooves having contained angles of 60, 90 and 120 deg., subjected to torsion. His experiments were confined to values of from $\frac{1}{2}$ to 9 of the ratio d/r, where d is the depth of the groove and r is the root radius of the groove. In the present experiments, however, d has a constant value of 0·02 in. and r varies from 0·0002 to 0·0015 in., thus giving a range of from 13·3 to 100 for values of d/r so that the results of Griffith's work are not directly applicable, and a rather wide extrapolation from his results would be necessary to provide a basis for comparison. More recently, stress concentration factors have been determined experimentally, using photoelastic and other methods, for the hyperbolic and circular form of notch, but again, the recorded values of d/r fall below those used in the present experiments.

Inglis[17] made an exact analytical treatment of a small elliptical hole in a plate subjected to tensile loading and showed that the stress concentration factor—the ratio of the stress at the bottom of the notch to the nominal stress in the plate—was $(1 + 2\sqrt{(d/r)})$. The case of a small semi-elliptical groove in a circular shaft subjected to bending stress has not been solved analytically but, from a consideration of the above analysis by Inglis, the stress concentration factor of $(1 + 2\sqrt{(d/r)})$ is probably applicable, with small error, also to such a groove. For the same small elliptical groove in a circular shaft under torsion, the stress concentration factor is $(1 + \sqrt{(d/r)})$: this is an exact theoretical result from Inglis' analysis. Griffiths' results on the torsion of shafts containing a Vee groove, using three values of included angle of groove, show that the stress concentration factor diminishes as the angle of the notch increases. Hence, writing the two formulae relating to the elliptical groove in the form, stress concentration factor equals $(1 + K\sqrt{(d/r)})$, values of K rather less than unity may be appropriate for the present Vee groove. Moreover, the effect of the limited diameter of the test piece at the bottom of the notch has a similar effect—this is known from photo-elastic measurements—and, again, the form $(1 + K\sqrt{(d/r)})$, where K is less than unity, is usually a good approximation. For the case of torsion, it appears possible that the value of K, for the present 55 deg. Vee groove 0·02 in. deep on a diameter of 0·3 in. may be as low as 0·6, but for direct or bending stress the defect below 2 is probably much less in proportion.

For the present purpose of approximate correction of the experimental results for variations in value of d/r, the following values of stress concentration factors, therefore, will be assumed :—

(a) for bending :— $1 + 1{\cdot}7\sqrt{(d/r)}$

(b) for torsion :— $1 + 0{\cdot}6\sqrt{(d/r)}$

These corrections can only be made to the two cases of reversed plane bending stresses ($\theta = 0$ deg.) and reversed torsional stresses ($\theta = 90$ deg.) : the factors are not applicable to the intermediate cases of combinations of these stresses.

TABLE 9

SUMMARY OF RESULTS OF COMBINED STRESS FATIGUE TESTS ON NOTCHED SPECIMENS ; ALSO COMPARISON WITH SOLID SPECIMENS

Note.—All nominal stresses are calculated on root diameter, ignoring stress concentration due to presence of notch.

Material	Value of θ deg.	Notched Specimens, Fatigue Limits					Solid Specimens		Relative Strength of Notched Specimen A/B per cent. (Uncorrected)
		Nominal Range of Direct Stress due to Bending, f t/in²	Nominal Range of Shear Stress due to Torsion, q t/in²	Nominal Maximum Shear Stress, S, t/in²		Reliability Index	Fatigue Limit in terms of Maximum Shear Stress, S. t/in² (B)	Reliability Index	
				Value (A)	Ratio S/S_0				
0·4% C. Steel (Normalised)	0	±11·6	0	± 5·8	1·00	R	±10·7₅	R	54
	15	±11·6	± 1·6	± 6·0	1·03	R	±11·0	R	55
	30	±10·7	± 3·1	± 6·2	1·07	R	±11·1	R	56
	45	± 9·5	± 4·7	± 6·7	1·16	R	±11·6	R	58
	60	± 7·7	± 6·7	± 7·7	1·33	R	±12·2₅	R	63
	75	± 4·7	± 8·8	± 9·1	1·57	R	±12·7	LR	72
	90	0	±11·4	±11·4	1·97	R	±13·4	R	85
3% Ni. Steel (30/35 ton)	0	±13·6	0	± 6·8	1·00	R	±11·1	R	61
	15	±13·5	± 1·8	± 7·0	1·03	R	±11·0	R	64
	30	±12·6	± 3·7	± 7·3	1·07	R	±11·4	R	64
	45	±10·9	± 5·4	± 7·7	1·13	R	±12·2	R	63
	60	± 8·0	± 6·9	± 8·0	1·18	R	±12·3	R	65
	75	± 4·6	± 8·5	± 8·8	1·29	R	±13·0	R	68
	90	0	± 9·8	± 9·8	1·44	R	±13·3	R	74
3/3½% Ni. Steel (45/50 ton)	0	±19·6	0	± 9·8	1·00	R	±14·4	R	68
	15	±18·5	± 2·5	± 9·6	0·98	LR	±14·1	R	68
	30	±17·1	± 5·0	± 9·9	1·01	R	±14·7	R	67
	45	±13·8	± 6·9	± 9·8	1·00	R	±15·2	LR	65
	60	±11·2	± 9·7	±11·2	1·14	R	±15·9	R	70
	75	± 6·0	±11·1	±11·5	1·17	R	±16·6	R	69
	90	0	±11·9	±11·9	1·21	R	±17·3	R	69
Cr. Va. Steel (45/50 ton)	0	±14·0	0	± 7·0	1·00	R	±13·9	R	50
	15	±13·5	± 1·8	± 7·0	1·00	LR	±13·7₅	R	51
	30	±13·5	± 3·9	± 7·8	1·11	LR	±14·2₅	LR	55
	45	±11·1	± 5·6	± 7·9	1·13	R	±15·2	R	52
	60	± 8·9	± 7·7	± 8·9	1·27	R	±15·9	LR	56
	75	± 5·1	± 9·5	± 9·8	1·40	LR	±16·5	R	59
	90	0	±10·4	±10·4	1·49	R	±16·7	R	62
3½% Ni. Cr. Steel (Normal Impact).	0	±17·4	0	± 8·7	1·00	R	±17·5	R	50
	15	±18·9	± 2·5	± 9·8	1·13	R	±18·1	R	54
	30	±17·0	± 4·9	± 9·8	1·13	R	±18·4	R	53
	45	±14·7	± 7·4	±10·4	1·20	R	±18·8	R	55
	60	±10·9	± 9·4	±10·9	1·25	R	±21·3	R	51
	75	± 6·5	±12·1	±12·5	1·44	R	±22·4	R	56
	90	0	±15·3	±15·3	1·76	R	±22·8	R	67
3½% Ni. Cr. Steel (Low Impact).	0	±16·0	0	± 8·0	1·00	R	±16·5	R	48
	15	±15·4	± 2·1	± 8·0	1·00	R	±17·3	R	46
	30	±14·7	± 4·3	± 8·5	1·06	R	±17·6	LR	48
	45	±13·0	± 6·5	± 9·2	1·15	R	±18·3	R	50
	60	±10·5/11·5	± 9·1/10·0	±10·5/11·5	1·31/1·44	LR	±20·4	R	51/56
	75	± 5·4/5·8	±10·0/10·7	±10·4/11·1	1·30/1·39	LR	±21·0	R	50/53
	90	0	±11·8	±11·8	1·47	R	±21·0	R	56
Ni. Cr. Mo. Steel (75/80 ton)	0	±17·6	0	± 8·8	1·00	R	±21·4	LR	41
	15	±17·2	± 2·3	± 8·9	1·01	R	±21·0	LR	42
	30	±16·4	± 4·8	± 9·5	1·08	R	±20·4	R	47
	45	±15·5	± 7·8	±11·0	1·25	R	±23·2	R	47
	60	±11·0	± 9·5	±11·0	1·25	R	±23·0	R	48
	75	± 6·7	±12·5	±12·9	1·47	R	±23·0	R	56
	90	0	±15·6	±15·6	1·77	R	±22·2	R	70

The values estimated on these bases are included in Table 10. In that table, the materials have been arranged in order of ascending tensile strength. The fourth column of the table states the average measured value of r, the root radius, in each series of tests.

Estimated Stress Concentration Factor, K_t. In the 5th and 6th columns of the table, the much greater effect of the stress concentration for bending stresses as compared with torsional stresses, is clearly shown, also the increase in stress concentration factor with the sharpness of the notch. The estimated value of K_t, under bending stresses, varies from 18 ($r = 0{\cdot}0002$ in.) to 7·2 ($r = 0{\cdot}0015$ in.) and, for torsional stresses, from 7·0 ($r = 0{\cdot}0002$ in.) to 3·8 ($r = 0{\cdot}0009$ in.).

Fatigue Strength Reduction Factor, K_f. This factor relates solely to the ratio of the experimental results obtained (see Table 9), thus :—

$$K_f = \frac{\text{Fatigue strength of solid specimens}}{\text{Fatigue strength of grooved specimens}}.$$

Comparison of K_t and K_f. This is shown by the values of the ratio K_t/K_f given in column (A) of Table 10 for the seven materials both in bending and torsion. In all cases, the estimated Stress Concentration Factor, corrected for variations of d/r, is considerably greater than the experimentally determined Fatigue Strength Reduction Factor. For bending stresses, the ratio value falls steadily, if irregularly, with increase in tensile strength of the material; the same general trend is observed for torsional stressing, although the results are more irregular.

In Column (B), the ratio K_t(bending)/K_t(torsion) shows the ratio of the estimated values of the Stress Concentration Factors (corrected for root radius) for each material. Column (C) shows the equivalent ratio K_f(bending)/K_f(torsion) of the actual fatigue strength values. If the Stress Concentration Factors were independent of the material, the values in columns (B) and (C) should be in agreement; the actual discrepancy between theory and experiment is brought out by the values of the ratio (B)/(C) given in the following column; these values vary from 2·14 to

TABLE 10

STRESS CONCENTRATION FACTORS, FATIGUE STRENGTH REDUCTION FACTORS AND FATIGUE NOTCH SENSITIVITIES

Material	U.T.S. t/in²	Type of Stressing†	Measured Values of r (In. $\times 10^{-3}$) *	Stress Concentration Factor, K_t		Fatigue Strength Reduction Factor, K_f		Ratios					Fatigue Notch Sensitivity Index, q	
				Bending $1+1{\cdot}7\sqrt{d/r}$	Torsion $1+0{\cdot}6\sqrt{d/r}$	Bending	Torsion	K_t/K_f (A) Bending	K_t/K_f (A) Torsion	K_t (bending)/K_t (torsion) (B)	K_f (bending)/K_f (torsion) (C)	(B)/(C)	Bending	Torsion
3% Ni. Steel ..	34·1	B	0·2	18	—	1·63	—	11·0	—	2·57	1·20	2·14	0·03$_7$	0·06
		T	0·2	—	7	—	1·36	—	5·1					
0·4% C. Steel .. (Normalised)	42·0	B	0·2	18	—	1·85	—	9·7	—	2·57	1·57	1·64	0·05	0·03
		T	0·2	—	7	—	1·18	—	5·9					
3/3½% Ni. Steel ..	46·8	B	0·4	13	—	1·47	—	8·8	—	2·36	1·01	2·34	0·03$_9$	0·10
		T	0·35	—	5·5	—	1·45	—	3·8					
Cr. Va. Steel ..	48·7	B	0·35	13·8	—	1·99	—	6·9	—	2·89	1·24	2·33	0·07$_7$	0·16
		T	0·5	—	4·8	—	1·61	—	3·0					
3½% Ni. Cr. Steel (Normal Impact)	58·0	B	0·8	9·5	—	2·01	—	4·7	—	2·53	1·35	1·87	0·12	0·18
		T	0·95	—	3·75	—	1·49	—	2·5					
3½% Ni. Cr. Steel (Low Impact)	58·1	B	0·85	9·2$_5$	—	2·06	—	4·5	—	2·43	1·16	2·10	0·13	0·28
		T	0·9	—	3·8	—	1·78	—	2·1					
Ni. Cr. Mo. Steel (75/80 ton)	80·5	B	1·5	7·2	—	2·43	—	3·0	—	1·89	1·71	1·11	0·23	0·15
		T	0·9	—	3·8	—	1·42	—	2·7					

Notes.—K_t = Stress Concentration Factor = Ratio of theoretical stress at bottom of notch to nominal stress.

K_f = Fatigue Strength Reduction Factor = $\frac{\text{Fatigue Strength of Solid Specimens}}{\text{Fatigue Strength of Grooved Specimens}}$ (Experimental values from Table 9)

q = Fatigue Notch Sensitivity Index = $\frac{K_f - 1}{K_t - 1}$

* Values recorded in Part I, Appendix 3.

† B denotes tests under reversed plane bending stresses ($\theta = 0$ deg.)
T denotes tests under reversed torsional stresses ($\theta = 90$ deg.)

1·11 in a very irregular manner. The materials clearly respond quite differently to the effects of the presence of the discontinuity of section, a result for which elastic theory makes no provision.

Fatigue Notch Sensitivity Index, q. A factor which is often used to express, for a material, the measure of agreement between theory and experiment of the effect of a discontinuity of section on the fatigue strength of that material. Thus :—

$$q = (K_f - 1)/(K_t - 1)$$

The limiting values of q are (1) zero, when $K_f = 1$, i.e. when the discontinuity produces no reduction in the fatigue strength and (2) unity, where $K_f = K_t$, i.e. when the full theoretical effect of the discontinuity is fulfilled in the fatigue test.

The values of q for each of the seven materials (for reversed bending and reversed torsion) are as stated in the last two columns of Table 10. If these values are plotted against Tensile Strength, the values of q (bending) show a fairly regular trend to increase with Tensile Strength, but this does not apply to values of q (torsion).

The main conclusion derived from these comparisons is the wide discrepancy between the values of stress concentration factor estimated from theory and the very much smaller effects actually established by fatigue tests on small test pieces. These discrepancies are very much greater than can possibly be accounted for by an error in the assumptions made in assessing the theoretical effects : discrepancies in that direction have been met by numerous investigators using forms of discontinuity whose theoretical effects could be predicted with considerable accuracy by exact analysis or by photo-elastic or other experimental methods.

But the possible influence of size effect must not be overlooked. As pointed out in the introduction to this paper, although present knowledge indicates that, whereas, with smooth specimens free from discontinuities of section, the fatigue strength is either unaffected appreciably or decreased only slightly with increase in size of specimen, a much greater decrease in fatigue strength with increase in size in specimens containing a discontinuity of section can be regarded as established. Unfortunately, really reliable experiments have hitherto been mainly confined to diameters not exceeding 2 or 3 in. (within which, of course, the present specimens fall). Whether a really close approach to, or coincidence with, the theoretical stress concentration factor would be realised with much larger sizes remains to be determined, also, whether all engineering steels would behave similarly in this respect.

Returning to the actual experimental results, as summarised in Table 9, the figures given in the last column of that table—the percentage relative fatigue strength of the notched specimens to that of the unnotched—or, alternatively, their reciprocals—the Fatigue Strength Reduction Factor (K_f)—are of special interest for design purposes. If either of these relative strengths are plotted to some base, say θ deg., some of the curves obtained show considerable irregularity of form for the values of θ intermediate between 0 and 90 deg. These irregularities may be real : on the other hand, they may result from cumulative errors due to the combination of uncorrected fatigue strengths of the plain and notched specimens. Discussion will, therefore, be deferred until, in the next section of the paper, all the combined fatigue stress results are examined in the attempt to find any relation that may exist between the values of the fatigue strengths as the applied stressing system changes from reversed bending to reversed torsion through the intermediate combinations of stress : the required 'smoothing-out' of irregular data will then be made.

V. EXAMINATION AND DISCUSSION OF THE RESULTS OF THE COMBINED STRESS FATIGUE EXPERIMENTS

A. RELATION BETWEEN THE COMPONENTS OF BENDING AND SHEARING STRESSES

The results will be examined to ascertain if any general relationship exists between the various values of the fatigue limits as the applied stress system changes from reversed bending stresses to reversed torsional stresses through the five intermediate combinations of those stresses.

Although previous study of the deformation and fatigue characteristics of metals, using the methods of mechanical testing, the metallurgical microscope and precision X-rays, has led to some understanding of the mechanism of fatigue in relation to the crystalline structure and atomic arrangement of metals, no quantitative theory of fatigue exists to provide an established basis of examination of the data now made available.

In two previous papers[9, 11] on combined fatigue stresses, two purely empirical relations were derived. One of these fitted the results obtained with each of two ductile steels : the other, of a slightly different form, represented satisfactorily the data obtained from tests on four cast irons. The greater number and variety of the present results provide a wider opportunity of determining whether either or both of these empirical relations are of general or special application ; if so, they will have a useful application as a basis of engineering design. The manner in which these two empirical relations were derived may be recalled.

Various hypotheses have been advanced, and much experimental work has been carried out, in the endeavour to ascertain the static stress or strain conditions which govern the failure of primitive elasticity under combined stresses ; given the value of the static elastic limit under simple direct, bending or shearing stress, the problem being to determine the stress conditions at elastic failure under any applied complex system of loading. The basic assumptions made in such theories regarding the properties of the material under investigation are those generally adopted in the classical theory of elasticity :— an initial state of perfect elasticity, homogeneity, continuity of structure, isotropy and obedience to Hooke's law. These hypotheses were never advanced to account for fatigue failure ; nevertheless, as representing the only quantitative theories relating to materials, their possible application was explored. Each of the theories examined covered the general case of three-dimensional stress, whereas the fatigue experiments, in which combinations of cyclic bending and torsional stresses only are used, are two-dimensional only, the third principal stress always being zero. Therefore, it was, and now is, possible only to compare the fatigue data with the two-dimensional representation of the selected theoretical criteria for static failure of primitive elasticity. To make this comparison, expressions were derived, as set out below, for the various criteria in terms of Maximum Shear Stress. It was also necessary to assume as legitimate the substitution of a range of stress, $\pm S$, in fact a fatigue limit, for the single stress value, S, to which each theoretical criterion originally referred. To suit the nomenclature employed for fatigue tests made on the present type of testing machine, the symbol S_0 (really $\pm S_0$) denotes the maximum shear stress when $\theta = 0$ deg. (reversed plane bending stresses) ; S_{90} (really $\pm S_{90}$) when $\theta = 90$ deg. ; S (really $\pm S$) at any other value of θ between these limits. The following expressions were obtained :—

1. Maximum Shear Stress Theory :—Failure is determined by a constant value of half the greatest difference of principal stresses. According to this criterion :—

$$S = S_0 = S_{90} \quad .. \quad .. \quad .. \quad .. \quad .. \quad (1)$$

2. Maximum Shear Strain Energy Theory :—Failure occurs at a constant value of the energy of shear strain contained in unit volume of the material, i.e. potential energy stored due to purely elastic strains, excluding the stress due to volumetric stress (three equal and mutually perpendicular direct stresses), or

$$(p_1 - p_2)^2 + (p_2 - p_3)^2 + (p_3 - p_1)^2 = \text{a constant}$$

from which the following relation was derived :—

$$S = 2S_0/\sqrt{(3 + \cos^2\theta)} \quad .. \quad .. \quad .. \quad (2)$$

3. Theory of Constant Energy of Deformation :—Failure occurs at a constant value of the total elastic strain energy contained in unit volume of the material, i.e.

$$\tfrac{1}{2}E\,[p_1^2 + p_2^2 + p_3^2 - 2\sigma\,(p_1p_2 + p_2p_3 + p_3p_1)] = \text{a constant}$$

According to this criterion :—

$$S = \frac{S_0\sqrt{2}}{\sqrt{\{(1 + \sigma) + (1 - \sigma)\cos^2\theta\}}} \quad .. \quad .. \quad (3)$$

where σ is Poisson's ratio.

4. Maximum Principal Strain Theory :—Failure is determined by a limiting value of positive elastic extension, $p_1/E - \sigma p_2/E =$ a constant, where E is Young's Modulus and σ is Poisson's ratio. From this expression, the following relation was derived :—

$$S = \frac{2S_0}{(1 + \sigma) + (1 - \sigma)\cos\theta} \quad .. \quad .. \quad (4)$$

5. Maximum Principal Stress Theory :—Failure is determined by a value of the maximum principal stress, regardless of the values of the other two principal stresses, i.e. $p_1 =$ constant. If this relation holds, then

$$S = 2S_0/(\cos\theta + 1) \quad .. \quad .. \quad .. \quad .. \quad (5)$$

The above five well-known criteria were selected as involving only known quantities, i.e., the three principal stresses and the two elastic constants for the material in the original expressions and Poisson's ratio, θ and S_0 in the derived relations. Thus, the value of S, for any required value of θ, can be written down.

The criteria for elastic failure due to Mohr and Guest were not overlooked.

Mohr's Theory :—Failure is determined by the maximum value of the shearing stress which is itself dependent on the normal stress acting across the plane of shearing stress and also dependent on the material, i.e. if $p_1 > p_3 > p_2$, failure occurs at a value of $\frac{1}{2}(p_1 - p_2)$ which must be a function of $(p_1 + p_3)$ whose form depends on the material.

Guest's Theory :—Failure is determined when the shearing force, together with a small fraction of the volumetric stress, reaches a certain value, or

$$(p_1 - p_2) + \lambda\,(p_1 + p_2) = C,$$

where λ has a value associated with the particular material under test.

Thus, in both of these theories, some unknown property of each material is involved, and no general expression—like those of equations (1) to (5)—can be written down for purposes of direct comparison.

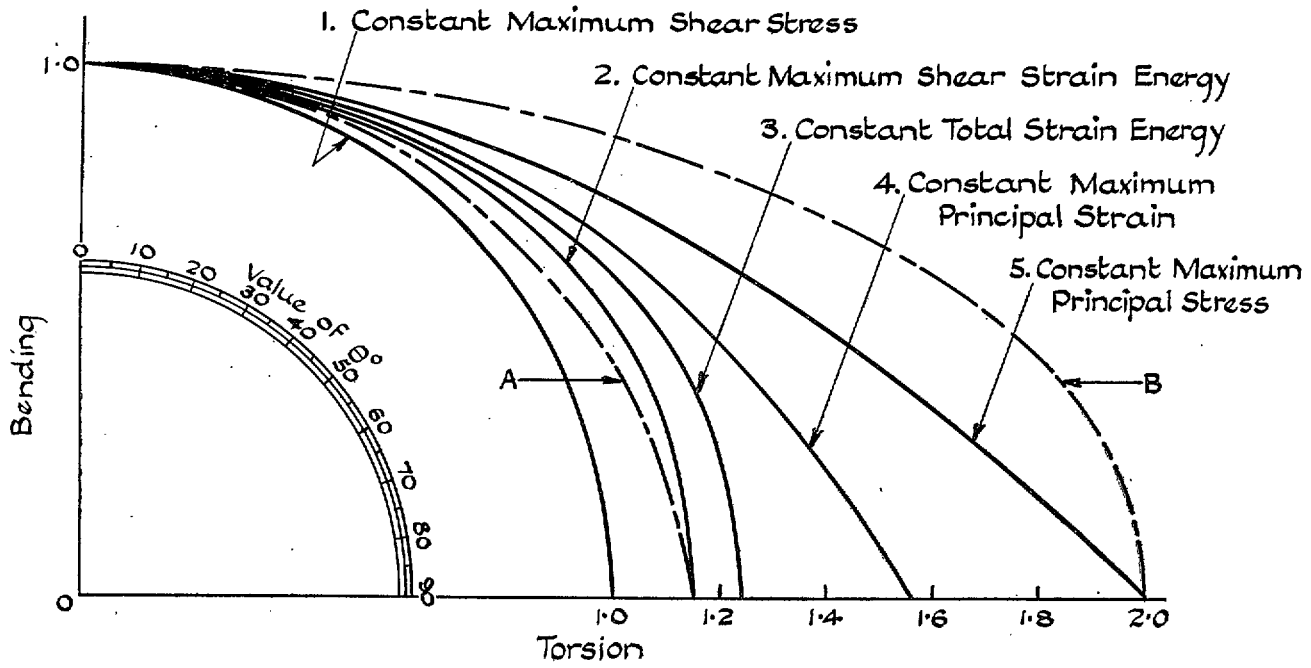

Note:- The radial co-ordinate is the value of the ratio S/S_0
where S = The maximum shear stress value of the applied stress conditions at angle θ°
S_0 = The maximum shear stress value under reversed bending stresses, i.e. when $\theta^\circ = 0$

FIG. 15. Polar Diagram representing 2-dimensional form of various Theories of Static Elastic Failure.

In Fig. 15, equations (1) to (5) have been plotted in the form of polar diagrams of which the polar co-ordinates are θ and S; references will be made later to the dotted curves A and B. For the criteria involving strain—Curves 3 and 4—the value of 0·284 has been taken for Poisson's ratio. Each of the five criteria predicts a fixed value for the ratio S_{90}/S_0, i.e. for the ratio of the elastic limit in static torsion to that in static tension or bending, or, if applicable to fatigue stresses, a constant ratio of the limiting fatigue range under reversed torsional stresses to that under reversed bending stresses. These constant values are irrespective of the material under test and are as follows :—

Criterion of Failure	*Indicated Value of* S_{90}/S_0
Constant Maximum Shear Stress ..	1·0
Constant Maximum Shear Strain Energy	1·154
Constant Total Strain Energy	1·248
Constant Maximum Principal Strain ..	1·558
Constant Maximum Principal Stress ..	2·0

Now the experimental values of these ratios given by the fatigue tests made on solid specimens, as taken from Table 5, are :—

Material	*U.T.S.* t/in.²	*Experimental Value of* S_{90}/S_0
1. 0·1% C. Steel (Normalised)	27·9	1·13
2. 0·4% C. Steel (Normalised)	42·0	1·25
3. 0·4% C. Steel (Spheroidised)	30·9	$1\cdot13_5$
4. 0·9% C. Steel (Pearlitic) ..	54·9	1·37
5. 3% Ni. Steel	34·1	1·20
6. 3/3½% Ni. Steel	46·8	1·20
7. Cr. Va. Steel	48·7	1·20
8. 3½% Ni. Cr. Steel (Normal Impact)	58·0	$1\cdot30_5$
9. 3½% Ni. Cr. Steel (Low Impact)	58·1	1·27
10. Ni. Cr. Mo. Steel (60/70 ton)	64·8	1·08/1·17
11. Ni. Cr. Mo. Steel (75/80 ton)	80·5	1·04
12. Ni. Cr. Steel (95/105 ton) ..	108	$1\cdot17_5$
13. 'Silal' Cast Iron	14·9	1·82
14. 'Nicrosilal' Cast Iron ..	14·2	1·67

The values of S_{90}/S_0 for the twelve ductile steels thus lie between the limits of 1·04 and $1\cdot30_5$, distributed as follows :—five lie between predicted values of 1·0 (Maximum Shear Stress) and $1\cdot15_4$ (Maximum Shear Strain Energy); four between $1\cdot15_4$ (Maximum Shear Strain Energy) and $1\cdot24_8$ (Total Strain Energy): the remaining three exceed $1\cdot24_8$. No experimental value is coincident with the special value associated with any of these criteria. It will be noticed, incidentally, that the experimental values of S_{90}/S_0 bear no relation to the tensile strengths of the materials.

The two values for cast iron are sharply distinct—being much higher—than the values for the ductile steels. They lie between the critical values of $1\cdot55_8$ and 2·0 for the criteria for Maximum Principal Strain and Maximum Principal Stress, respectively, but are coincident with neither.

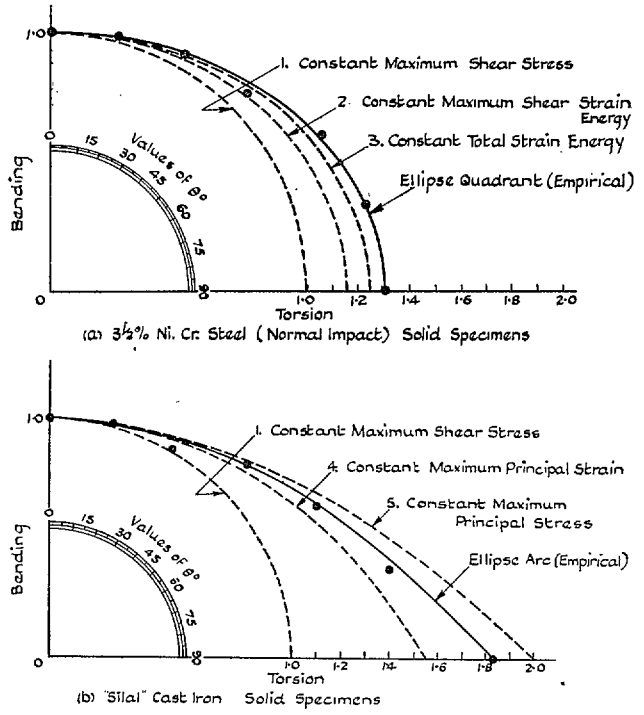

FIG. 16. Experimental Results of a Ductile Steel and a Cast Iron plotted on Polar Diagrams.

Now in the previous publications, the results of two of the ductile steels only were available—the same 0·1% C. Steel and 3½% Ni. Cr. Steel (Normal Impact) as now reported (materials 1 and 8 in above list). Plotted in the form of a polar diagram like Fig. 15 the mild steel results fell very near to the Maximum Shear Strain Energy curve. The data for the Ni. Cr. Steel, plotted as in Fig. 16 (*a*), agreed with none of the three criteria shown and it seemed sound to assume that the apparent agreement of the mild steel data with the Misés-Hencky relation was probably accidental and to look for an empirical relation of a form that would cover both sets of data while permitting variations in the value of the ratio S_{90}/S_0. Allowing for irregularities in the materials under test, some regular form of curve would be anticipated, probably similar to curves 1, 2 and 3 for corresponding values of S_{90}/S_0 between 1·0 and 1·3. Now inspection of equations (1), (2) and (3) shows that curves 1, 2 and 3 are, in fact, ellipse quadrants. Disregarding these particular ellipse quadrants, it is permissible to try the ellipse quadrant which will pass through the two end points, the ratio of the axes being thus decided only by the experimental results. The general expression for this ellipse quadrant, similarly expressed in terms of the polar co-ordinates θ and S, is

$$\frac{1}{S^2} = \frac{1}{c^2} - \left(\frac{1}{c^2} - \frac{1}{d^2}\right) \sin^2 \theta \qquad .. \qquad (6)$$

where

$\pm S$ is Fatigue Limit, in terms of Maximum Shear Stress

$\pm c$ is Minor Axis of Ellipse

= Fatigue Limit under reversed bending stresses $= \pm S_0$

$\pm d$ is Major Axis of Ellipse

= Fatigue Limit under reversed torsional stresses $= \pm S_{90}$

In Fig. 16 (*a*), the full line represents such an ellipse quadrant drawn through the end points : it provides a satisfactory fit to the experimental data.

The polar diagram is convenient to use when making a trial plot of experimental data ; it has, however, little or no value for reference purposes or for use in design. For these purposes, a plot to rectangular axes, having as co-ordinates the components of applied bending and shear stresses, is much more convenient. Converting equation (6) to this form, the following expression is obtained :—

$$f^2/b^2 + q^2/t^2 = 1 \qquad .. \qquad .. \qquad .. \qquad .. \qquad (7)$$

where

$\pm f$ is range of direct stresses due to bending

$\pm q$ is range of shear stresses due to torsion

} at the fatigue limit of the combination.

and

$\pm b$ is fatigue limit (direct stress) under reversed bending stresses only.

$\pm t$ is fatigue limit (shear stress) under reversed torsional stresses only.

The ellipse quadrant of equations (6) and (7) was thus derived as a purely empirical relation. It fitted satisfactorily the data of the two ductile steels and catered for the well-known variation, from steel to steel, of the value of the ratio b/t. It was, therefore, suggested that it might provide a reasonable basis for design, as far as ductile steels are concerned, until such time as the results of the complete investigation were available, when its validity could be more thoroughly examined. It was not suggested as applicable to a brittle material like cast iron, of which, at that time, the results of only one material, ' Silal ', were available.

In the subsequent combined fatigue stress investigation[11] made on materials for cast crankshafts, four cast irons were tested ; a Copper-Chromium iron (U.T.S. = 32·3 t/in.²), an Inoculated iron (U.T.S. = 23·3 t/in.²), a Chrome-Molybdenum iron (U.T.S. = 20·8 t/in.²) and a Nickel-Chrome iron (U.T.S. = 18·8 t/in.²). The experimental values of S_{90}/S_0 for the cast irons were, respectively, 1·58, 1·77, 2·02 and 1·68. The complete data, $\theta = 0$, 15, 30, 45, 60, 75 and 90 deg., for these materials, when plotted in polar diagrams similar to Fig. 15, fell on curves of the same geometrical type as curves 4 and 5 of that figure. An empirical formula was, therefore, devised to give, on the polar diagram, curves of that

general shape which would all pass through the point $S_0 = 1$ and also through any desired value of S_{90}/S_0. This formula is provided by the general polar equation for a conic section having the focus as the pole, i.e.

$$r = \frac{r_c(1+e)}{1+e\cos\theta}$$

where e = the eccentricity of the conic. Writing $e = (S_{90}/S_0) - 1$, we obtain

$$\frac{S}{S_0} = \frac{S_{90}}{S_0 + \cos\theta\,(S_{90} - S_0)} \quad .. \quad (8)$$

From the properties of a conic, if $e = 1$, $e > 1$, $e < 1$ we obtain, respectively, a parabola, a hyperbola and an ellipse, corresponding to the cases where S_{90}/S_0 has the value, respectively, of 2, values greater than 2, and values between 1 and 2. It will be seen, by inspection of equation (5), that curve 5 (the two-dimensional trace of the Maximum Principal Stress Theory) of Fig. 15, is, in fact, the parabola given by equation (8). Also, inspection of equation (4) shows that, provided k has values between 0 and 1, curve 4 (and similar curves representing the two-dimensional trace of the Maximum Principal Strain Theory) is also represented by equation (8), although in such cases the curves are arcs of ellipses.

Thus, the purely empirical relation expressed by equation (8), provides the required series of geometrical curves similar in form and including the explicit relations expressed by curves 4 and 5 of Fig. 15, but which can be used for any value of S_{90}/S_0 which is greater than unity ; in the limiting case of $S_{90}/S_0 = 1$, the ellipse arc of equation (8) becomes an ellipse quadrant having equal major and minor axes, i.e., the circular quadrant coinciding with curve 1 (the two-dimensional trace of the Maximum Shear Stress Theory).

In the polar diagram of Fig. 16 (*b*), the experimental fatigue results obtained with ' Silal ' (solid specimens) are plotted. The full curve shown drawn between the end points ($\theta = 0$ and 90 deg.) is an ellipse arc to equation (8). With the exception of the value at $\theta = 30$ deg. (probably subnormal due to irregularities of material or defects in the specimens tested) the empirical curve fits the data satisfactorily.

In regard to the four cast irons previously tested and reported elsewhere, the data for three of the irons plotted extremely closely to ellipse arcs given by equation (8) : with the fourth iron, five of the seven fatigue values fell satisfactorily on an ellipse arc, while two values plotted irregularly. Thus, within the limits of the data available, the empirical relation of equation (8) represented satisfactorily the behaviour under combined fatigue stresses of materials which exhibit brittle characteristics.

Polar diagrams to equation (8), using the ratio S/S_0, are unsuitable for general use. The more convenient form of diagram, on which the shearing and bending components at the fatigue limit are plotted to rectangular axes, is given by the following expression, derived from equation (8) by direct substitution :—

$$\frac{q^2}{t^2} + \frac{f^2}{b^2}\left(\frac{b}{t} - 1\right) + \frac{f}{b}\left(2 - \frac{b}{t}\right) = 1 \quad .. \quad (9)$$

where

$\pm f$ is range of direct stresses due to bending

$\pm q$ is range of shear stresses due to torsion

} at the fatigue limit of the combination.

and

$\pm b$ is fatigue limit (direct stress) under reversed bending stresses only.

$\pm t$ is fatigue limit (shear stress) under reversed torsional stresses only.

As in every set of data to be plotted, the values of b/t lie between 1 and 2 (corresponding to values of S_{90}/S_0 lying between 2 and 1), the corresponding curves given by equation (9) will all be ellipse arcs and will be referred to as such. The f axis will contain the major axis of the parent ellipse, while the q axis will be parallel to the minor axis of that ellipse ; the origin of the rectangular axes will not, of course, in the general case, be co-incident with the focus of the ellipse.* The complete data of the combined stress tests have been plotted in the form of these f/q diagrams. On each diagram, curves have been added corresponding to the relations given by equations (7) and (9) and passing through the same end point values at $f = 0$ and $q = 0$. Inspection of the equations shows that the ellipse quadrant and the ellipse arc are co-incident when $b/t = 2$ and diverge increasingly as b/t approaches unity value. In regard to this variation of discrimination, dependent, with each material, on the ratio of the fatigue range under reversed bending to that under reversed shearing stresses, a final reference may be made to Fig. 15 to bring out this point on that type of diagram. As the values of S_{90}/S_0 change from 2 to unity, the family of ellipse quadrants change gradually from curve B until they coincide with curve 1 (Constant Maximum Shear Stress), which is a quadrant of a circle. Similarly, the family of ellipse arcs gradually change from the nearest possible approach to curve 5 (Constant Maximum Principal Stress) until they also become co-incident with curve 1. To show the divergence at an intermediate point, the dotted curve A has been drawn through the end points of curve 2 (Constant Maximum Shear Strain Energy) which is itself, as pointed out previously, an ellipse quadrant.

The ellipse quadrant and arc relations were thus derived : they were regarded as empirical, being chosen because these two simple geometrical forms fitted reasonably well those examples of the two apparently

* *Note.*—The focus will remain at the origin if the shearing stress is plotted to twice the scale of the bending stress.

distinct groups of ' ductile ' steels and ' brittle ' cast irons which were then available and, equally important, they could be drawn through any given pair of ' end point ' values. However, in discussing the results given in the first paper[9], Stanfield suggested that the results on the ductile and brittle materials could be reconciled by assuming, with Perry, that the resistance to shear involves an ' internal frictional resistance ' whose value is directly proportional to the normal stress acting across the shear plane. The normal resistance to shear is increased by the frictional resistance, failure occurring when the sum of the two terms reaches a limiting value given by $S + \mu p$, or $\lambda S + \mu p$: the planes of failure would not be principal planes but as determined by a relation of the type $\alpha p_1 - \beta p_2 = \text{constant}$, where p_1 and p_2 are the principal stresses. On this assumption, and by choosing appropriate values of the constants, Stanfield obtained a relation, which is mathematically identical with the present equation (8). Stanfield plotted the combined fatigue stress data then available—the two steels and Silal—and concluded that his relation represented the Silal data satisfactorily but did not fit the data for the ductile steels as closely as the ellipse quadrant. During the same discussion and, later, in a separate paper[18], Guest shows that his criterion for failure of primitive elasticity under static stressing, i.e.

$$(p_1 - p_2) + \lambda (p_1 + p_2) = C$$

can be rewritten to give exactly the expression given in equation (9), by taking the value of λ equal to $(2t/b - 1)$. The second term on the left hand side of Professor Guest's relation represents, as originally defined by its author, a fraction of the volumetric stress and is not, necessarily, associated with the conception of internal friction to which may exist serious objections on physical grounds ; the value of λ is a constant for a given material and varies with different materials.

During the course of preparing this paper, I have also heard with great interest from my former colleague, Mr. H. L. Cox, M.A., of the National Physical Laboratory, that, in the course of a mathematical examination of the effect of internal flaws (which is about to be published), he has found that the relation between the bending and shearing stress components is, again, represented by formula (9).

Thus, the present position in regard to the two curves adopted initially as empirical convenient geometrical forms to fit the early results is that, while no-one has put forward any physical interpretation for the ellipse quadrant, three separate explanations, based on physical grounds, have been advanced, any one of which could form the basis of the ellipse arc. Further experiments of a different nature would be necessary to decide between these possible explanations.

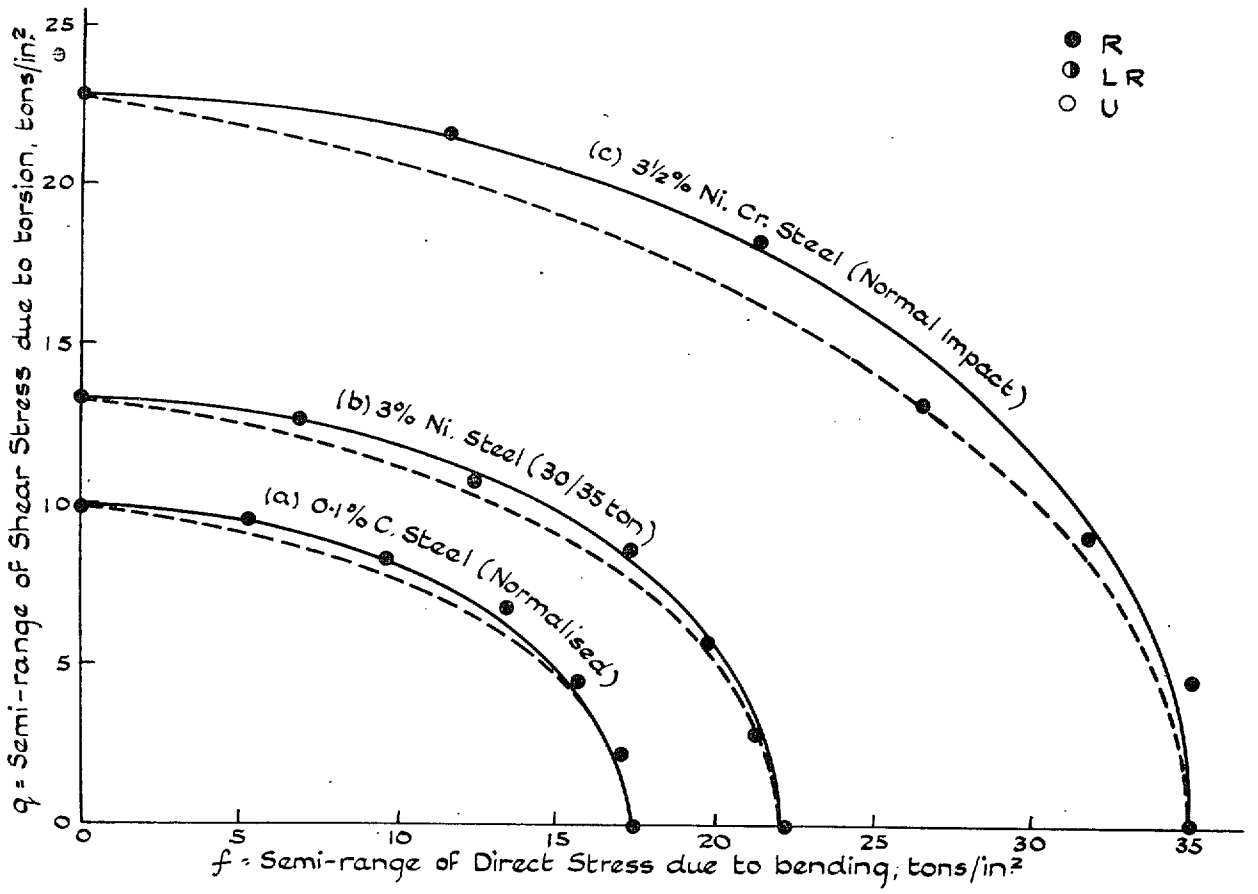

FIG. 17. *f/q* Curves. Experiments on Solid Specimens.

Comparison of Data with the Ellipse Quadrant and the Ellipse Arc

For each of the fourteen materials tested and for each form of specimen used, the limiting ranges of stress have been plotted in the form of an f/q diagram to give Figs. 17 to 24 inclusive. For each material, the appropriate ellipse quadrant and ellipse arc have been drawn, as calculated from equations (7) and (9), from common end points. With one exception only—solid specimens of the Ni. Cr. Steel (95/105 ton), see Fig. 20 (*c*)—the end points chosen are the experimentally-determined values of the fatigue limits for reversed bending and reversed torsional stress, no attempt being made to find a curve giving the best fit to all the seven results of each series of test. In carrying out the actual experiments, these end-point values were determined first, particular care being taken, as far as the uniformity of the material and the use of a reasonable number of specimens permitted, to establish reliable values of these end-points ; the intermediate five values were then obtained. In the only adjustment made, to the Ni. Cr. Steel (95/105 ton), the recorded value of $\pm$ 50·0 t/in.^{2} was definitely classed as 'LR' (see Fig. 44). With some considerable hesitation, the curve has been drawn through the higher value of $b = \pm 52\frac{1}{2}$ t/in.^{2}, in order to make a closer approach to the next two test values, both of which had been classed 'R' as fatigue tests.

Making due allowance in those series of tests in which one or more test points plot irregularly, examination of Figs. 17 to 24 leads to the following assessment of the agreement, or otherwise, of the test data with either of the two curves ; for convenience, the materials have been arranged, in this assessment, in decreasing order of values of b/t as the separation between any corresponding pair of curves depends on the value of that ratio. The actual tensile strengths of the materials are also inserted.

SOLID SPECIMENS

(i) Ni. Cr. Mo. Steel (80·5 t/in.^{2}). Fig. 20 (*b*). $b/t = 1{\cdot}93$. Data are conservatively represented by the ellipse quadrant which is, therefore, the better fit. But the curves are very close to each other and, hence, the ellipse arc could be taken without serious additional quantitative error.

(ii) Ni. Cr. Steel (108 t/in.^{2}). Fig. 20 (*c*). $b/t = 1{\cdot}792$. The two curves, which are in close proximity, jointly cover the data, with the exception of the inconsistent 'b'

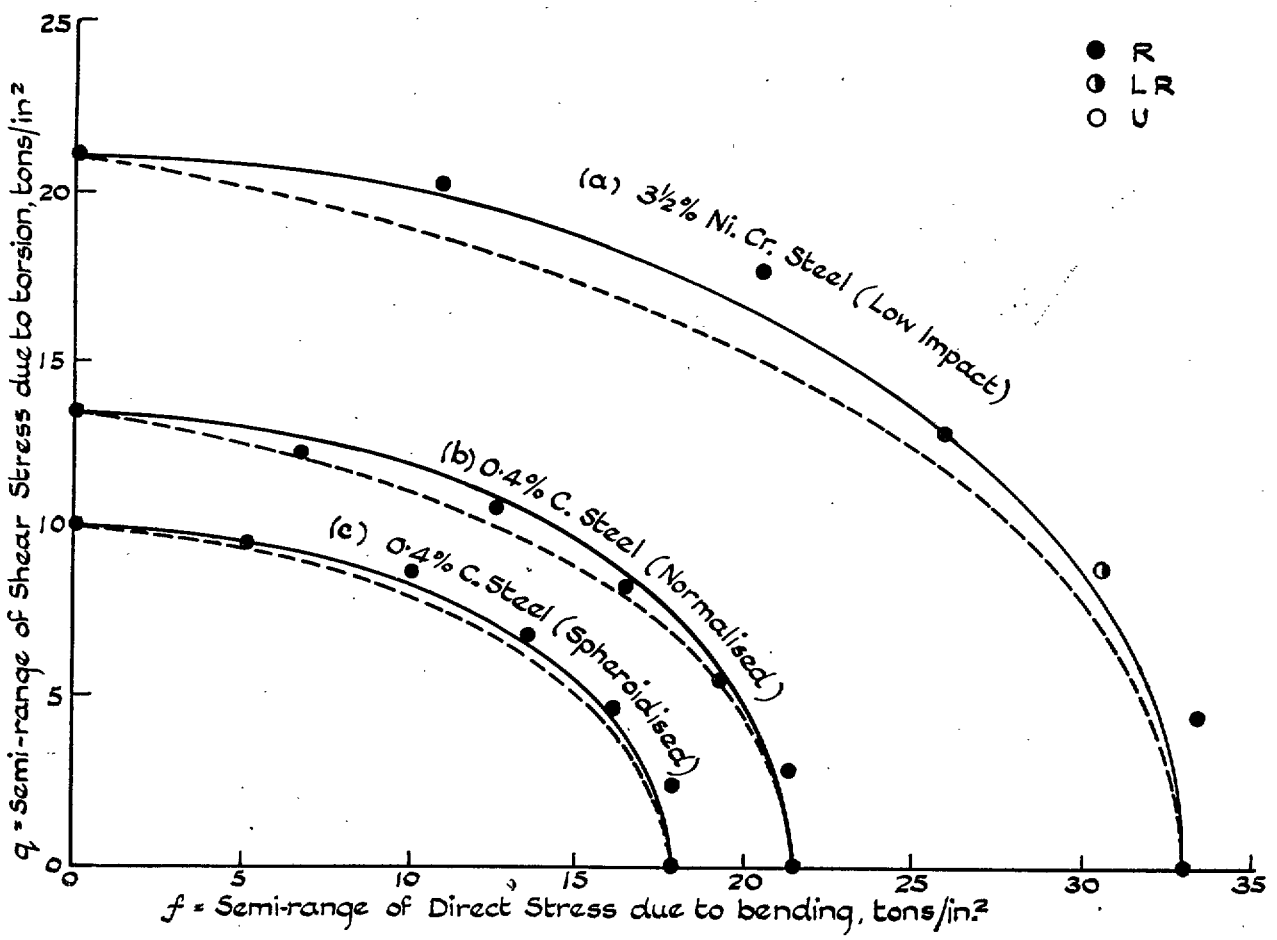

FIG. 18. f/q Curves : Experiments on Solid Specimens.

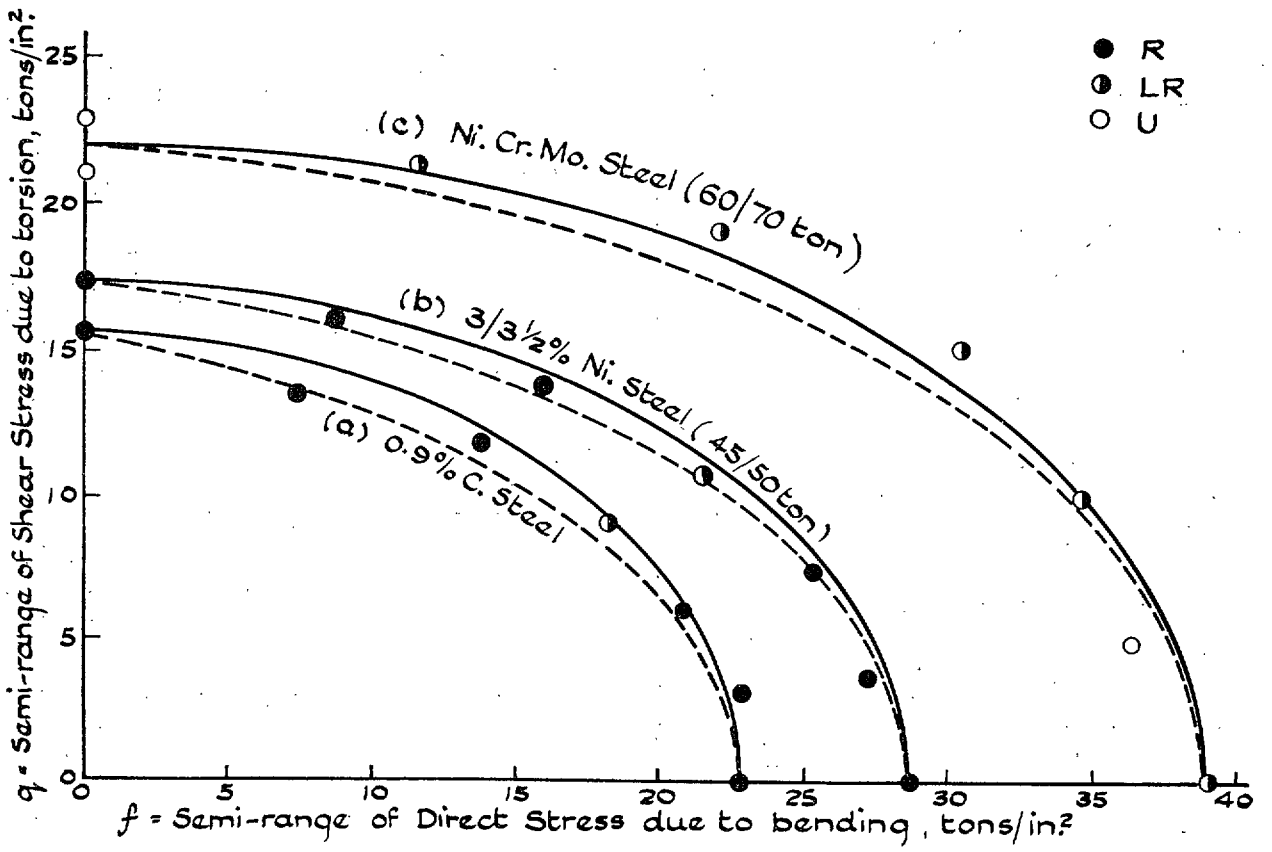

FIG. 19. *f*/*q* Curves : Experiments on Solid Specimens.

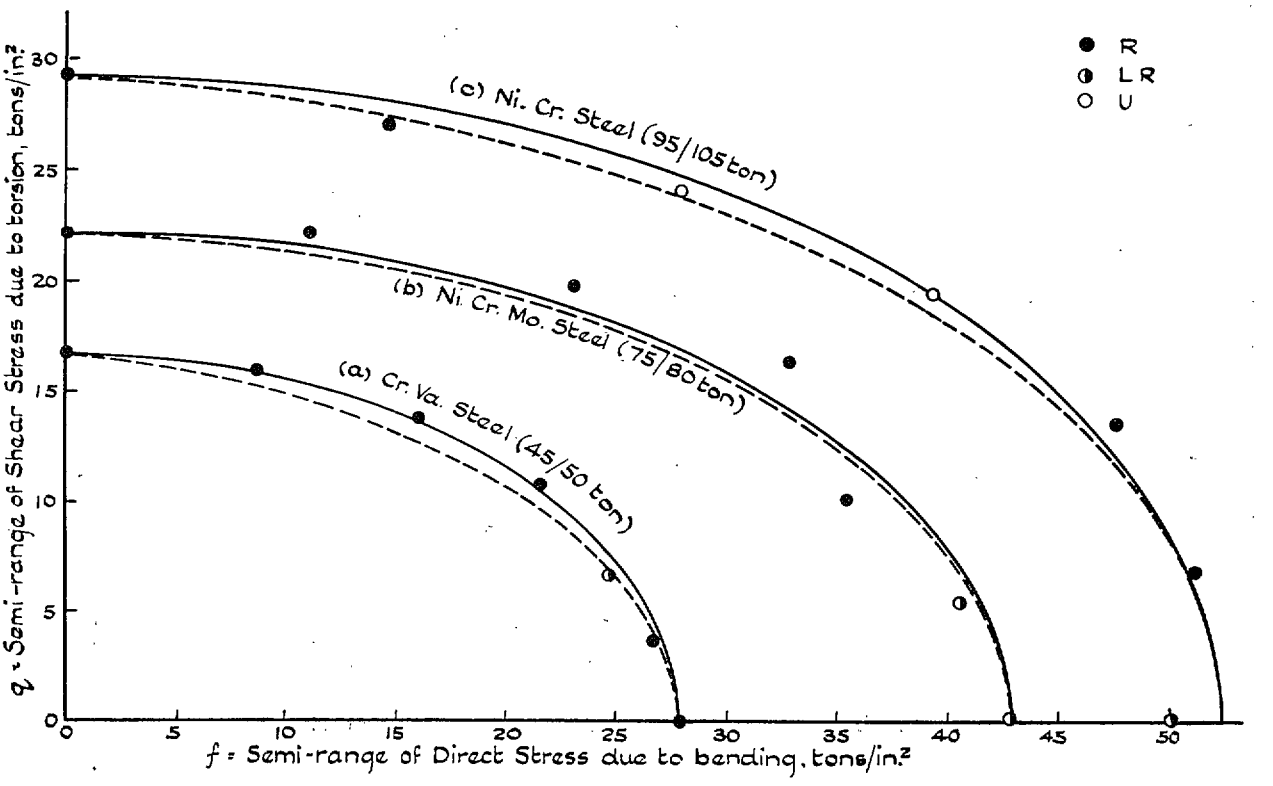

FIG. 20. *f*/*q* Curves : Experiments on Solid Specimens.

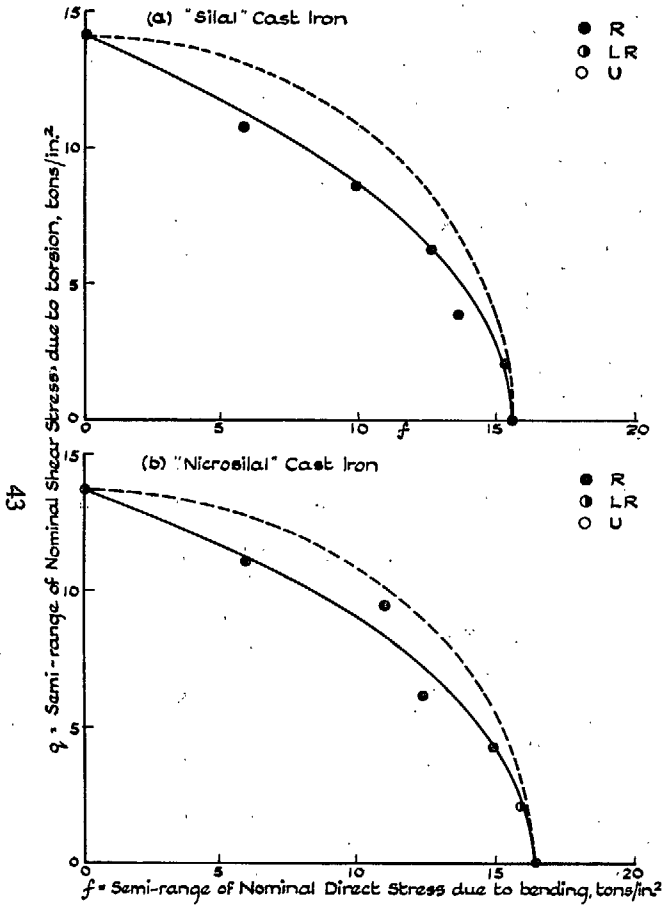

FIG. 21. *f/q* Curves: Experiments on Solid Specimens.

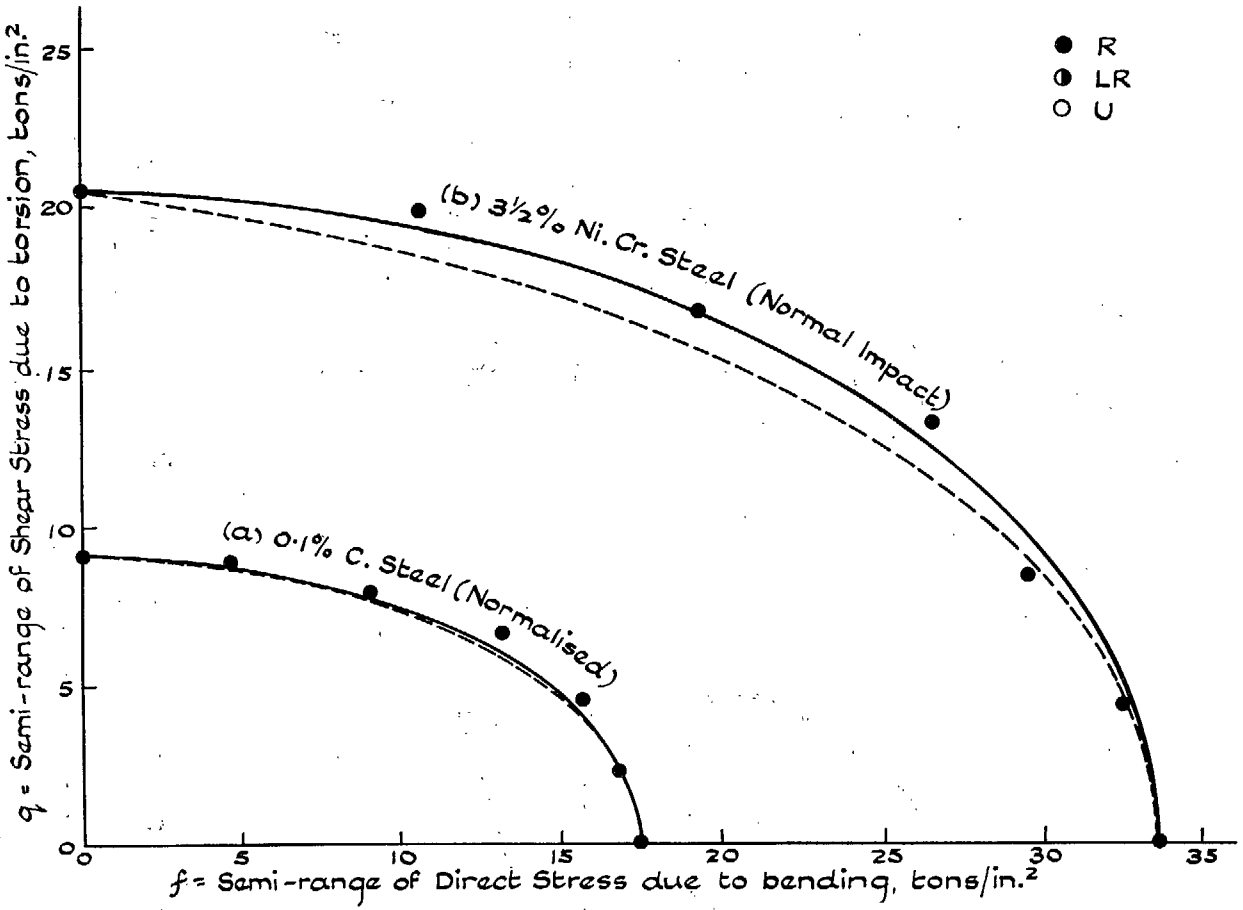

FIG. 22. *f/q* Curves: Experiments on Hollow Specimens.

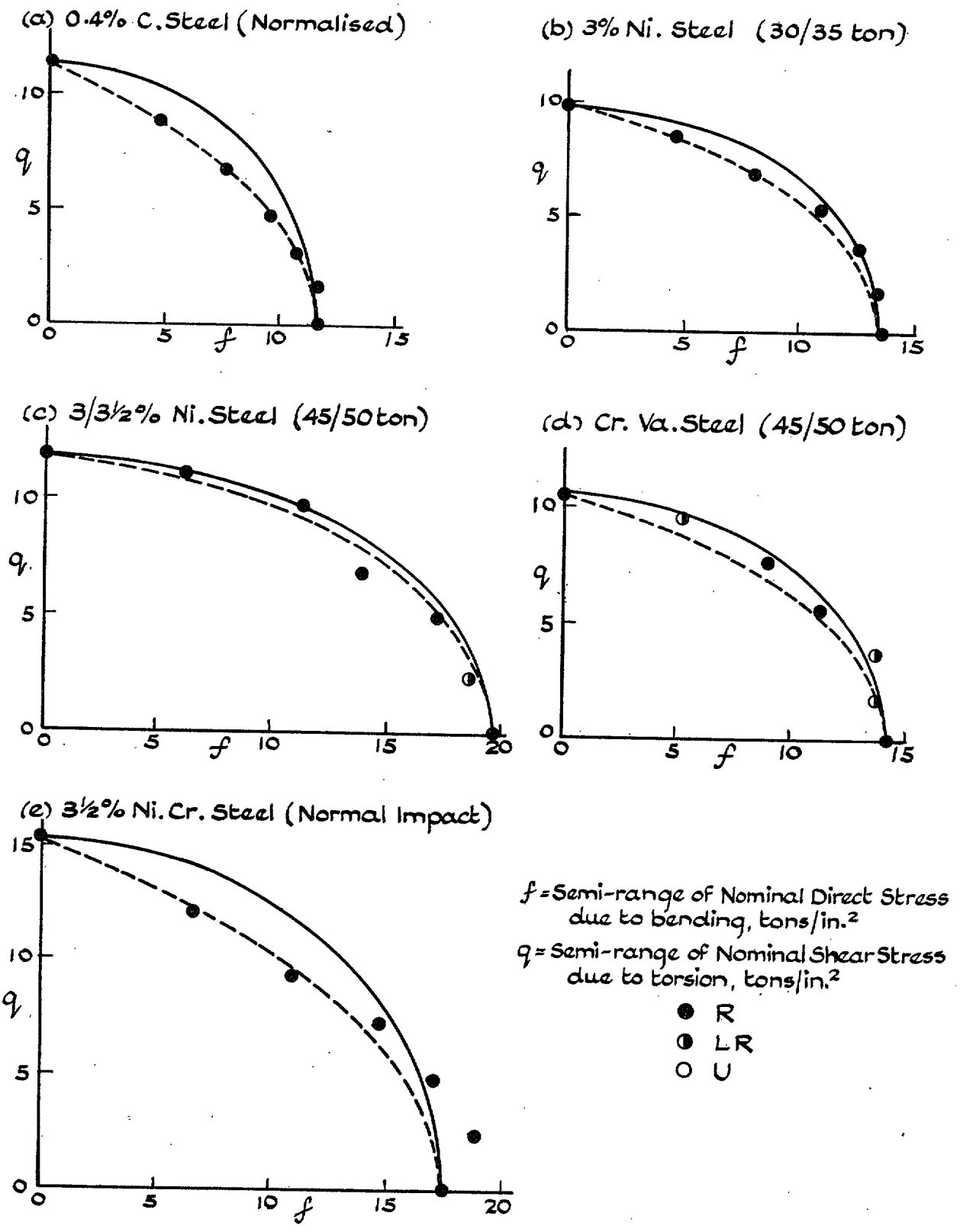

FIG. 23. *f/q* Curves : Experiments on Grooved Specimens.

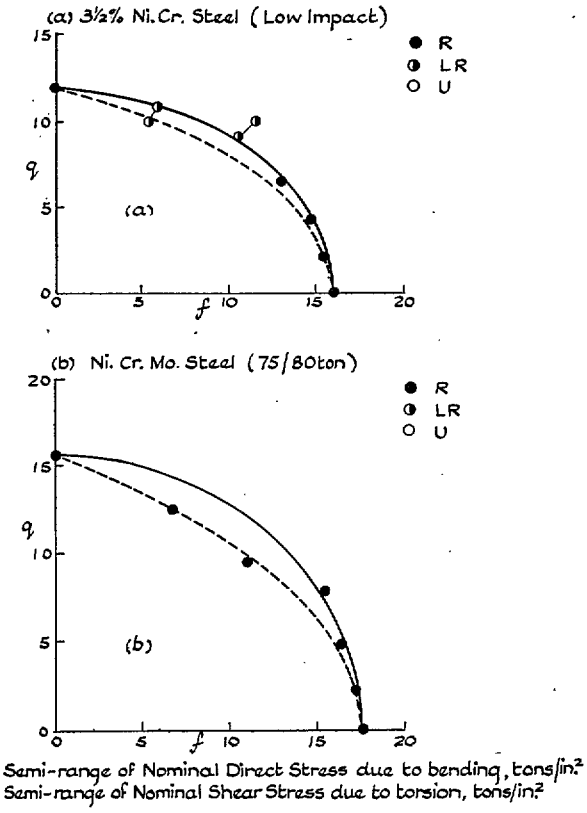

FIG. 24. *f/q* Curves: Experiments on Grooved Specimens.

end-point. Either criterion could be selected; the slight scatter of the test data at this value of b/t renders it impossible to make a critical choice.

(iii) Ni. Cr. Mo. Steel (64·8 t/in.²). Fig. 19 (c). $b/t = 1{\cdot}773$. The ellipse quadrant fits the test data satisfactorily, definitely closer than the ellipse arc.

(iv) 0·1% C. Steel (Normalised) (27·9 t/in.²). Fig. 17 (*a*). $b/t = 1{\cdot}767$. The ellipse quadrant fits the data very closely and definitely closer than the ellipse arc.

(v) 0·4% C. Steel (Spheroidised) (30·9 t/in.²). Fig. 18 (*c*). $b/t = 1{\cdot}762$. The ellipse quadrant fits the data very closely and definitely closer than the arc.

(vi) 3% Ni. Steel (34·1 t/in.²). Fig. 17 (*b*). $b/t = 1{\cdot}669$. The ellipse quadrant is the better fit and is preferred, but no serious error would be involved by using the ellipse arc. The curves are still in close proximity.

(vii) Cr. Va. Steel (48·7 t/in.²). Fig. 20 (*a*). $b/t = 1{\cdot}665$. The ellipse quadrant fits the data very closely.

(viii) 3/3½% Ni. Steel (46·8 t/in.²). Fig. 19 (*b*). $b/t = 1{\cdot}665$. With the exception of one point which falls inside both curves, the data fit the ellipse arc satisfactorily. The two curves are not widely separated.

(ix) 0·4% C. Steel (Normalised) (42·0 t/in.²). Fig. 18 (*b*). $b/t = 1{\cdot}605$. Either curve gives a good fit, a slight preference in favour of the ellipse quadrant.

(x) 3½% Ni. Cr. Steel (Low Impact) (58·1 t/in.²). Fig. 18 (*a*). $b/t = 1{\cdot}571$. The ellipse quadrant fits the data satisfactorily: the ellipse arc is well below every test point.

(xi) 3½% Ni. Cr. Steel (Normal Impact) (58 t/in.²). Fig. 17 (*c*). $b/t = 1{\cdot}535$. With the exception of one point, the ellipse quadrant provides a very close fit to the data: the ellipse arc is definitely conservative.

(xii) 0·9% C. Steel (Pearlitic) (54·9 t/in.²). Fig. 19 (*a*). $b/t = 1{\cdot}462$. If one test point were excluded, the ellipse quadrant would provide the preferred fit. This irregular test point falls on the ellipse arc and, as one other point is mid-way between the two curves the estimate must be that either curve can be accepted; the average value given by the ellipse arc would be less than the average of the test data.

(xiii) 'Nicrosilal' Cast Iron (14·2 t/in.²). Fig. 21 (*b*). $b/t = 1{\cdot}197$.

(xiv) 'Silal' Cast Iron (14·9 t/in.²). Fig. 21 (*a*). $b/t = 1{\cdot}099$. With both cast irons, and in spite of some scatter of the test data, the ellipse arc provides a good fit to the results: the ellipse quadrant is not applicable. The ellipse arc relation was, of course, specially developed to cover cast materials, to which, from the earliest tests, it was found that the quadrant was not applicable. However, it is now brought out that Nicrosilal behaves similarly in this respect to the five cast irons previously tested.

HOLLOW SPECIMENS

(i) 0·1% C. Steel (Normalised) (27·9 t/in.²). Fig. 22 (*a*). $b/t = 1{\cdot}913$. The two curves are nearly coincident. The data fit the ellipse quadrant very closely and slightly better than the ellipse arc.

(ii) 3½% Ni. Cr. Steel (Normal Impact) (58 t/in.²). Fig. 22 (*b*). $b/t = 1{\cdot}639$. The ellipse quadrant provides a good fit to the data, the ellipse arc clearly does not.

GROOVED SPECIMENS

(i) 3/3½% Ni. Steel (46·8 t/in.²). Fig. 23 (*c*). $b/t = 1{\cdot}647$. The data are too irregular to provide a critical assessment, but the ellipse arc fits the data satisfactorily and slightly better than the ellipse quadrant; no serious error, however, would be involved if the latter were used.

(ii) 3% Ni. Steel (34·1 t/in.²). Fig. 23 (*b*). $b/t = 1{\cdot}388$. In spite of a small irregularity of the test data, the ellipse arc provides a good fit to the data, and is preferred to the ellipse quadrant.

(iii) $3\frac{1}{2}\%$ Ni. Cr. Steel (Low Impact) (58·1 t/in.²). Fig. 24 (*a*). $b/t = 1{\cdot}356$. Two of the fatigue limits are not clearly defined and render assessment difficult, but the ellipse quadrant definitely provides a good fit to the whole series : the ellipse arc does not.

(iv) Cr. Va. Steel (48·7 t/in.²). Fig. 23 (*d*). $b/t = 1{\cdot}346$. The data are a little irregular. The ellipse quadrant provides a good fit, better than does the ellipse arc.

(v) Ni. Cr. Mo. Steel (80·5 t/in.²). Fig. 24 (*b*). $b/t = 1{\cdot}128$. The ellipse arc definitely provides a good fit : the ellipse quadrant does not. The two curves are critically separated.

(vi) $3\frac{1}{2}\%$ Ni. Cr. Steel (Normal Impact) (58 t/in.²). Fig. 23 (*e*). $b/t = 1{\cdot}137$. One test result is well removed from both curves. If this is neglected the ellipse arc definitely provides the better fit to the series as a whole.

(vii) 0·4% C. Steel (Normalised) (27·9 t/in.²). Fig. 23 (*a*). $b/t = 1{\cdot}018$. The ellipse arc fits all the data very closely indeed.

Discussion

Inspection of Figs. 17 to 24 inclusive, shows that, neglecting an occasional abnormal result, the test data for all materials—twelve steels and two cast irons—in each of the three forms of specimen used—solid, hollow or grooved—fall very satisfactorily within or in close proximity to the area enclosed by the appropriate quadrant and ellipse arc. This is quite an important first conclusion for design purposes.

Analysing more closely the foregoing assessment in order to ascertain the relative capabilities of the ellipse quadrant or ellipse arc, the results fall broadly into three groups :—(*a*) solid and hollow specimens of the steels, (*b*) the cast irons, and (*c*) grooved specimens of the steels. A real difficulty arises owing to the effect of the varying b/t ratio, whose value determines the separation between a pair of curves.

Steels (Solid and Hollow Specimens). With solid specimens, eleven of the twelve series of data fit the quadrant curve satisfactorily ; one series is closely represented by the ellipse arc, but small error would be involved in using the quadrant.

In seven of those eleven cases, the quadrant is definitely a better fit than the arc ; in three of the seven, the arc is sufficiently removed from the quadrant so that appreciable error would be involved if the arc were adopted, while in four of the seven, the curves are so close to each other that little error would be involved. In the remaining four cases, slight irregularities of the plotted data leave it open as to whether the quadrant or the arc is the better fit, but small differences only are involved in taking either criterion. In one case (0·9% C. Steel) the data are distributed between the curves.

With the two sets of data from hollow specimens, the ellipse quadrant provides a very close fit for each, but in one, the curves are practically coincident.

Cast Iron (Solid Specimens). For both materials, the test data are represented very satisfactorily by the ellipse arc : the ellipse quadrant does not apply.

Steel (Grooved Specimens). Of the seven series of tests, the test data of four conform definitely to the ellipse arc. Of the remainder, in one case, the quadrant gives a better fit to the data, but two scattered points render that conclusion open to doubt. In the remaining two series, either criterion could be adopted : the test points are distributed irregularly about the area enclosed by the two curves, one pair of which are, in fact, very close to each other. The general conclusion emerges that, within limits of error which, in most cases, are not greater than those limits within which a fatigue range can usually be determined experimentally, the ellipse arc represents the f/q relation of the present seven series of tests on steel grooved specimens.

General Conclusions as to the form of the f/q Relation

Twelve ductile steels, covering a range of tensile strengths from 27·9 to 108 t/in.² and six cast irons having tensile strengths from 14·2 to 32·3 t/in.² have now been tested in fatigue under reversed plane bending stresses, reversed torsional stresses and five combinations of these stresses. All have been tested using solid cylindrical specimens free from discontinuities of section : two of the steels have also been tested using hollow cylindrical specimens similarly free from discontinuities of section ; seven of the steels have also been tested using solid cylindrical specimens having a discontinuity of section in the form of a circumferential sharp 55 deg. Vee groove.

In all cases, after allowing for normal irregularities of some of the individual results, the bending and shearing stress components, $\pm f$ and $\pm q$, at the fatigue limits plot satisfactorily on regular f/q curves between the test limits of $\pm f = 0$ (reversed shear stresses) and $\pm q = 0$ (reversed bending stresses).

The form of this f/q relation has been examined and it is found that

(i) The f/q relation for data relating to solid and hollow specimens of all ductile steels is represented satisfactorily by the ellipse quadrant given by the expression

$$f^2/b^2 + q^2/t^2 = 1 \quad .. \quad .. \quad .. \quad (7)$$

No physical meaning can, at present, be attached to this relation which must be regarded as empirical.

(ii) The f/q relation for data relating to solid specimens of the cast irons, also for the grooved specimens (nominal stresses calculated at the bottom of the groove and

neglecting the stress concentration due to the presence of the groove) of the seven steels, is represented satisfactorily by the ellipse arc given by the expression

$$\frac{q^2}{t^2}+\frac{f^2}{b^2}\left(\frac{b}{t}-1\right)+\frac{f}{b}\left(2-\frac{b}{t}\right)=1 \quad .. \qquad (9)$$

This expression, originally derived empirically, in the manner described, may have any one of the three physical bases propounded by Guest, Stanfield or Cox.

Thus, given the experimentally-determined values of b and t—the fatigue limits under simple reversed bending and reversed torsional stresses, respectively—the fatigue limits under combinations of those stresses can be calculated from the appropriate formula.

A further simplification of the combined stress problem would have resulted if it could have been reported that all the results of the present investigation conformed to the ellipse arc relation but such a conclusion is not justified. It has been pointed out, however, that the quantitative difference between results calculated from equations (7) and (9) depends on the actual value of the ratio b/t: this difference is zero when b/t is 2 and increases as the value of b/t diminishes from 2 to 1. All the results relating to solid and hollow specimens of the ductile steels lie between the limits of 1·93 and 1·462.

Estimates of resistance to combined fatigue stresses based on the ellipse arc relation are always more conservative than those based on the ellipse quadrant; if designers are prepared to accept a single rule at the expense of lower accuracy in some cases, the former relation could be adopted as a simple design rule throughout the whole scope of the present investigation. In the absence of experimental evidence, it cannot be assumed that the f/q relation found to apply to specimens containing a sharp Vee groove is, necessarily, of general application to other forms of discontinuity of section.

In the present investigation, it has been possible only to study the effect of variation of two of the three principal stresses; the value of the third principal stress was zero throughout. The data afforded may be helpful in the design of a variety of engineering components subjected to such a two-dimensional stressing system. Nevertheless, the study of the effect of the third principal stress is of fundamental importance and a necessity in arriving at a more complete understanding of the stress conditions governing failure under combined fatigue stresses. Such a study of fatigue failure under a three-dimensional stress system well deserves the attention of future investigators.

B. RESULTS OF TESTS ON GROOVED SPECIMENS: FATIGUE STRENGTH REDUCTION FACTORS

In Part I, Section 4, the results of the tests on the grooved specimens were summarised. An estimation was also made and discussed of the theoretical stress concentration factors involved in the cases of reversed bending stresses and reversed torsional stresses only; the discrepancy between the theoretical and actual reductions of fatigue strength due to the presence of the notch for these two special cases was pointed out and discussed.

In regard to the evaluation, for the complete series of seven values associated with each of the seven materials tested, of the Fatigue Strength Reduction Factor, K_f, where

$$K_f=\frac{\text{Fatigue strength of solid specimens}}{\text{Fatigue strength of grooved specimens}}$$

as each of the two quantities concerned in this ratio are subject to independent irregularities—experimental, material, etc.—the evaluation of K_f was deferred until the data could be corrected, using whatever f/q relation was found to be the best fit to each series of data: cumulative errors due to the combination of uncorrected fatigue strengths of the plain and notched specimens thus being eliminated or reduced.

In order to be able to compare the relative sensitivities of the seven steels to the presence of the groove on a single diagram, the corrections have been made to the test data expressed in terms of Maximum Shear Stress. Taking the experimentally determined end points ($\theta = 0$ and 90 deg.), the corrected intermediate five points ($\theta = 15$, 30, 45, 60, 75 deg.) have been calculated to the ellipse quadrant (equation 6) for the solid specimens and the ellipse arc (equation 8) for the grooved specimens. The uncorrected and corrected values of the fatigue limits and the corresponding values of K_f, are as stated in Table 11; as before, the fatigue strengths of the grooved specimens refer to nominal stresses calculated on root diameter without taking into account the stress concentration due to the presence of the notch; the materials are listed in the order of ascending tensile strengths.

The corrected values of the Fatigue Strength Reduction Factor, given in the last column of Table 11, have been plotted on the convenient base of values of θ, to give the interesting curves of Fig. 25. The most significant feature brought out is the wide variation between the effect of the groove on the fatigue resistance of the various materials. Under reversed bending stresses ($\theta = 0$ deg.), the value of the reduction factor, K_f, increases with increasing tensile strength, with a single exception, the 3/3½% Ni. Steel, but, under reversed torsional stresses ($\theta = 90$ deg.), the values of K_f bear no relation to the tensile strengths. With five materials, the value of K_f diminishes continuously from $\theta = 0$ deg. to $\theta = 90$ deg., but with the 3/3½% Ni. Steel and, to a lesser extent, with the 3½% Ni. Cr. Steel (low impact), the maximum value of K_f does not occur at $\theta = 0$ deg. The effect of embrittling the 3½% Ni. Cr. Steel produces a slight drop in

TABLE 11

CORRECTED VALUES OF FATIGUE STRENGTH REDUCTION FACTOR, K_f

Material	Value of θ deg.	Fatigue Limit in Terms of Maximum Shear Stress, S. t/in²				Fatigue Strength Reduction Factor, Kf	
		Solid Specimens		Grooved Specimens			
		Experimental A	After Correction (to Ellipse Quadrant) B	Experimental C	After Correction (to Ellipse Arc) D	Experimental A/C	Corrected B/D
3% Ni. Steel (U.T.S. = 34·1 t/in²)	0	±11·1	±11·1	± 6·8	± 6·8	1·63	1·63
	15	±11·0	±11·2	± 7·0	± 6·9	1·57	$1·62_5$
	30	±11·4	$±11·5_5$	± 7·3	± 7·1	1·56	1·62
	45	±12·2	$±12·0_5$	± 7·7	± 7·5	$1·58_5$	$1·60_5$
	60	±12·3	$±12·6_5$	± 8·0	± 8·0	1·54	1·58
	75	±13·0	±13·1	± 8·8	± 8·8	$1·47_5$	1·49
	90	±13·3	±13·3	± 9·8	± 9·8	$1·35_5$	$1·35_5$
0·4% C. Steel (Normalised) (U.T.S. = 42·0 t/in²)	0	$±10·7_5$	$±10·7_5$	± 5·8	± 5·8	$1·85_5$	$1·85_5$
	15	±11·0	±10·9	± 6·0	± 5·9	$1·83_5$	$1·84_5$
	30	±11·1	$±11·2_5$	± 6·2	± 6·2	1·79	$1·81_5$
	45	±11·6	$±11·8_5$	± 6·7	± 6·8	1·73	$1·74_5$
	60	$±12·2_5$	$±12·5_5$	± 7·7	± 7·7	1·59	1·63
	75	±12·7	$±13·1_5$	± 9·1	± 9·1	$1·39_5$	$1·44_5$
	90	±13·4	±13·4	±11·4	±11·4	$1·17_5$	$1·17_5$
3/3½% Ni. Steel (U.T.S. = 46·8 t/in²)	0	±14·4	±14·4	± 9·8	± 9·8	1·47	1·47
	15	±14·1	$±14·5_5$	± 9·6	± $9·8_5$	1·47	$1·47_5$
	30	±14·7	±15·0	± 9·9	$±10·0_5$	$1·48_5$	1·49
	45	±15·2	$±15·6_5$	± 9·8	±10·3	1·55	1·52
	60	±15·9	±16·4	±11·2	$±10·7_5$	1·42	$1·52_5$
	75	±16·6	$±17·0_5$	±11·5	$±11·2_5$	$1·44_5$	$1·51_5$
	90	±17·3	±17·3	±11·9	±11·9	$1·45_5$	$1·45_5$
Cr. Va. Steel (U.T.S. = 48·7 t/in²)	0	±13·9	±13·9	± 7·0	± 7·0	$1·98_5$	$1·98_5$
	15	$±13·7_5$	$±14·0_5$	± 7·0	± 7·1	$1·96_5$	1·98
	30	$±14·2_5$	$±14·4_5$	± 7·8	± 7·3	$1·82_5$	1·98
	45	±15·2	±15·1	± 7·9	$± 7·7_5$	$1·92_5$	1·95
	60	±15·9	$±15·8_5$	± 8·9	$± 8·3_5$	$1·78_5$	1·90
	75	±16·5	$±16·4_5$	± 9·8	$± 9·2_5$	$1·68_5$	1·80
	90	±16·7	±16·7	±10·4	±10·4	$1·60_5$	$1·60_5$
3½% Ni. Cr. Steel (Normal Impact) (U.T.S. = 58·0 t/in²)	0	±17·5	±17·5	± 8·7	± 8·7	2·01	2·01
	15	±18·1	$±17·7_5$	± 9·8	± $8·8_5$	$1·84_5$	2·01
	30	±18·4	±18·5	± 9·8	$± 9·2_5$	$1·87_5$	2·00
	45	±18·8	$±19·6_5$	±10·4	± $9·9_5$	1·81	$1·97_5$
	60	±21·3	$±21·0_5$	±10·9	±11·1	$1·95_5$	$1·89_5$
	75	±22·4	±22·3	±12·5	±12·8	1·79	1·74
	90	±22·8	±22·8	±15·3	±15·3	1·49	1·49
3½% Ni. Cr. Steel (Low Impact) (U.T.S. = 58·1 t/in²)	0	±16·5	±16·5	± 8·0	± 8·0	$2·06_5$	$2·06_5$
	15	±17·3	±16·7	± 8·0	± 8·1	2·16	2·06
	30	±17·6	$±17·3_5$	± 8·5	$± 8·3_5$	2·07	2·08
	45	±18·3	$±18·3_5$	± 9·2	$± 8·8_5$	1·99	$2·07_5$
	60	±20·4	$±19·5_5$	±10·5/11·5	± $9·5_5$	1·94/1·77	$2·04_5$
	75	±21·0	±20·6	±10·4/11·1	±10·5	2·02/1·89	1·96
	90	±21·0	±21·0	±11·8	±11·8	1·78	1·78
Ni. Cr. Mo. Steel (75/80 ton) (U.T.S. = 80·5 t/in²)	0	±21·4	±21·4	± 8·8	± 8·8	2·43	2·43
	15	±21·0	$±21·4_5$	± 8·9	$± 8·9_5$	2·36	$2·39_5$
	30	±20·4	±21·6	± 9·5	$± 9·3_5$	$2·14_5$	2·31
	45	±23·2	±21·8	±11·0	±10·1	2·11	2·16
	60	±23·0	±22·0	±11·0	$±11·2_5$	2·09	$1·95_5$
	75	±23·0	$±22·1_5$	±12·9	±13·0	$1·78_5$	1·70
	90	±22·2	±22·2	±15·6	±15·6	$1·42_5$	1·42

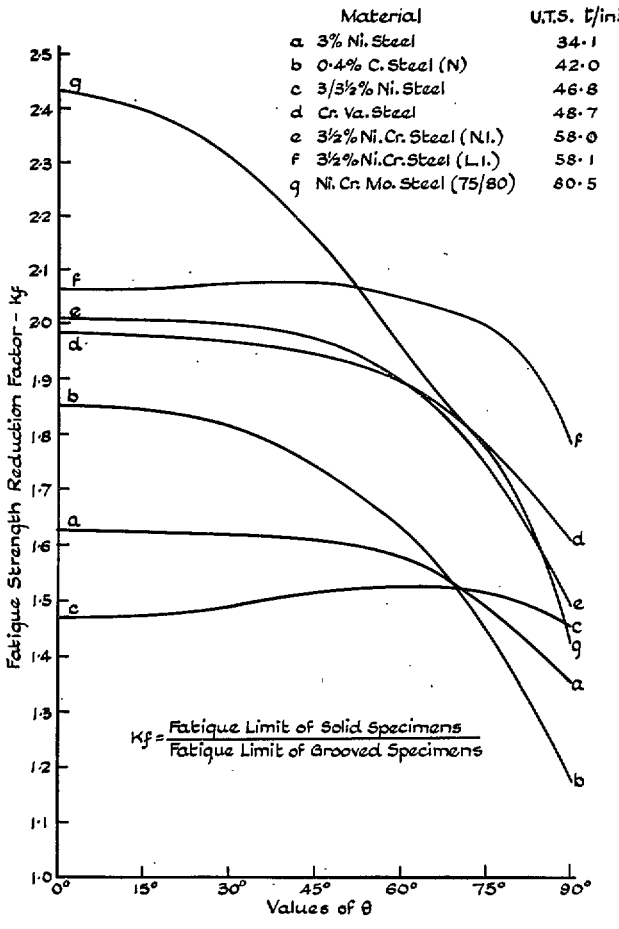

FIG. 25. Fatigue Strength Reduction Factors due to 55 deg. Vee Groove.

the fatigue strength under reversed bending stresses and a greater drop in the fatigue resistance to reversed torsional stresses, but these reductions are insignificant in comparison with the relative single blow impact values, 76 ft. lb. and 5½ ft. lb. respectively, a further confirmation of the well-established fact that the limiting fatigue resistance of a material, with or without notches, bears no relation to its impact notched bar value.

It is evident from a combined study of these curves and the data of Table 10, in which available theory has been used to correct for the measured variations in root radius at the bottom of the notch, that the widely varying effects of the presence of the notch on the fatigue resistance of the various steels cannot, at present, be defined or reconciled. We have already seen (Table 10) that the actual strength reduction factor, K_f, is in all cases much less than the estimated theoretical stress concentration factor, K_t ; the values of K_t/K_f vary from 11 to 3 for reversed bending stresses and from 5·9 to 2·1 for reversed torsional stresses. The shape of curve (c) on Fig. 25, brings out an additional remarkable and inexplicable characteristic of the 3/3½% Ni. Steel. For while the estimated theoretical value of the ratio of K_t (bending)/K_t (torsion) is 2·36, the experimental value of K_f (bending)/K_f (torsion) is only 1·01. By contrast, the corresponding theoretical and experimental ratio values for the Ni. Cr. Mo. Steel (75/80) are, 1·89 and 1·71, a fairly near approach. The ratio values for the remaining five steels lie variously between these extremes. No explanation can be offered of these wide variations in behaviour of the materials tested : consideration of the various chemical compositions or forms of microstructure also afford no clue.

VI. COMPARISION OF THE FATIGUE STRENGTHS AS DETERMINED USING THE C.S. MACHINE, THE WOHLER ROTATING BAR MACHINE AND THE STROMEYER ALTERNATING TORSION MACHINE

The values of the fatigue strengths under reversed bending and reversed torsional stresses, as determined using the three machines employed in the present investigation, are collected and compared in Table 12, where the steels are arranged in order of ascending tensile strengths. In both series of comparisons, the differences are brought out by listing the percentage excess of the combined stress machine value over that determined using the corresponding machine. Two inherent reasons for such differences may be mentioned.

Firstly, the design and method of operation of the Combined Stress machine is such that no restraint whatever is imposed on inserting a specimen in the holders and applying the load. This entire freedom from initial stress in the specimens is, of course, a most desirable feature of any testing machine but one which in many types is extremely difficult to satisfy. Considerable care and experience are required in setting up a specimen in a rotating bar machine so as to avoid a slight initial vibration and, hence, some inertia stresses ; however, when special precautions are observed, the error due to this cause should be small. With the Stromeyer machine, greater care is required to ensure that the specimen is free from initial strain : the specimen has to be locked firmly into position so that its axis is exactly coincident with the common axis of the two holder shafts which are definitely located by the long journal bearings in which they oscillate. Every precaution was duly taken in the rotating bar and Stromeyer tests, and any errors in the fatigue strength values due to initial strains in the specimens are probably small in amount, as is indicated by the regular plotting on S/N curves of the majority of the test data ; if and where they exist, however, they will tend towards producing a positive value of the ratios (CS–W)/CS and (CS–S)/CS.

Secondly, the impressed conditions of test are very important. In this respect, the conditions in the reversed torsion tests as made on the Combined Stress and

Stromeyer machines are identical. The specimen, in each case, it subject to pure alternating couples ; also, if the range of strain of the specimen increases slightly, the applied stress similarly increases. As far as impressed conditions are concerned, the machines should, therefore, give the same fatigue values for any given material. Turning to the reversed bending stress tests, the types of straining imposed on the specimens in the Combined Stress and Wohler machines are quite different ; in the Combined Stress machine, zones at the extremities of a single fixed diameter only are exposed to maximum strain, whereas, in the rotating bar specimen, all fibres equidistant from the axis are similarly strained. Thus, a correspondingly greater proportion of the material is subjected to super-elastic straining, within the fatigue range, in the Wohler test and the calculated ' nominal ' values of the fatigue strengths would be expected to differ. The effect of the impressed conditions of tests has been discussed in Part I, Section 3, and it is unnecessary to expand that discussion. In general, it is found that the fatigue range of a ductile steel under reversed direct stresses is less than the Wohler fatigue range determined using solid specimens, which in turn usually exceeds the Wohler value obtained using hollow specimens (see also Table 4) ; this difference between solid and hollow specimens has also been brought out in the present test on two materials tested over the whole applied range of combined stresses (see Tables 5 and 7). It is, therefore, to be expected that the rotating bar value will be lower than the value for reversed plane bending stresses as determined in the Combined Stress machine. The extent of the differences is dependent on the static stress/strain relations of the material under test and will thus vary from material to material.

Comparing corresponding pairs of fatigue limits listed in Table 12, the following points emerge :—

DUCTILE STEELS

(i) Reversed Bending Stresses :—In every case, the Combined Stress value exceeds the Wohler value by amounts which certainly vary from + 0·6 to + 8·6% ; some doubt attaches to the reliability of the + 10% value recorded for the Ni. Cr. Steel (95/105), as this material behaved so irregularly under both types of test. The constancy of the plus sign is strong evidence of the reality of the influence of the differing impressed test conditions ; as previously pointed out, the type of

TABLE 12

COMPARISON OF THE FATIGUE LIMITS OBTAINED USING THREE TYPES OF TESTING MACHINES

C.S. = Combined Stress Machine ; W = Wohler Rotating Bar Machine ; S = Stromeyer Alternating Torsion Machine

Material	U.T.S. t/in²	Form of Specimen	F.Lt ; Reversed Bending Stresses* (t/in²)			F.Lt ; Reversed Torsional Stresses* (t/in²)			Fatigue Ratios (C.S. Machine) $= \frac{\text{F.Lt}}{\text{U.T.S.}}$	
			C.S.	W.	$\frac{\text{CS–W}}{\text{CS}} \times 100$	C.S.	S.	$\frac{\text{CS–S}}{\text{CS}} \times 100$	Reversed Bending	Reversed Torsion
0·1% C. Steel (Normalised)	27·9	Solid	±17·4	±17·0	+ 2·3	± 9·8₅	± 9·6	+ 2·5	0·62	0·35
	27·9	Hollow	±17·5	±16·5	+ 5·7	± 9·1₅	± 8·7	+ 4·9	0·63	0·33
0·4% C. Steel (Spheroidised)	30·9	Solid	±17·8	±15·9/17·4 (U)	—	±10·1	± 9·6	+ 5·0	0·58	0·33
3% Ni. Steel (30/35) ..	34·1	Solid	±22·2	±20·3	+ 8·6	±13·3	±12·7	+ 4·5	0·65	0·39
0·4% C. Steel (Normalised)	42·0	Solid	±21·5	±20·8	+ 3·3	±13·4	±13·5	− 0·75	0·51	0·32
3/3½% Ni. Steel (45/50)	46·8	Solid	±28·8	±26·5	+ 8·0	±17·3	±18·0	− 4·0	0·62	0·37
Cr. Va. Steel (45/50) ..	48·7	Solid	±27·8	±26·5	+ 4·7	±16·7	±17·5 (LR)	(− 4·8)	0·57	0·34
0·9% C. Steel (Pearlitic)	54·9	Solid	±22·8	±22·2	+ 2·6	±15·6	±16·3	− 4·5	0·42	0·28
3½% Ni. Cr. Steel (Normal Impact)	58·0	Solid	±35·0	±33·7	+ 3·7	±22·8	±22·6	+ 0·9	0·60	0·39
	58·0	Hollow	±33·6	±33·4	+ 0·6	±20·5	±21·5	− 4·9	0·58	0·35
3½% Ni. Cr. Steel (Low Impact)	58·1	Solid	±33·0	±31·9	+ 3·3	±21·0	±21·7	− 3·3	0·57	0·36
Ni. Cr. Mo. Steel (60/70)	64·8	Solid	±39·0	±37·5	+ 3·8	±21/22¾ (U)	±21·5 (U)	—	0·60	—
Ni. Cr. Mo. Steel (75/80)	80·5	Solid	±42·8 (L.R.)	±39·0 (U)	—	±22·2	±23·8	− 7·2	(0·53)	0·28
Ni. Cr. Steel (95/105) ..	108	Solid	±50 (L.R.)	±45 (L.R.)	(+10)	±29·3	±28·5	+ 2·7	(0·46)	0·27
' Nicrosilal ' Cast Iron	14·2	Solid	±16·4	±14·0	+14·6	±13·7	±11·8	+13·9	1·15	0·97
' Silal ' Cast Iron ..	14·9	Solid	±15·6	±14·9	+ 4·5	±14·2	±12·9	+ 9·2	1·05	0·95

*Note.—Except where otherwise stated, the fatigue limit values have a ' Reliability Index ' of ' R.' No ratio value is stated where a ' U ' value is involved : where an ' LR ' value is concerned, the ratio value is enclosed in brackets.

machine employed is only a secondary influence, the primary cause is the modification in the stress/strain relation set up in the specimen due to super-elastic straining of the material within the fatigue range. As to be expected, the variations in the values of the (CS–W)/CS ratio bear no relation to tensile strengths.

(ii) Reversed Torsional Stresses :—Some of the ' CS ' values are greater, some less, than the corresponding S values, the (CS–W)/CS ratio varying between $-7{\cdot}2$ and $+5\%$. With the exception of the $7{\cdot}2\%$ value, which is rather high, the majority of the remainder have little significance for design purposes, the corresponding stress difference values being small and comparable with variations which may be expected to result from different bars of a heat-treated batch. The occurrence of six plus signs and seven minus signs, distributed quite irregularly in relation to the tensile strength and ductility of the materials, confirms the conclusion derived from consideration of impressed test conditions that, given uniformity of the material and freedom from applied initial strains, both machines should give the same value of the fatigue limit under reversed torsional stresses.

CAST IRONS

The Combined Stress machine gives higher values than the other two machines. The percentage differences are high, $14{\cdot}6$ and $4{\cdot}5$ for bending, $13{\cdot}9$ and $9{\cdot}2$ for torsion. It is probable that, as the specimens used in the Stromeyer machine had a relatively long parallel test portion, greater opportunity occurred for occasional flaws to give a lower value of the fatigue limit ; unavoidable initial stresses may have been partly responsible. Otherwise, no explanation can be offered of the fact that plus (CS–S)/CS values, were obtained in both comparisons.

Conclusions

In Part I, Section 5, it has been shown, within the range of the materials investigated, that the resistance to combined fatigue stresses consisting of reversed plane bending and reversed torsion with combinations of these stresses, when expressed in terms of their bending and shearing stress components, $\pm f$ and $\pm q$, plot satisfactorily on regular f/q curves between the limits of $\pm f = 0$ (reversed shear stresses) and $\pm q = 0$ (reversed bending stresses). Hence, given these ' end ' values, the intermediate combinations can be calculated for design purposes. Examination of the present data has shown that rotating bar values—as determined using a form of machine that is widely available—gives a value that, in general, will be lower than can be safely applied to the design of components to be subjected to plane bending stresses. On the other hand, the results obtained from any reliable form of reversed torsional fatigue testing machine can be used for the shearing end point in the calculation. This conclusion definitely holds for all the ductile steels investigated and is consistent with considerations of the effect of the impressed conditions of testing. Some reservation must be attached, at present, to its applicability to the design of cast iron components.

FATIGUE RATIOS

The opportunity has been taken to record in Table 12, the values of the Fatigue Ratios $\left(\frac{\text{Fatigue limit}}{\text{Ultimate tensile strength}}\right)$ for reversed bending and reversed torsional stresses, as determined using the Combined Stress machine.

As far as the steels are concerned, the data show the usual relation, i.e. that the fatigue limit under reversed bending stresses is roughly proportional to the tensile strength within fairly small variations : this increase of fatigue strength with tensile strength, in the present range of steels, is largely independent of chemical composition and heat-treatment. The two exceptions in the present series are the $0{\cdot}9\%$ C. Steel (Pearlitic), which exhibits relatively poor fatigue resistance, and, to a lesser extent, the $0{\cdot}4\%$ C. Steel (Normalised).

The fatigue ratios for the two cast irons have abnormally high values, all in the neighbourhood of unity, which means that fracture under static and fatigue stressing is primarily determined by principal stress or principal strain : this is also demonstrated by the established identity of the fracture planes.

APPENDIX No. 1

RESULTS OF CHEMICAL ANALYSES AND MICROSCOPICAL EXAMINATION OF MATERIALS

A. DUCTILE ENGINEERING STEELS

1. $0{\cdot}1\%$ Steel (Normalised)

This steel was tested in one condition, i.e. normalised from 900° C.: it was supplied in the form of $\frac{7}{8}$ in. diameter bars, in the heat-treated condition.

RESULTS OF CHEMICAL ANALYSIS :—

C	$0{\cdot}12\%$	P	$0{\cdot}016\%$
Si	$0{\cdot}185\%$	Ni	$0{\cdot}06\%$
Mn	$0{\cdot}61\%$	Cr	Trace
S	$0{\cdot}012\%$	Cu	$0{\cdot}075\%$

RESULTS OF MICROSCOPICAL EXAMINATION :—

Transverse sections through a bar were examined, by means of sulphur printing and by etching in a cupric chloride reagent, to detect possible segregations of sulphur and phosphorus. It was found that these impurities were present only in small proportions and were regularly distributed throughout the section.

Microscopical examination of a polished but unetched longitudinal section of a bar has shown the steel to

contain only a very small proportion of non-metallic inclusions, which are present as fine filaments. Longitudinal sections were also examined after etching in a solution of nitric acid in alcohol. The structure consists largely of ferrite together with some pearlite, as shown in Fig. 7 (*a*), at a magnification of 150 diameters. The pearlite, finely lamellar in structure, is somewhat banded in the direction of rolling. The appearance of the pearlite and ferrite, at a magnification of 500 diameters, is shown in Fig. 7 (*b*).

2. **0·4% C. Steel**

This steel has been completely investigated in each of two forms of heat-treatment and constitutes one of the series of experiments aimed at determining the effect of the structure of the material on its resistance to combined fatigue stresses. The types of structure employed are :—

(*a*) Ferrite and Pearlite, as in normalised carbon steels.

(*b*) Uniform Matrix containing Spheroidised Cementite, as in fully annealed steels of moderate carbon content.

In this case, while the chemical composition is, of course, the same in both cases (the results given below of independent analyses of each batch show only trifling differences as commonly encountered in the same cast), the tensile strengths in the normalised and spheroidised conditions are, respectively, 42 and 31 t/in.^{2}.

Heat Treatment :—The normalised material was tested in the condition as received from the makers, i.e. after normalising at 850° C.

The spheroidised material had also been heat-treated at the maker's works to produce the required condition:—subjected to two periods of heating at 700° C. for 48 hours each, followed by slow cooling. A micro-examination at the N.P.L. showed that the material was not completely spheroidised. It was, therefore, given further heat-treatment consisting of a preliminary normalising treatment (heating to 900° C. for 20 minutes and cooling in air) followed by heating for six days at 650° C. and allowing to cool slowly. It was tested in the condition following this further heat-treatment.

2 (*a*). **0·4% C. Steel** (Normalised)

RESULTS OF CHEMICAL ANALYSIS :—

C	0·38%	P	0·020%
Si	0·22%	Mn	0·65%
S	0·018%	Ni	0·10%

RESULTS OF MICROSCOPICAL EXAMINATION:—

Specimens from each bar were examined to ensure uniformity throughout the whole batch.

The microstructures of all the specimens examined are similar, the most marked features being the irregularity in the size of the pearlitic areas. The bars have also a banded structure but this is not strongly developed. The irregularity of the structure is not eliminated by normalising at 850° C. or 900° C. Fig. 7 (*c*) is a representative photo-micrograph of the structure.

2 (*b*). **0·4% C. Steel** (Spheroidised)

RESULTS OF CHEMICAL ANALYSIS :—

C	0·40%	P	0·019%
Si	0·24%	Mn	0·66%
S	0·016%	Ni	0·14%

RESULTS OF MICROSCOPICAL EXAMINATION :—

Fig. 7 (*d*) shows the appearance of the structure, at 1,500 diameters, of a representative section after polishing and etching in a dilute solution of nitric acid in alcohol. The cementite is well spheroidised but there are a number of larger granules of carbide present and the distribution of carbide particles has been determined by the position of the pearlitic areas.

3. **0·9% C. Steel** (Pearlitic)

This crucible melted carbon steel, having the eutectic composition, was included in the programme to provide one of the four series of representative microstructures (ferrite and pearlite ; pearlitic : uniform matrix containing spheroidised cementite ; hardened and tempered) to provide some information on the effect of the structure of steels on their resistance to combined stresses. The steel was tested in the normalised condition to produce the pearlitic structure ; the heat-treatment, applied at the maker's works, was normalising from 820° C.

RESULTS OF CHEMICAL ANALYSIS :—

C	0·86%	S	0·026%
Si	0·05%	P	0·020%
Mn	0·13%		

RESULTS OF MICROSCOPICAL EXAMINATION :—

Typical microstructures of the material are shown in Fig. 8 (*a*) and 8 (*b*) at magnifications of 150 and 500, respectively. There is a complete absence of free ferrite and primary cementite. The whole of the structure consists of pearlite. The steel contains an appreciable number of fine non-metallic inclusions, but there are no obvious defects which would render the material unsuitable for the purposes of the research.

4. **3% Nickel Steel** (Low Carbon) (H. and T.)

In regard to tensile strength, this steel was selected to represent the 30/35 t/in.^{2} class. The heat-treatment, applied at the maker's works, was :—Oil-hardened from 850° C. ; tempered at 700° C. ; air cooled.

RESULTS OF CHEMICAL ANALYSIS :—

C	0·11%	P	0·011%
Si	0·22%	Ni	3·18%
Mn	0·42%	Cr	Trace
S	0·011%		

RESULTS OF MICROSCOPICAL EXAMINATION :—

The examination of polished but unetched longitudinal sections shows the material to contain only a small proportion of elongated low metallic inclusions.

The microstructure, developed by etching in a dilute solution of nitric acid in alcohol, is shown in Figs. 8 (*c*) and 8 (*d*) at magnifications of 150 and 500, respectively. The structure consists mainly of ferrite together with cementite formed from martensite as the result of heavy tempering. The material suffers from pronounced banding, brought about by sluggish diffusion during heat-treatment ; probably, the duration of heating above the higher critical point was insufficient. The banding might lead to marked directional properties in the material.

5. 3/3½% Nickel Steel (O.H. and T.)

In regard to tensile strength, this steel was selected to represent the 45/50 tons per sq. in. class. The heat-treatment, applied at the maker's works, was :—Oil-hardened from 850° C. ; tempered at 610° C. ; air cooled.

RESULTS OF CHEMICAL ANALYSIS :—

C	0·34%	Mn	0·57%
Si	0·17%	Ni	3·25%
S	0·007%	Cr	0·06%
P	0·011%		

RESULTS OF MICROSCOPICAL EXAMINATION :—

The microstructure corresponds to that of a Nickel Steel after the stated heat-treatment. Fig. 9 (*a*) shows the appearance of the structure, after etching in a solution of nitric acid in alcohol, at a magnification of 300 diameters, revealing a well-defined martensitic structure, which, at the higher magnification of 1,500 diameters, as shown in Fig. 9 (*b*), clearly indicates the separation of a well formed carbide. This is indicative of a high tempering temperature following upon a hardening operation on the material from above the critical temperature.

A few streaks of non-metallic inclusions were observed in the material, as shown in Fig. 9 (*a*), but the steel is relatively free from non-metallic material or other defects.

6. Chrome-Vanadium Steel (O.H. and T.)

This steel, suitably heat-treated to produce a tensile strength in the 45/50 tons per sq. in. range, duplicates in this respect the 3/3½% Nickel Steel. It was selected to show the effect, if any, on the fatigue properties of differing chemical composition of two steels having the same tensile strength.

The heat-treatment, applied at the maker's works, was :—Oil-hardened from 850° C. ; tempered at 700° C. ; air cooled.

RESULTS OF CHEMICAL ANALYSIS :—

C	0·41%	P	0·017%
Si	0·23%	Cr	1·27%
Mn	0·71%	Va	0·28%
S	0·006%		

RESULTS OF MICROSCOPICAL EXAMINATION :—

Longitudinal and transverse sections were examined. The non-metallic inclusions observed in the unetched sections are normal in number and size for this type of steel. Fig. 9 (*c*) shows the microstructure, at a magnification of 500 diameters, of a longitudinal section etched in a 4% solution of nitric acid in alcohol. The material has a uniform fine grain : the carbide occurs as well separated particles clearly seen at this magnification. The microstructure is typical of a steel of this composition after hardening and tempering at a temperature higher than 550° C.

7. 3½% Ni. Cr. Steel

This material, supplied in the form of ⅞ in. diameter bars, has been investigated in two conditions.

Firstly, in the hardened and tempered condition as normally used in engineering practice, having a tensile strength of 55/60 t/in.^{2} The heat-treatment applied was :—Oil-hardened from 830° C. ; tempered 620° C. and cooled in water. The tensile strength obtained was 58·0 t/in.^{2} associated with an Izod notched bar value of 75·5 ft. lb.

Secondly, it was subjected to a heat-treatment which, while leaving the tensile strength unchanged, produced a very low notched-bar value. The heat-treatment applied in this case was :—Oil-hardened from 830° C. ; tempered for 1¾ hours at 620° C. and slowly cooled from that temperature to 100° C. in 42 hours. The tensile strength obtained was 58·1 t/in.^{2}, associated with an Izod notched bar value of 5·4 ft. lb.

All bars were from the same cast ; the common chemical composition will be evident from the results, given below, of independent analyses of each batch. The two materials jointly provide an excellent example for examining the relative resistances to combined fatigue stresses of differing heat-treatment (and microstructures), but identical chemical composition and tensile strength.

7 (*a*). 3½% Ni. Cr. Steel (Normal Impact)

RESULTS OF CHEMICAL ANALYSIS :—

C	0·31%	P	0·017%
Si	0·21%	Ni	3·65%
Mn	0·58%	Cr	0·85%
S	0·002%		

RESULTS OF MICROSCOPICAL EXAMINATION :—

Transverse and longitudinal sections through a bar were examined, by sulphur printing and by etching in a cupric chloride reagent, to detect possible segregation of sulphur and phosphorus. The small content of sulphur appeared to be evenly distributed and there is no gross segregation of the phosphorus, but the etched longitudinal section exhibited numerous fine parallel bands in the direction of rolling.

Microscopical examination of a polished but unetched longitudinal section showed the steel to contain only a very small proportion of non-metallic inclusions which

are elongated in the direction of rolling. Longitudinal sections were also examined after etching in a solution of nitric acid in alcohol; the microstructure consists of martensite which has been somewhat altered by tempering. This microstructure is characteristic of a hardened nickel-chromium steel tempered sufficiently to bring about separation of carbide. The structure is uniform throughout the section, but, at low magnifications, banding is revealed in the direction of rolling. The appearance of the microstructure at magnifications of 150 and 500 diameters, respectively, is shown in Fig. 10 (*a*) and Fig. 10 (*b*).

7 (*b*). **3½% Ni. Cr. Steel** (Low Impact)

RESULTS OF CHEMICAL ANALYSIS :—

C	0·30%	P	0·019%
Si	0·21%	Ni	3·60%
Mn	0·59%	Cr	0·86%
S	0·010%		

RESULTS OF MICROSCOPICAL EXAMINATION :—

Transverse and longitudinal sections through the specimen were examined by sulphur printing, and by etching in cupric chloride reagent, to detect possible segregation of sulphur and phosphorus. The sulphur is distributed evenly and there is no appreciable segregation of phosphorus, but the etched longitudinal section exhibits fine parallel bands which run in the direction of rolling.

Microscopical examination of a polished but unetched section of the material has shown the steel to contain only a very small proportion of non-metallic inclusions; these are elongated in the direction of rolling.

Longitudinal sections were also examined after etching in a solution of nitric acid in alcohol. The microstructure consists of martensite which has been somewhat altered by tempering, which has been sufficient to bring about separation of carbide. The structure is illustrated in Fig. 10 (*c*) and Fig. 10 (*d*) at magnifications of 150 and 500 diameters, respectively. It will be seen that the austenite grains from the martensite have been formed, are very clearly defined and, at the higher magnification, appear to be bounded by fine black lines.

As austenitic grain boundaries are not usually seen distinctly in martensitic steels, it was thought that these fine lines were an abnormal feature of the microstructure associated with low notched bar impact value and that they might even be fine cracks, either present in the steel before etching or formed during etching in regions of high internal stress. The former possibility was investigated by examining unetched specimens which had been polished by a method which generally reveals intercrystalline cracks when present in steel, namely, hand polishing on magnesia. No cracks were observed on such specimens before etching. Impact fractures of the material contained branching cracks which lie in the grain boundaries.

It was considered useful to demonstrate that this 'embrittled' steel could be restored to its original, and normal, impact value by subsequent heat-treatment. It was found that either re-hardening and tempering or tempering alone, followed by water cooling, effected this restoration: the Izod values obtained were 79 and 81 ft. lb., respectively. After such further treatment, examination under the microscope showed that the austenitic grain boundaries were still clearly defined but fracture under impact occurred without the propagation of branching intercrystalline cracks. It was, therefore, clear that the fine black lines observed microscopically in the 'embrittled' material were not cracks.

8. **Ni. Cr. Mo. Steel** (O.Q. and T.) (65 ton)

This steel was selected to represent the 60/70 t/in.² range of tensile strength. It was heat-treated, at the National Physical Laboratory, as follows :—Normalised at 900° C.; oil-hardened from 850° C.; tempered at 640° C.; air cooled.

RESULTS OF CHEMICAL ANALYSIS :—

C	0·24%	Ni	3·06%
Si	0·20%	Cr	1·29%
Mn	0·57%	Mo	0·54%
S	0·004%	Va	0·25%
P	0·015%		

RESULTS OF MICROSCOPICAL EXAMINATION :—

The material in the 'as received' condition was heavily banded; the relation of these bands to the martensitic structure is shown in Fig. 11 (*a*). Heat-treatment above the critical point tends to eliminate the banding: Fig. 11 (*b*) shows the uniform character of the structure after such heat-treatment.

The material is of good quality, the number of non-metallic inclusions is reasonably low and there is no appreciable segregation of impurities in any part of the bars.

9. **Ni. Cr. Mo. Steel** (O.Q. and T.) (80 ton)

This steel was selected to represent the 75/80 t/in.² range of tensile strength. It was heat-treated, at the maker's works, as follows :—Oil-hardened from 850° C.; tempered at 600° C.; air cooled.

RESULTS OF CHEMICAL ANALYSIS :—

C	0·24%	Ni	3·10%
Si	0·27%	Cr	1·33%
Mn	0·57%	Mo	0·41%
S	0·007%	Va	0·25%
P	0·011%		

RESULTS OF MICROSCOPICAL EXAMINATION :—

Specimens were polished and etched in a dilute solution of nitric acid in alcohol. A uniform structure of tempered martensite was revealed, as shown in Fig. 11 (*c*) and Fig. 11 (*d*), at 150 and 500 magnifications, respectively. Non-metallic inclusions were not unduly prominent.

10. **Ni. Cr. Steel** (A.H. and T.) (105 ton)

This air-hardening nickel-chromium steel was selected to represent the 95/105 t/in.^{2} range of tensile strength. It was heat-treated, at the maker's works, as follows :— Air-hardened from 820° C.; tempered at 200° C.; air cooled.

RESULTS OF CHEMICAL ANALYSIS :—

C	0·28%	P	0·018%
Si	0·23%	Ni	4·42%
Mn	0·48%	Cr	1·36%
S	0·004%		

RESULTS OF MICROSCOPICAL EXAMINATION :—

A longitudinal section was cut from the central part of the heat-treated material. On polishing and etching in a dilute solution of nitric acid in alcohol, a tempered martensitic structure was revealed as shown, at a magnification of 500 diameters, in Fig. 9 (*d*).

Small isolated areas of ferrite occur throughout the section, indicating that a slightly higher temperature might have been employed before quenching in order to obtain an entirely martensitic structure.

B. CAST IRONS

Two cast irons have been investigated: 'Silal' was selected as an interesting example of a close approach to a brittle material, 'Nicrosilal' as representing a comparatively ductile cast iron. It is well known that the strength of cast iron is dependent on the size and shape of the section under test. To obtain comparable results, the irons were cast in the nearest practicable approach to the size in which they were subsequently tested, patterns being prepared of the actual forms of the various specimens plus an allowance for machining to the required finished dimensions (see Fig. 5). Both materials were tested in the 'as cast' condition as received from the makers. Some of the castings contained blowholes; no tests were made on specimens which, on inspection after final machining, were found to exhibit defects, while careful note was made of other specimens the fracture of which, after completion of the test, appeared to have been influenced by surface or internal defects.

11. '**Silal**' **Cast Iron** (as cast)

RESULTS OF CHEMICAL ANALYSIS :—

C	2·09%	Total—1·99% Graphitic Carbon	
		0·10% Combined Carbon	
Si	6·39%		
Mn	1·13%		
S	0·031%		
P	0·047%		
Al	0·08%		

RESULTS OF MICROSCOPICAL EXAMINATION :—

Cross-sections of ½-in. square bars were polished and etched in a dilute solution of nitric acid in alcohol. The structure, illustrated by Figs. 12 (*a*) and 12 (*b*), is seen to consist of elongated dendrites of primary constituent (transforming to silico-ferrite on cooling) together with a fine infilling eutectic composed of fine graphite and ferrite. In addition to the dendritic structure, the sections present a coarse cellular structure apparently quite independent of the former and more particularly noticeable at low magnifications (see Fig. 12 (*a*)). The outline of the cell walls can be seen even more clearly before the section is etched. These cell walls are characterised by the presence of a rather larger form of graphite, accompanied possibly by small cavities and the presence of a constitutent which, on etching, is rather like pearlite. Examination suggests that the cellular structure was established just before the material solidified, but its origin is obscure. The constituent resembling pearlite, which is associated with the cell walls, has been previously observed in 'Silal' but has not been definitely identified. A longitudinal section through the centre of the bar indicates that the cells are, more or less, equiaxially arranged.

12. '**Nicrosilal**' **Cast Iron** (as cast)

RESULTS OF CHEMICAL ANALYSIS :—

C	1·88%	Total —1·51% Graphitic Carbon	
		0·37% Combined Carbon	
Si	4·25%		
Mn	0·60%		
S	0·039%		
P	0·033%		
Ni	17·74%		
Cr	2·39%		

RESULTS OF MICROSCOPICAL EXAMINATION :—

The structure of a sample taken from a bar ½-in. square is shown in Figs. 12 (*c*) and 12 (*d*). The austenite dendrites are clearly developed, while the graphite present is mostly of the finely divided inter-dendritic type usually associated with Nicrosilal. A third constituent, probably carbide, is also present, this being often found in irons containing over 2% of chromium. Apart from the finely divided graphite, there is a certain amount of this constituent present in larger nodular masses or thin flakes. This is sometimes associated with slight porosity and, for this reason, several other samples, taken from differently sized bars, were also examined. The nodular or flaky graphite was found to be present to some extent in all sections but in no instance was any porosity discovered.

APPENDIX 2

RESULTS OF SUPPLEMENTARY MECHANICAL TESTS

The forms of all the specimens used are shown in Figs. 4, 5 and 6.

1. **Static Tensile Tests**

Four specimens of each material were tested to destruction. Duplicate tests were made, on the standard type of tensile specimen, in a single-lever vertical testing machine, strain measurements, up to the yield point, being taken by means of a double-rhomb mirror extensometer of the Martens type; these tests afforded the usual tensile data. In addition, duplicate tests to destruction were carried out with a Dalby optical load-extension recorder on the special type of specimen required; the additional data of special interest thus

TABLE 13

RESULTS OF STATIC TENSILE TESTS

Material	Stresses, t/in²					Elongation %		Reduction of Area at Fracture %	Value of Young's Modulus (E) lb/in² × 10^{-6}	Remarks* on Fracture
	Limit of Proportionality	Upper yield point	Lower yield point	Ultimate Tensile (on original area)	Breaking Stress (on final area)	On standard gauge length ($l=4\sqrt{A}$)	On 8 dias.			
0·1% C. Steel (Normalised)	12·5	16·6	15·6	27·9	61	40½	33½	70	28·8	Cup and Cone
0·4% C. Steel (Normalised)	14·5	23·4	22·9	42·0	76½	31	24¼	58¼	30·0	Cup and Cone: silky crystalline
0·4% C. Steel (Spheroidised)	14·9	18·6	16·8	30·9	67	39½	31¾	67	30·1	Cup and Cone: silky crystalline
0·9% C. Steel (Pearlitic)	7·7	No definite yield point	—	54·9	65	13¾	13½	18	29·3	Crystalline: brittle type.
3% Ni. Steel (30/35 ton)	15·8	No definite yield point	—	34·1	81	40½	30	72½	29·2	Cup and Cone
3/3½% Ni. Steel (45/50 ton)	26·0	38·0	No drop at yield	46·8	90	26½	19½	67½	29·2	Shear failure: also axial separation.
Cr. Va. Steel (45/50 ton)	31·5	44·1	41·0	48·7	96½	26½	19¼	66	30·3	Shear failure: also axial separation.
3½% Ni. Cr. Steel (Normal Impact)	18·3	49·2	No drop at yield	58·0	103	25	17	65	29·0	Shear failure: also axial separation.
3½% Ni. Cr. Steel (Low Impact)	13·5	48·9	No drop at yield	58·1	99	24	16¼	60½	28·9	Shear failure: also axial separation.
Ni. Cr. Mo. Steel (60/70 ton)	47·0	61·3	60·8	64·8	118	23½	14	67	29·1	Shear failure: also axial separation.
Ni. Cr. Mo. Steel (75/80 ton)	21(14/28)	No definite yield point	—	80·5	129	20½	12	60	29·2	Shear failure: also axial separation.
Ni. Cr. Steel (95/105 ton)	24	No definite yield point	—	108(106/112)	166	16	10½	52	30·0	Cup and cone: silky crystalline.
'Silal' Cast Iron ..	1·9	No definite yield point	—	14·9	14·9	½	¼	0	17·5	Brittle.
'Nicrosilal' Cast Iron ..	1·9	No definite yield point	—	14·2	14·4	1	1	1·3	19·6	Fine crystalline.

**Note.*— 'Shear Failure, also axial separation' is used to describe the shape, somewhat resembling an end milling cutter, which is so often associated with the tensile fracture of an alloy steel.

provided being :—(*a*) autographic complete load/extension diagram to fracture, (*b*) upper and lower (when exhibited) yield stresses and (*c*) breaking stress calculated on final cross-sectional area.

The results obtained, from specimen to specimen, were usually very consistent and it appears unnecessary to tabulate in detail the individual results of the fifty-six (4 × 14) tests. For each material, therefore, the average result only is recorded in Table 13, except that where appreciable variation was exhibited, the maximum and minimum values are also given (in brackets).

For each material tested, one (of the pair obtained) autographic tensile load/elongation diagram recorded in the Dalby machine is reproduced to form Fig. 13.

2. Static Torsion Tests

Static torsion tests to fracture were made on duplicate specimens of each material. A single-lever testing machine of the usual type was employed, while strain readings, up to the yield point, were recorded using a double -mirror extensometer of the Martens type. As in the case of the tensile test data, it is necessary only to record the average values when the results are in good agreement ; in other cases, both values are given in brackets. The results are given in Table 14. It will be noted that whereas the direction of fracture of all the steels indicated the usual failure by shear, the helicoidal type of fracture of both cast irons suggests failure on planes associated with principal stress (or strain).

3. Static Indentation Tests

Steels :—To check the uniformity of the heat-treatment throughout the bar in the case of the engineering steels, indentation tests have been made on ground surfaces of four specimens of each material, so prepared that these surfaces were parallel to the axis of the bar and situated at distances of 0·15, 0·2, 0·25 and 0·3 in. from the axis (the actual thickness of the specimens being equal to twice these amounts ; see Fig. 4). A number of indentation tests were made on each surface using (*a*) a 5 mm. ball and 750 kg. load in an Avery machine, (*b*) a 2 mm. ball and 120 kg. load in a Vickers hardness testing machine, and (*c*) a diamond pyramid (angle 136 deg.) and 50 kg. load, also in a Vicker's machine. All these results are on record but, as each of the three sets of results are very consistent indicating the same kind of hardness variation with position in the bar, it will be sufficient to present one series of results ; the results obtained with the 2 mm. ball and 120 kg. load only are, therefore, given in Table 15. Small variations occur in hardness at various depths but the results indicate that the heat-treatments applied have been successful in producing a reasonable degree of uniformity throughout each bar.

Cast Irons :—With these materials, in which greater variation might be expected from bar to bar, it was considered more informative to carry out a number of tests on the surfaces of random test specimens of different types, and, also, on some sectioned cast bars. These, also, were made using the same three methods of tests

TABLE 14

RESULTS OF STATIC TORSION TESTS

Material	Stresses, t/in²			Total twist at fracture on 2½ in. gauge length (degrees)	Modulus of Rigidity, *G* lb/in² × 10^{-6}	Remarks on Fracture
	Limit of Proportionality	Yield point	Modulus of Rupture			
0·1% C. Steel (Normalised)	8·5	11·7	32·7	2859(2795/2923)	11·5	Ductile : transverse
0·4% C. Steel (Normalised)	10·5	16·8	41·7	1600	11·8	Ductile : transverse
0·4% C. Steel (Spheroidised)	5·2	11·7	36·3	2190	11·8	Ductile : transverse
0·9% C. Steel (Pearlitic)	7·5(6·6/8·4)	No definite yield point	48·9(46·5/51·3)	552	11·4	Ductile : transverse
3% Ni. Steel (30/35 ton)	9·0	No definite yield point	38·0	2014(1850/2178)	11·5	Ductile : transverse
3/3½% Ni. Steel (45/50 ton)	19·0	27·8	44·3	1991	11·4	Ductile : transverse
Cr. Va. Steel (45/50 ton)	24·5	30·8	46·2	1402(1286/1517)	12·1	Ductile : transverse
3½% Ni. Cr. Steel (Normal Impact) ..	23·7	37·8	52·3	1230(1139/1322)	11·4	Ductile : transverse
3½% Ni. Cr. Steel (Low Impact) ..	18·3	No definite yield point	51·2	1150	11·5	Ductile : transverse
Ni. Cr. Mo. Steel (60/70 ton)	31·4	46·3	57·3	2085(2054/2116)	11·5	Ductile : transverse
Ni. Cr. Mo. Steel (75/80 ton)	26·6	59·1	67·5	1066(1204/927)	11·6	Ductile : transverse
Ni. Cr. Steel (95/105 ton)	28·8	No definite yield point	89·2	630(597/660)	11·3	Ductile : transverse
'Silal' Cast Iron	4·4	No definite yield point	23·8	8	7·6	Brittle : double helicoidal
'Nicrosilal' Cast Iron	2·3(2·7/1·9)	No definite yield point	32·5	170(125/215)	8·6	Silky : single helicoidal

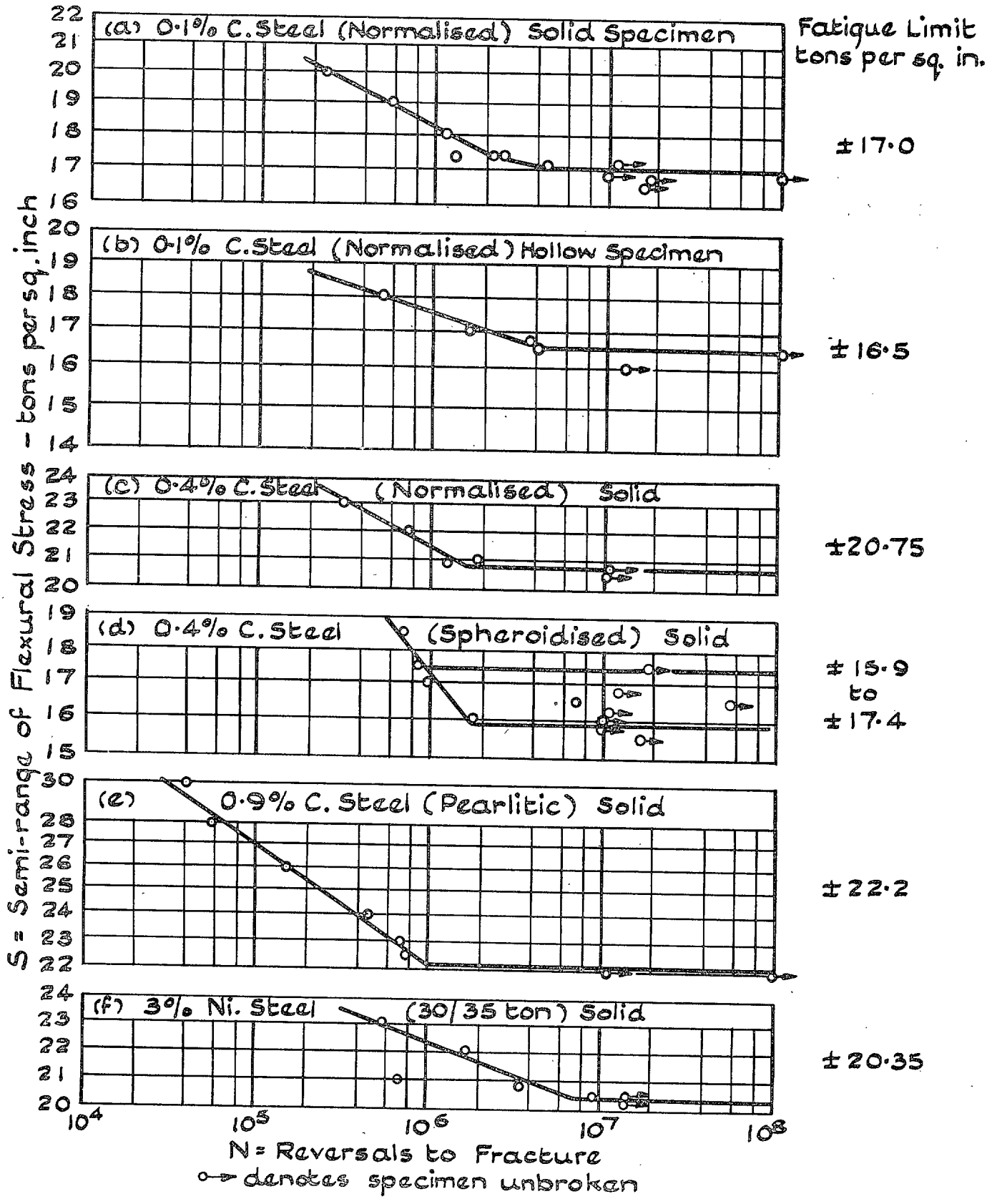

FIG. 26. *S/N* diagrams (Rotating Bar Fatigue Machine).

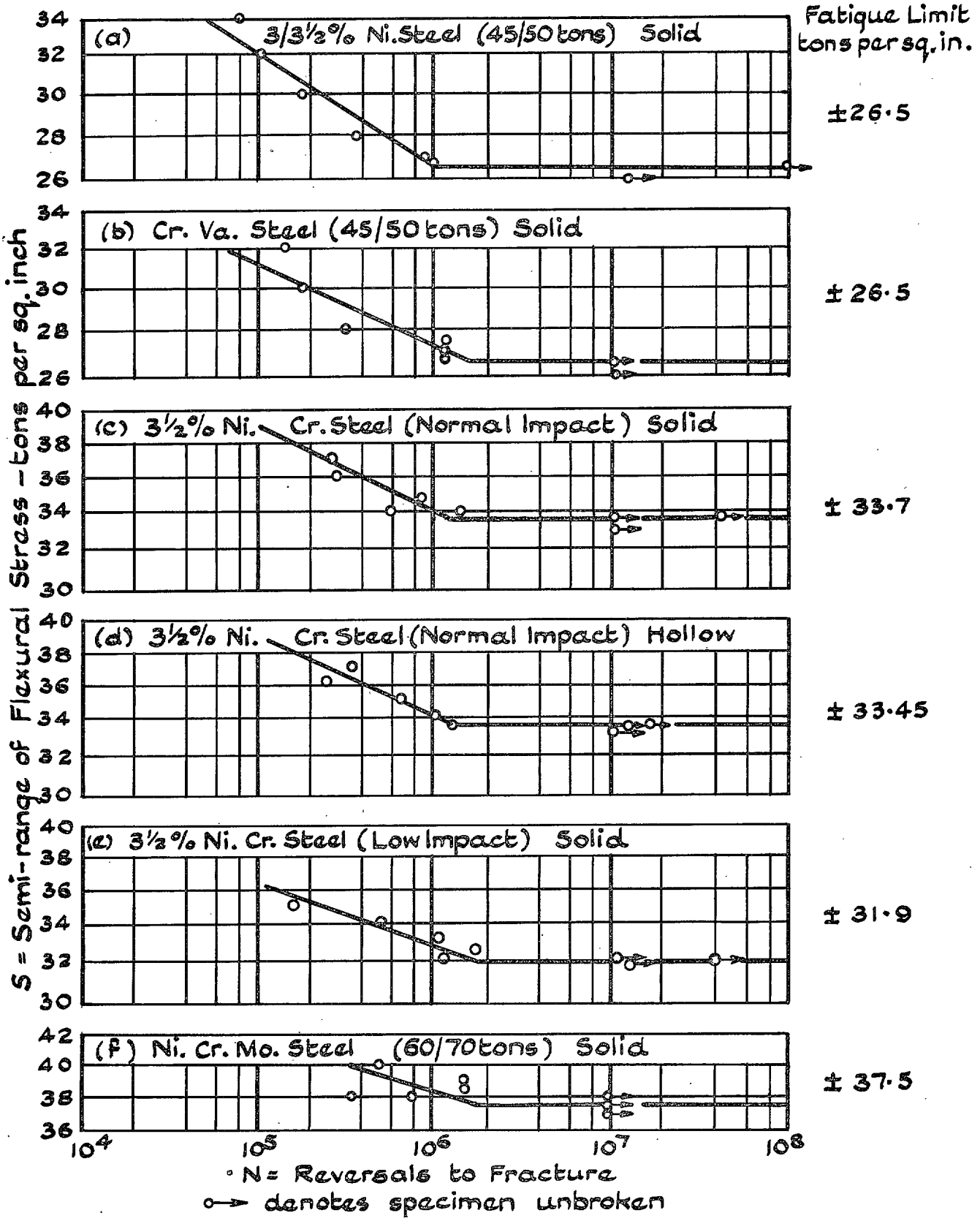

FIG. 27. *S/N* diagrams (Rotating Bar Fatigue Machine).

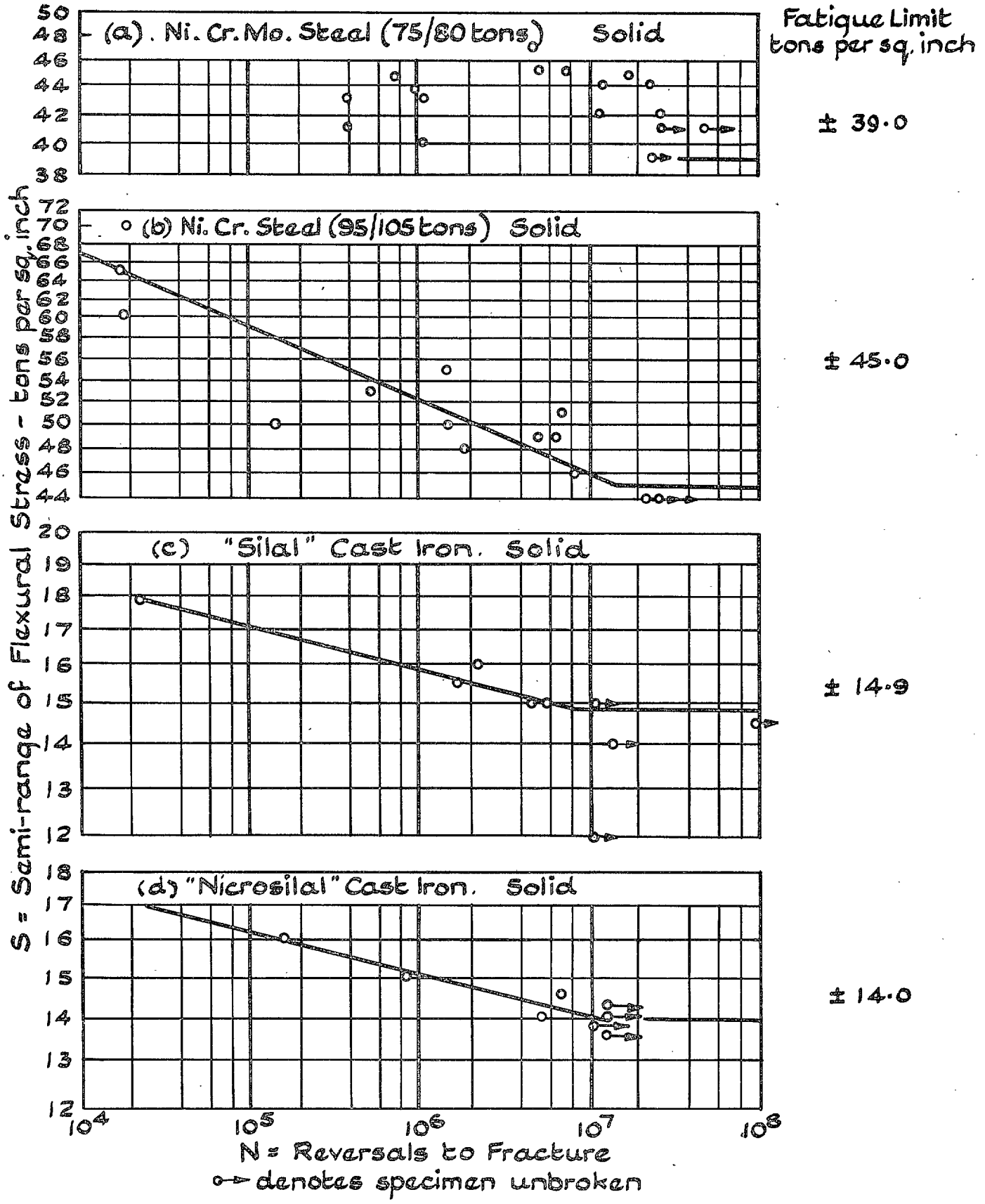

FIG. 28. *S/N* diagrams (Rotating Bar Fatigue Machine).

TABLE 15

RESULTS OF HARDNESS INDENTATION TESTS (2mm. ball, 120 kg. load)

Material	Brinell Hardness No.*	
0·1% C. Steel (Normalised) ..	127, 125, 123, 132.	Av. 127
0·4% C. Steel (Normalised) ..	186, 194, 197, 202.	Av. 195
0·4% C. Steel (Spheroidised) ..	140, 147, 142, 146.	Av. 144
0·9% C. Steel (Pearlitic)	246, 256, 251, 240.	Av. 248
3% Ni. Steel (30/35 ton)	161, 163, 168, 168.	Av. 165
3/3½% Ni. Steel (45/50 ton) ..	231, 239, 240, 238.	Av. 237
Cr. Va. Steel (45/50 ton)	228, 234, 228, 228.	Av. 229
3½% Ni. Cr. Steel (Normal Impact)	282, 284, 281, 279.	Av. 282
3½% Ni. Cr. Steel (Low Impact)	273, 281, 279, 281.	Av. 278
Ni. Cr. Mo. Steel (60/70 ton) ..	325, 330, 320, 325.	Av. 325
Ni. Cr. Mo. Steel (75/80 ton) ..	394, 395, 395, 392.	Av. 394
Ni. Cr. Steel (95/105 ton) ..	486, 485, 472, 474.	Av. 479
'Silal' Cast Iron	At various positions.	Av. 322
'Nicrosilal' Cast Iron	185, 163, 216, 164.	Av. 182

*Note — For each material, the four values quoted, reading from left to right, represent the average of readings taken on indented surfaces parallel to the axis of the bar and distant from it at 0·15, 0·20, 0·25 and 0·30 in., respectively.

as for the steels, the results of one of which have been included in Table 15. The results show, as expected, a much greater variation than in the case of the steels. The variations in 'Nicrosilal' are, perhaps, not unduly excessive in view of the nature of the material and the fact that the size of the cast bars included ½ in. square and $\frac{15}{16}$ in. round bars.

4. Notched Bar Impact Tests

Notched bar impact tests were made on four specimens of each steel and on six specimens of each cast iron. The specimens were of the British Standard form, 10 mm. × 10 mm., as shown in Fig. 4. A single-blow Izod impact machine, having a capacity of 120 ft. lb., was used and in all cases the full striking energy of 120 ft. lb. was employed. The results are as stated in Table 16.

The embrittling treatment applied to the 3½% Ni. Cr. Steel has reduced the normal impact figure of 76 to 5½. The 0·9% C. Steel (Pearlitic) also has a very low impact value (3.3). The remainder of the steels—including the air-hardened Ni. Cr. Steel—have good impact resistances. Both the cast irons exhibit notched-bar brittleness.

5. Rotating Bar Fatigue Tests :—

The fatigue limit of each material, under cycles of reversed bending stresses, has been determined by lengthy endurance tests. The form of Wohler rotating bar machine, developed at the National Physical Laboratory and described by Gough[19], has been used, operating at a frequency of 2,400 stress cycles per minute. The specimen is in the form of a rotating cantilever with a single end-load applied at a horizontal distance of 3 in. from the plane of maximum stress of the test portion of the specimen. For the forms of the hollow and solid specimens used, see Fig. 6.

The results obtained are reproduced, as *S/N* diagrams, plotted to logarithmic co-ordinates, in Fig. 26, 27 and 28.

The values of the fatigue limits are assembled in Table 17 to which has been added the values of the 'Fatigue Ratio', obtained by dividing the fatigue limit by the ultimate tensile strength.

With only two exceptions, all the steels gave very regular results, free from appreciable 'scatter' and having clearly defined fatigue limits.

The *S/N* diagram for 0·4% C. Steel (Normalised) shows how irregularly this material behaved. Examination of the fractured surfaces of the three specimens

TABLE 16

RESULTS OF NOTCHED BAR IMPACT TESTS

Material	Energy Absorbed in Fracture		Remarks on Fracture
	Ft. lb.	Average	
0·1% C. Steel (Normalised) ..	89, 89, 91, 89	89	Fractures partly complete. Silky fibrous.
0·4% C. Steel (Normalised) ..	31, 30, 29, 29	30	Fractures nearly complete. Finely crystalline.
0·4% C. Steel (Spheroidised) ..	31, 33, 32, 32	32	Fractures nearly complete. Finely crystalline.
0·9% C. Steel (Pearlitic)	3·7, 3·1, 3·1, —	3·3	Brittle. Crystalline.
3% Ni. Steel (30/35 ton)	101, 96, 100, 101	100	Fractures about ½ complete. Silky. Horn type.
3/3½% Ni. Steel (40/45 ton).. ..	84, 87, 87, 85	86	Fractures not complete. Silky. Horn type.
Cr. Va. Steel (45/50 ton)	95, 96, 98, 97	96	Fractures about ¾ complete. Slightly fibrous. Horn type.
3½% Ni. Cr. Steel (Normal Impact)	73, 78, 75, 76	76	Fractures not quite complete. Silky fibrous.
3½% Ni. Cr. Steel (Low Impact) ..	6·2, 5·8, 6·1, 3·4	5·4	Brittle. Dull grey.
Ni. Cr. Mo. Steel (60/70 ton) ..	91, 90, 90, 88	90	Fibrous. Horn type.
Ni. Cr. Mo. Steel (75/80 ton) ..	54, 56, 56, 55	55	Fractures nearly complete. Horn type. Silky crystalline.
Ni. Cr. Steel (95/105 ton)	24, 23, 24, 25	24	Horn type. Silky.
'Silal' Cast Iron	0·3, 0·5, 0·4, 0·4, 0·5, 0·6	0·5	Brittle. Finely crystalline.
'Nicrosilal' Cast Iron	1·6, 1·4, 1·4, 1·3, 1·3, 1·4	1·4	Brittle. Finely crystalline with silky spots.

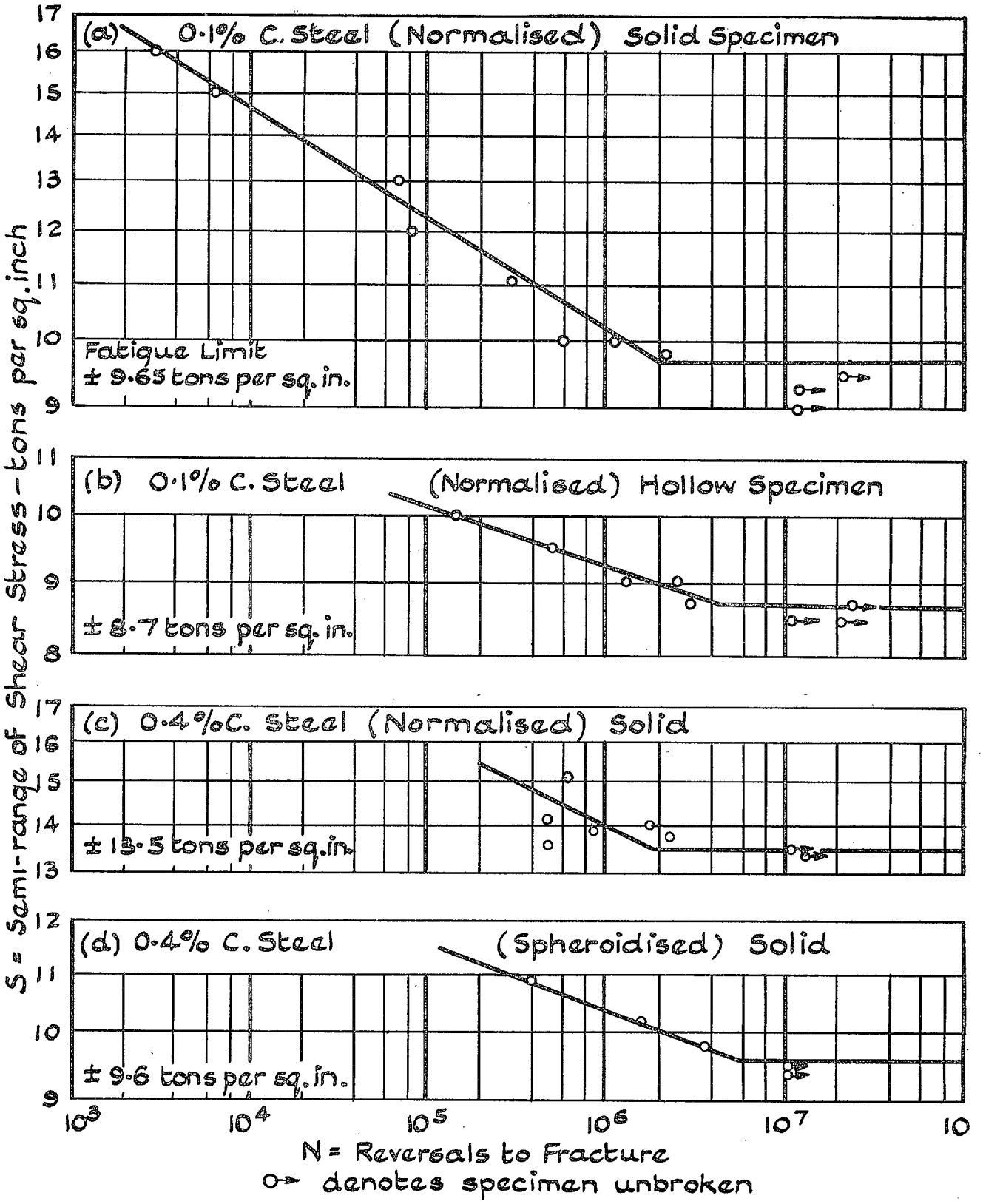

FIG. 29. *S/N* diagrams. Reversed Torsional Fatigue (Stromeyer Machine).

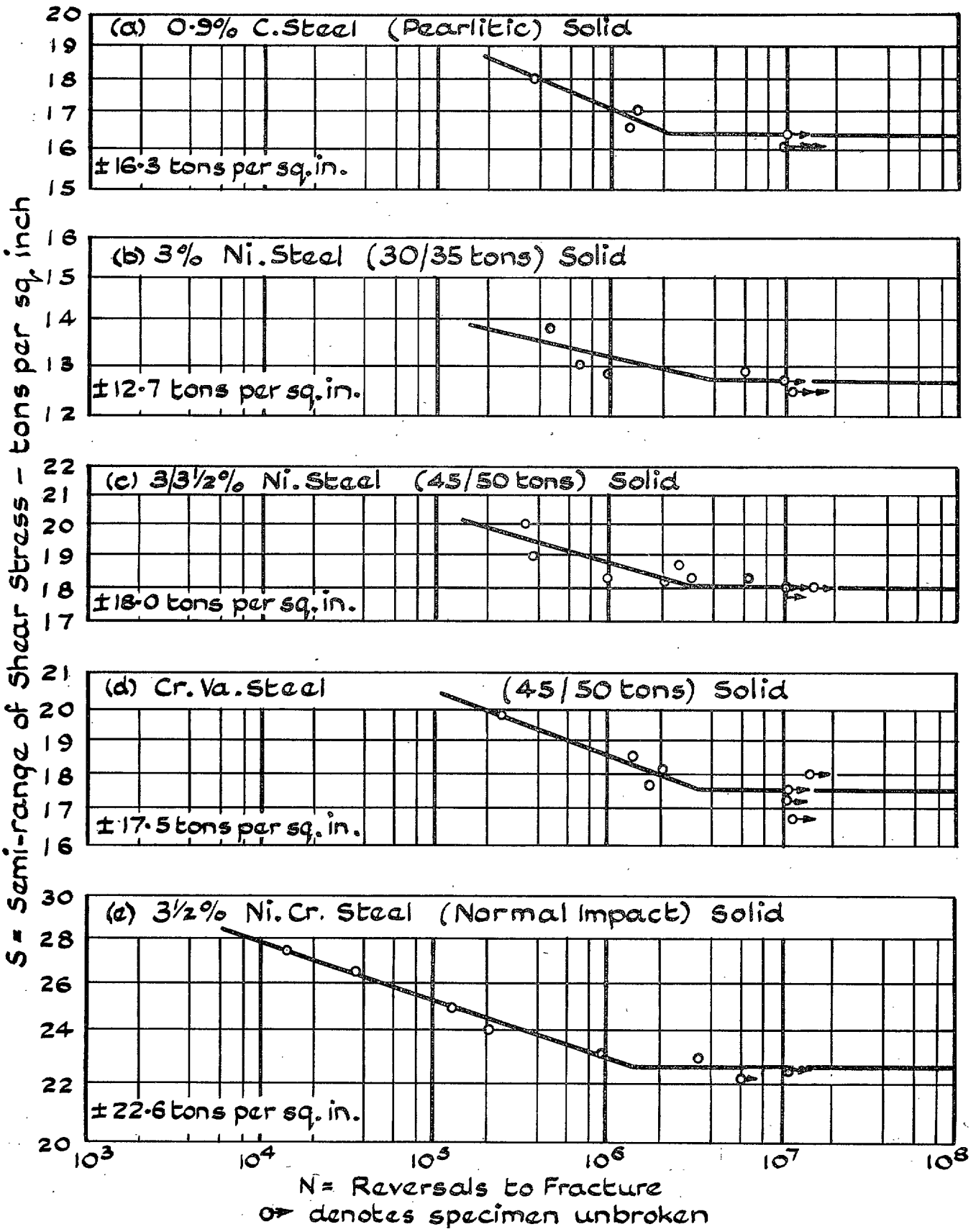

FIG. 30. *S/N* diagrams. Reversed Torsional Fatigue (Stromeyer Machine).

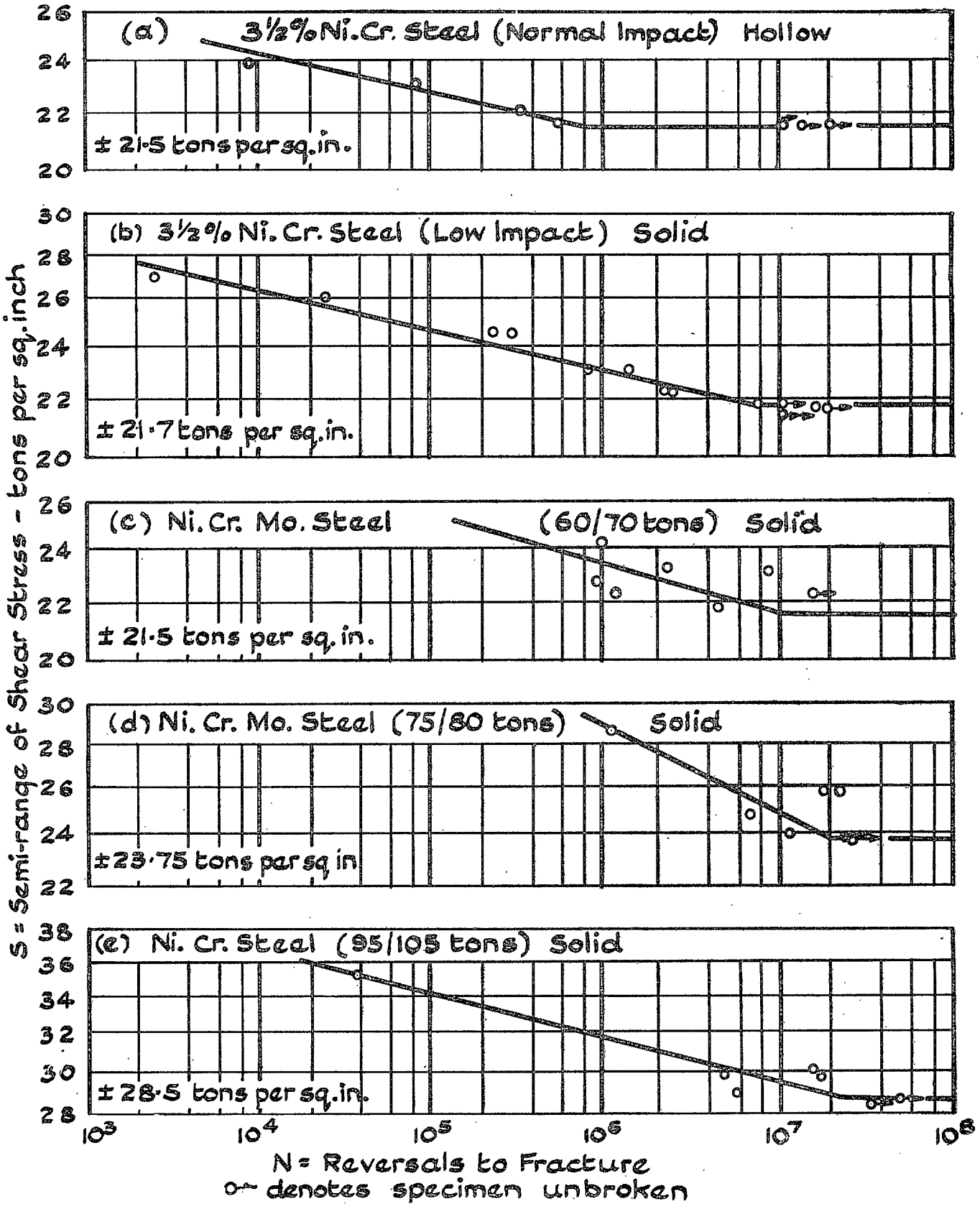

FIG. 31. *S/N* diagrams. Reversed Torsional Fatigue (Stromeyer Machine).

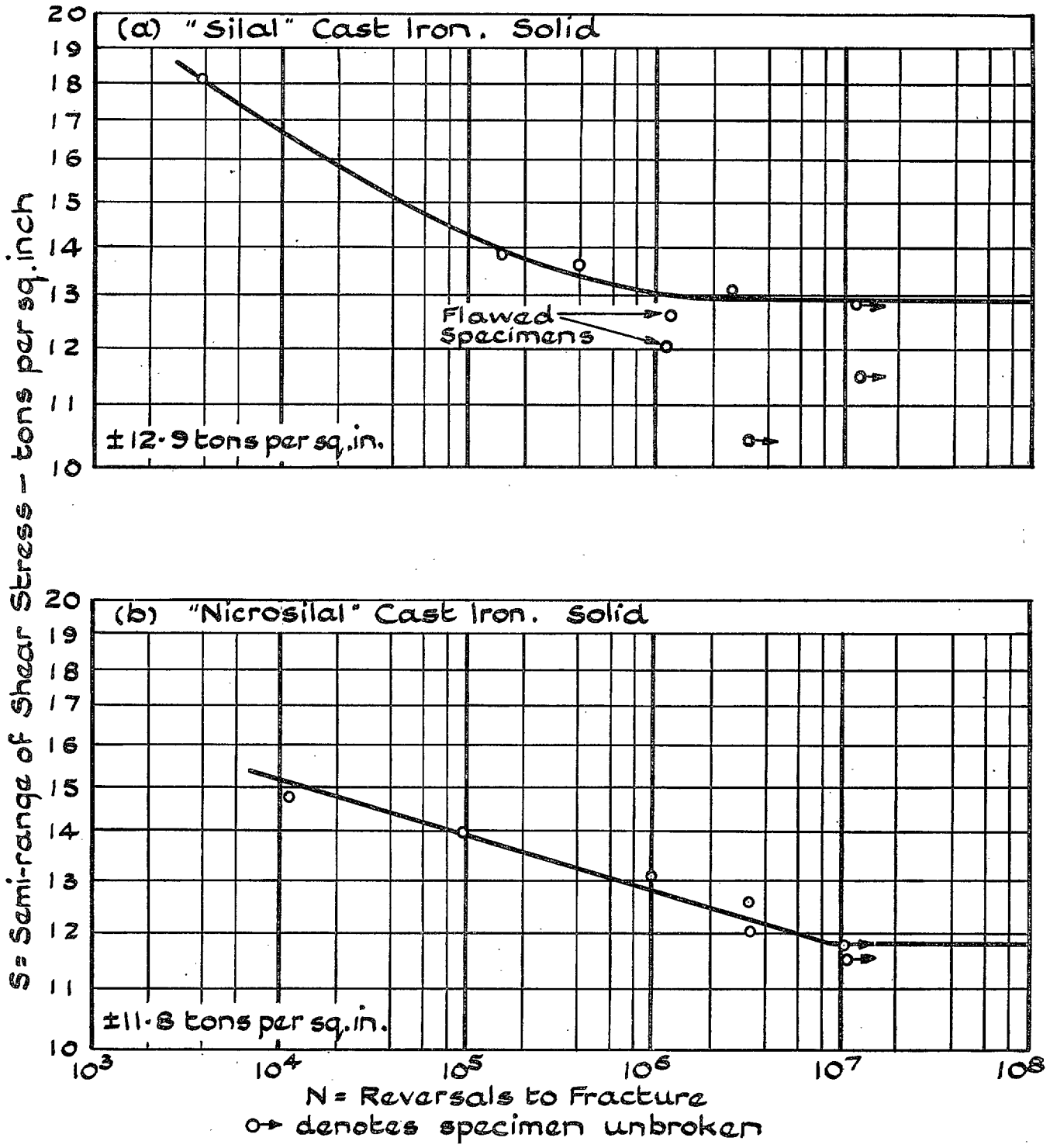

FIG. 32. *S/N* diagrams. Reversed Torsional Fatigue (Stromeyer Machine).

which behaved inconsistently revealed no obvious defects ; the fatigue limit can only be recorded as the bracket values, $\pm$ 15·9 to $\pm$ 17·4 t/in.^{2}. A greater ' scatter ' of results was exhibited by the Ni. Cr. Mo. Steel (75/85 ton) and no reliable value of the fatigue limit emerged ; the approximate value of $\pm$ 39 t/in.^{2} is recorded.

The fatigue properties of ' Silal ' and ' Nicrosilal ' are noteworthy. The actual values of the fatigue limits—$\pm$ 14·9 and $\pm$ 14·0 t/in.^{2}, respectively—are high for cast irons. But it is the ' fatigue ratio ' values of 1·0 and 0·98 which are really remarkable. The typical shapes of the *S/N* curves for these irons show that each material is clearly undergoing fatigue at nominal stresses exceeding the static tensile strength. Even if cast iron is pictured as a metal full of ' flaws ' due to the presence of the graphite flakes, it is surprising to find that the limiting cyclic stress, on a very lengthy endurance basis, sufficient to cause these flaws to develop into cracks, has the same value as the static stress which produces fracture on a single application.

6. Reversed Torsional Fatigue Tests

These tests were made on the machine designed by the late Dr. C. E. Stromeyer, O.B.E., M.I.Mech.E., and presented by him, many years ago, to the National Physical Laboratory ; it has been fully described elsewhere.[19] As the machine applies to the specimen inertia forces due to rocking shafts and flywheels, a close control of speed is essential. This was formerly obtained by using an automatic speed governor designed by the writer. It was further improved, prior to the commencement of the present tests, by replacing the D.C. motor and speed governor by a synchronous A.C. motor ; a 3-speed gear-box was also fitted. Variations in speed were then too small to be detected, provided a suitable source of A.C. was used. During the present tests, the machine was operated at 1,000 stress cycles per minute.

The results of the tests are fully recorded in the *S/N* diagrams of Figs. 29, 30, 31 and 32 and summarised in Table 18. In this table the general direction of the fracture plane, particularly at the apparent source of the principal fatigue cracks, is also noted.

In a bar subjected to a pure torsional couple (static or cyclic), the two sets of planes subjected to wholly tangential stresses (shear) are those perpendicular to the axis of the bar and, also, those containing the axis ; the two sets of mutually perpendicular principal planes are inclined at 45 deg. to the axis of the specimen. Failure under shear would, therefore, normally be associated with transverse and longitudinal fracture planes : failure under principal stress (or strain) with one or both sets of fracture planes inclined at 45 deg. with the former and producing a single-helicoidal fracture (under a unidirectional couple) or a double-helicoidal fracture (under reversed couples). Yet such spiral fractures are a common feature of crankshafts made of steels which are essentially ductile and this curious fact was an unsolved problem of considerable scientific interest for many years. A combined analytical and experimental investigation, by Southwell and Gough[20], supplied an explanation. It was shown that the effect of a small spherical flaw on the surface of a shaft, subjected to a torsional couple, producing a nominal shear stress, *S*,

TABLE 17

RESULTS OF ROTATING BAR FATIGUE TESTS (REVERSED BENDING STRESSES)

Material	Form of Specimen	Fatigue Limit		Ultimate Tensile Strength t/in^2	Fatigue Ratio (F.Lt/U.T.S.)
		t/in^2	Reliability Index		
0·1% C. Steel (Normalised)	Solid	$\pm$17·0	R	27·9	0·61
0·1% C. Steel (Normalised)	Hollow	$\pm$16·5	R	27·9	0·59
0·4% C. Steel (Normalised)	Solid	$\pm$20·8	R	42·0	0·50
0·4% C. Steel (Spheroidised)	Solid	$\pm$15·9 to $\pm$17·4	U	30·9	0·51/0·56
0·9% C. Steel (Pearlitic)	Solid	$\pm$22·2	R	54·9	0·40
3% Ni. Steel (30/35 ton)	Solid	$\pm$20·3	R	34·1	0·60
3/3½% Ni. Steel (45/50 ton)	Solid	$\pm$26·5	R	46·8	0·57
Cr. Va. Steel (45/50 ton)	Solid	$\pm$26·5	R	48·7	0·54
3½% Ni. Cr. Steel (Normal Impact)	Solid	$\pm$33·7	R	58·0	0·58
3½% Ni. Cr. Steel (Normal Impact)	Hollow	$\pm$33·4	R	58·0	0·58
3½% Ni. Cr. Steel (Low Impact)	Solid	$\pm$31·9	R	58·1	0·55
Ni. Cr. Mo. Steel (60/70 ton)	Solid	$\pm$37·5	R	64·8	0·58
Ni. Cr. Mo. Steel (75/80 ton)	Solid	$\pm$39	U	80·5	0·49
Ni. Cr. Steel (95/105 ton)	Solid	$\pm$45	LR	108	0·42
' Silal ' Cast Iron	Solid	$\pm$14·9	R	14·9	1·00
' Nicrosilal ' Cast Iron	Solid	$\pm$14·0	R	14·2	0·98

Note.—With above three exceptions, the Endurance Limit of all materials was clearly defined.

was as follows :—The stress at the surface of the flaw would range from a maximum tension at some point in one principal plane passing through the flaw to a maximum compression of the same amount, $2{\cdot}7S$, at some point on the other, and mutually perpendicular, principal plane also passing through the flaw. If the torsional couple was reversed in sign, the sign of these stresses was also reversed. This intensification was independent of the magnitude of the flaw, provided the latter was infinitesimal compared with the external dimensions of the shaft. Once a crack had commenced on such a helicoidal path, it could be expected to continue to propagate, for some appreciable distance at least, on the same path or paths under the additional stress concentration due to the sharp end of the crack and assisted by the principal tensile stress operating across the edges of the crack. It was concluded that the ' flaws ' responsible for producing helicoidal fractures under fatigue could be (*a*) small surface defects, or (*b*) ultra-microscopic flaws inherent in the structure of the material. The experiments made afforded striking confirmation of the analysis and theory. Reversed torsional fatigue tests were made on two materials, a 0·27% C. Steel and a 0·65% C. Steel ; both were essentially ductile materials, although the latter was, of course, a ' harder ' steel. Hollow thin-walled specimens, with carefully prepared surfaces, were employed. Under reversed torsional fatigue stresses, the 0·27% C. Steel always gave transverse fractures ; the 0·65% C. Steel always gave helicoidal fractures. The tests were then repeated on similar specimens of each material, but having a small radial hole, drilled through one side-wall of the tube, to represent a small flaw. The 0·27% C. Steel then gave perfect double-helicoidal fractures intersecting at the small drilled hole where they originated : the 0·65% C. Steel continued to give helicoidal fractures, also originating at the drilled hole.

The reference to this earlier investigation is relevant to any discussion of the type of fractures observed in the present tests on materials under reversed torsional fatigue. A helicoidal fracture is not necessarily evidence of failure due to principal stress or to a state of inherent brittleness, although either is possible ; it could be produced by the presence of minute surface defects or, possibly, of intrinsic flaws in a material which, by all the tests normally applied in the testing of metals, would be definitely classed as ' ductile '.

Some features of the tabulated results (Table 18) and the *S/N* diagrams call for remark.

Considering first the twelve steels. In four cases, the *S/N* curves show some scatter, but, with one exception, the value of the fatigue limit is fairly closely defined. The striking exception is the Ni. Cr. Mo. Steel (60/70 ton) which gave such great irregularity that only an estimated value of the fatigue limit can be given. No less than eight out of the twelve steels gave helicoidal fractures, but the values of the corresponding ' Fatigue Ratios ' exclude any possibility of failure by principal stress (or strain). With the 3½% Ni. Cr. Steel, whereas the material in its normal form of heat-treatment gave transverse or longitudinal fractures, one effect of the embrittling treatment is to change the fracture to the helicoidal path.

TABLE 18

RESULTS OF REVERSED TORSIONAL FATIGUE TESTS (STROMEYER MACHINE)

Material	Form of Specimen	Fatigue Limit		Plane of Fracture	Ultimate Tensile Strength t/in²	Fatigue Ratio F.Lt/U.T.S.
		t/in²	Reliability Index			
0·1% C. Steel (Normalised) ..	Solid	± 9·6	R	Transverse or Longitudinal	27·9	0·34
0·1% C. Steel (Normalised) ..	Hollow	± 8·7	R	Transverse or Longitudinal	27·9	0·31
0·4% C. Steel (Normalised) ..	Solid	±13·5	R	Helicoidal	42·0	0·32
0·4% C. Steel (Spheroidised) ..	Solid	± 9·6	R	1 Transverse : 2 Helicoidal ..	30·9	0·31
0·9% C. Steel (Pearlitic)	Solid	±16·3	R	Helicoidal	54·9	0·30
3% Ni. Steel (30/35 ton)	Solid	±12·7	R	Helicoidal	34·1	0·37
3/3½% Ni. Steel (45/50 ton) ..	Solid	±18·0	R	Transverse	46·8	0·38₅
Cr. Va. Steel (45/50 ton)	Solid	±17·5	LR	Helicoidal	48·7	0·36
3½% Ni. Cr. Steel (Normal Impact)	Solid	±22·6	R	Transverse or Longitudinal ..	58·0	0·39
3½% Ni. Cr. Steel (Normal Impact)	Hollow	±21·5	R	Transverse or Longitudinal ..	58·0	0·37
3½% Ni. Cr. Steel (Low Impact) ..	Solid	±21·7	R	Helicoidal	58·1	0·37
Ni. Cr. Mo. Steel (60/70 ton) ..	Solid	±21·5 (estimated)	U	Helicoidal	64·8	0·33 (estimated)
Ni. Cr. Mo. Steel (75/80 ton) ..	Solid	±23·8	R	Transverse	80·5	0·30
Ni. Cr. Steel (95/105 ton)'	Solid	±28·5	R	Helicoidal	108	0·26
' Silal ' Cast Iron	Solid	±12·9	R	Helicoidal	14·9	0·87
' Nicrosilal ' Cast Iron	Solid	±11·8	R	Helicoidal	14·2	0·83

Turning to the cast irons. Justifiably rejecting two specimens, the fractured surfaces of which contained quite large defects, the torsional fatigue limit of ' Silal ' is clearly defined at $\pm$ 12·9 t/in.^{2}, giving the abnormally high value of 87% for the Fatigue Ratio. Every specimen fractured along a single or double helicoidal path. These two facts in combination give a strong indication that this is a brittle material whose fracture is largely controlled by principal stress (or strain). As shown in the S/N diagram, ' Nicrosilal ' gave extremely consistent results, with a clearly defined fatigue limit of $\pm$ 11·8 t/in.^{2} ; also, as with the ' Silal ', an exceptionally high value of the Fatigue Ratio, in this case 83% (Silal 87%). All the fractures were of the single helicoidal type. Further discussion of the degree of correspondence of the fracture planes of both irons with the planes of principal stress (or strain) is deferred until the results of the combined stress experiments are discussed.

APPENDIX 3

RESULTS OF TESTS MADE IN THE NO. 1 COMBINED FATIGUE STRESS MACHINES

The machine has been fully described in Part I, Section 1 of this paper, also the stressing system applied by the machine. Each individual machine was run at its experimentally-determined resonant frequency which varied only slightly from machine to machine.

Fatigue limits were determined by the usual method of endurance tests, carried out on a minimum reversals basis of 10^7. Wherever possible, sufficient numbers of specimens and small differences of applied stress range were used to evaluate the fatigue limit within close limits. As special importance was attached to a close evaluation of the 'end points'—$\theta = 0$ deg. (reversed plane bending) and $\theta = 90$ deg. (reversed torsion)—a greater number of specimens was usually devoted to these particular tests. As a result, the majority of the materials gave fatigue values on which considerable reliance can be placed ; in a few cases, the irregularity of the material produced an unfavourable ' scatter ' of results.

Each machine is fitted with a trip gear which switches off the driving motor when a small increase occurs, during the test, in the cyclic range of strain of the specimen. This trip gear lends itself to very close adjustment of setting and by this means, in tests made on the steels, the majority were stopped in the very early stages of crack development. In fact, only rarely did a steel specimen fracture ; in many cases, the crack was so small that it could not be detected visually without the aid of a low-power microscope. On every specimen which failed during the endurance test, observations and measurements were made of the trace of the crack on the surface of the specimen at and near the apparent origin of the crack ; the inclinations to the trace of a transverse reference plane passing through the same point were recorded. Such two-dimensional surface measurements are clearly not sufficient, even in the most favourable circumstances, to define either original fracture planes or the planes along which fatigue cracks have propagated. For fatigue cracks in general rarely follow regularly a definite path, but tend to branch and change direction, often in an apparently entirely haphazard manner. But it was considered of worthwhile interest to make the observations, particularly as the regular variation of applied stress conditions—from $\theta = 0$ deg. to $\theta = 90$ deg.—furnished an exceptional opportunity of observing if the crack directions exhibited any consistent changes, which could be correlated with the variations in those stress conditions. Where the recorded observations have proved to be so irregular or so ambiguous as to be misleading, no reference to those observations is included in the following record of the results. Where, however, the direction of the initial crack and/or the subsequent path followed shows some definite and consistent tendency as the stress conditions change, the limit values of the inclinations are recorded and, for comparison, the inclination (always equal to $\theta/2$) of the trace of the plane of maximum principal stress to the transverse reference plane is given.

Referring to Fig. 3, for each material and form of specimen, the fatigue limit was determined at seven values of θ, the angle between the vertical planes containing the axes of the loading arm and specimen. The values are :—$\theta = 0$ deg. (reversed plane bending), $\theta = 90$ deg. (reversed torsion) and seven combinations, given by $\theta = 15$, 30, 45, 60 and 75 deg.

We have seen (Part I, Section 1) that :—

Flexural stress, f, due to bending moment $= \pm KM \cos\theta$

Shear stress q, due to twisting moment $= \pm \frac{1}{2}KM \sin\theta$

Maximum shear stress, S $= \pm \frac{1}{2}KM$.

where M is the moment applied to the specimens through the loading arm and K is a constant, determined entirely by the form and dimensions of the specimen. It is convenient to use the maximum shear stress value, also, stating, of course, the relevant value of θ, to express applied stress conditions in any particular series of experiments in which K has a constant value ; the corresponding values of f and q are directly given by $2S \cos\theta$ and $S \sin\theta$, respectively. The stress-endurance diagrams are thus presented as Maximum Shear Stress/N diagrams.

Because of the very large number of experiments made, the results are presented in the three separate groups of tests which form the programme, i.e. using (*a*) solid round specimens, (*b*) hollow circular specimens, and (*c*) solid round specimens containing a discontinuity in the form of a ' sharp ' Vee groove.

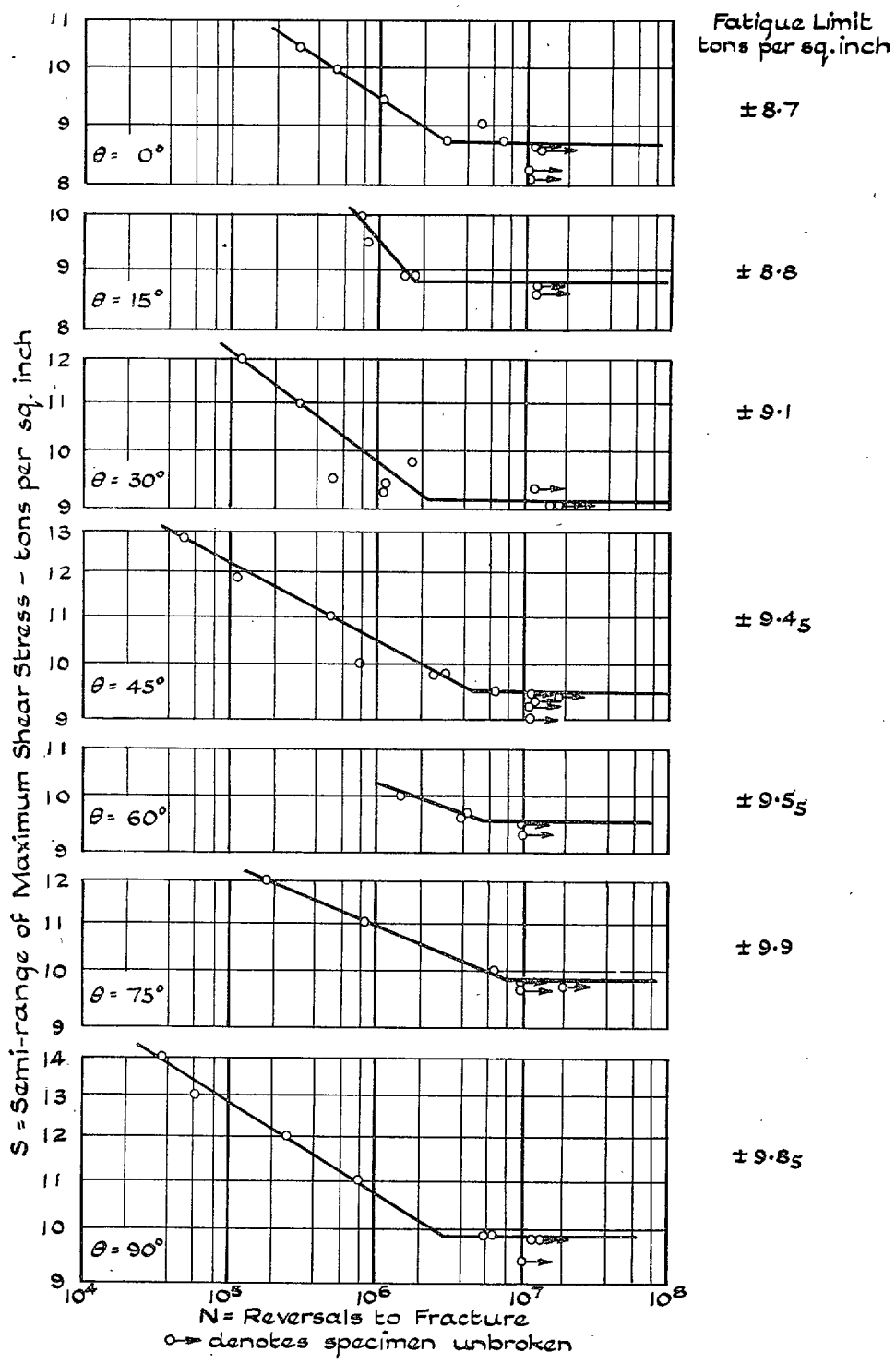

FIG. 33. *S/N* diagrams for 0·1% C. Steel (Normalised). Solid Specimens.

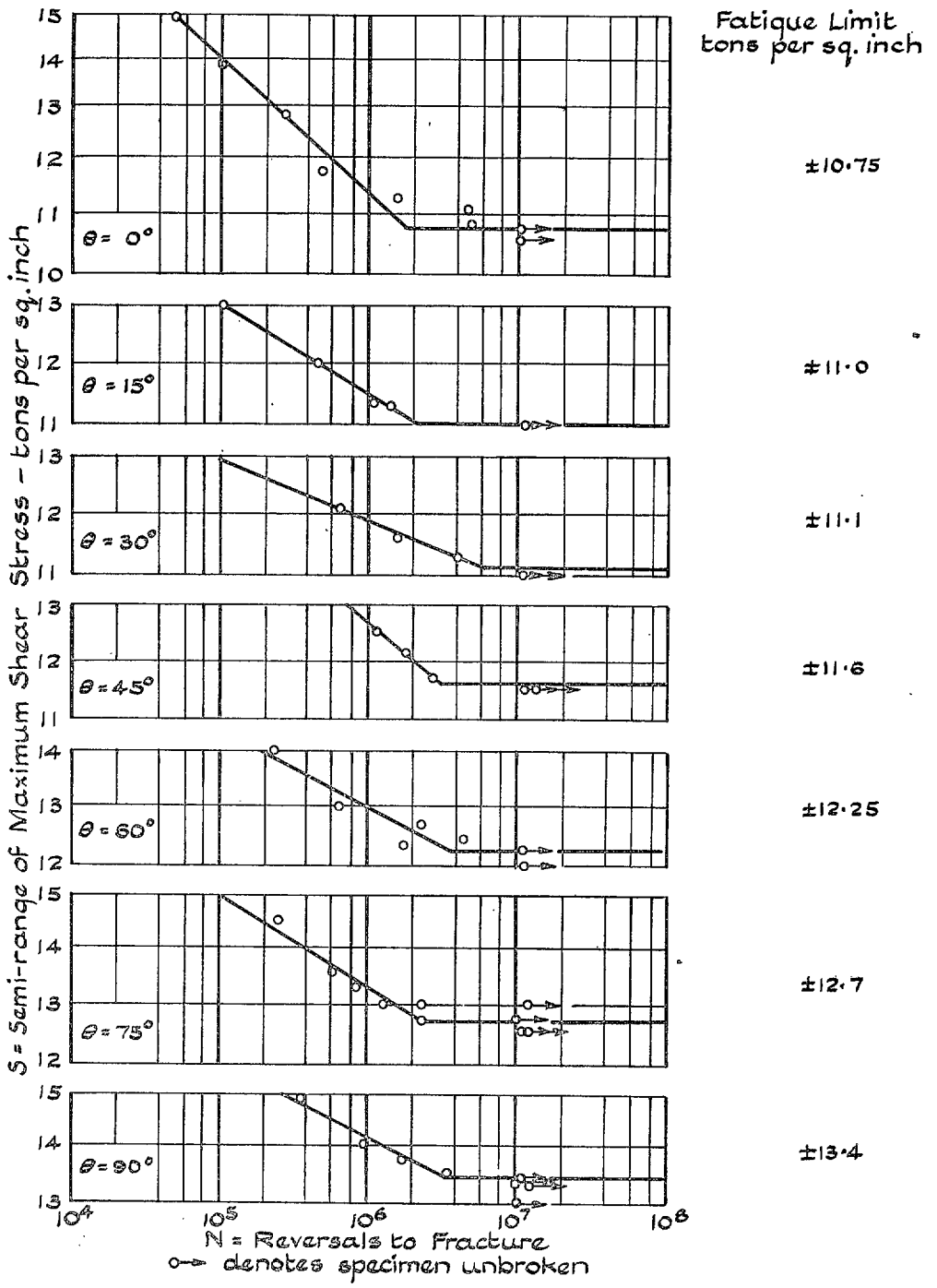

FIG. 34. *S/N* diagrams for 0·4% C. Steel (Normalised). Solid Specimens.

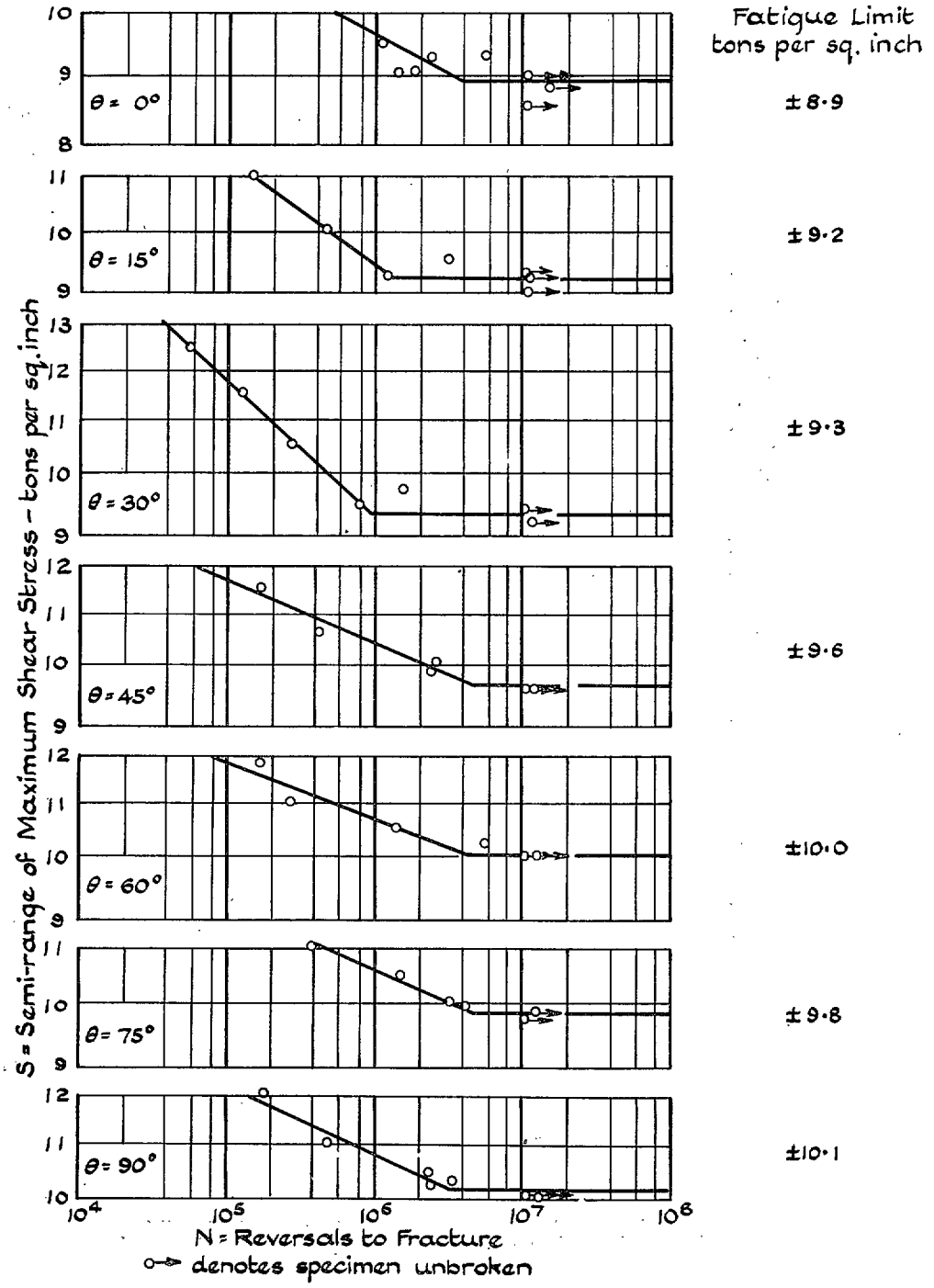

FIG. 35. *S/N* diagrams for 0·4% C. Steel (Spheroidised). Solid Specimens.

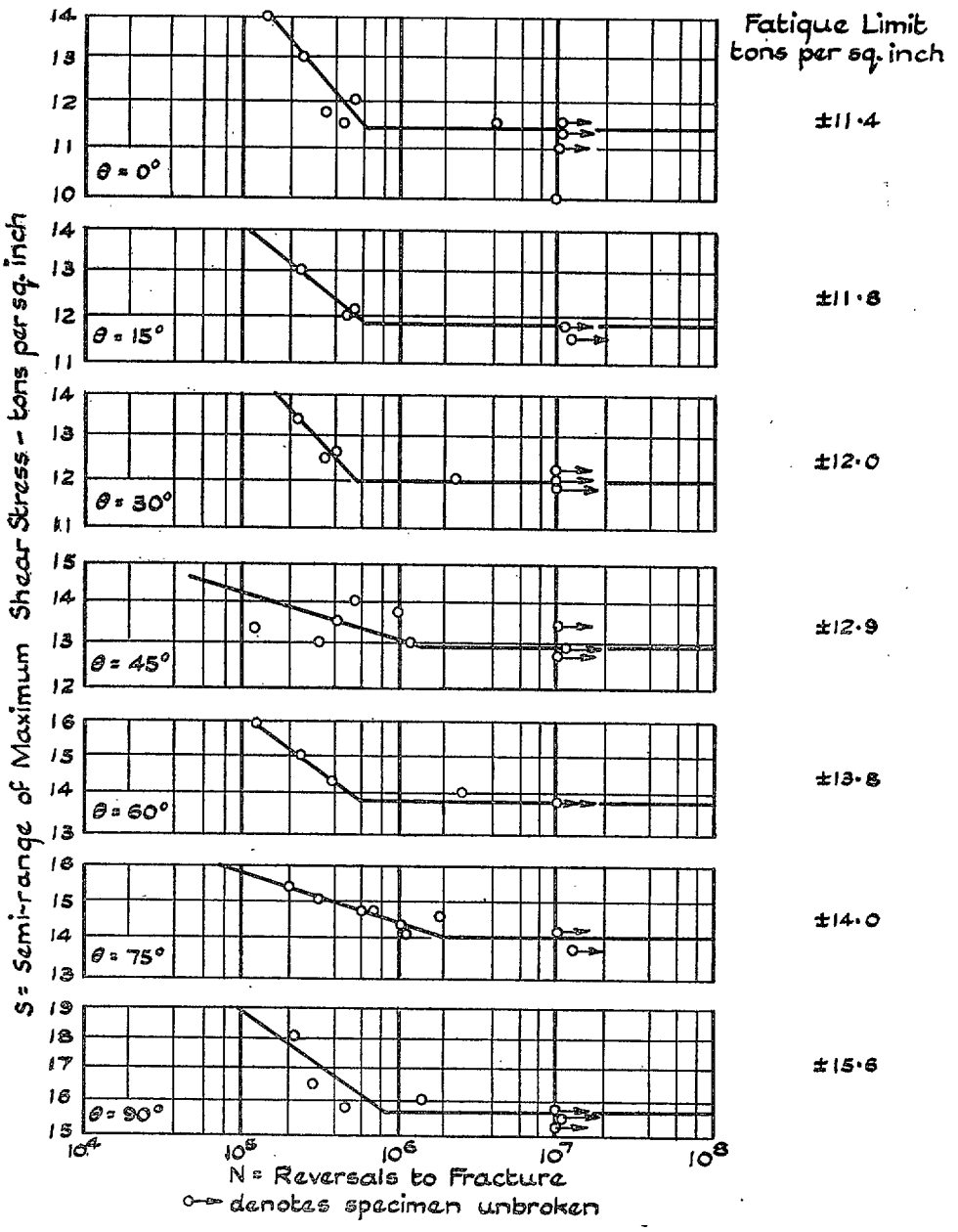

FIG. 36. *S/N* diagrams for 0·9% C. Steel (Pearlitic). Solid Specimens.

RESULTS OF COMBINED FATIGUE TESTS MADE ON SOLID SPECIMENS OF CIRCULAR SECTION

The form and dimensions of the specimen are as shown in Fig. 4.

(*a*) 0·1% C. Steel (Normalised). The *S/N* diagrams are shown in Fig. 33. The results plot very regularly and the fatigue limits are clearly defined within very close limits. The measurements of the traces of the fatigue cracks gave very irregular results and revealed no consistent tendency to change with the change in the applied stressing conditions ; although under pure shear ($\theta = 90$ deg.) failure obviously occurred on planes of maximum shear, under no conditions of combined stress did this occur. In their simplest form, the fatigue limits can be expressed thus :—

Value of θ deg.	*Fatigue Limit* (Max. shear stress) t/in.²	*Reliability Index*
0	±8·7	R
15	±8·8	R
30	±9·1	R
45	$\pm 9{\cdot}4_5$	R
60	$\pm 9{\cdot}5_5$	R
75	±9·9	R
90	$\pm 9{\cdot}8_5$	R

(*b*) 0·4% C. Steel (Normalised). The *S/N* diagrams are shown in Fig. 34. The results plot regularly and, with the possible exception at $\theta = 75$ deg., all the fatigue limits are closely defined. The traces of some of the fatigue cracks were typically ragged and the measurements taken at the apparent origins of the cracks were irregular. As the cracks developed and branched, there was some measure of agreement with their traces and those of planes of maximum principal stress.

The results are as follows :—

Value of θ deg.	*Fatigue Limit* (Max. shear stress) t/in.²	*Reliability Index*
0	$\pm 10{\cdot}7_5$	R
15	±11·0	R
30	±11·1	R
45	±11·6	R
60	$\pm 12{\cdot}2_5$	R
75	±12·7	LR
90	±13·4	R

As noted in Table 18, this material, when tested in the Stromeyer machine, exhibited helicoidal fractures.

(*c*) 0·4% C. Steel (Spheroidised). The *S/N* diagrams are shown in Fig. 35. The results plot regularly, a few specimens excepted, and the fatigue limits are closely defined. At each angle of test, with the exceptions of $\theta = 30$ deg. (where fairly good agreement with maximum principal stress planes was observed in every specimen) and $\theta = 0$ deg. (where fracture always occurred on transverse or longitudinal planes), some specimens gave transverse fractures, while others agreed quite well with planes of maximum principal stress. The material thus appeared to be almost equally liable to these two forms of fracture : similar behaviour was observed in the Stromeyer tests. Alternatively, the results can be dismissed as irregular. (See Table 18.) The results are as follows :—

Value of θ deg.	*Fatigue Limit* (Max. shear stress) t/in.²	*Reliability Index*	*Inclination to Transverse Plane* (degrees) (*a*) *Of plane of max. princ. stress*	(*b*) *Of measured traces of cracks*
0	± 8·9	R	0	0 to 1
15	± 9·2	R	7½	2 to 7
30	± 9·3	R	15	11 to 17
45	± 9·6	R	22½	−3 : also 22 to 26
60	±10·0	R	30	0 and 3, also 30
75	± 9·8	R	37½	2 also 37
90	±10·1	R	45	−14 to 5, branching at 28 to 60.

(*d*) 0·9% C. Steel (Pearlitic). The *S/N* diagrams are shown in Fig. 36. With one exception ($\theta = 45$ deg.) the data plot regularly and the fatigue limits are closely defined. At all values of θ, the traces of the cracks are in fair general agreement with the trace of the plane of maximum principal stress. The results are as follows :—

Value of θ deg.	*Fatigue Limit* (Max. shear stress) t/in.²	*Reliability Index*	*Inclination to Transverse Plane* (degrees) (*a*) *Of plane of max. princ. stress*	(*b*) *Of measured traces of cracks*
0	±11·4	R	0	0 to 1½
15	±11·8	R	7½	7½ to 9½
30	±12·0	R	15	13½ to 14½
45	±12·9	LR	22½	21 to 23
60	±13·8	R	30	28½ to 34
75	±14·0	R	37½	37 to 42
90	±15·6	R	45	42 to 57

(*e*) 3% Ni. Steel (30/35 ton). The *S/N* diagrams are shown in Fig. 37. With the exception of the tests at 60 deg., the data plot regularly : all the fatigue limits are closely defined. The traces of some of the cracks were approximately transverse, others appeared to be in rough agreement with the trace of the maximum principal stress plane ; both types often occurred on different

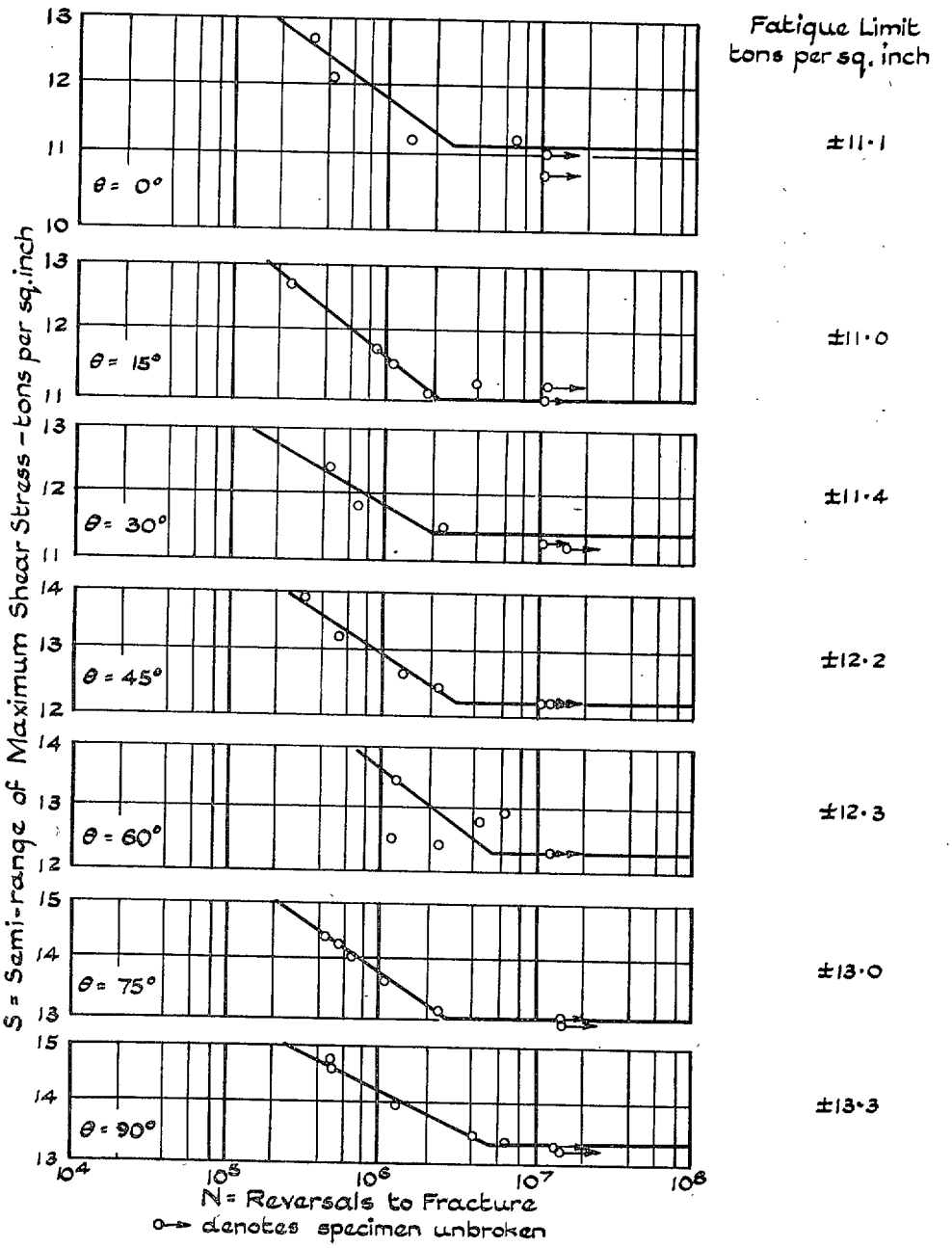

FIG. 37. *S/N* diagrams for 0·3% Ni. Steel (30/35 ton). Solid Specimens.

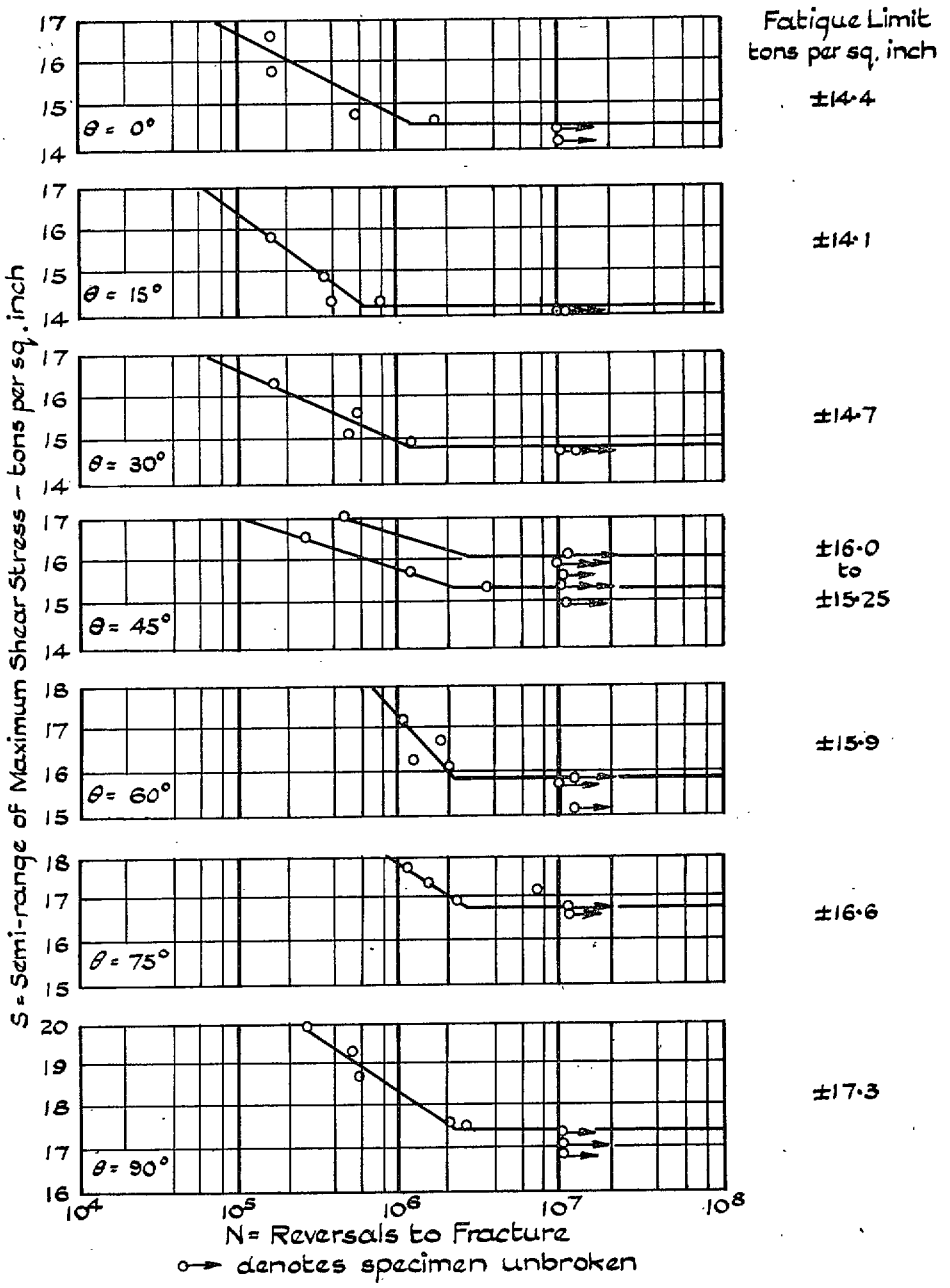

FIG. 38. *S/N* diagrams for 3/3½% Ni. Steel (45/50 ton). Solid Specimens.

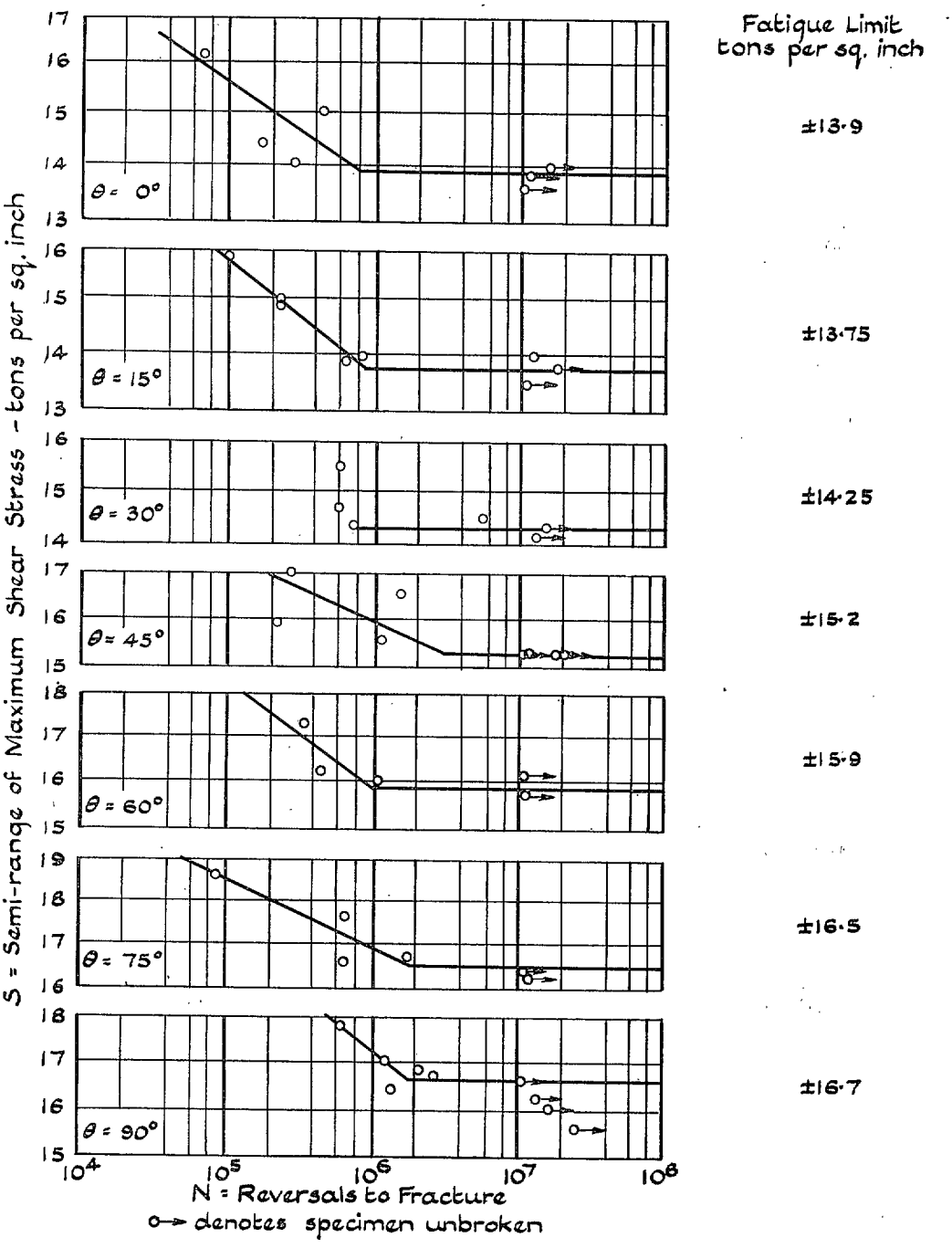

FIG. 39. *S/N* diagrams for Cr. Va. Steel (45/50 ton). Solid Specimens.

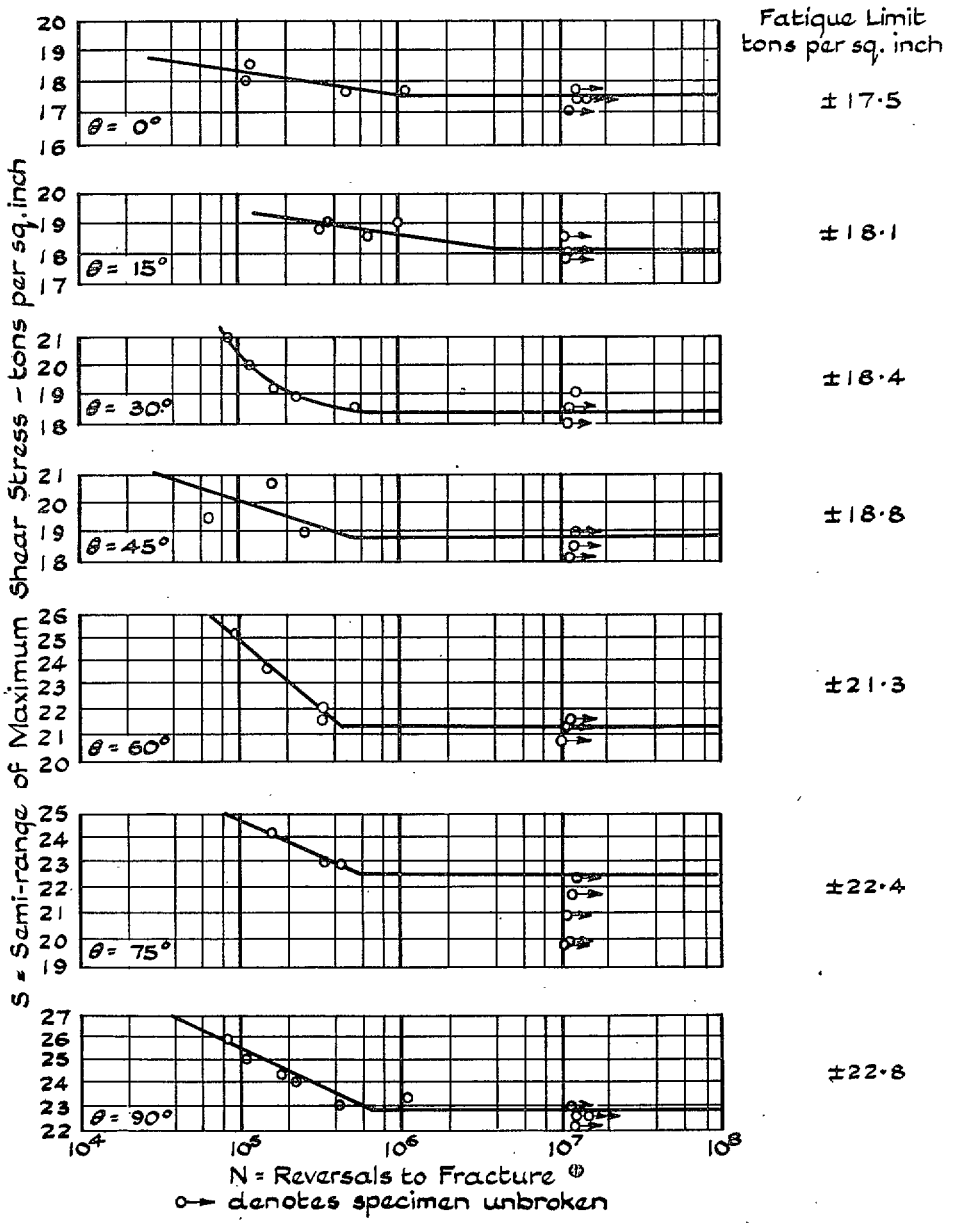

FIG. 40. *S/N* diagrams for 3½% Ni. Cr. Steel (Normal Impact). Solid Specimens.

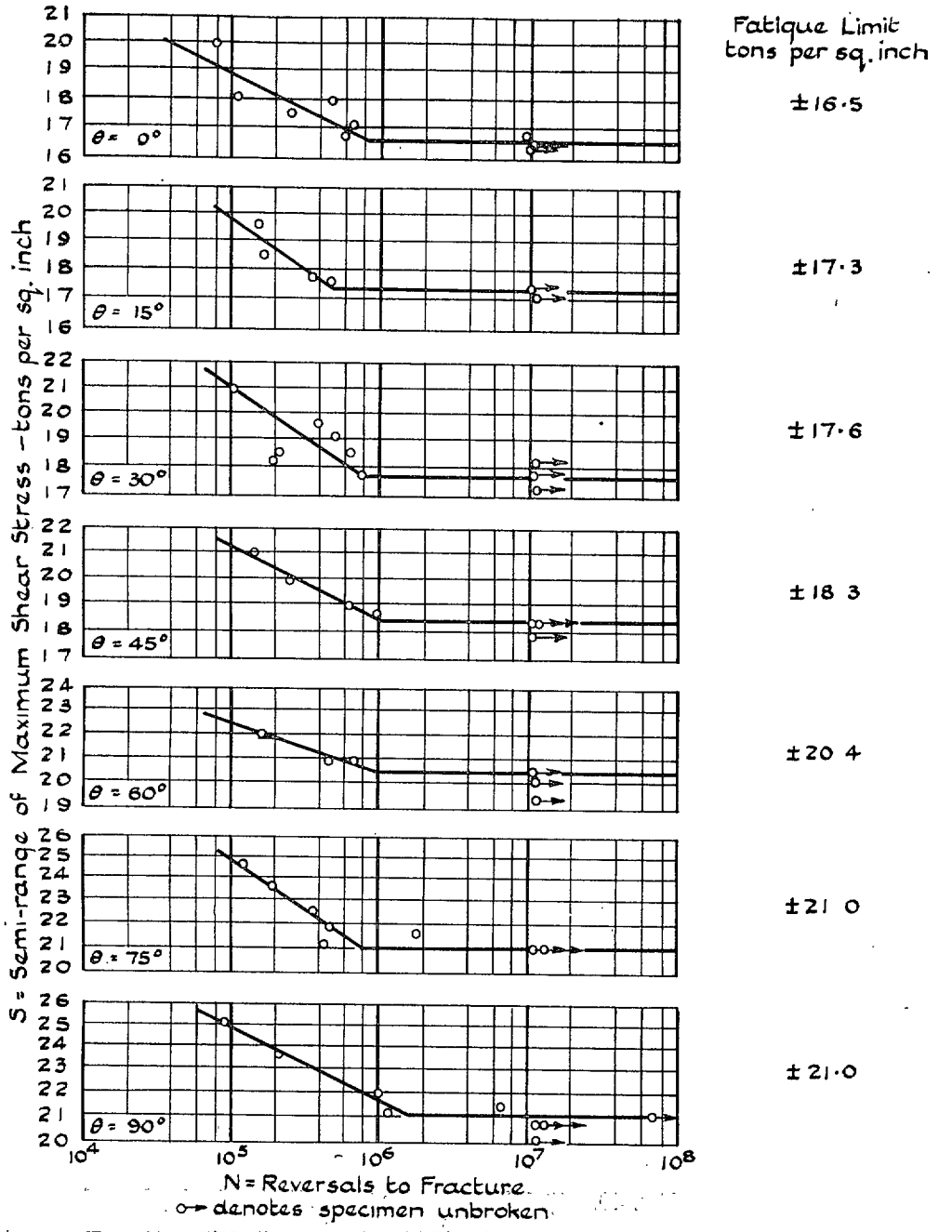

FIG. 41. *S/N* diagrams for $3\frac{1}{2}\%$ Ni. Cr. Steel (Low Impact). Solid Specimens.

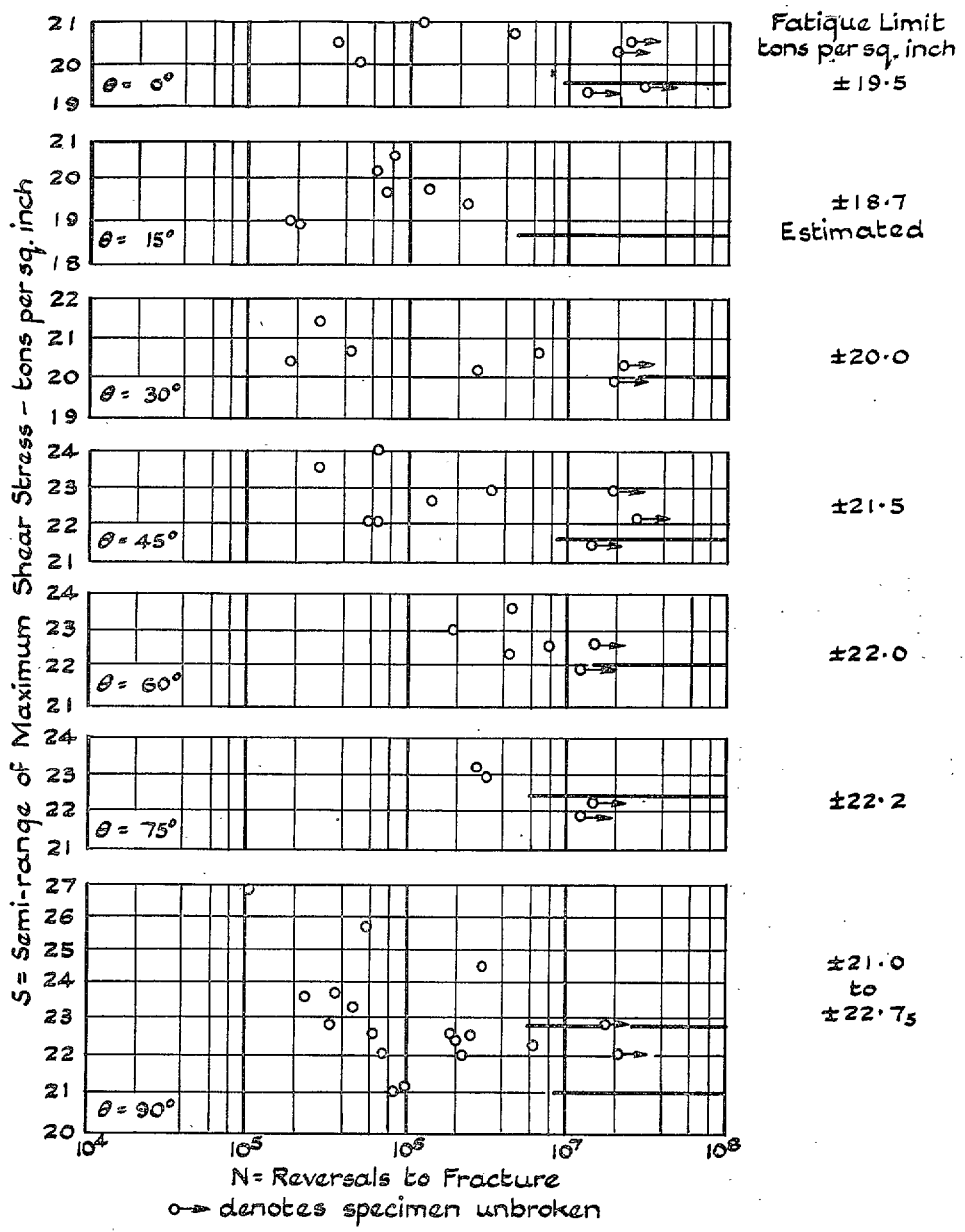

FIG. 42. *S/N* diagrams for Ni. Cr. Mo. Steel (60/70 ton). Solid Specimens.

specimens tested at the same θ value. But the irregularity is so great that no real significance can be attached to the observations. The results are as follows :—

Value of θ deg.	*Fatigue Limit* (Max. shear stress) t/in.²	*Reliability Index*
0	±11·1	R
15	±11·0	R
30	±11·4	R
45	±12·2	R
60	±12·3	R
75	±13·0	R
90	±13·3	R

(*f*) 3/3½ Ni. Steel (45/50 ton). The *S/N* diagrams are shown in Fig. 38. With one exception ($\theta = 45$ deg.) the data plot regularly and the fatigue limits are clearly defined. In the tests at $\theta = 45$ deg., although the bracket values of ± 15¼ to ± 16·0 t/in.² are noted on the *S/N* diagram, the two fractures at ± 15·3 and ± 15·6 t/in.² cannot be ignored and the safe value of ± 15¼ t/in.² has been adopted. Wide irregularity was observed in the inclinations of the fracture planes ; there was some evidence that as the cracks developed they tended to follow the trace of the plane of maximum principal stress but this is really uncertain. The results are as follows :—

Value of θ deg.	*Fatigue Limit* (Max. shear stress) t/in.²	*Reliability Index*
0	±14·4	R
15	±14·1	R
30	±14·7	R
45	±15·2₅	LR
60	±15·9	R
75	±16·6	R
90	±17·3	R

(*g*) Cr. Va. Steel (45/50 ton). The *S/N* diagrams are shown in Fig. 39. Some scatter occurred in some groups, but the fatigue limits at each of the seven conditions of stressing are satisfactorily definite. The measured traces of the cracks even in any one group of θ value, showed very wide irregularity among themselves. The results are as follows :—

Value of θ deg.	*Fatigue Limit* (Max. shear stress) t/in.²	*Reliability Index*
0	±13·9	R
15	±13·7₅	R
30	±14·2₅	LR
45	±15·2	R
60	±15·9	LR
75	±16·5	R
90	±16·7	R

(*h*) 3½% Ni. Cr. Steel (Normal Impact). The *S/N* diagrams are shown in Fig. 40. The results plot remarkably regularly and the fatigue limits are closely defined. All specimens failed by cracks whose directions showed merely slight and irregular deviations from the transverse direction. The results are as follows :—

Value of θ deg.	*Fatigue Limit* (Max. shear stress) t/in.²	*Reliability Index*
0	±17·5	R
15	±18·1	R
30	±18·4	R
45	±18·8	R
60	±21·3	R
75	±22·4	R
90	±22·8	R

(*i*) 3½% Ni. Cr. Steel (Low Impact). The *S/N* diagrams are shown in Fig. 41. With few exceptions, all the data plot regularly and all the fatigue limits are closely defined. The inclinations of the traces of the fatigue cracks were so irregular as to afford no indication as to any common identification. The results are as follows :—

Value of θ deg.	*Fatigue Limit* (Max. shear stress) t/in.²	*Reliability Index*
0	±16·5	R
15	±17·3	R
30	±17·6	LR
45	±18·3	R
60	±20·4	R
75	±21·0	R
90	±21·0	R

(*j*) Ni. Cr. Mo. Steel (60/70 ton). The *S/N* diagrams are shown in Fig. 42 and reveal the extremely irregular manner in which this material behaved under test. Such irregularity is often obtained with high-tensile heat-treated steels which, moreover, are sensitive to small surface defects. The magnitude of the whole programme simply did not permit the multiplication of specimens used to the point at which a ' statistical ' value of the fatigue limit would emerge. The scatter is so pronounced that little real significance can be attached to the tabulated values of the fatigue limits : they can be taken only as indications. The orientation of the traces of the cracks, many of which ' branched ', were most irregular and apparently random. The results are as follows :—

Value of θ deg.	*Fatigue Limit* (Max. shear stress) t/in.²	*Reliability Index*
0	±19·5	LR
15	±18·7	U
30	±20·0	LR
45	±21·5	LR
60	±22·0	LR
75	±22·2	LR
90	±21 to ±22¾	U

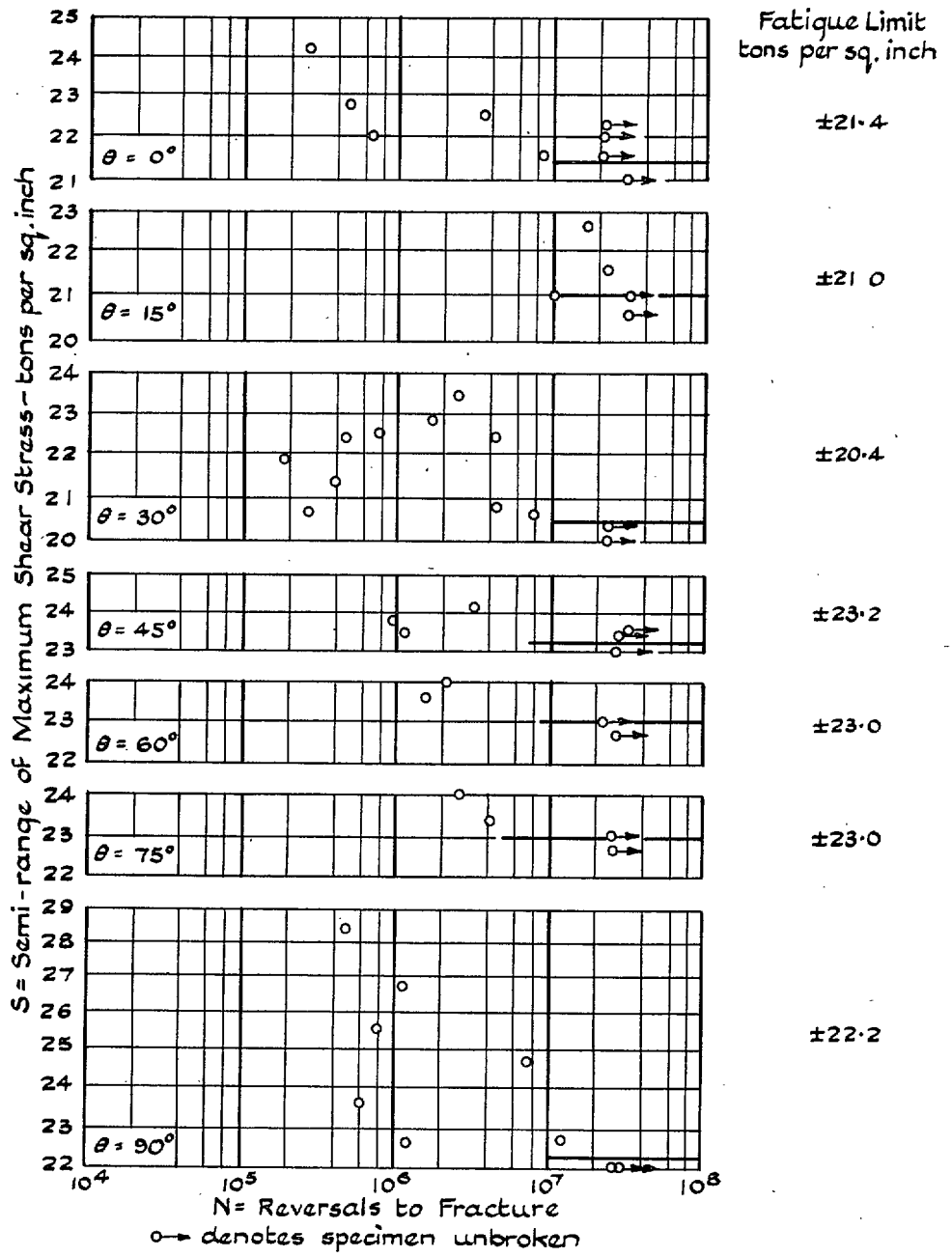

FIG. 43. *S/N* diagrams for Ni. Cr. Mo. Steel (75/80 ton). Solid Specimens.

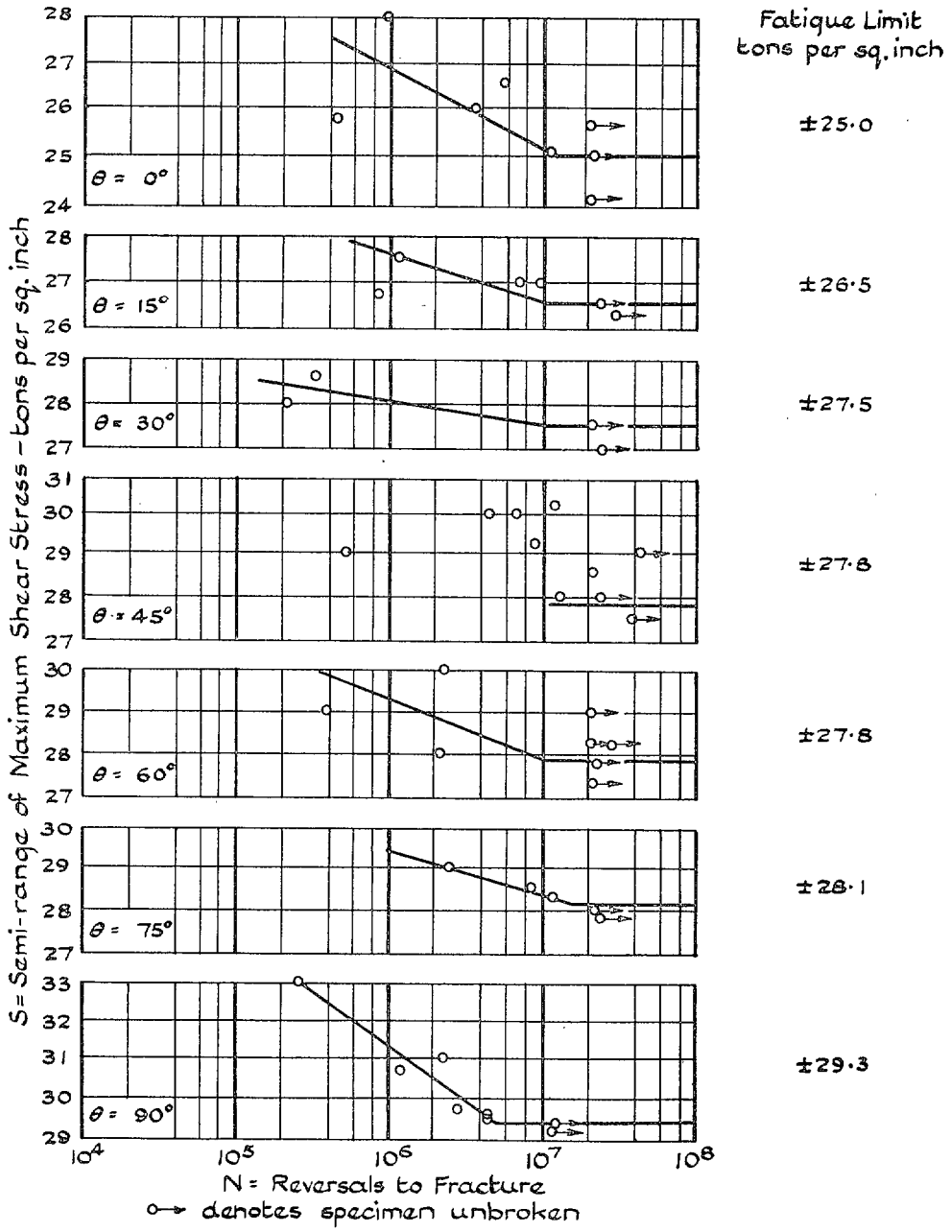

FIG. 44. *S/N* diagrams for Ni. Cr. Steel (95/105 ton). Solid Specimens.

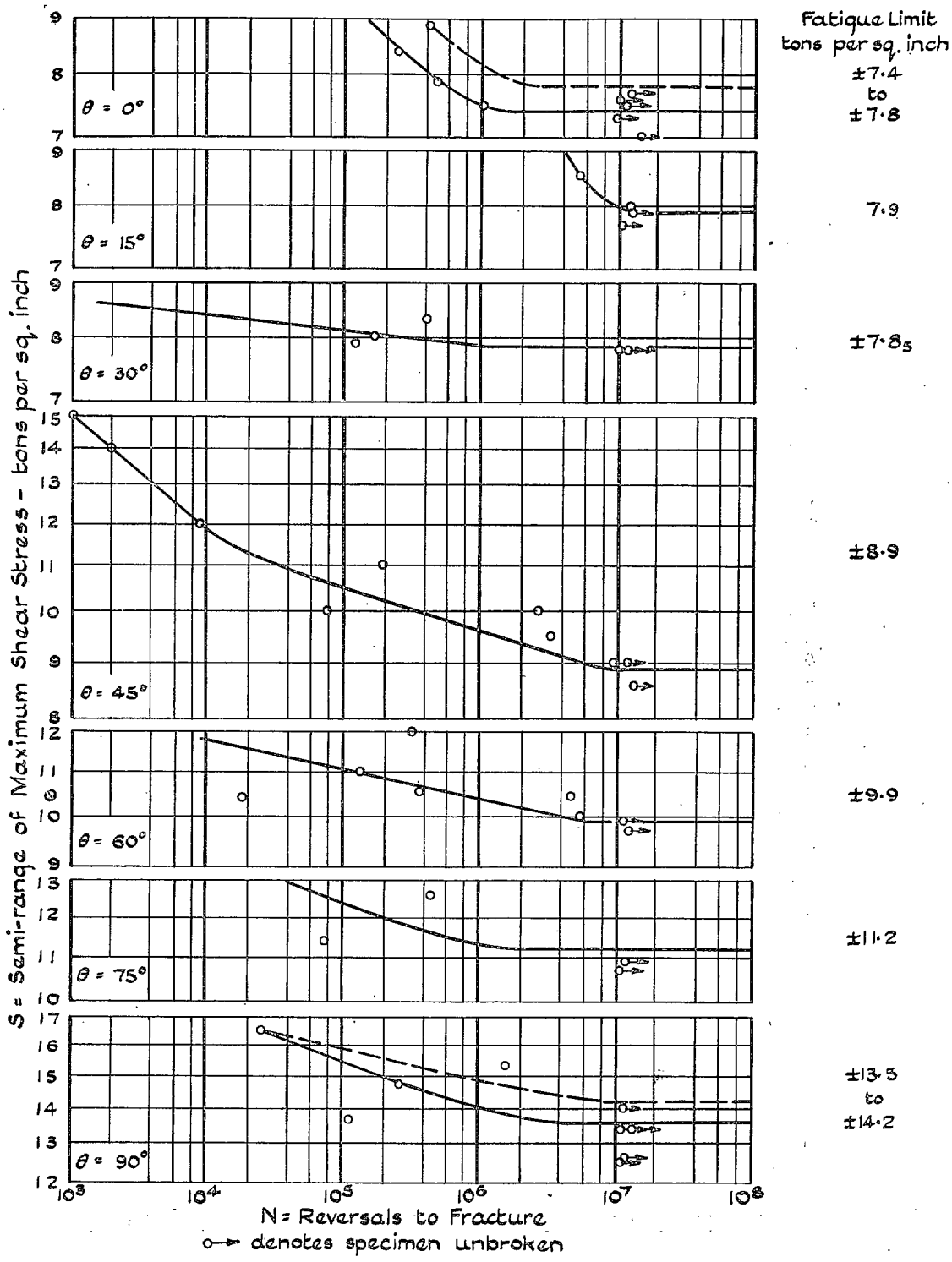

FIG. 45. *S/N* diagrams for ' Silal ' Cast Iron. Solid Specimens.

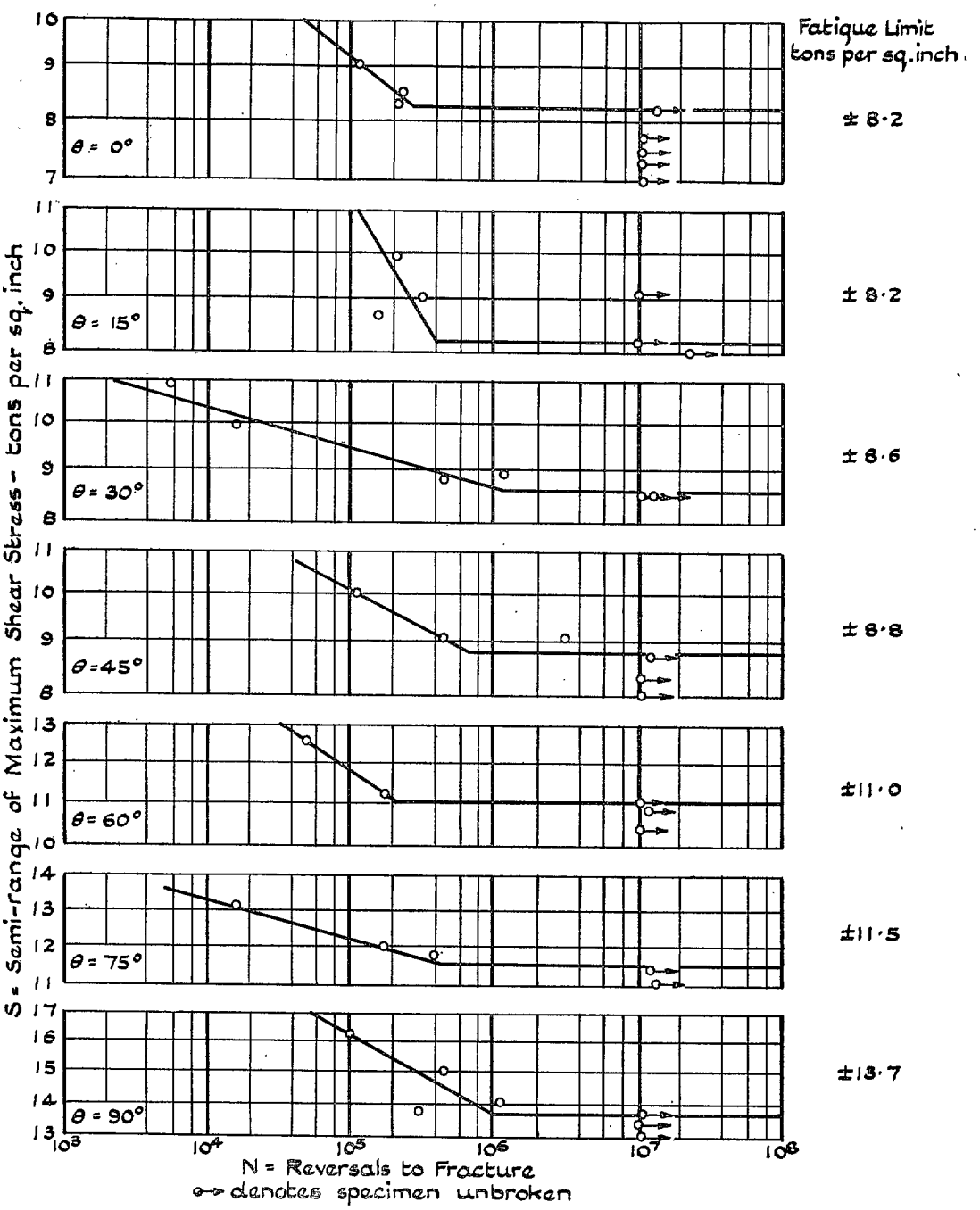

FIG. 46. *S/N* diagrams for ' Nicrosilal ' Cast Iron. Solid Specimens.

(*k*) Ni. Cr. Mo. Steel (75/80 ton). The *S/N* diagrams are shown in Fig. 43. This material also behaved very irregularly and the results cannot be regarded as satisfactory, although more reliance can, perhaps, be placed on the fatigue limit values than on those of the preceding 60/70 steel of the same type. The direction of the cracks bore some signs of following generally the traces of the maximum principal stress plane but many were indefinite or irregular. The results are as follows :—

Value of θ deg.	*Fatigue Limit* (Max. shear stress) t/in.²	*Reliability Index*
0	±21·4	LR
15	±21·0	LR
30	±20·4	R
45	±23·2	R
60	±23·0	R
75	±23·0	R
90	±22·2	R

(*l*) Ni. Cr. Steel (95/105 ton). The *S/N* diagrams are shown in Fig. 44. The data for $\theta = 90$ deg. and 75 deg. plot regularly, also perhaps, those at 15 and 30 deg., but much 'scatter' is seen in the other results ; this material, also, has behaved irregularly. The directions of the cracks showed no consistent tendency. The results are as follows :—

Value of θ deg.	*Fatigue Limit* (Max. shear stress) t/in.²	*Reliability Index*
0	±25·0	LR
15	±26·5	R
30	±27·5	R
45	±27·8	U
60	±27·8	U
75	±28·1	R
90	±29·3	R

(*m*) 'Silal' Cast Iron. The *S/N* diagrams are shown in Fig. 45. There can be little doubt that these results obtained on a cast material exhibit a degree of uniformity that is remarkable and surprising. With the exception of three specimens only, all fractures were essentially sound, being free from blowholes, inclusions or discolourations. Some inconsistency is seen in the two series of tests made at $\theta = 0$ and 90 deg. Interpreting these data literally, the fatigue limits may be expressed as falling within certain limits — ± 7·4/7·8 t/in.² in plane bending, and ± 13·5/14·2 t/in.² in torsion. In the *S/N* diagram for plane bending ($\theta = 0$ deg.), the inconsistency is caused by a single specimen which fractured, after $1{\cdot}04 \times 10^6$ reversals, under an applied range of ± 7·5 t/in.² : yet five other specimens safely withstood, for 10^7 or more reversals, applied stress ranges of from ± 7·0 up to ± 7·7 t/in.². Similarly, under reversed torsion ($\theta = 90$ deg.), the inconsistency is again caused by a single specimen only fracturing, after $1{\cdot}14 \times 10^5$ reversals, under an applied range of ± 13·6 t/in.², while five other specimens safely withstood, for more than 10^7 reversals, applied stress ranges of from ± 12·5 up to ± 14·0 t/in.². Therefore, although the fractured surfaces of these two specimens showed no visible flaw, it is considered that these specimens behaved abnormally and that they could be reasonably excluded in deducing the fatigue limits for their respective groups : this course has been followed.

The fractures are of great interest. In spite of the close setting of the machine trip gear, every specimen of 'Silal' fractured completely, the face of the fractures having an essentially brittle appearance. Every fracture face was a very close approach to a single plane ; the readings recorded below of the limiting measured angles show how very closely this plane agreed with the plane of maximum principal stress for all the applied stress systems. The results were as follows :—

Value of θ deg.	*Fatigue Limit* (Max. shear stress) t/in.²	*Reliability Index*	*Inclination to Transverse Plane (deg.)* (*a*) *Of plane of max. princ. stress*	(*b*) *Of measured traces of cracks*
0	± 7·8*	R	0	0 to 1½
15	± 7·9	R	7½	8 and 8½
30	± 7·8₅	R	15	15½ and 19½
45	± 8·9	R	22½	19 to 24
60	± 9·9	R	30	30 to 32
75	±11·2	R	37½	37 and 38
90	±14·2*	R	45	40 to 48

* Rejecting one inconsistent specimen in each case.

(*n*) 'Nicrosilal' Cast Iron. The *S/N* diagrams are shown in Fig. 46. Considering that this is a cast material under test, the data plot extremely consistently (even more so than those obtained with 'Silal') ; some irregularity occurs in the three specimens of the group $\theta = 15$ deg. and tested at stress ranges of ± 8½ and ± 9 t/in.², but, otherwise, the values of the fatigue limits are clearly defined. The fractures were more ragged than in the case of 'Silal' and in some cases the origin of the fracture was doubtful. But the measurements made at the point of maximum calculated stress are worth recording and the average values show good general agreement with the trace of the plane of maximum principal stress (or strain). The results are as follows :—

Value of θ deg.	*Fatigue Limit* (Max. shear stress) t/in.²	*Reliability Index*	*Inclination to Transverse Plane (deg.)* (*a*) *Of plane of max. princ. stress*	(*b*) *Of measured traces of cracks*
0	± 8·2	R	0	— 2 to 0
15	± 8·2	LR	7½	6 to 7
30	± 8·6	R	15	14 to 15
45	± 8·8	R	22½	21 to 23
60	± 11·0	R	30	29 and 32
75	± 11·5	R	37½	37 to 40
90	± 13·7	R	45	45 and 46

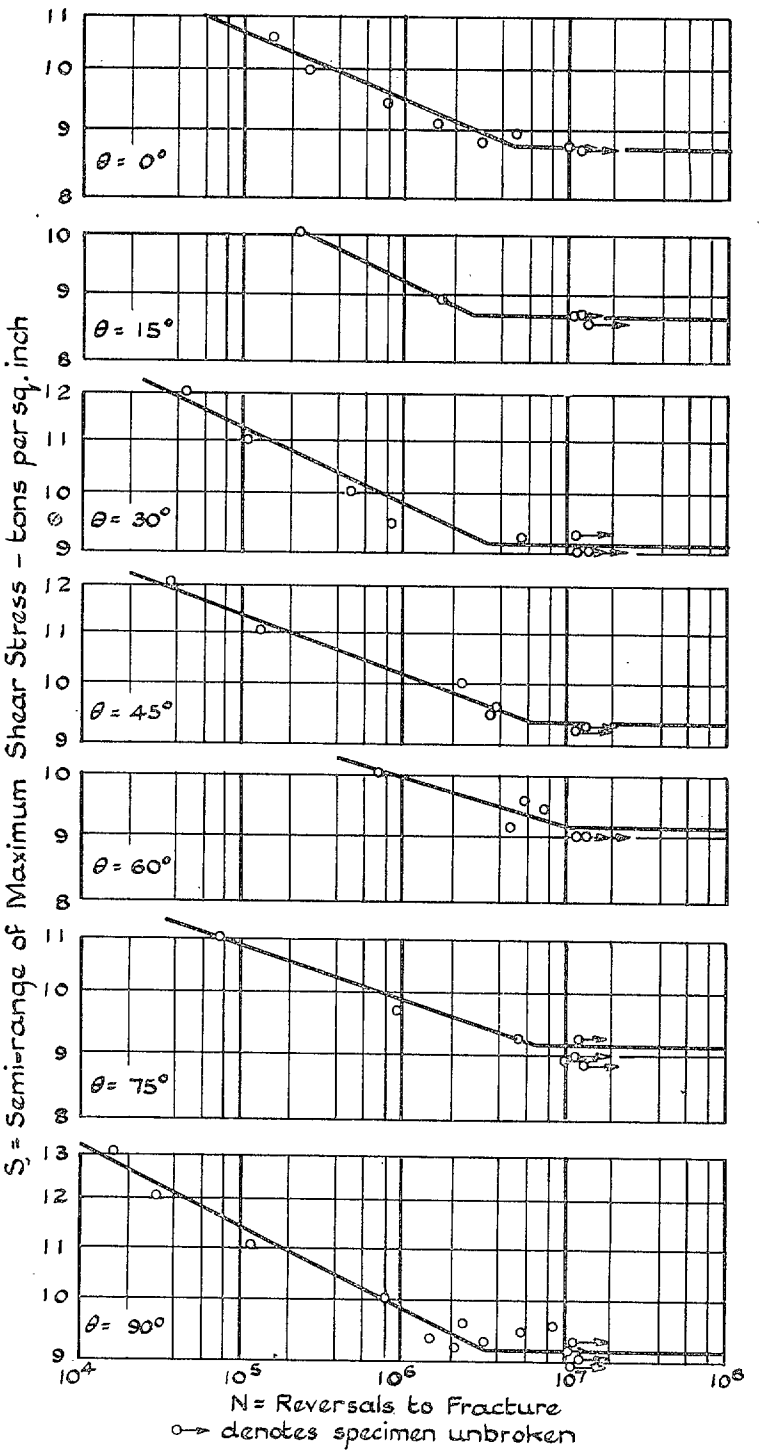

FIG. 47. *S/N* diagrams for 0·1% C. Steel (Normalised).
Hollow Specimens.

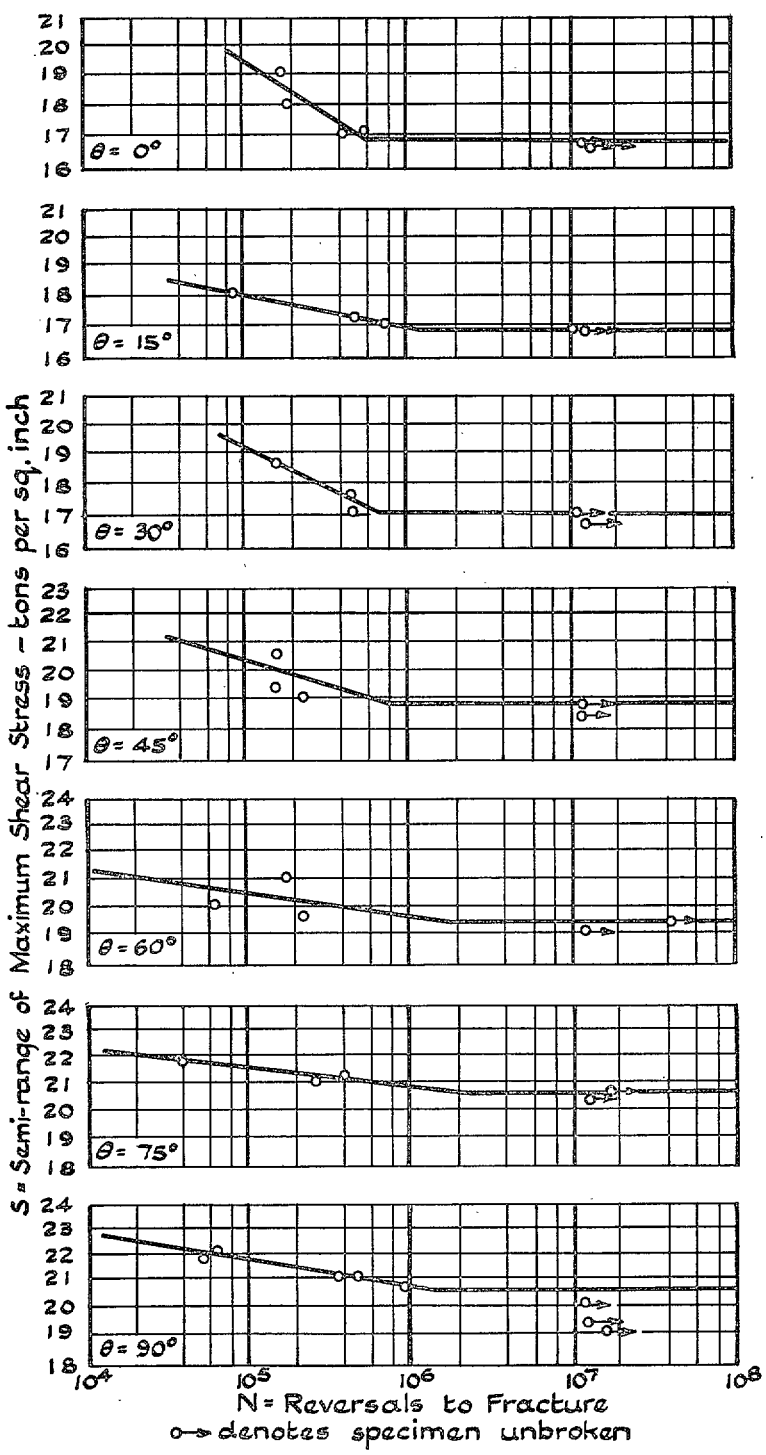

FIG. 48. *S/N* diagrams for 3½% Ni. Cr. Steel (Normal Impact). Hollow Specimens.

RESULTS OF COMBINED FATIGUE TESTS MADE ON HOLLOW SPECIMENS OF CIRCULAR SECTION

Experience in ordinary fatigue tests has established that the specimen form may affect the actual value of the fatigue limits determined by endurance tests. The main object of the present tests was to ascertain if the substitution of a hollow for the solid section would modify the general manner in which the fatigue limits varied as the applied stress system changed from reversed bending stresses to reversed torsional stresses through the intermediate combinations of these stresses. The two ductile steels selected for this comparison were chosen to represent one class which exhibits a definite drop of stress at yield—the 0·1% C. Steel (Normalised), also, by comparison, the second class which did not possess this characteristic—the 3½% Ni. Cr. Steel (Normal Impact).

The form and dimensions of the test specimens are shown in Fig. 6. The nominal external and internal diameters of the test specimen are 0·4 in. and 0·32 in., respectively, being the same as used for the corresponding Wohler and Stromeyer tests. Great care was taken in the machining of the bore of all the hollow specimens in order to reduce to an absolute minimum the occurrence of machine marks and lack of concentricity. The internal diameters of the specimens were carefully measured by special means devised in the Metrology Division of the National Physical Laboratory. The tests were carried out using exactly the same procedure as with the solid specimens. The fatigue limits were determined by endurance tests on a minimum reversals basis of 10^7.

No measurements were made of the orientation of the fatigue cracks.

(*a*) 0·1% C. Steel (Normalised). The *S/N* diagrams are shown in Fig. 47. With the exception of the tests made at $\theta = 90$ deg., where a little 'scatter' occurs, the data plot regularly and consistently. In all cases, the fatigue limit is clearly defined. The summarised results are as follows :—

Value of θ deg.	*Fatigue Limit* (Max. shear stress) t/in.²	*Reliability Index*
0	± 8·7₅	R
15	± 8·7	R
30	± 9·1	R
45	± 9·3₅	R
60	± 9·1	R
75	± 9·1₅	R
90	± 9·1₅	R

(*b*) 3½% Ni. Cr. Steel (Normal Impact). The *S/N* diagrams are shown in Fig. 48. With the exception of one specimen only, the fatigue data plot extremely regularly and consistently : all the fatigue limits are closely defined. The summarised results are as follows :—

Value of θ deg.	*Fatigue Limit* (Max. shear stress) t/in.²	*Reliability Index*
0	±16·8	R
15	±16·8	R
30	±17·0	R
45	±18·7₅	R
60	±19·3	R
75	±20·6	R
90	±20·5	R

RESULTS OF COMBINED FATIGUE TESTS MADE ON SOLID SPECIMENS CONTAINING A CIRCUMFERENTIAL 55 deg. SHARP Vee NOTCH

Of the fourteen materials, whose resistance to combined fatigue stresses had already been determined using solid specimens, seven were selected for this series of tests made to investigate the effect of the presence of a discontinuity on fatigue resistance. The 3½% Ni. Cr. Steel, in both the normal and embrittled conditions, was selected for inclusion in this series of tests. With each of the seven materials, the fatigue resistance has been determined under each of the seven applied stress conditions corresponding to $\theta = 0$, 15, 30, 45, 60, 75 and 90 deg. The form and dimensions of the specimen used is shown in Fig. 6. The stress concentration has been produced by machining a 55 deg. 'sharp' Vee notch round the circumference of the test portion of the specimen, the depth of the groove being 0·02 in. It will be noticed that the root diameter at the base of the notch is 0·3 in., equal to the diameter of the solid circular specimens used in the main series of tests. A comparison of the results of the two series of tests will thus give directly the decrease in fatigue resistance due to the presence of the notch, as such. The nominal maximum shear stress values reported below are calculated on the diameter at the root of the notch and take no account of any stress concentration due to the presence of the notch.

Every effort was made to produce the bottom of the notch as sharp as possible by sharpening the tool before each final cut, for which the specimen was turned by hand. Each notch in fact had a blunted bottom approximating to a root radius. This radius was carefully measured on every specimen by the method previously described in Part I, Section 2, of this paper. The average

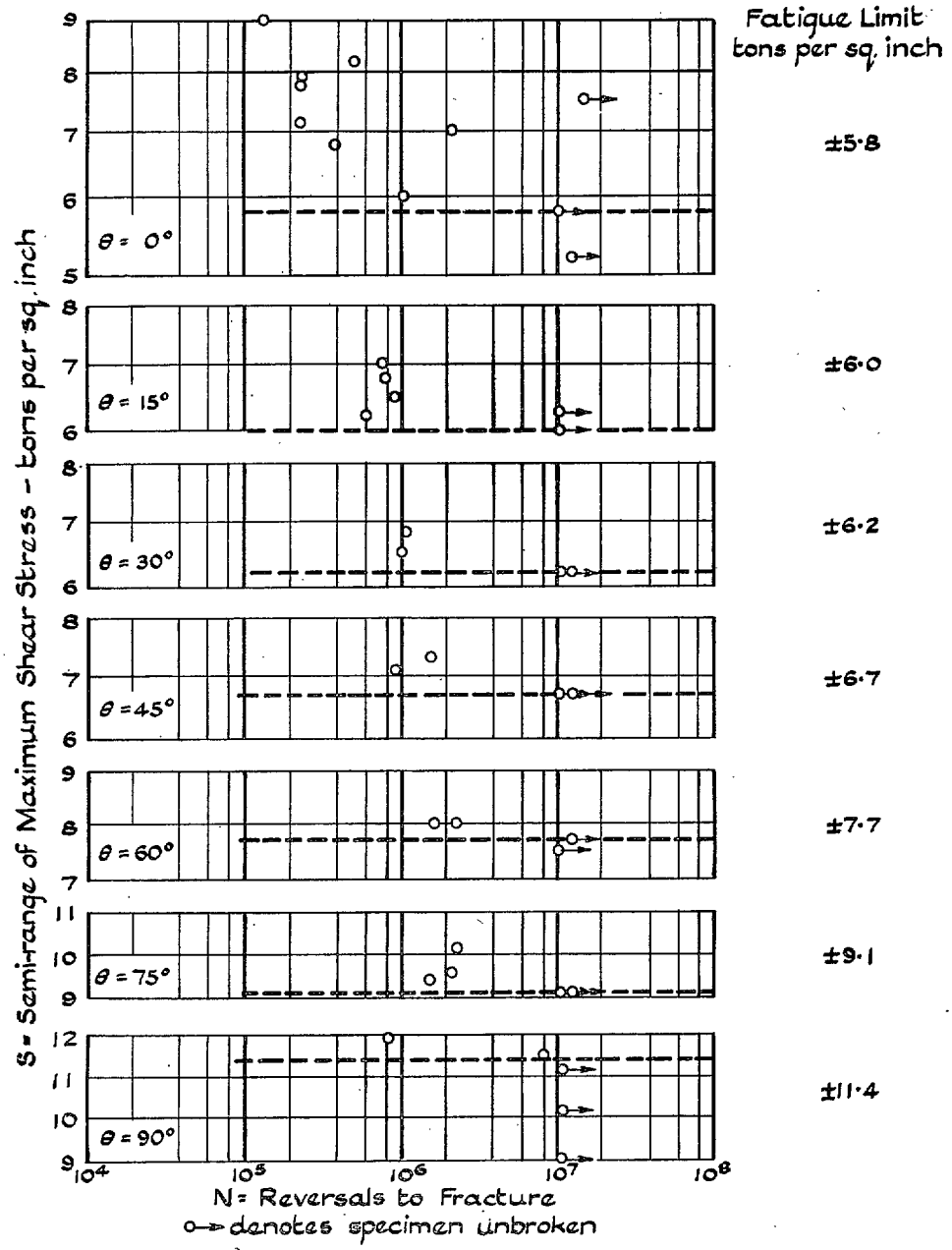

FIG. 49. *S/N* diagrams for 0·4% C. Steel (Normalised).
Notched Specimens.

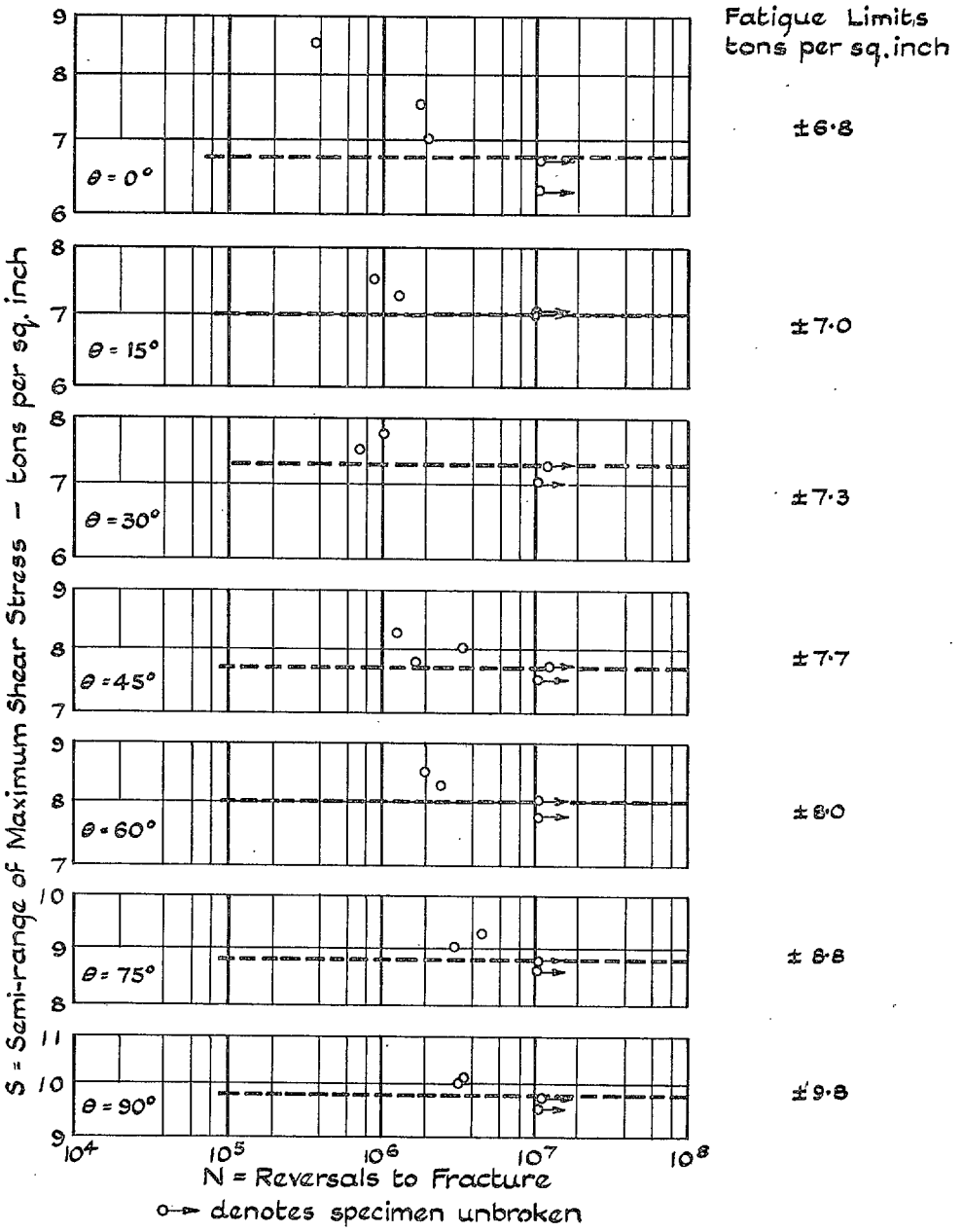

FIG. 50. *S/N* diagrams for 3% Ni. Steel (30/35 ton). Notched Specimens.

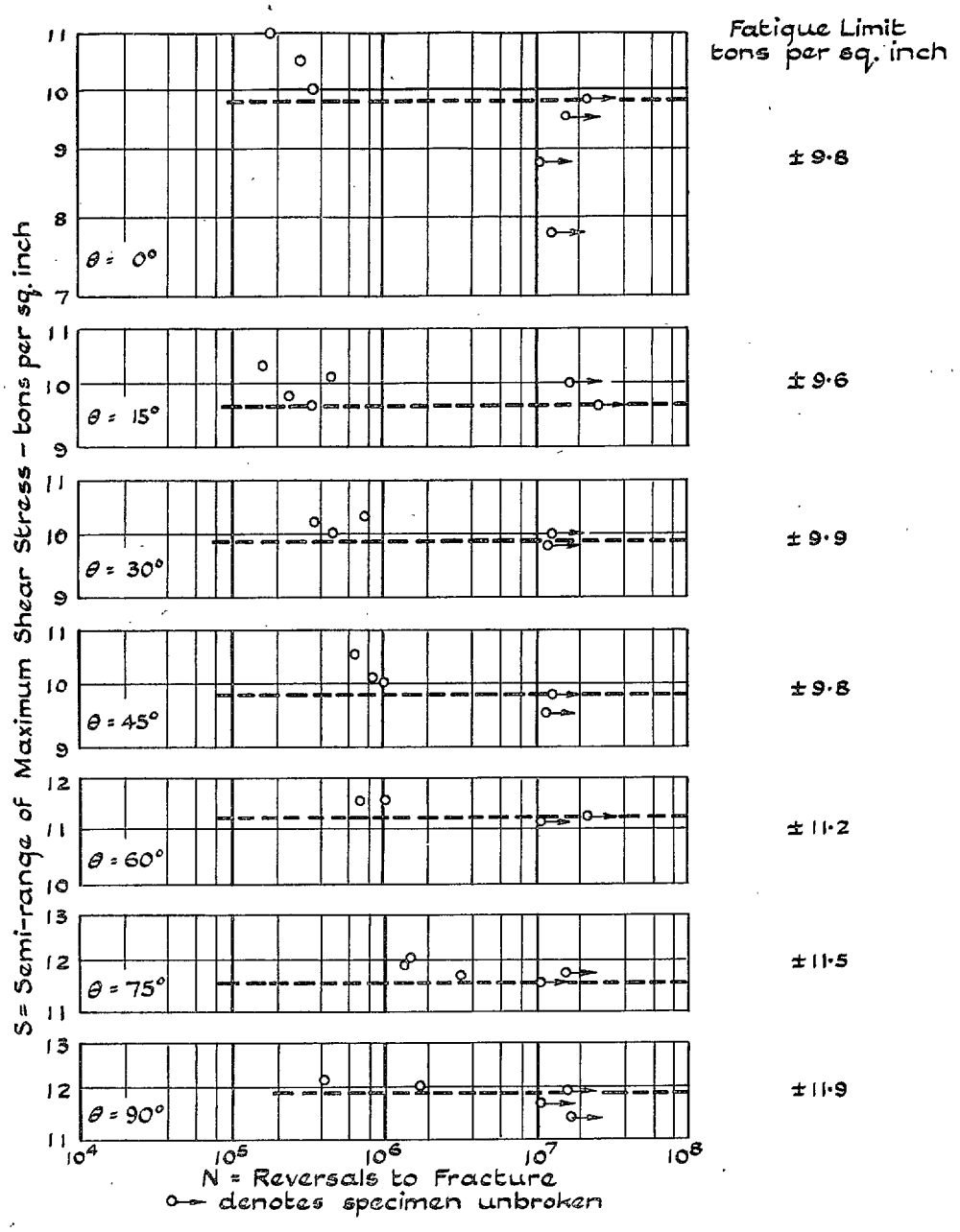

FIG. 51. *S/N* diagrams for 3/3½% Ni. Steel (45/50 ton). Notched Specimens.

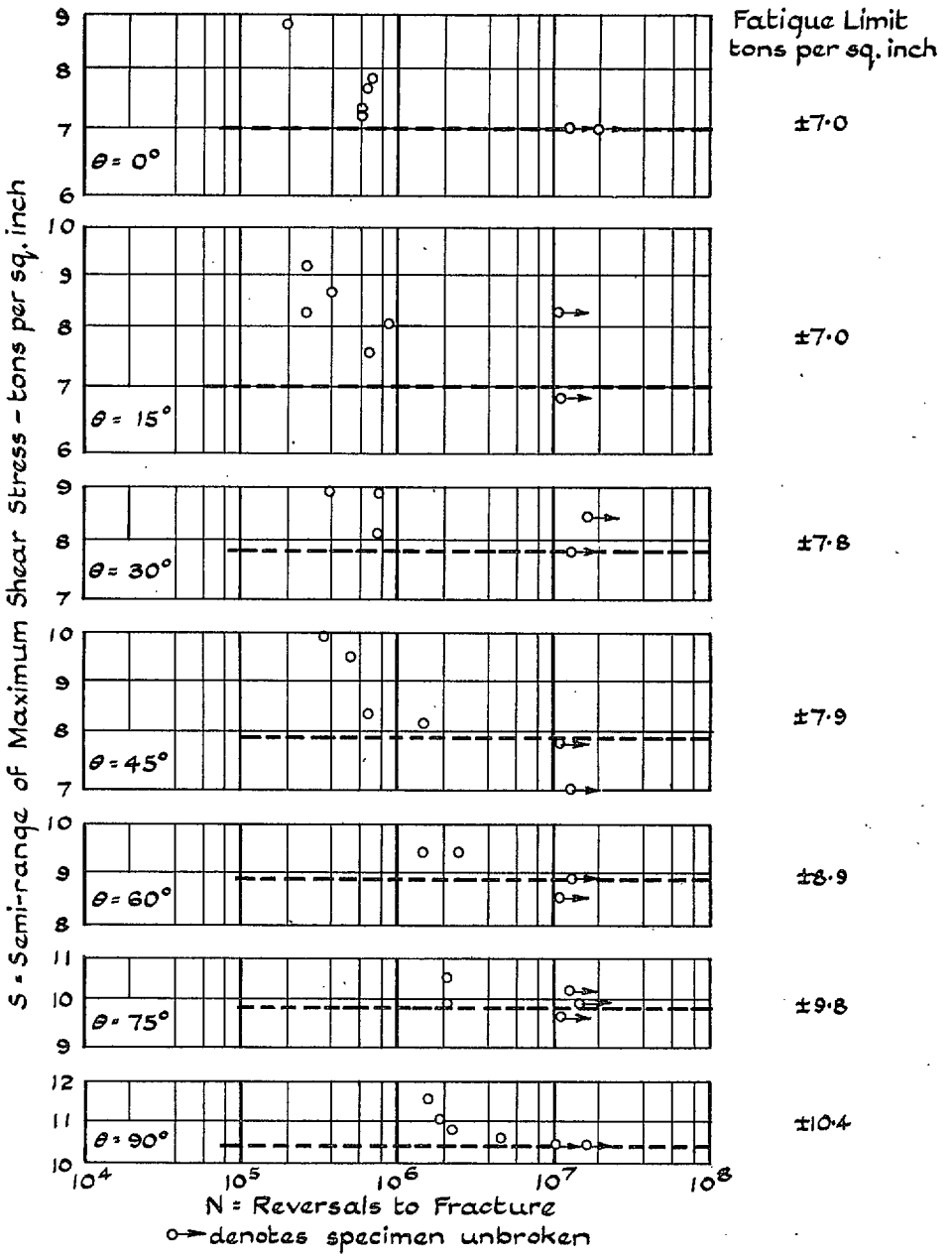

FIG. 52. *S/N* diagrams for Cr. Va. Steel (45/50 ton). Notched Specimens.

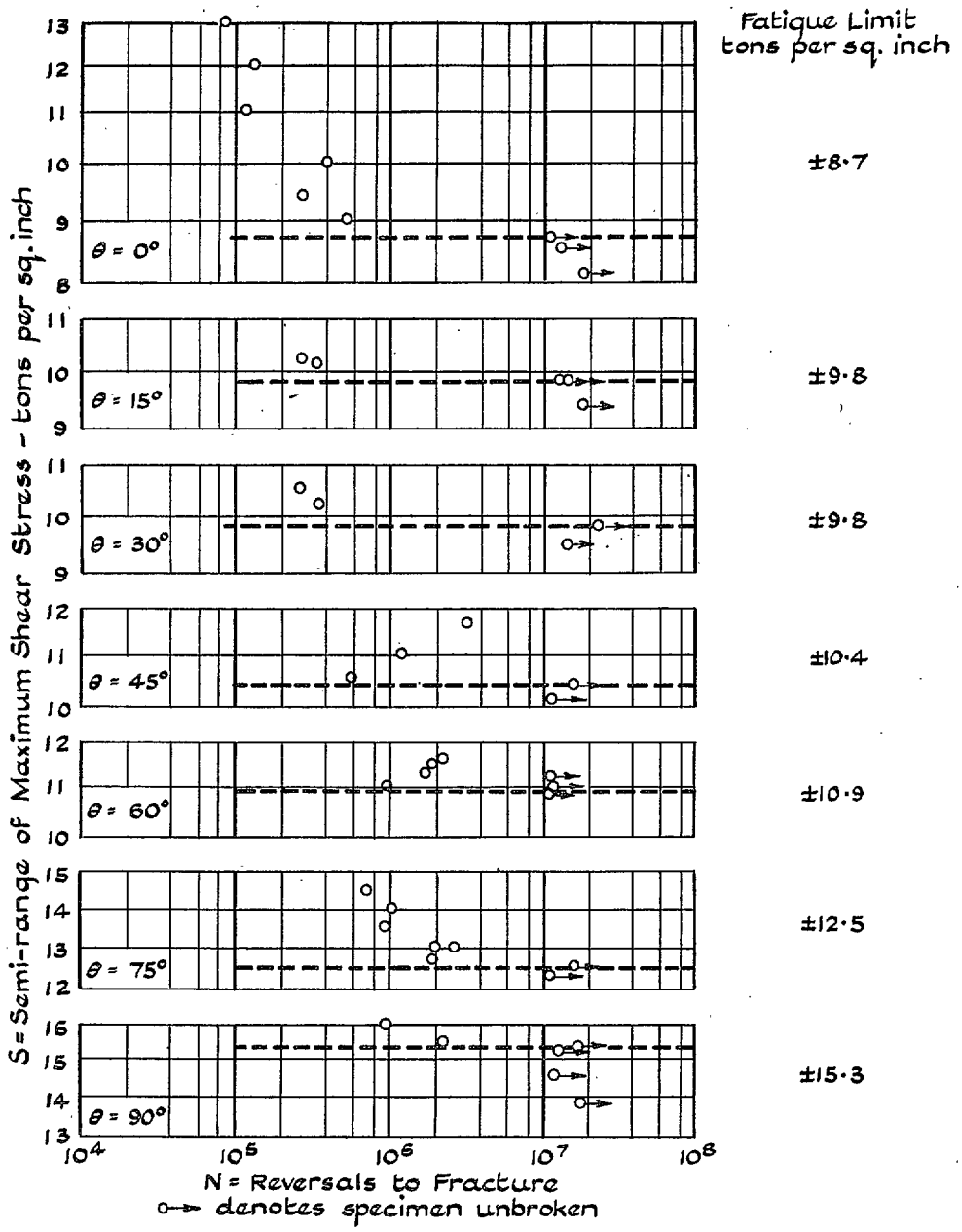

FIG. 53. *S/N* diagrams for 3½% Ni. Cr. Steel (Normal Impact). Notched Specimens.

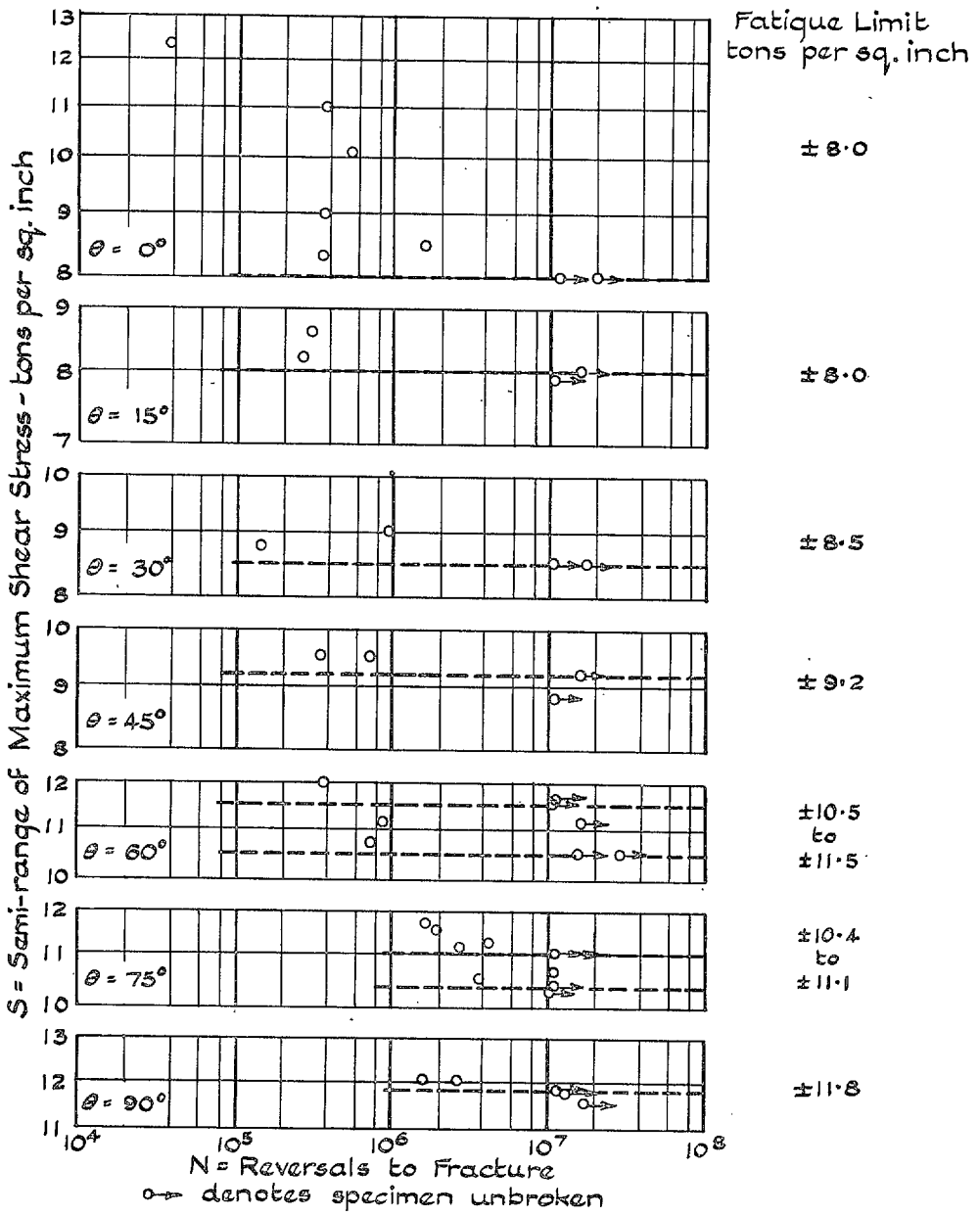

FIG. 54. *S/N* diagrams for 3½% Ni. Cr. Steel (Low Impact). Notched Specimens.

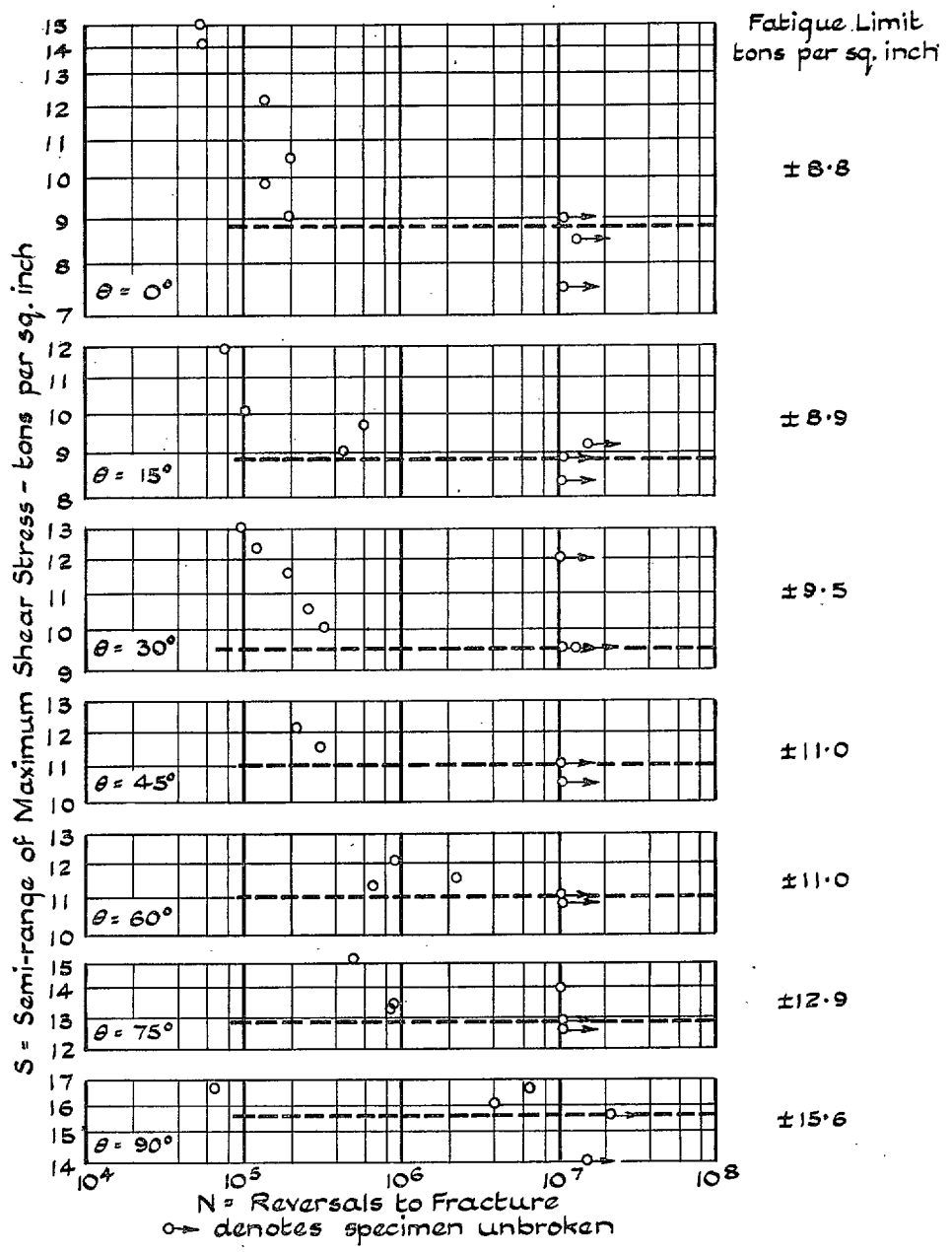

FIG. 55. *S/N* diagrams for Ni. Cr. Mo. Steel (75/80 ton). Notched Specimens.

value of the root radius varied from material to material (as would be expected with such variations in hardness and machinability) but was reasonably consistent for any one material. But variations did occur from specimen to specimen. It will be seen later that, with some materials, the plotted *S/N* curves showed greater irregularities than the corresponding tests made on plain specimens. Each result was then carefully analysed to find if these irregularities could be accounted for by the differences in the root sharpness as measured of the various notches. The result was entirely negative ; for example, several specimens each yielding a certain value of the measured 'root radius' would, under test, have greater fatigue resistances than other specimens each having a larger root radius as measured. The conclusion was inescapable that, within the variations of shape of root encountered, the effect of differences of root radius as measured was completely masked by other factors. This is not really an unexpected conclusion, when regarded in relation to experience of fractures by fatigue of engineering components in practice. For, visualising what the profile of such a notch would look like, if sectioned and examined microscopically, it might be expected that discontinuities of that profile, inseparable from a machining operation, would affect the fatigue resistance to a greater extent than apparently larger, but smoother, variations in the overall shape of the profile itself. Thus, no useful object would be served by tabulating every specimen with its measured 'root radius' value ; the results might be misleading. Instead, the maximum and minimum values of the specimens which failed are noted : they may have some interest from a machining point of view. To a designer, the main interest must lie in the effect on the fatigue resistance of the materials used as resulting from a careful attempt to produce in the workshop a sharp 55 deg. Vee notch.

(*a*) 0·4% C. Steel (Normalised). The *S/N* diagrams are shown in Fig. 49. They show considerable scatter but, with the exception of one specimen, tested at $\theta = 0$ deg., which it is reasonable to reject, the data are consistent and the following recorded values of the fatigue limits are definitely indicated.

Value of θ deg.	*Nominal Fatigue Limit* (Max. shear stress) t/in.²	*Reliability Index*	*Measured Value of Root Radius* inches × 10^{-3}	
			Limits	*Average*
0	± 5·8	R	0·1/0·3	0·2
15	± 6·0	R	0·1	0·1
30	± 6·2	R	0·1/0·2	$0·1_5$
45	± 6·7	R	0·1/0·2	$0·1_5$
60	± 7·7	R	0·1/0·2	$0·1_5$
75	± 9·1	R	0·1/0·2	$0·1_5$
90	±11·4	R	0·2	0·2

(*b*) 3% Ni. Steel (30/35 ton). The *S/N* diagrams are shown in Fig. 50. The results are consistent and the fatigue limits closely defined, as follows :—

Value of θ deg.	*Nominal Fatigue Limit* (Max. shear stress) t/in.²	*Reliability Index*	*Measured Value of Root Radius* inches × 10^{-3}	
			Limits	*Average*
0	± 6·8	R	0·1/0·3	0·2
15	± 7·0	R	0·3/0·5	0·4
30	± 7·3	R	0·1/0·6	0·3
45	± 7·7	R	0·1/0·2	$0·1_5$
60	± 8·0	R	0·2	0·2
75	± 8·8	R	0·2/0·3	$0·2_5$
90	± 9·8	R	0·2	0·2

(*c*) 3/3½% Ni. Steel (45/50 ton). The *S/N* diagrams are shown in Fig. 51. The data relating to tests at $\theta = 15$ deg. are inconsistent ; in the other six series of tests, the data plot satisfactorily and the fatigue limits are closely defined, as follows :—

Value of θ deg.	*Nominal Fatigue Limit* (Max. shear stress) t/in.²	*Reliability Index*	*Measured Value of Root Radius* inches × 10^{-3}	
			Limits	*Average*
0	± 9·8	R	0·2/0·6	0·4
15	± 9·6	LR	0·3/0·5	0·4
30	± 9·9	R	0·4/0·5	$0·4_5$
45	± 9·8	R	0·3/0·6	0·4
60	±11·2	R	0·4	0·4
75	±11·5	R	0·4/0·5	$0·4_5$
90	±11·9	R	0·3/0·4	$0·3_5$

(*d*) Cr. Va. Steel (45/50 ton). The *S/N* diagrams are shown in Fig. 52. The data plot regularly in the groups of $\theta = 0$, 45, 60 and 90 deg. and give well defined limiting values ; the others suffer from scatter and more tests are required to establish reliable results. With these reservations, the results are recorded as follows :—

Value of θ deg.	*Nominal Fatigue Limit* (Max. shear stress) t/in.²	*Reliability Index*	*Measured Value of Root Radius* inches × 10^{-3}	
			Limits	*Average*
0	± 7·0	R	0·3/0·5	$0·3_5$
15	± 7·0	LR	0·5/0·7	0·6
30	± 7·8	LR	0·6/0·8	0·7
45	± 7·9	R	0·5/0·8	0·7
60	± 8·9	R	0·4/0·9	$0·6_5$
75	± 9·8	LR	0·5	0·5
90	±10·4	R	0·4/0·6	0·5

(*e*) 3½% Ni. Cr. Steel (Normal Impact). The *S/N* diagrams are shown in Fig. 53. In spite of some irregularity in a few results, the limiting values are closely defined in all seven groups, as follows :—

Value of θ deg.	*Nominal Fatigue Limit* (Max. shear stress) t/in.²	*Reliability Index*	*Measured Value of Root Radius* inches × 10^{-3}	
			Limits	*Average*
0	± 8·7	R	0·6/1·0	0·8
15	± 9·8	R	0·7/0·8	$0·7_5$
30	± 9·8	R	0·7/1·0	$0·8_5$
45	±10·4	R	0·6/0·9	0·8
60	±10·9	R	0·5/1·4	0·9
75	±12·5	R	0·4/1·5	0·8
90	±15·3	R	0·9/1·0	$0·9_5$

(*f*) 3½% Ni. Cr. Steel (Low Impact). The *S/N* diagrams are shown in Fig. 54. From tests made at $\theta = 0$, 15, 30, 45 and 90 deg., the data plot regularly, although more tests could, with advantage, have been used for the intermediate three. The tests made at $\theta = 60$ and 75 deg. warrant only the assigned ' bracket ' values for the fatigue limits.

Value of θ deg.	*Nominal Fatigue Limit* (Max. shear stress) t/in.²	*Reliability Index*	*Measured Value of Root Radius* inches × 10^{-3}	
			Limits	*Average*
0	± 8·0	R	0·5/1·3	$0·8_5$
15	± 8·0	R	0·7/1·0	$0·8_5$
30	± 8·5	R	1·0	1·0
45	± 9·2	R	0·6	0·6
60	±10·5/±11·5	LR	0·8/2·0	1·6
75	±10·4/±11·1	LR	0·3/1·4	0·8
90	±11·8	R	0·8/1·0	0·9

(*g*) Ni. Cr. Mo. Steel (75/80 ton). The *S/N* diagrams are shown in Fig. 55. With the exception of a single specimen tested at $\theta = 30$ deg., the result on which can be reasonably rejected, all the data plot very consistently, with occasional scatter, giving well defined limiting values of stress.

Value of θ deg.	*Nominal Fatigue Limit* (Max. shear stress) t/in.²	*Reliability Index*	*Measured Value of Root Radius* inches × 10^{-3}	
			Limits	*Average*
0	± 8·8	R	1·2/2·0	1·5
15	± 8·9	R	0·5/1·0	$0·7_5$
30	± 9·5	R	0·8/1·2	1·0
45	±11·0	R	0·6/1·8	1·2
60	±11·0	R	0·7/0·8	$0·7_5$
75	±12·9	R	0·5/1·8	0·9
90	±15·6	R	0·8/1·2	0·9

PART II

Fatigue Strength of a Nickel-Chromium-Vanadium-Molybdenum Steel under Combinations of Reversed Bending Stresses, Reversed Torsional Stresses and Superimposed Static Bending and Torsional Stresses (Four Independent Variables)

by

H. J. GOUGH, F.R.S. and W. J. CLENSHAW, B.Sc.

I. THE No. 2 COMBINED STRESS FATIGUE TESTING MACHINE

This No. 2 type of machine was developed directly from the No. 1 type which has been fully described in Part I of the present paper. In both machines, the alternating loading forces are generated by the centrifugal forces of revolving unbalanced discs, the inertia of the remaining vibrating and rotating parts being balanced by a spring system, on which they are supported : the working speed of each machine is that at which the mass of the moving parts resonates on the supporting springs. In each machine, this suspensory spring system consists of two pairs of double cantilever springs in parallel. In the No. 1 machine, the sole function of the suspensory spring system is to eliminate from the test specimen all forces other than those due to the out-of-balance weights attached to the revolving discs. They also discharge this function in the No. 2 machine, but, in addition, are so mounted that initial deflections can be given to the springs which thus superimpose on the specimen a static loading moment to produce a required bending and/or torsional moment. Thus, while the No. 1 machine applies a required combination of two variables, i.e. cycles of reversed bending and reversed torsional stresses, the No. 2 machine applies a desired combination of four variables, i.e. static bending and static shearing stresses superimposed on the same two cyclic stress variables as with the No. 1 machine.

1. Description of the machine

Fig. 56 shows the general arrangement of the No. 2 machine. One end of the specimen S is rigidly clamped on a bracket K which can be rotated about a vertical axis to any desired position and then bolted firmly to the casting G, which is rigidly attached to the baseplate B. The other end of the specimen is held in a balanced adaptor C to which the lever arm A is pivoted about a vertical axis passing through the centre of the specimen. Two balanced discs D carry the out-of-balance weights W and are attached to a spindle F which runs in bearings suitably housed and clamped to the ends of the springs E. The spindle F carries a pulley, located centrally between the discs D, which is belt-driven from the synchronous motor M whose speed is 1,500 r.p.m. The housings on the ends of the springs E are connected to the centre of percussion of the arm A by links L and side-arms H. These links L have spherical seatings at their lower ends and, also, at their upper points of attachment, U, to the ends of the side-arms H : this system of spherical seatings avoids undesirable constraint of the specimen as the latter deflects. The lengths of the links L are adjustable. The vertical components of the out-of-balance forces developed at the axle carrying the discs are transmitted, via links L and lever arm A, to produce alternating moments on the specimen. The speed of the disc is adjusted, by varying the ratio of the pulley diameters, to the resonant frequency of all the moving parts vibrating on the outer ends of the springs E ; this adjustment is effected by the use of a very flexible ' specimen ' which is, effectively, only a ' crossed-strip ' pivot having negligible stiffness. The foregoing description of the origin and application of the alternating loading covers, in principle, both the No. 1 and No. 2 types of machine, although these machines differ in detailed design.

The new feature of the No. 2 machine lies in the superimposition of static moments on the specimens : this is effected by initial deflections of the suspensory spring system, as follows :—

The rear ends of each pair of springs E are held in a massive steel clamp N : the centre block of each clamp can slide in a horizontal direction parallel to the length of the springs in grooves cut in the Vee shaped casting, V. The casting V can be adjusted vertically to any desired position by means of the screwed spindle Q and attached handwheel. These horizontal and vertical adjustments having been effected, the whole assembly is locked rigidly to the casting J by means of the bolts O and the spring plate P : the casting J is bolted rigidly both to the baseplate B and the casting G. The rear ends of each pair of springs can thus be deflected independently from the zero position corresponding to zero static load.

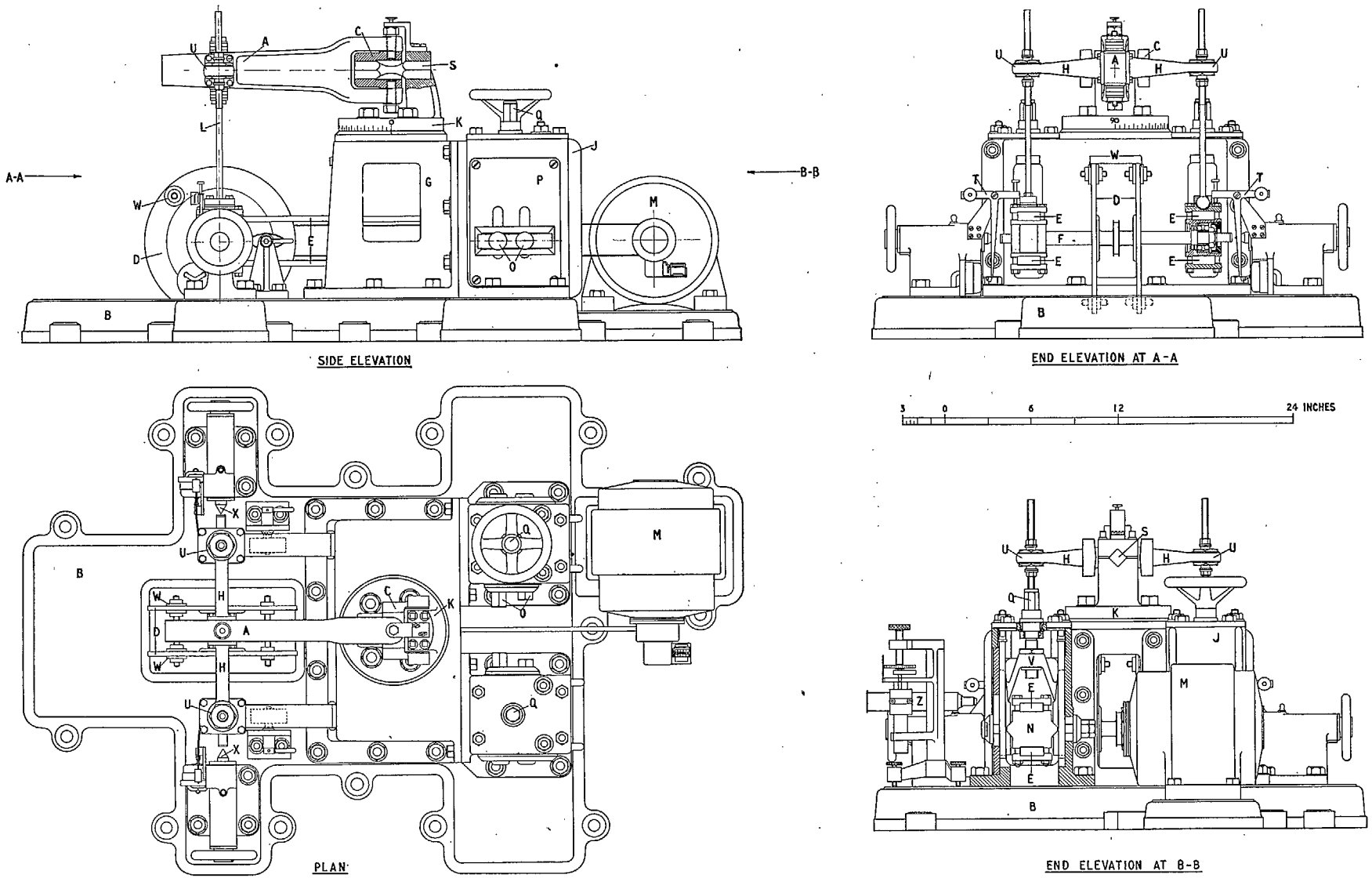

FIG. 56. General Arrangement of No. 2 Combined Stress Fatigue Testing Machine.

The zero position of the springs is accurately determined as follows. At the front end of the machine, a headstock, carrying an adjustable centre X, is mounted accurately on each side of the baseplate so that the pair have a common, and horizontal, axis. The adjustable centres fit the ends of the spindle F (into which they can be advanced or retracted as desired by the headstock handwheels), thus accurately locating that spindle, together with the front end of the springs, at a fixed height above the baseplate ; this fixed height can also be checked by two special vertical height gauges which can be placed in position resting on the baseplate and just touching the lower surface of the spindle F at each of its ends. Thus when, with the links L removed, both the screwed spindles Q have been so adjusted that the spindle F is horizontal and accurately co-axial with the headstock centres X, then the rear ends of both springs are also accurately sited in the zero position. The zero position of the rear end of each pair of springs is located, in regard to the baseplate of the machine, by a reference mark engraved on each of the castings V, the height of which, in relation to the machined baseplate extensions at the rear of the machine, is measured by vertical measuring microscopes which can be mounted on these extensions : these microscopes are shown in position on Figs. 57, 58 and 59.

When it is desired to carry out a test in which static loading is superimposed on the cyclic loading, the equivalent deflection of each pair of springs is calculated. After removing the links L, the positions of the rear ends of the springs are adjusted, using the handwheels and screws Q, until microscope readings made on the reference marks show that the rear ends of the springs have been correctly located in positions corresponding to the required vertical deflections. The springs are as yet unstrained, the spindle F having been free to depart from its original horizontal position. The links L are now replaced and their lengths adjusted until the spindle F has again assumed a horizontal position co-axial with the headstock centres, as determined using the height gauges and checked by the headstock centres. The springs are now in the deflected and strained position, the specimen being subjected to the required static loading through the links L, the side arms H and the lever arm A.

In regard to the cyclic loading, the effect of setting the arm A at an angle θ to the axis of the specimen is exactly the same as with the No. 1 type machine as described in Part I of this report. The applied cyclic bending and cyclic torsional moments are proportional, respectively, to cos θ and sin θ.

It will be seen that the nature of the superimposed static loading on the specimen, for any given deflections of the springs, is also dependent on the angle of setting of the specimen. For example, when the specimen is set at $\theta = 0$ deg. and thus subjected to cyclic bending stresses, the application of equal and upward spring loads superimpose a static bending moment on the specimen : equal but opposite spring loads will superimpose a static torsional moment on the specimen. When, however, the specimen is set at $\theta = 90$ deg. and thus subjected to cyclic torsional stresses, the effect of the same spring loads is reversed ; equal spring loads acting in the same direction superimpose a static torsional moment on the specimen, while equal spring loads acting in opposite directions superimpose a static bending moment. For intermediate values of θ, any combination of static bending and torsional moments may be applied by an appropriate choice of spring loads.

Figs. 57, 58, 59 and 60 show the machine adjusted to apply a typical combination of stress and illustrate most of the external details referred to in the above description of the machine ; the right- and left-hand sides of the machine are designated as by an observer looking at the machine from the disc spindle end, corresponding to end elevation A of Fig. 56. The specimen is set at $\theta = 53{\cdot}1$ deg., to give a ratio of applied cyclic bending to applied cyclic torsional stress of $1\frac{1}{2} : 1$. The spring loads have been adjusted to produce, on the standard specimen of 0·5 in. diameter, superimposed static bending and torsional stresses of $34\frac{1}{2}$ and $22\frac{1}{4}$ t/in.^{2}, respectively. The photographs show the out-of-balance weights, which generate the cyclic stresses, attached to the discs at two diametrically opposite positions. The weights not in use are seen housed on the arm A at its centre of percussion ; this practice maintains constant through all tests a mean weight distribution of the moving parts. By a suitable choice of these weights, ranges of maximum shear stress (on a standard specimen) varying from $\pm \frac{1}{4}$ to $\pm 30\frac{1}{4}$ t/in.^{2}, with intermediate steps of $\pm \frac{1}{4}$ t/in.^{2}, are available using five pairs of weights only : a pair of equal weights is necessary for each stress value as both discs must be equally loaded.

2. Calibration of machine

(*a*) CALIBRATION OF SPRINGS

Fig. 61 illustrates the arrangement. The links L are removed, thus disconnecting the springs from the lever arm and specimen. Two 4 : 1 levers are placed in position resting on hard steel balls which fit into the lower spherical seatings in which the links L normally rest. The fulcra of these levers are hard steel knife edges which rest against special hard steel flat seatings mounted on the casting G. The loading ends of the levers are fitted with knife-edge seatings on which rests a cross-bar carrying a scale pan at its mid-length. Before commencing the calibration, both pairs of springs are accurately adjusted and locked in their zero position, the spindle F being truly horizontal. The spring calibration is then carried out by applying weights to the scale pan, the deflection of the springs—as indicated by vertical movements of spindle F—being accurately measured by Ames dials or slip gauges and providing a load/deflection calibration diagram. To adjust the machine for an actual fatigue test, the required spring deflections—as taken from the calibration diagram—are applied by raising or

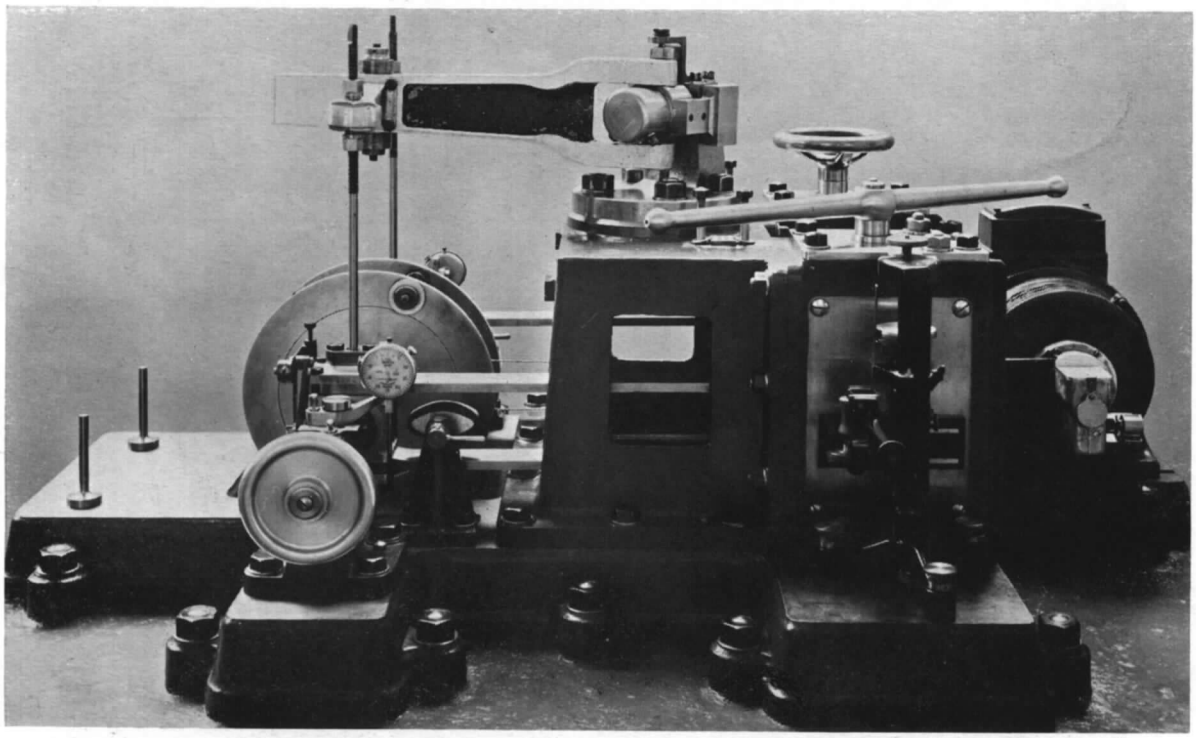

FIG. 57. No. 2 Fatigue Machine. View of right-hand side.

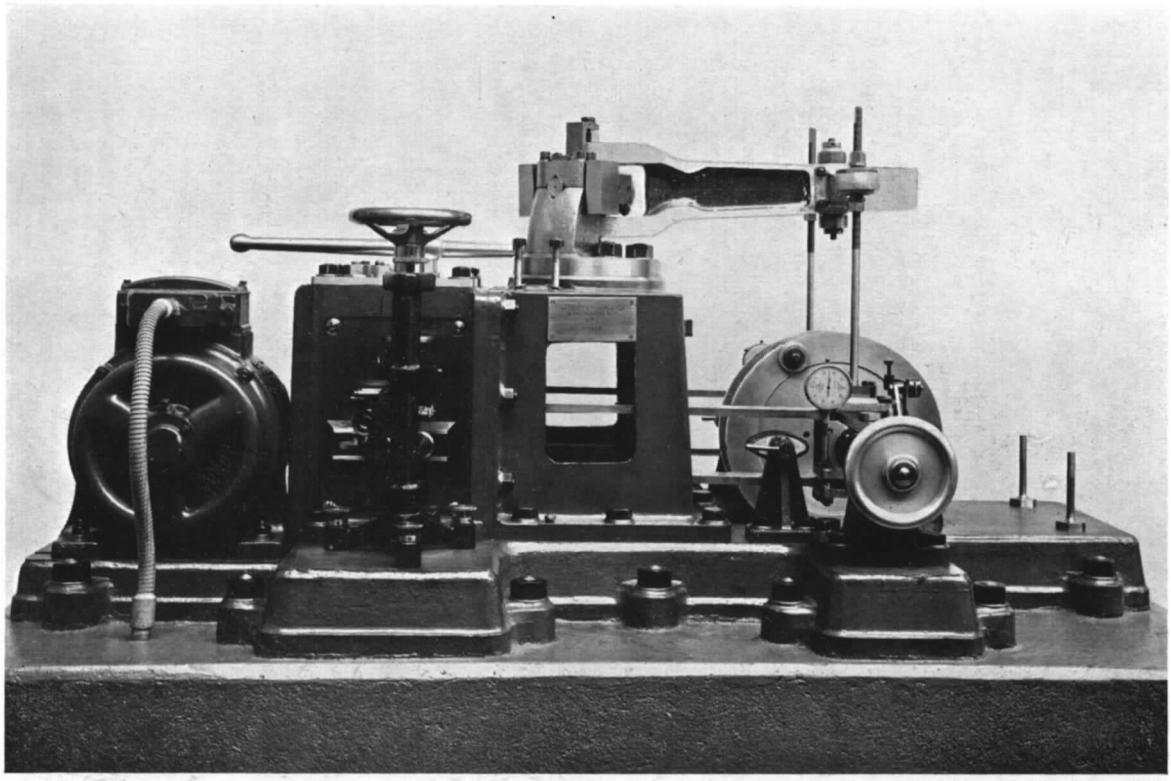

FIG. 58. No. 2 Fatigue Machine. View of left-hand side.

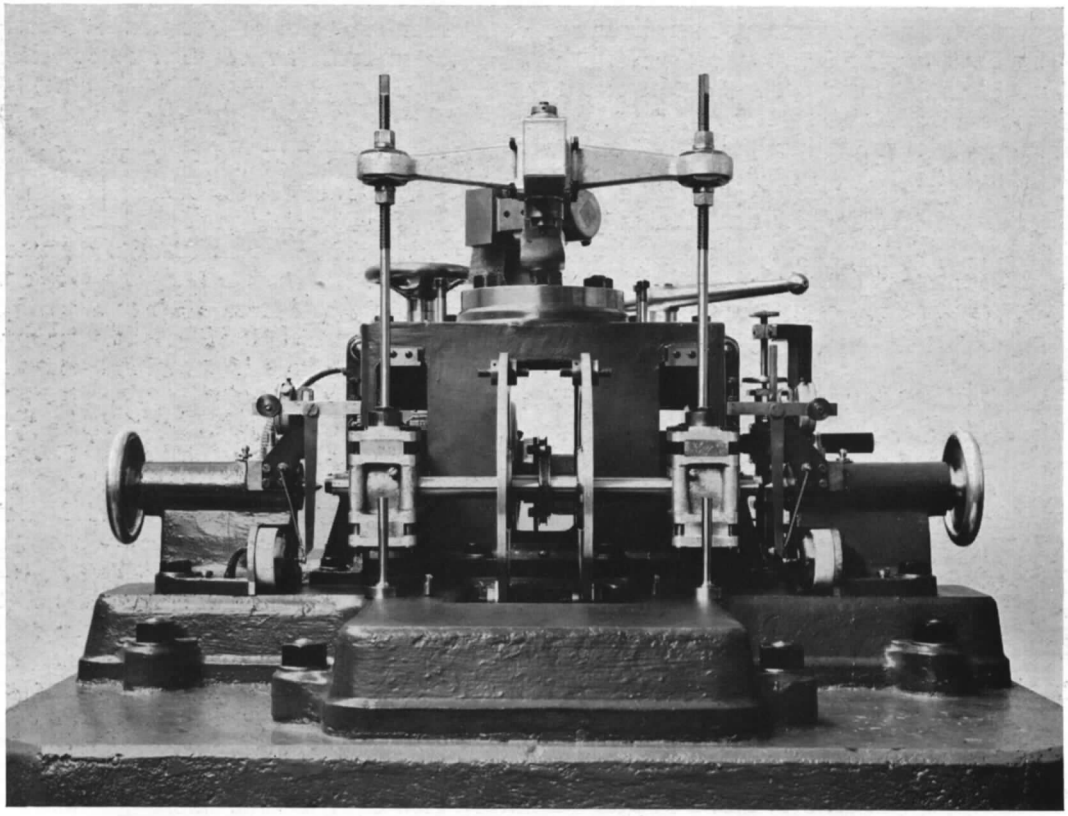

FIG. 59. No. 2 Fatigue Machine. View of Front End.

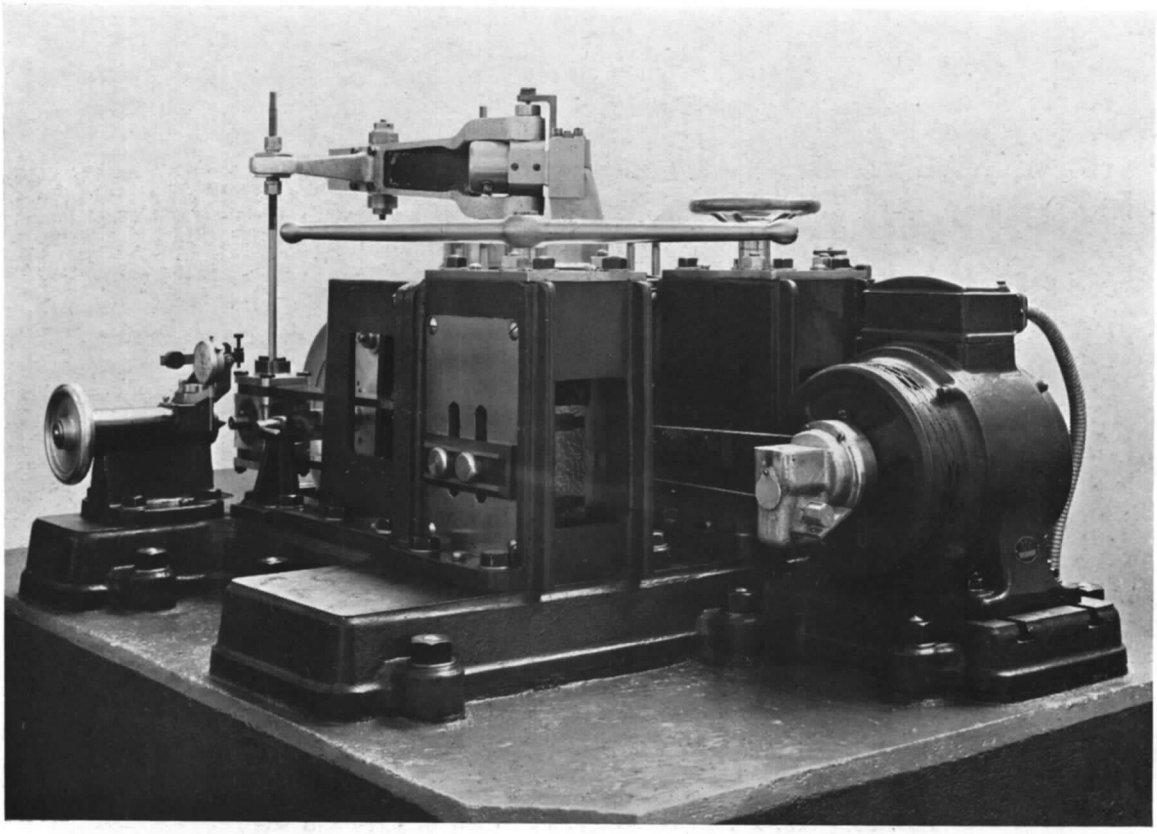

FIG. 60. No. 2 Fatigue Machine. Oblique View.

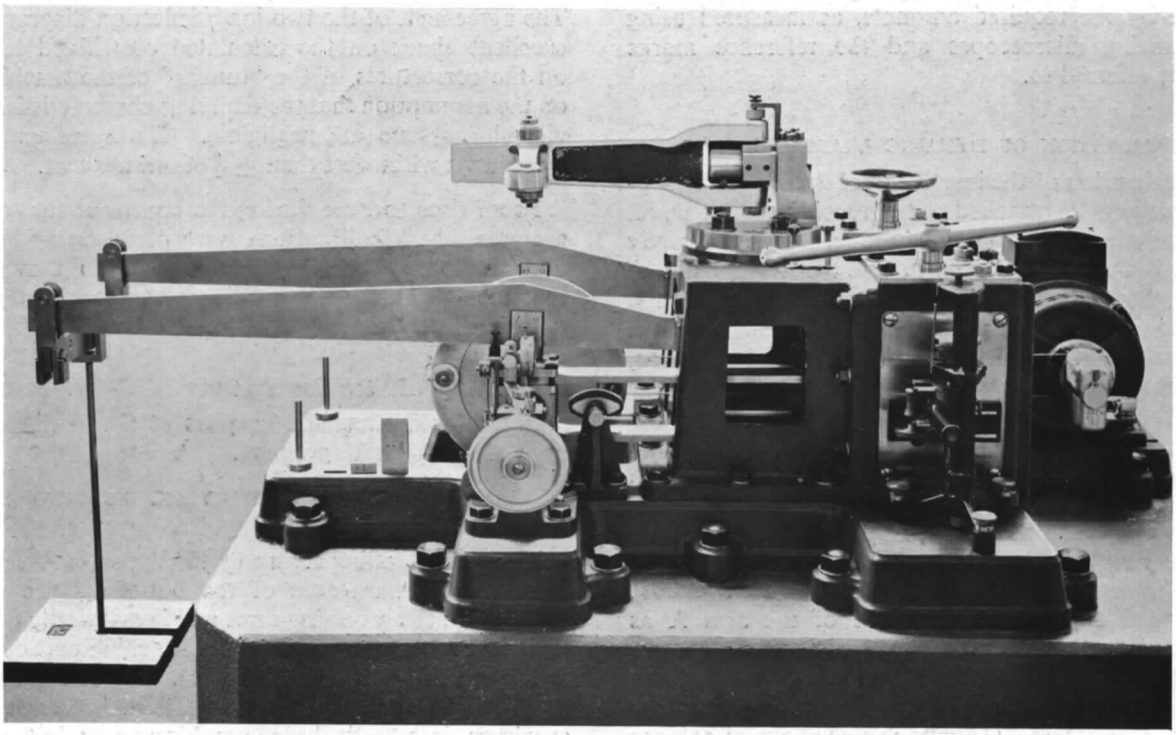

FIG. 61. Method of Calibration of Springs : No. 2 Fatigue Machine.

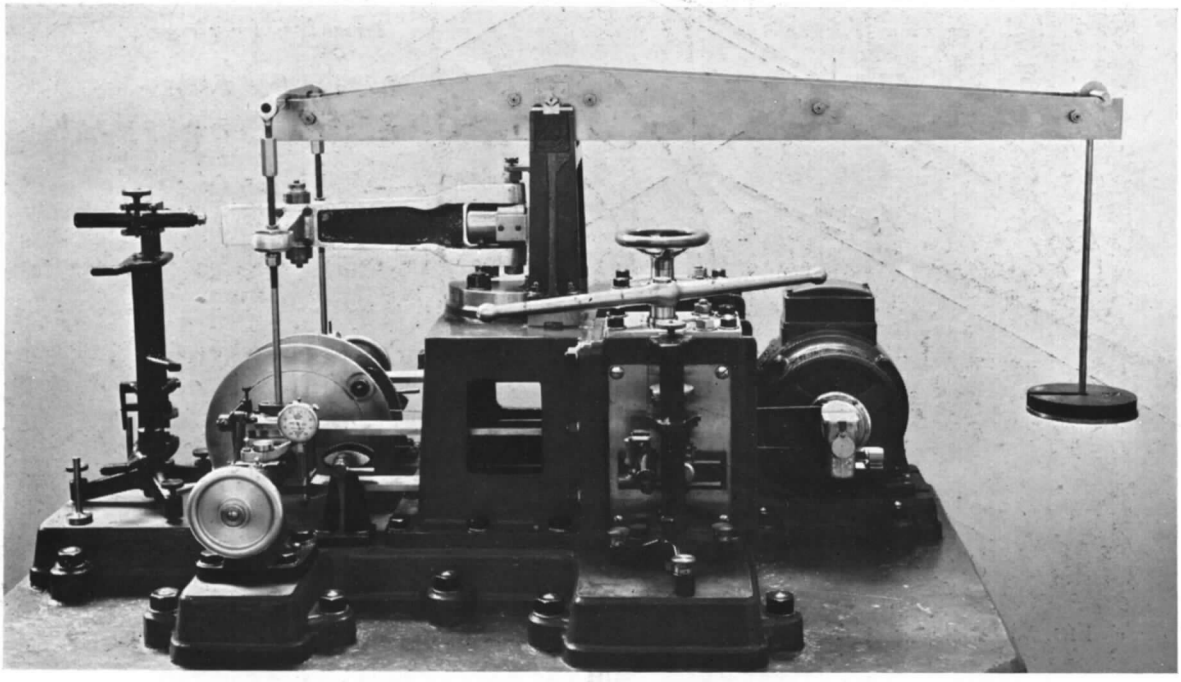

FIG. 62. Method of Calibration of Dynamic Loading Forces : No. 2 Fatigue Machine.

lowering the rear ends of the springs in relation to the baseplate by the required amounts, as measured using the measuring microscopes and the reference marks previously referred to.

(*b*) CALIBRATION OF DYNAMIC LOADING FORCES

For the estimation of the inertia forces due to the out-of-balance weights W attached to the revolving discs D, all that is really necessary, provided the machine is correctly ' tuned ', is the accurate measurement of the masses of these weights, together with the observed speed of the discs. An independent static calibration is carried out by the method illustrated in Fig. 62. A special specimen, reserved for calibration purposes, is placed in the machine which is set in the $\theta = 0$ deg. position. The links L are disconnected at their lower ends from the spindle and spring system. A 2 : 1 lever is mounted as shown in Fig. 62 and attached by links to the cross arm H. Applying weights to the scale pan attached to the right-hand end of the lever, a static load/deflection curve for the specimen is obtained : the recorded deflections are those of cross-lines engraved on the end of the arm A as observed through the measuring microscope shown. The calibration lever is then removed and the links L again connected so that the machine is correctly assembled for operation. Using each pair of out-of-balance weights, singly and in combination, a load/deflection curve is determined under running conditions, the loads being calculated from the masses of the weights and the disc speed : as before, vertical deflections of the end of lever A are observed by the measuring microscope. The agreement of the two load/deflection diagrams is an excellent check on the calculated centrifugal loadings, on the correctness of the ' tuning ' of the machine and on the assumption that the damping characteristics of the vibrating system are negligible. The agreement found was always within less than $\pm \frac{1}{2}$ of one per cent.

From time to time during the course of the test programme, check calibrations were made on springs and dynamic loading of each testing machine : they showed that the accuracy of the machines was excellently maintained throughout.

3. The Applied Stressing System

Fig. 63 is a schematic diagram of the loading system applied to the test specimen.

(*a*) IMPOSED RANGE OF CYCLIC LOADING DUE TO DYNAMIC FORCES

The cyclic loading set up by the dynamic forces arises from the inertia forces of the out-of-balance weights attached to the revolving discs and is essentially the same as induced in the No. 1 Fatigue Machine and described in Section I of Part I of this report. An alternating load, $\pm P$, is applied, at a distance L from the centre of the specimen, in a vertical plane making an angle θ with the vertical plane containing the axis of the specimen. A moment $\pm PL$ equal, say to $\pm M$, is thus imposed : the imposed range of direct shearing force $\pm P$ is, relatively, very small and may be neglected.

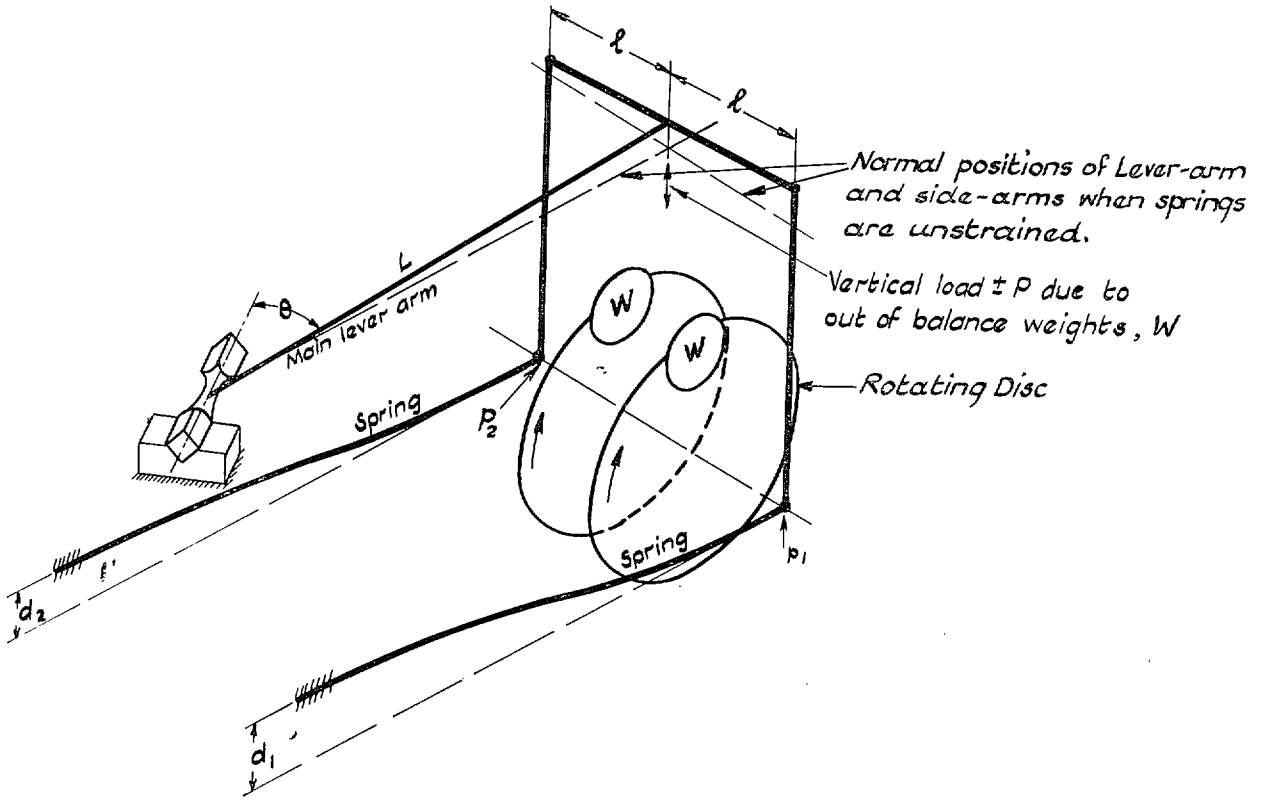

FIG. 63. Schematic Diagram of the Loading System of the No. 2 Fatigue Machine.

The specimen is thus subjected to bending and twisting moments of $\pm M \cos\theta$ and $\pm M \sin\theta$, respectively, which produce the following maximum nominal flexural and shearing fibre stresses :—

Range of Flexural stress, $\pm f$,
due to bending moment $= \pm KM \cos\theta$ (1)

Range of Shear Stress, $\pm q$,
due to twisting moment $= \pm \frac{1}{2} KM \sin\theta$ (2)

where $K = d/2I$ where d is the diameter of the specimen and I is the second plane moment of specimen section. As previously shown, the value of the range of maximum shear stress $\pm S$ induced (half the greatest difference of the principal stresses) is $\frac{1}{2} KM$: thus, a constant value of $\pm M$ at all angles of θ induces the same value of range of maximum shear stress on specimens of the same diameter and it will be convenient to use the maximum range of shear stress value in recording the results obtained in the combined fatigue stress tests on this machine as in the tests made using the No. 1 type machine.

The values of the cyclic ranges of flexural and shear stresses, $\pm f$ and $\pm q$ are, of course, independent of any static stresses which may be superimposed.

(*b*) SUPERIMPOSED STATIC STRESSES

Referring to Fig. 63, by the upward deflections, d_1 and d_2, of the rear ends of the springs, upward forces of p_1 and p_2, are applied to the lower ends of the links and transmitted to the specimen through the side arms, each of length l, and the main lever arm of length L. Let B and T be the bending and twisting moments applied to the specimen by the static forces p_1 and p_2. Then we have :—

The Moments due to p_1 are :—

$$B = p_1 L \cos\theta - p_1 l \sin\theta$$
$$T = p_1 L \sin\theta + p_1 l \cos\theta$$

The Moments due to p_2 are :—

$$B = p_2 L \cos\theta + p_2 l \sin\theta$$
$$T = p_2 L \sin\theta - p_2 l \cos\theta$$

giving the Total Moments due to p_1 and p_2 :—

$$B = p_1 (L \cos\theta - l \sin\theta) + p_2 (L \cos\theta + l \sin\theta) \quad .. \quad .. \quad (3)$$

$$T = p_1 (L \sin\theta + l \cos\theta) + p_2 (L \sin\theta - l \cos\theta) \quad .. \quad .. \quad (4)$$

Thus, from equations (3) and (4) and the known constants of the machine, the superimposed static bending and torsional moments applied to the specimens by any forces p_1 and p_2 due to the springs may be evaluated. But in the actual operation of the machine, it is usually required to find p_1 and p_2 for predetermined values of B and T: it is convenient to re-write the above equations in the forms

$$p_1 = T\left(\frac{\cos\theta}{2l} + \frac{\sin\theta}{2L}\right) - B\left(\frac{\sin\theta}{2l} - \frac{\cos\theta}{2L}\right) \quad (5)$$

$$p_2 = B\left(\frac{\sin\theta}{2l} + \frac{\cos\theta}{2L}\right) - T\left(\frac{\cos\theta}{2l} - \frac{\sin\theta}{2L}\right) \quad (6)$$

or

$$p_1 = aT - bB \quad .. \quad .. \quad .. \quad .. \quad (7)$$
$$p_2 = cB - dT \quad .. \quad .. \quad .. \quad .. \quad (8)$$

where a, b, c and d are constants for any specific value of θ.

A further step for the convenience of practical operation of the machine was to express the static bending and twisting moments, B and T, in terms of the static bending and shearing stresses, f_s and q_s, imposed on the standard solid circular specimen of diameter d. The constants are thereby modified and the final expressions for the spring loads required for any combination of superimposed flexural and torsional stresses become

$$p_1 = \alpha q_s - \beta f_s \quad .. \quad .. \quad .. \quad .. \quad (9)$$
$$p_2 = \gamma f_s - \delta q_s \quad .. \quad .. \quad .. \quad .. \quad (10)$$

where

$$\alpha = \frac{\pi}{16} d^3 \left(\frac{\cos\theta}{2l} + \frac{\sin\theta}{2L}\right)$$
$$\beta = \frac{\pi}{32} d^3 \left(\frac{\sin\theta}{2l} - \frac{\cos\theta}{2L}\right)$$
$$\gamma = \frac{\pi}{32} d^3 \left(\frac{\sin\theta}{2l} + \frac{\cos\theta}{2L}\right)$$
$$\delta = \frac{\pi}{16} d^3 \left(\frac{\cos\theta}{2l} - \frac{\sin\theta}{2L}\right)$$

In the programme which was carried out, five values of θ were employed ; the ratio of f/q is determined solely by θ according to the relation, $f/q = 2 \cot\theta$. The constants of the machine are $L = 12$ in. and $l = 6$ in. Hence, expressing stresses (f_s and q_s) in t/in.^{2} and the spring loads (p_1 and p_2) in pounds, the values of the constants of equations (9) and (10) are stated in Table 19 with regard to a standard solid specimen of 0·500 in. in diameter.

TABLE 19

EQUATION CONSTANTS FOR EVALUATING SPRING LOADS ON A STANDARD SPECIMEN

Dynamic Ratio f/q	θ deg.	Constants			
		α	β	γ	δ
∞	0	4·581	—1·145	1·145	4·581
$3\frac{1}{2}$	29·75	5·114	0·142	2·131	2·841
$1\frac{1}{2}$	53·15	4·581	1·145	2·520	0·916
$\frac{1}{2}$	75·95	3·333	1·945	2·500	—1·111
0	90	2·291	2·291	2·291	—2·291

The diameters of some of the specimens were not exactly to standard size and a simple table of correction factors was prepared and used : the spring loads for any specified stress are directly proportional to the cube of the specimen diameter. The use of these tables in conjunction with equations (9) and (10) enabled all the required spring loads to be easily and quickly estimated.

II. THE TEST MATERIAL

In the investigation described in Part I in which two variables were explored, a series of seven fatigue determinations, using the No. 1 combined stress fatigue machine, was sufficient for each material investigated. The result of substituting four variables for two, in quite a conservative programme, has involved the determination of a minimum of seventy-one fatigue limits for one material, while the time required to carry out these tests has approached about three years, in spite of the fact that four fatigue testing machines were employed for at least half that time ; the operation of setting the No. 2 type of machine for a test was, naturally, more complicated than in the case of the simpler type. A preliminary estimate, made when the research was planned, of the effort involved in carrying out endurance tests of this complicated type and in such numbers, made it clear that it would be impracticable to include a wide range of materials in the programme. It was decided to concentrate on a very limited number of representative aircraft-engine steels, say three, choosing these to cover a practical range of tensile strengths, say 30, 60 and 90 t/in.^{2}, commencing with the intermediate strength. A Ni. Cr. Mo. Va. steel to British Standard Specification S.65A was chosen as possessing special interest and the present report covers the work that has been carried out on that material : in what follows it will be referred to as the S.65A steel.

1. Origin and Description

By arrangement with the Air Ministry and with Messrs. Thomas Firth and John Brown Ltd., a special 32½-ton cast of alloy steel to B.S.S. S.65A was cast at the Sheffield works of that firm. The heat was melted in a basic-lined electric-arc furnace : the latest techniques of high-taper mould and casting methods were employed to produce ingots which were to be as homogenous as possible in their usable portions. The cast yielded forty-seven ingots. The forty-fifth ingot was made the subject of a preliminary investigation at the Brown-Firth Research Laboratories : this ingot was sectioned, sulphur-printed and macro-etched, and chemical analyses were made of samples taken from a variety of positions on a vertical cross-section of the ingot ; a report on this work has been published[13] by the late Dr. W. H. Hatfield, F.R.S. From this examination, Dr. Hatfield concluded that the degree of heterogeneity in the body was so small that the steel in the usable part of the ingot could be considered homogenous in regard to chemical composition.

One ingot provided material for all the experiments made on this steel and described in this report. That ingot was rolled down, at the makers' works, to produce about 300 feet of 1 in. square bar ; this bar stock was sent to the National Physical Laboratory. The remaining ingots were reserved, at Sheffield, for a proposed future programme of fatigue tests which would include an investigation of ' size effect,' in which specimens of diameters of 2½ in. or more would be used.

The bar stock was received from the makers in the annealed condition. All test-pieces were rough machined nearly to size before being heat-treated ; the heat-treatment was carried out in Sheffield by Messrs. Firth-Brown. This heat-treatment consisted of a preliminary normalising (900 deg. C for 1 hour : cooled in air), reheating and quenching in oil (850 deg. C for 1 hour: O.Q) and tempering (640 deg. C for 3 hours : cooled in air). The normalising process was carried out on batches of specimen blanks taken ten at a time : the two subsequent heat treatments, each on batches of blanks taken five at a time. This batch method was unavoidable but every precaution was taken to preserve uniform conditions of heat-treatment throughout. Duplicate static tests on specimens of the material have yielded extremely consistent results, but, in some cases, the endurance test data displayed a most undesirable degree of ' scatter.' It is, of course, recognised that, under some of the more complex and severe imposed stress conditions, the material may have been in a somewhat unstable condition while it is common experience that, under the searching fatigue test, very rarely does a heat-treated high-alloy steel behave as consistently as, for example, a normalised mild steel. Nevertheless, the uncertainty attached to the accuracy of some of the fatigue data obtained is a cause for some disappointment. The final machining operations on all the test specimens were made after the heat-treatment had been carried out on the rough machined specimen blanks.

In addition to the extensive series of tests made on this material in the No. 2 Combined Stress Fatigue Machine, it was of interest also to make one series of combined fatigue stress tests using the No. 1 type of machine. The results of the latter tests have already been reported in Part I of this paper. It should, therefore, be noted that the Ni. Cr. Mo. Steel (60/70 ton) of Part I (see Table 1) and the S.65 Steel of Part II represent the same identical material, tested in the same heat-treated condition and having the common identification mark JZP.

2. Results of Chemical Analysis and Metallurgical Examination

The chemical analysis and heat-treatment have been reported in Tables 1 and 2, while a brief summary of the results of the metallurgical examination is given in Appendix I. The appearances of typical microstructures, before and after heat-treatment are reproduced in Figs. 11 (*a*) and 11 (*b*) at magnifications of 150 and 500 diameters, respectively. As the metallurgical examination made on this material at the National Physical Laboratory was extensive, it may be of interest to amplify somewhat the description previously given. The material was first examined in the annealed condition as received from the makers. An estimation, using the Bolsover method, showed that the number of non-metallic

inclusions was reasonably low. A grain size determination, using the McQuaid and Ehn method, showed that the principal grain size was equivalent to about 320,000 grains per square inch of surface. As seen in Fig. 11 (*a*) the microstructure of the annealed condition showed heavy banding which tended to be eliminated by subsequent heating above the critical point.

The material was also examined in the heat-treated condition as tested. Fig. 11 (*b*) shows the structure: some banding is still present. The steel is of good quality, the sulphur and phosphorus contents are low, while the amounts of the added elements fall within the limits specified by the British Standard Specification, S.65A. The number of non-metallic inclusions is low and they are distributed satisfactorily. There is no appreciable segregation of impurities.

3. Results of Supplementary Mechanical Tests

The usual complete programme of supplementary mechanical tests—as described in Part I, Section 2, B—were carried out on this material with the results as stated in Appendix 2, Part I and summarised in Table 3. The record tensile strength of 65 (64·7) t/in.^{2} is a normal value for this material which also possesses excellent ductility (67% R.A.) and notched bar Izod value (90 ft. lb). The Dalby load/elongation diagrams to fracture, one of which is reproduced as Fig. 13 (*k*), exhibit a well-marked drop at yield. The Wohler fatigue limit, $\pm 37{\cdot}5$ t/in.^{2} is clearly defined as shown in Fig. 27 (*f*), and is classed as 'reliable (R).' In the reversed-torsion tests carried out on the Stromeyer machine, however, the material behaved very irregularly (*see* Fig. 31) and the value of this torsional fatigue limit can only be estimated at $\pm 21\frac{1}{2}$ t/in.^{2} and is definitely classed as 'unreliable (U).'

4. Results of Tests Made in the No. 1 Combined Stress Fatigue Testing Machine

The results of these combined stress fatigue tests are fully reported in Part I, Appendix 3 and summarised in Table 5 of Part I, Section 4. The *S/N* curves (Fig. 42) show such an unsatisfactory degree of 'scatter' that little accuracy is attached to the recorded values; plotted in Fig. 19 (*c*), in the form of an *f/q* curve, they appear to conform to the "ellipse quadrant" relation.

III. PROGRAMME OF COMBINED STRESS FATIGUE TESTS

The test programme, carried out on the No. 2 Combined Stress Fatigue Testing Machine, divides naturally into two parts. The first relates to the determination of what may be termed the intrinsic fatigue limits of the material, using polished solid specimens of circular cross-section, associated with the size of specimen used and the imposed combined stress conditions. The second part of the programme relates to the determination of the effect of selected rapid changes of section, also discontinuities of section, on the previously determined intrinsic fatigue limits of the material.

1. Tests on Solid Cylindrical Specimens

This section of the programme was planned to survey in outline the intrinsic fatigue resistance of the material under practical combinations of the four stress component variables—cycles of reversed bending stress, cycles of reversed torsional stress, superimposed static bending stress and superimposed static torsional stress. The actual values of the applied stresses were selected to cover the field of practical interest in connection with the aeroplane engine crankshaft and similar problems. For, as the fatigue limit is dependent on the mean stress of the cycle which can have any value between zero and the ultimate strength of the material in bending or shear, theoretically an enormous scope of applied stress combinations is possible. The first practical limit imposed is the limitation of number of specimens and testing time: the second, that stress combinations under which failure by fatigue is preceded by an appreciable amount of plastic yielding have little, if any, design interest.

It was decided to build a programme around three values of each type of superimposed static stress; also, to couple with each combination of static mean stresses not more than five combinations, i.e. five values of θ, of reversed bending and reversed torsional cyclic stresses. (As against seven combinations of cyclic stresses only used throughout Part I of the investigation).

The five values which have been employed are $\theta = 0$, 29·7, 53·1, 75·9 and 90 deg., the corresponding values of $\pm f/\pm q$ being:—∞ ($q = 0$), $3\frac{1}{2}$, $1\frac{1}{2}$, $\frac{1}{2}$ and 0 ($f = 0$). It will be convenient to refer to the ratio f/q (equal to 2 cot θ) as the 'dynamic ratio,' thus avoiding any confusion between the applied reversed cyclic stresses, to which f and q only refer, the superimposed static stresses and the complete imposed stress cycle which is a combination of the other two.

Superimposed static bending and static torsional stresses will be denoted by M and T, respectively, the suffix 0 denoting zero mean stress of the particular type, thus, M_0 and T_0. Of considerable practical interest is the case of repeated stress, in which the stresses at the fatigue limit—bending or torsion—vary cyclically from zero to a positive value: for this case, M_r and T_r will be used to denote the mean static stress. Clearly M_0 and T_0 (reversed stresses) and M_r and T_r (repeated stresses) must be selected as two of the three mean stress

values to be investigated. As it was necessary to keep the third type of stress cycle within the practical field of design interest, before this third value could be decided on, it was first necessary to determine, experimentally, the reversed and repeated stress fatigue limits.

This was done with the following results :—

(*a*) Fatigue Range (reversed plane bending), t/in.^{2} .. .. $= \pm 37\frac{3}{4}$

(*b*) Fatigue Range (repeated plane bending), t/in.^{2} .. .. $= 0$ to 69 or $34\frac{1}{2} \pm 34\frac{1}{2}$

(*c*) Fatigue Range (reversed torsion), t/in.^{2} .. .. $= \pm 24$

(*d*) Fatigue Range (repeated torsion) t/in.^{2}.. .. .. $= 0$ to $44\frac{1}{2}$ or $22\frac{1}{4} \pm 22\frac{1}{4}$

thus supplying the values :—$M_r = 34\frac{1}{2}$, $T_r = 22\frac{1}{4}$.

The high values obtained for the fatigue limits under repeated stresses show that the field of pulsating stresses ($M > M_r$ and $T > T_r$) lies outside the range of practical interest to the designer and it was decided to make the third series of tests midway between M_0, T_0 and M_r, T_r, corresponding to $M_r/2$ and $T_r/2$, i.e. having the actual mean stress values of $17\frac{1}{4}$ t/in.^{2} (bending) and 11 t/in.^{2} (torsion) rounding off the latter value.

The test programme was, therefore, built up round the mean stress values of M_0, $M_r/2$, M_r and T_0, $T_r/2$, T_r as represented schematically in Table 20 which requires some explanation.

Table 20 divides naturally into nine squares numbered in (bold) roman numerals. In each square are shown the fatigue limits to be determined. Each test is numbered for reference purposes : against each reference number is shown the corresponding value of the dynamic ratio to be used. The superimposed static bending and static torsional stresses, respectively, are given by the headings of the vertical and the horizontal columns in which the particular square is situated. Thus, squares **I**, **II** and **III** contain tests, in which the values of the static bending stress are M_0, $M_r/2$ and M_r, respectively, the value of the static torsional stress being zero throughout. Squares **I**, **IV** and **VII** form a similar series, substituting three values of static torsional stress coupled with zero static bending stress. Again, in each of squares **I**, **V** and **IX**, static bending and torsional stresses or corresponding amounts are simultaneously applied : M_0 and T_0, $M_r/2$ and $T_r/2$, M_r and T_r.

Regard for reasonable economy in numbers of specimens and testing time forbade the use of the full series of five dynamic ratios for each square. The importance of the stress combinations represented by squares **I**, **V** and **IX** appeared to merit the full series of the five ratio values. Next, squares **II** and **IV** where three ratio values have been inserted. In each of the remaining squares, **III**, **VII**, **VI** and **VIII** two ratios only are inserted. Even with this restricted programme, twenty-nine separate fatigue limit investigations are involved.

TABLE 20

SCHEMATIC REPRESENTATION OF THE TEST PROGRAMME CARRIED OUT ON SOLID CYLINDRICAL SPECIMENS

		Superimposed Static Bending Stress, t/in^2		
		$M_0 = 0$	$M_r/2 = 17\frac{1}{4}$	$M_r = 34\frac{1}{2}$
Superimposed Static Torsional Stress, t/in^2	$T_0 = 0$	(1) $f/q = \infty$ ($q = 0$) (19) $f/q = 3\frac{1}{2}$ (20) $f/q = 1\frac{1}{2}$ (21) $f/q = \frac{1}{2}$ (4) $f/q = 0$ ($f = 0$) 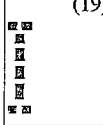	(2) $f/q = \infty$ (28) $f/q = 1\frac{1}{2}$ (13) $f/q = 0$ 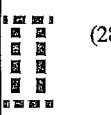	(3) $f/q = \infty$  (14) $f/q = 0$
	$T_r/2 = 11_{\cdot}$	(7) $f/q = \infty$  (29) $f/q = 1\frac{1}{2}$ (5) $f/q = 0$	(9) $f/q = \infty$ (22) $f/q = 3\frac{1}{2}$ (23) $f/q = 1\frac{1}{2}$ (24) $f/q = \frac{1}{2}$  (15) $f/q = 0$	(11) $f/q = \infty$  (16) $f/q = 0$
	$T_r = 22\frac{1}{4}$	(8) $f/q = \infty$  (6) $f/q = 0$	(10) $f/q = \infty$  (17) $f/q = 0$	(12) $f/q = \infty$ (25) $f/q = 3\frac{1}{2}$ (26) $f/q = 1\frac{1}{2}$ (27) $f/q = \frac{1}{2}$  (18) $f/q = 0$

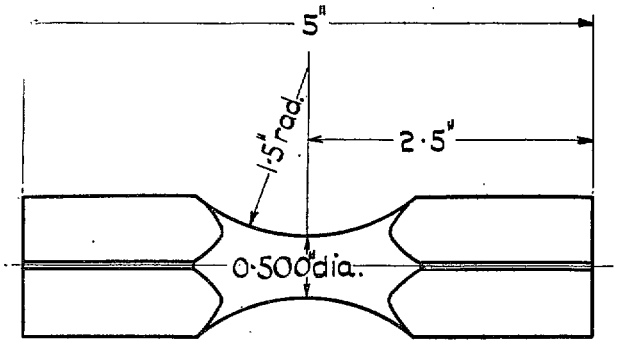

A. Solid Plain Specimen

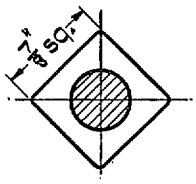

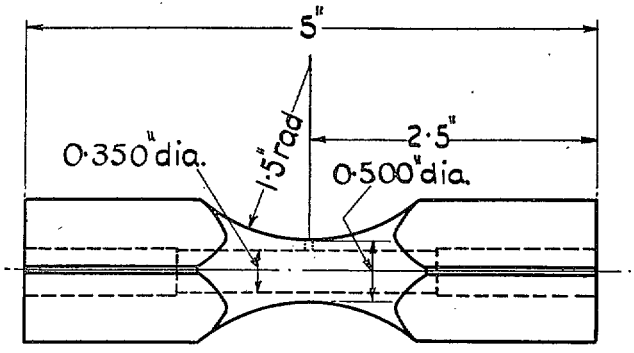

B. Hollow Specimen with radial hole.

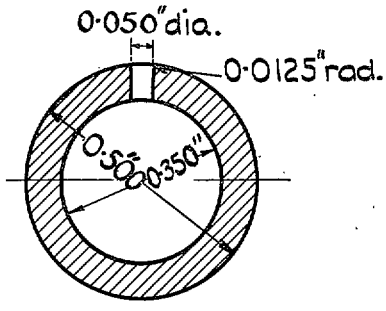

Enlarged Section

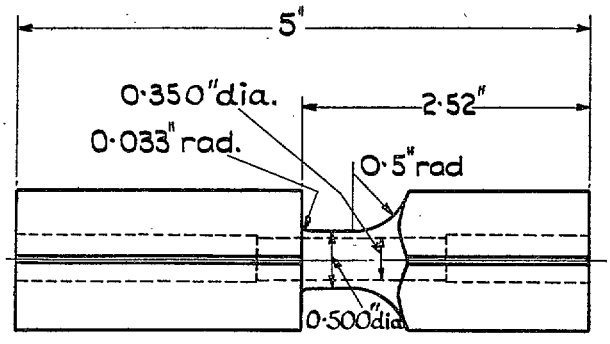

C. Hollow Specimen with Fillet ($\frac{r}{D} = \frac{1}{15}$)

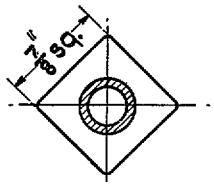

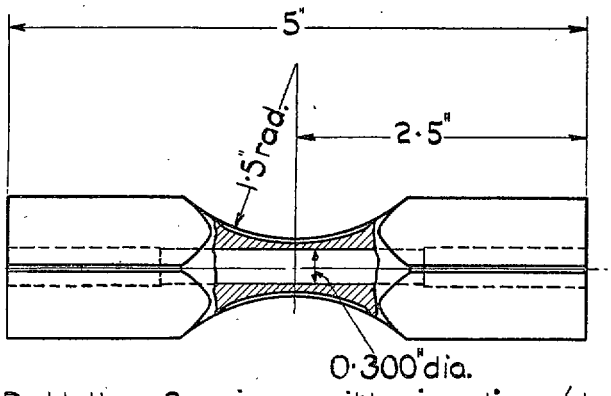

D. Hollow Specimen with six splines (deep)

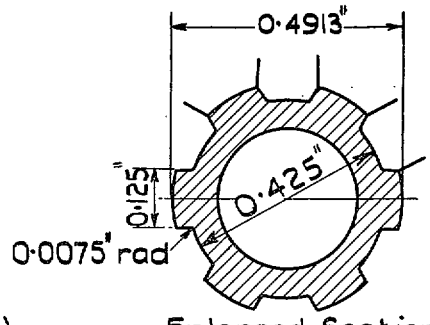

Enlarged Section

Splines based BSS Nº 46. Part 2 - 1929
Table XIV - U. K. Fit

FIG. 64. Test Specimens for Combined Stress Research.

It will be recognised that the results of tests (1), (2) and (3) will show the effect of imposing static bending stresses on the fatigue limit under reversed bending stress : similarly, the results of tests (4), (5) and (6) will show the effect on the reversed torsional fatigue limit of adding static torsional stress. The results of tests (1), (7) and (8) will show the effect on the reversed bending fatigue limit of superimposing static torsional stresses : correspondingly, tests (4), (13) and (14) will show the effect of superimposed static bending stresses on the fatigue limit under reversed torsional stresses. And so on.

Each fatigue limit was determined, on one of the No. 2 Combined Stress Machines, by the usual method of endurance testing, on a minimum basis of 10^7 cycles. The number of specimens tested and the applied ranges of stress were chosen to determine the limiting range within as close limits as permitted by the regularity of the behaviour of the material under test.

As the adjustment and manipulation of the testing machine under some of the complex stress systems of Table 20 naturally present some difficulties, it may be of interest to record two items of testing technique which were evolved from experience and which assisted to standardise the test procedure and to reduce experimental errors and operating time.

(1) The machine was fitted with a trip gear which cut out the motor when a sensible increase occurred in the range of strain of the specimen : this gear could be adjusted within very close limits and usually operated so early in the fatigue cracking stage that a complete fracture of the specimen was a rare occurrence. This close adjustment was also necessary in order that the required spring load should not be departed from during a test. This disadvantage would arise if, especially under very high values of static stress, the specimen underwent a small permanent strain in the early stages of the test : the machine would then stop and a complete readjustment and checking of spring loads would be necessary. Now it had previously been established, by Gough and Wood[21], that, under the severest conditions of direct stresses—pulsating tensile stress which caused considerable initial yielding—if a single sustained application of the maximum load of the cycle was applied statically, the specimen yielded : if the required stress cycle was then applied at its normal high frequency, and provided that cycle was below the safe range of stress, no appreciable further extension occurred. This observation was made use of in the present tests. Each specimen was pre-stressed *in situ* by one sustained application of those spring deflections of the machine which imposed the superior stress of the cycle to be subsequently applied : the value of the superior stress being the sum of the spring loads and half the cyclic load. The method was entirely successful.

(2) The diameters of some of the specimens varied slightly from the standard diameter of 0·500 in. To avoid resetting the springs for every specimen, the springs were accurately adjusted, in the rear end blocks, to suit the standard sized specimens : this spring position was then left unaltered throughout the whole series of tests required for the determination of that particular fatigue limit. The compensation for the deviation in specimen size was then made, in each test, by accurate adjustment of the vertical height of the disc-spindle F by using slip gauges. In this way, it was ensured that the clamping conditions of the springs were constant throughout the test series and that, therefore, the applied spring loads were also constant : variations in clamping conditions might have led to small differences in the spring loading.

Form of Specimen :—The form and dimensions of the specimens used for this series of tests are shown in Fig. 64A. They were of solid circular cross-section having a minimum diameter of 0·500 in. The transition radius of 1·5 in. was such ($r/d = 3$) that the fatigue properties of the specimens should not have been appreciably affected by the stress concentration effect due to this rate of change of section.

Surface of Specimens :—The fatigue strength of heat-treated alloy steels is often sensitive to small surface defects and some preliminary tests were made to determine a suitable surface finish. A batch of specimens was finish-machined and polished, in a circumferential direction, using 00 and 000 emery papers. Their appearance was good but, under the microscope, polishing marks were clearly visible. The fatigue range of this batch was determined, under reversed plane bending stresses, in the No. 2 type machine. An undesirable 'scatter' of test data resulted, coupled with some inconsistency. Further, there was evidence that some of the fractures had commenced at polishing marks. A further batch of specimens was prepared, the polishing being carried out in a more refined manner and always in the longitudinal direction, and the fatigue range re-determined. The data obtained were consistent indicating a clearly defined fatigue limit exceeding the previous value by nearly $\pm$ 1 t/in.^{2}. The longitudinal polishing method was, therefore, adopted as standard for the whole programme.

This steel is, undoubtedly, somewhat sensitive to surface defects and the 'scatter' of fatigue results which was subsequently encountered in some of the tests was probably partly due to this cause.

2. Tests on Specimens containing Discontinuities of Form

In consultation with representatives of the aircraft engine industry, it was decided that the effect of drilled oil-holes, sharp transition fillets and splines could usefully be investigated as representing types of unavoidable discontinuities of form and section associated with practical crankshafts ; the forms and dimensions of the

specimens selected are as shown in Fig. 64, being chosen to produce scale models of practical cases. The three types of specimen are :—

(*a*) Hollow specimen having a radial drilled oil-hole (Fig. 64B).

(*b*) Hollow specimen having a transition fillet of small radius (Fig. 64C).

(*c*) Hollow specimen having six deep splines based on the appropriate British Standard Specification. (Fig. 64D.)

A hollow form of specimen was adopted as representing a nearer approach to a practical engine component in which such discontinuities are present. The result, therefore, will not be strictly comparable with those relating to the solid specimens ; the hollow specimens can, however, be regarded as fairly ' thick-walled ' and the effect of removing the core will certainly be small when bending stresses are imposed and, probably, also small under torsional stresses ; in any case, this ' form ' effect will be very small in comparison with the stress concentration effect due to the presence of the discontinuities of form. Specialised machining facilities and experience are required for the accurate preparation of such specimens and this was kindly undertaken by the Bristol Aeroplane Company, Ltd. ; special acknowledgment is made of the valuable advice, co-operation and assistance rendered by that firm.

The adopted scheme of tests was based on that drawn up for the solid specimens, but it was considered that the high value of $M_r = 34\frac{1}{2}$ t/in.^{2} was beyond the range of practical design interest for these components. The test programme corresponds, therefore, to squares **I, II, IV** and **V** of Table 20 with the single amendment that three values of ' dynamic ratio ' only are investigated in the square corresponding to number **V** of Table 20 in place of the five values shown in that table. The test programme that was adopted, for each type of ' discontinuity ' specimen, is, therefore, as set out in Table 21.

TABLE 21

SCHEMATIC REPRESENTATION OF THE TEST PROGRAMME CARRIED OUT ON HOLLOW SPECIMENS CONTAINING ONE OF THREE FORMS OF DISCONTINUITY OF SECTION

Superimposed Static Torsional Stress, t/in2		Superimposed Static Bending Stress, t/in^2	
		$M_0 = 0$	$M_r/2 = 17\frac{1}{4}$
$T_0 = 0$		(1) $f/q = \infty$ ($q = 0$) (13) $f/q = 3\frac{1}{2}$ (9) $f/q = 1\frac{1}{2}$ (14) $f/q = \frac{1}{2}$ (5) $f/q = 0$ ($f = 0$)	(2) $f/q = \infty$ (10) $f/q = 1\frac{1}{2}$ (6) $f/q = 0$
$T_r/2 = 11$		(3) $f/q = \infty$ (11) $f/q = 1\frac{1}{2}$ (7) $f/q = 0$	(4) $f/q = \infty$ (12) $f/q = 1\frac{1}{2}$ (8) $f/q = 0$

For each type of specimen, four values of static stress are thus involved—M_0, T_0, $M_r/2$ and $T_r/2$ and fourteen fatigue ranges have to be determined. The method of testing and the test procedure adopted have been previously described. The following additional notes relate to the specimens and the tests.

(*a*) TESTS ON HOLLOW SPECIMENS CONTAINING A RADIAL DRILLED HOLE

This type of specimen (see Fig. 64B) was designed with the same external form as the solid specimen and has the ' standard ' test diameter of 0·500 in. The internal bore diameter is 0·350 in. ($d/D = 0{\cdot}7$), the diameter (δ) of the drilled hole is 0·050 in. ($\delta/D = 0{\cdot}1$).

The applied nominal stress ranges have been calculated neglecting the presence of the drilled hole. All specimens were inserted in the machine so that the drilled hole was in the region of maximum applied bending moment.

(*b*) TESTS ON HOLLOW SPECIMENS CONTAINING A TRANSITION FILLET OF SMALL RADIUS

The parallel test portion of the specimen (see Fig. 64C) has the standard diameter of 0·500 in. and length of $\frac{3}{8}$ in. : it is joined to the enlarged end of the specimen by a transition fillet of 0·033 in. radius ($r/D = 1/15$).

The applied nominal stress ranges have been calculated on the modulus of section of the hollow parallel portion of the specimen, neglecting the presence of the fillet. The external diameter of each specimen was measured using an optical projection apparatus at a magnification of 50 diameters : the bore diameter was accurately determined, to within a tolerance of $\pm 0{\cdot}001$ in., by plug gauges.

(*c*) TESTS ON HOLLOW SPECIMENS CONTAINING SIX SPLINES

The form and dimensions of the specimen are shown in Fig. 64D : it was designed so that the dimensions at the minimum diameter of the test portion conformed to British Standard Specification No. 46, Part 2, 1929, Table XIV, U.K. Fit.

It will be recalled that the plane of bending applied to a test piece mounted in the combined stress fatigue testing machine is the vertical plane containing the axis of the specimen and one diagonal of the enlarged square end of the specimen. Reference to Fig. 64D shows that a splined specimen may thus be mounted in two alternative positions, so that the maximum applied bending moment acts (*a*) at the centre of a spline crest, or (*b*) at the centre of a spline trough. Some preliminary experiments

(92759)

were made to determine the relative influence of these alternative positions on the fatigue resistance of the splined shafts. Using cycles of simple reversed bending stresses (Test (1) of Table 21), the fatigue limit was determined in each of the two alternative specimen positions. The results obtained are plotted in Fig. 76. in which the stresses stated are deduced using the calculated moment of inertia of each alternative position of the splines in relation to the axis of bending, taking into account the actual cross-sections of the shaft. The difference between the estimated values of the fatigue limits, $\pm 36\frac{1}{2}$ t/in.^{2} for the 'crest' position and ± 37 t/in.^{2} for the 'trough' position is very small. The S/N curve aa of Fig. 76 (*a*), is reproduced, as a dotted line, in the lower diagram, Fig. 76 (*b*) ; it is evident that all the data for both sets of experiments would fit a single S/N curve admirably, giving the estimated value of the common fatigue limit as $\pm 36\frac{1}{2}$ t/in.^{2}. However, the main programme of tests has been carried out with the specimens mounted in what may be the slightly weaker position, i.e. with the maximum bending moment always applied on the centres of an opposite pair of spline crests.

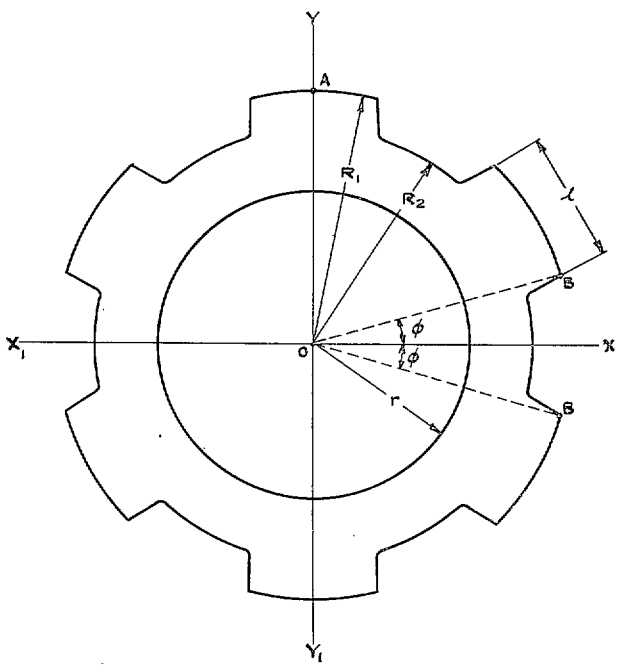

FIG. 65. Cross-section at the minimum diameter of the Splined Specimen.

The bore diameter of the splined specimens was reduced to 0·300 in., as compared with 0·350 in. for specimens containing a radial hole or small transition fillet, to preserve a sufficient thickness of material below the spline troughs.

Referring to Fig. 65, the polar moment of inertia, I_0, of the splined shaft section is given, approximately, by the expression :—

$$I_0 = \frac{\pi}{2}\left(R_2^4 - r^4\right) + 3\left(R_1^4 - R_2^4\right)\sin^{-1}\frac{l}{R_1 + R_2}$$

where R_1 is radius of section at spline crest

R_2 is radius of section at spline trough

r is radius of bore

l is width of spline crest.

and it may be shown that the moments of inertia of the section taken about the axes XX_1 and YY_1 are equal, i.e.

$$I_{xx} = I_{yy} = I_0/2$$

As mentioned above, the main programme of tests has been carried out with the specimens so mounted in the machine that the axis YY was always in the vertical plane. The stresses have been estimated using the calculated values of I_{yy}, and I_0 for bending and torsion, respectively. It will be seen from Fig. 65, that, in the preliminary bending fatigue tests made to determine the specimen setting, we have :—

$$\text{Bending Stress at A} = \frac{2M_A R_1}{I_0}$$

$$\text{Bending Stress at B} = \frac{2M_B R_1 \cos\phi}{I_0}$$

Longitudinal splines should have very little, if any, stress concentration effect under bending stresses ; as we have seen, the experimental fatigue limits for the 'crest' and 'trough' positions were in extremely good agreement, thus giving confidence in the method of calculation employed. Also, comparing these values ($\pm 36\frac{1}{2}$ and ± 37 t/in.^{2}) with the value obtained, in the preliminary tests, for the fatigue limit of solid specimens under reversed bending stresses, i.e. $\pm 37\frac{3}{4}$ t/in.^{2}, clearly the stress concentration effect of the splines is indeed small and, perhaps, non-existent ; the maximum difference between these values is 3% which might be due, wholly or in part, to small differences between batches of specimens, to the effect of solid versus hollow form, or to a combination of these effects.

IV. RESULTS OF THE COMBINED STRESS FATIGUE TESTS

The fatigue limit of the steel, with each form of specimen and combination of applied static and cyclic loading, was determined by the usual method of endurance testing, on a basis of 10^7 cycles. The method of adjusting the loading and the testing technique adopted have been previously described. Prior to the fatigue test and as a check on heat-treatment, four indentation tests were made on the enlarged ends of each specimen, using a 5 mm. ball and a load of 750 kg. : it seems unnecessary to include the resulting B.H.N. in this report. The trip gear of each machine was closely adjusted and most of the tests were stopped in the early stages of fracture :

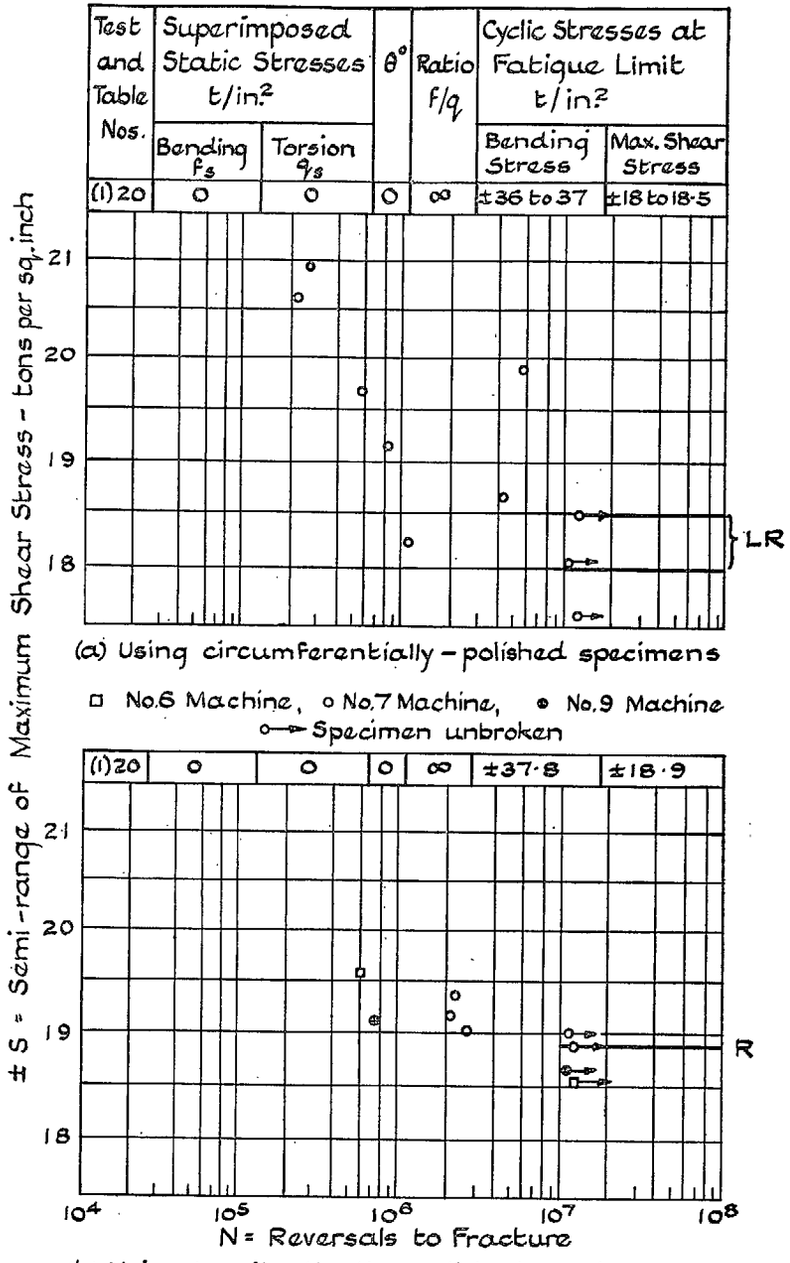

FIG. 66. *S/N* Diagrams. Solid Specimens. Test (1).

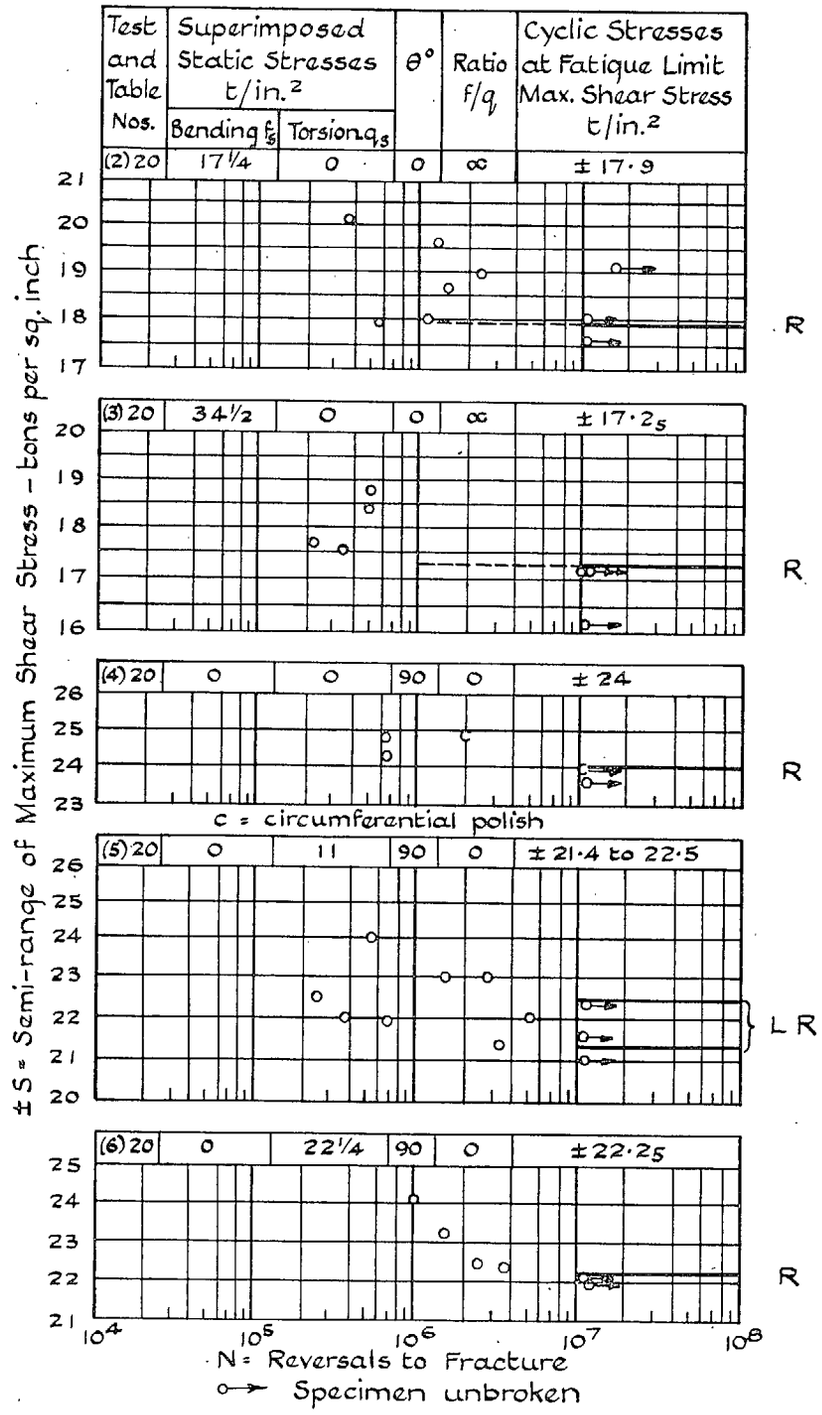

FIG. 67. *S/N* Diagrams. Solid Specimens. Tests (2) to (6).

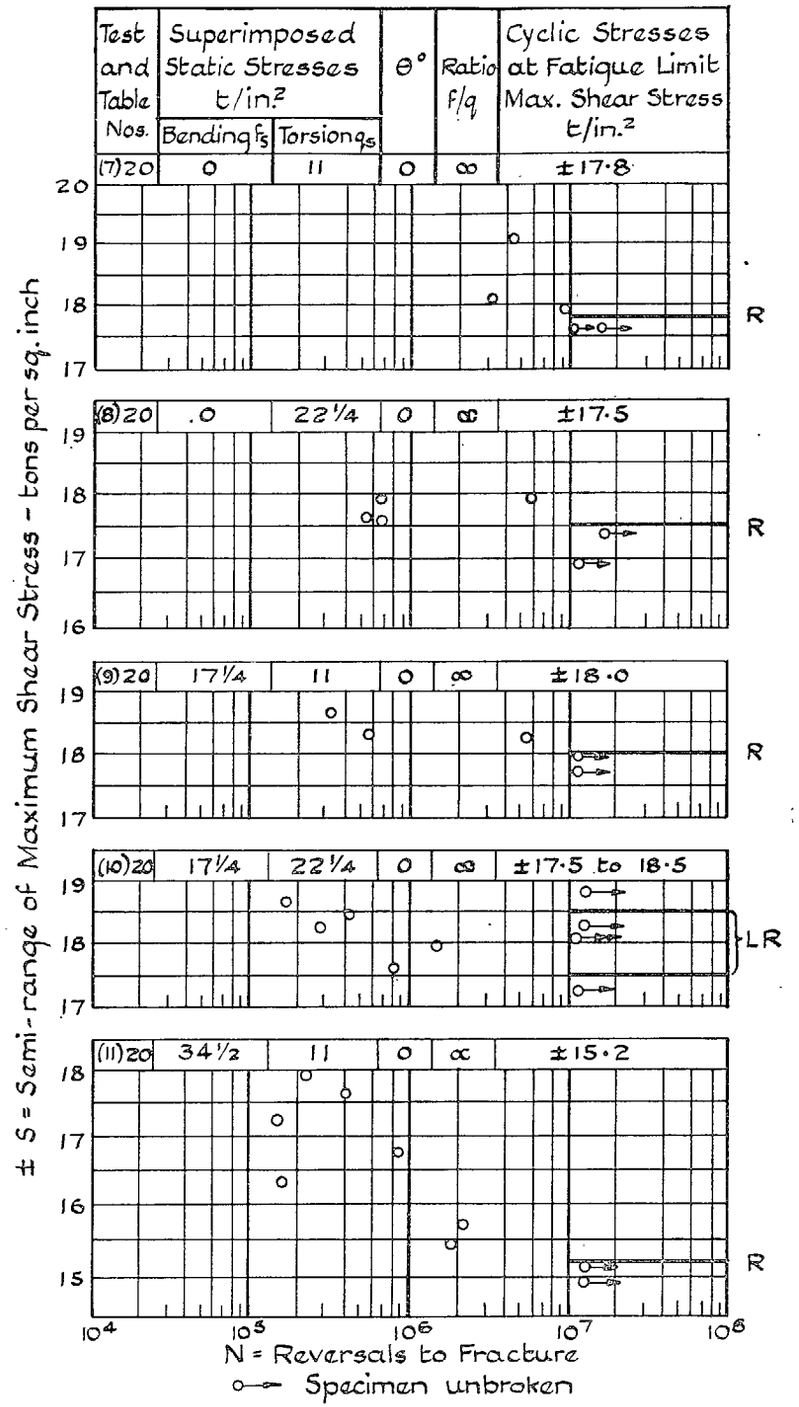

FIG. 68. *S/N* Diagrams. Solid Specimens. Tests (7) to (11).

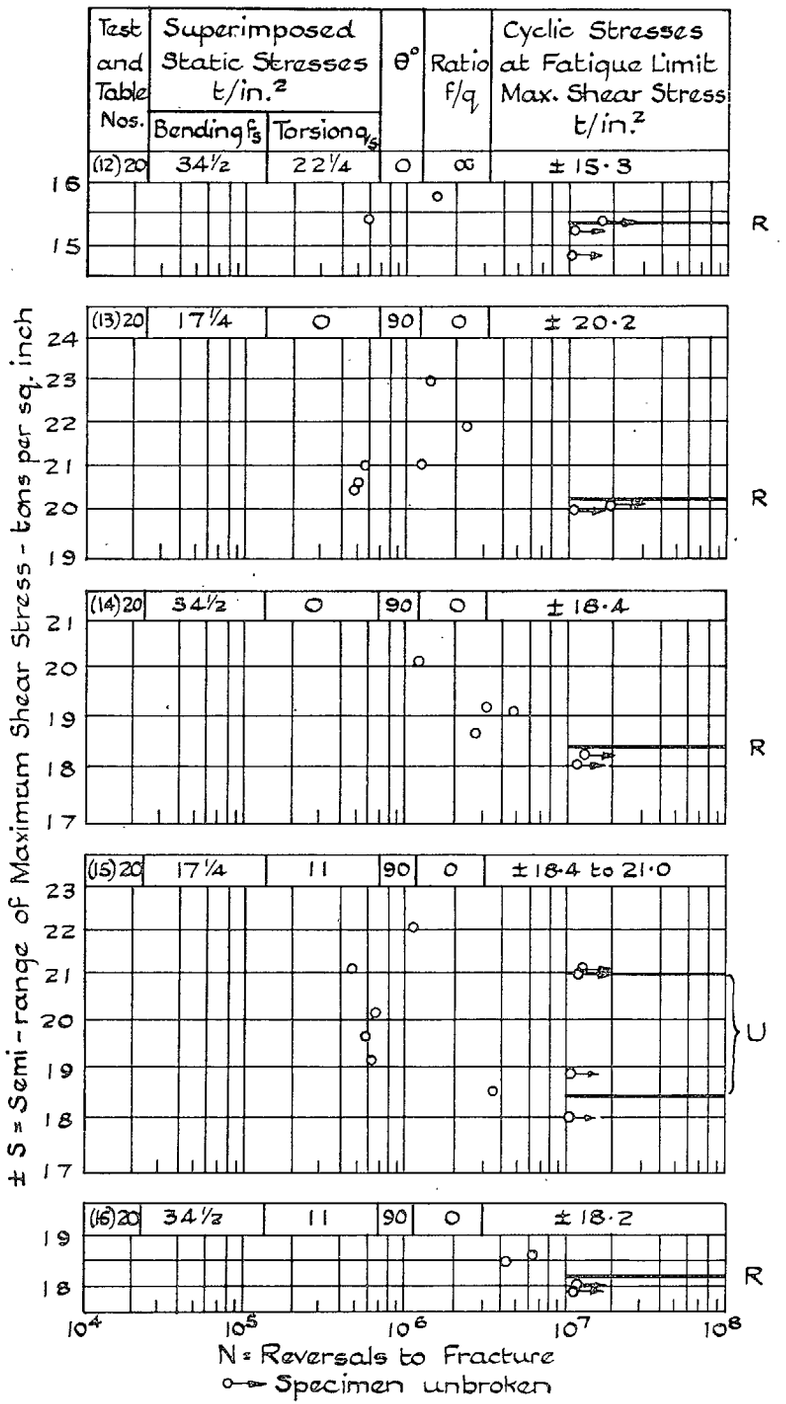

FIG. 69. *S/N* Diagrams. Solid Specimens. Tests (12) to (16).

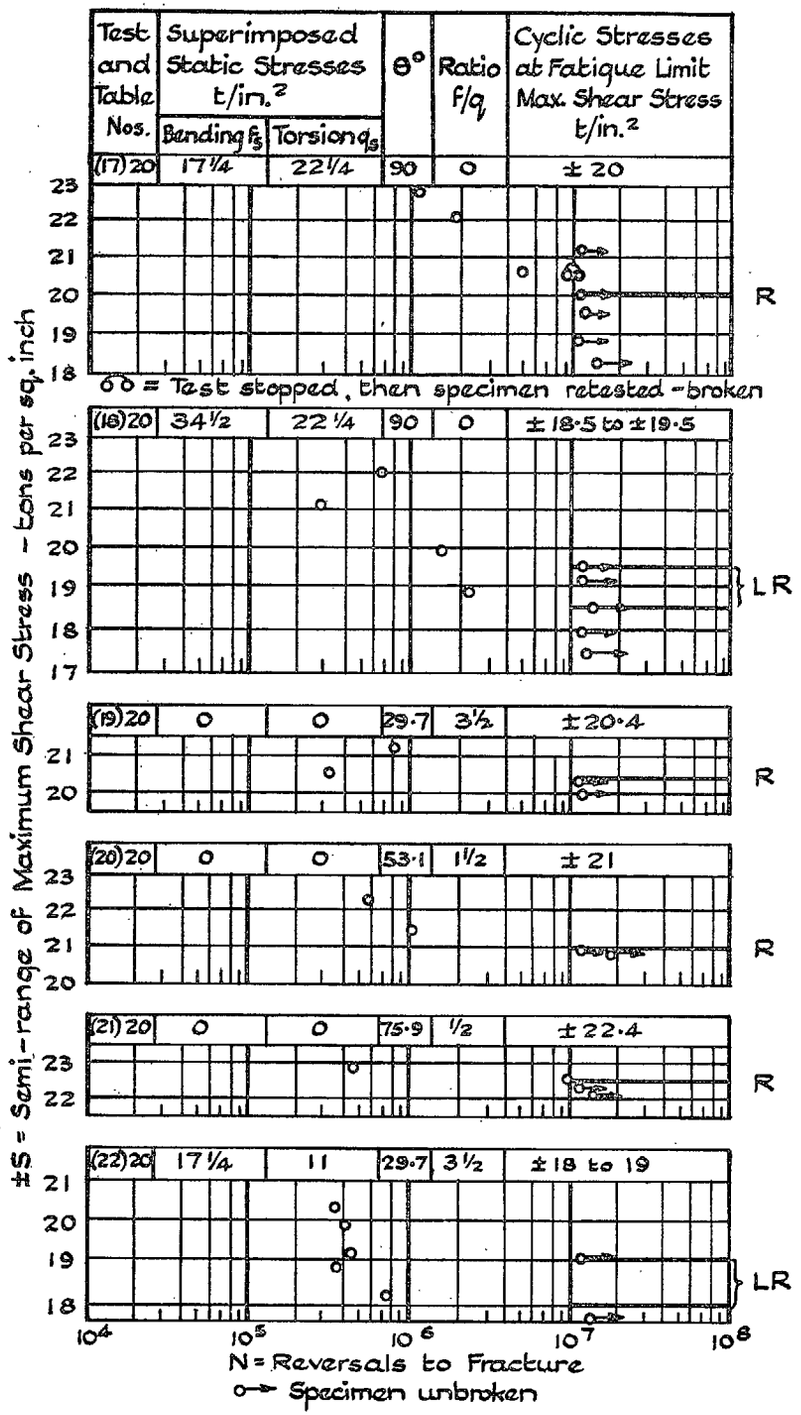

FIG. 70. *S/N* Diagrams. Solid Specimens. Tests (17) to (22).

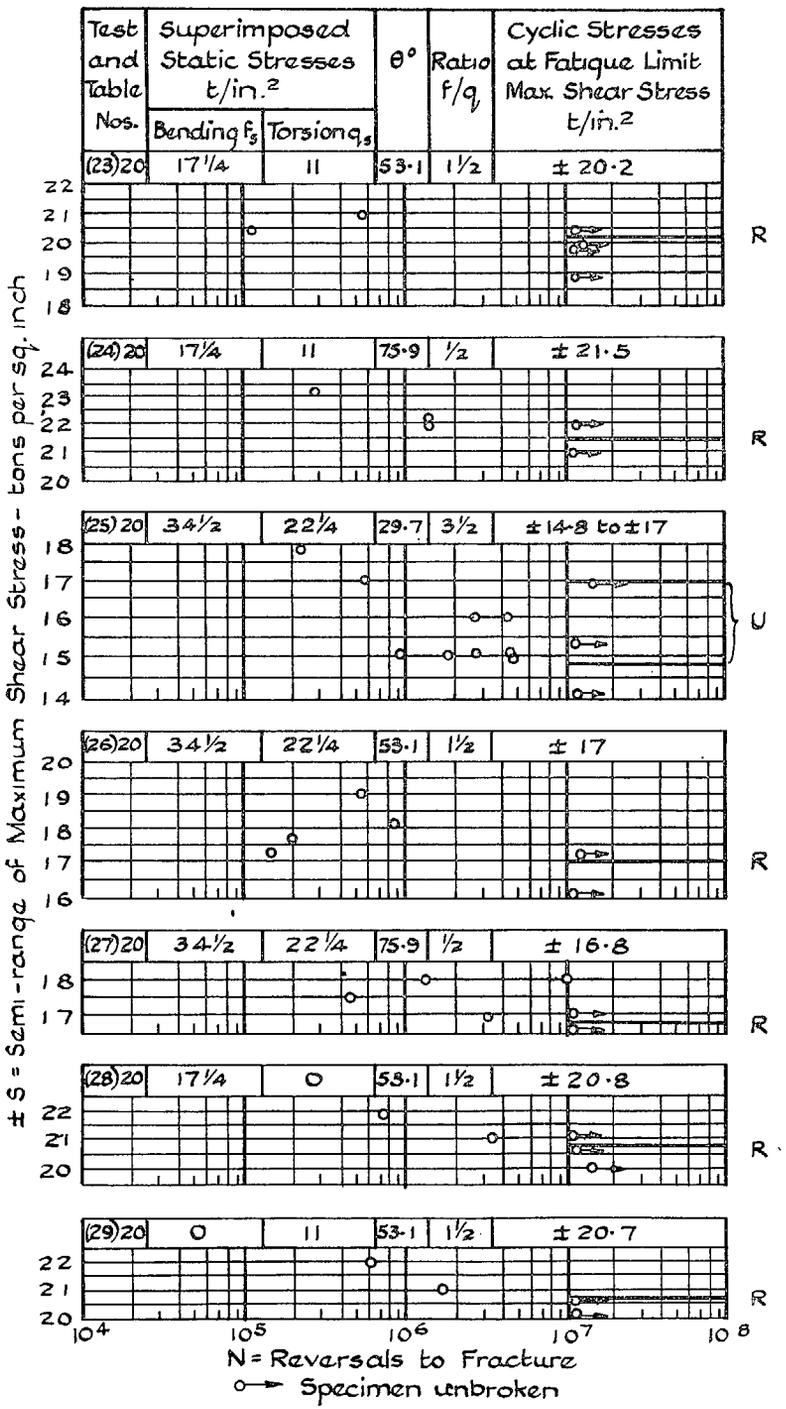

FIG. 71. *S/N* Diagrams. Solid Specimens. Tests (23) to (29).

the orientation of the trace of the origin of the principal fatigue crack was subsequently measured: where the results lead to some conclusion, the readings are reported.

The essential data of the tests can be fully presented in the form of (*a*) the *S*/*N* diagrams, and (*b*) a summary table for each of the four main groups of tests. The *S*/*N* diagram sheets have been reduced to a simple form. Each test is completely identified by the reference number given in the appropriate table (20 or 21): the superimposed static loading is shewn, while the cyclic stresses are expressed in terms of Maximum Shear Stress, *S*. In the summary tables, the calculated values of the cyclic bending and torsional stress components, f and q, are also given $\{S = \sqrt{f^2/4 + q^2}\}$. In regard to the accuracy of estimation of the fatigue limit, by inspection of the *S*/*N* diagram, the system, previously employed in connection with the fatigue tests of Part I of the investigation, of assigning a 'reliability index', has again been adopted. Thus, 'R' indicates a well-defined and apparently reliable value; 'LR' indicates a result less clearly defined but probably correct within the stated limits: 'U' indicates a result on whose accuracy little reliance can be placed, owing to the inconsistency or 'scatter' of the endurance data. The assigned reliability index is marked on each *S*/*N* diagram and given in the appropriate summary table. All experimental data are recorded.

1. Tests on Solid Specimens

The *S*/*N* diagrams are reproduced as Figs. 66 to 71 inclusive.

Fig. 66 relates to the two special series of tests, made to investigate a suitable final polishing process for the specimens, which have previously been referred to. The superiority of the longitudinal polishing is clearly established and it is of interest also to note the consistency of the results obtained with the three separate testing machines used for the latter test. These results, with those of similar check tests made from time to time during the course of the research, give considerable confidence in the accuracy of the calibration and operating reliability of the four machines employed.

TABLE 22

SUMMARY OF RESULTS OF COMBINED STRESS FATIGUE TESTS ON SOLID SPECIMENS (STEEL S.65A)

Test Reference No. (*see* Table 20)	Superimposed Static Stresses (t/in²)		Applied Cyclic Stresses					Assigned Reliability Index
			Value of θ	Dynamic Ratio	Fatigue Limits (t/in²)			
	Bending f_s	Torsion q_s	deg.	f/q	Range of Direct Stress due to bending f	Range of Shear Stress due to torsion q	Range of Maximum Shear Stress, S	
(1)	0	0	0	∞ ($q = 0$)	±37·8	0	±18·9	R
(2)	17¼	0	0	∞ ($q = 0$)	±35·8	0	±17·9	R
(3)	34½	0	0	∞ ($q = 0$)	±34·5	0	±17·2₅	R
(4)	0	0	90	0 ($f = 0$)	0	±24	±24·0	R
(5)	0	11	90	0 ($f = 0$)	0	±21·4 to ±22·5	±21·4 to ±22·5	LR
(6)	0	22¼	90	0 ($f = 0$)	0	±22·2₅	±22·2₅	R
(7)	0	11	0	∞ ($q = 0$)	±35·6	0	±17·8	R
(8)	0	22¼	0	∞ ($q = 0$)	±35·0	0	±17·5	R
(9)	17¼	11	0	∞ ($q = 0$)	±36·0	0	±18·0	R
(10)	17¼	22¼	0	∞ ($q = 0$)	±35 to ±37	0	±17·5 to ±18·5	LR
(11)	34½	11	0	∞ ($q = 0$)	±30·4	0	±15·2	R
(12)	34½	22¼	0	∞ ($q = 0$)	±30·6	0	±15·3	R
(13)	17¼	0	90	0 ($f = 0$)	0	±20·2	±20·2	R
(14)	34½	0	90	0 ($f = 0$)	0	±18·4	±18·4	R
(15)	17¼	11	90	0 ($f = 0$)	0	±18·4 to ±21	±18·4 to ±21	U
(16)	34½	11	90	0 ($f = 0$)	0	±18·2	±18·2	R
(17)	17¼	22¼	90	0 ($f = 0$)	0	±20·0	±20·0	R
(18)	34½	22¼	90	0 ($f = 0$)	0	±18·5 to ±19·5	±18·5 to ±19·5	LR
(19)	0	0	29·7	3½	±35·4₅	±10·1	±20·4	R
(20)	0	0	53·1	1½	±25·2	±16·8	±21·0	R
(21)	0	0	75·9	⅓	±10·9	±21·7₅	±22·4	R
(22)	17¼	11	29·7	3½	±31·3 to ±33	±8·9 to ±9·4	±18 to ±19	LR
(23)	17¼	11	53·1	1½	±24·2₅	±16·1₅	±20·2	R
(24)	17¼	11	75·9	⅓	±10·4₅	±20·8₅	±21·5	R
(25)	34½	22¼	29·7	3½	±26 to ±29·5	±7·3 to ±8·4	±14·8 to ±17	U
(26)	34½	22¼	53·1	1½	±20·4	±13·6	±17·0	R
(27)	34½	22¼	75·9	⅓	± 8·2	±16·3	±16·8	R
(28)	17¼	0	53·1	1½	±25·0	±16·6₅	±20·8	R
(29)	0	11	53·1	1½	±24·8₅	±16·5₅	±20·7	R

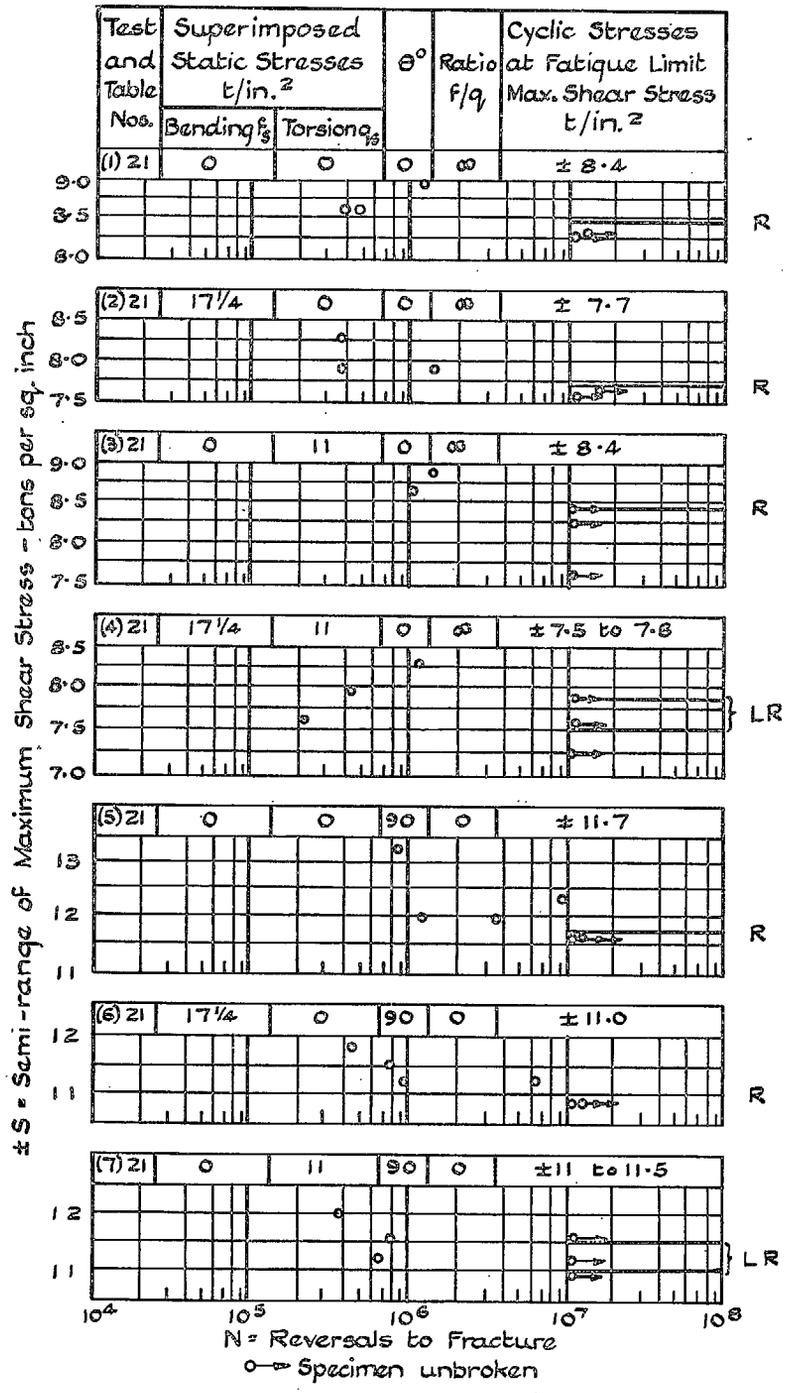

FIG. 72. *S/N* Diagrams. Hollow Specimens with Radial Drilled Hole. Tests (1) to (7)

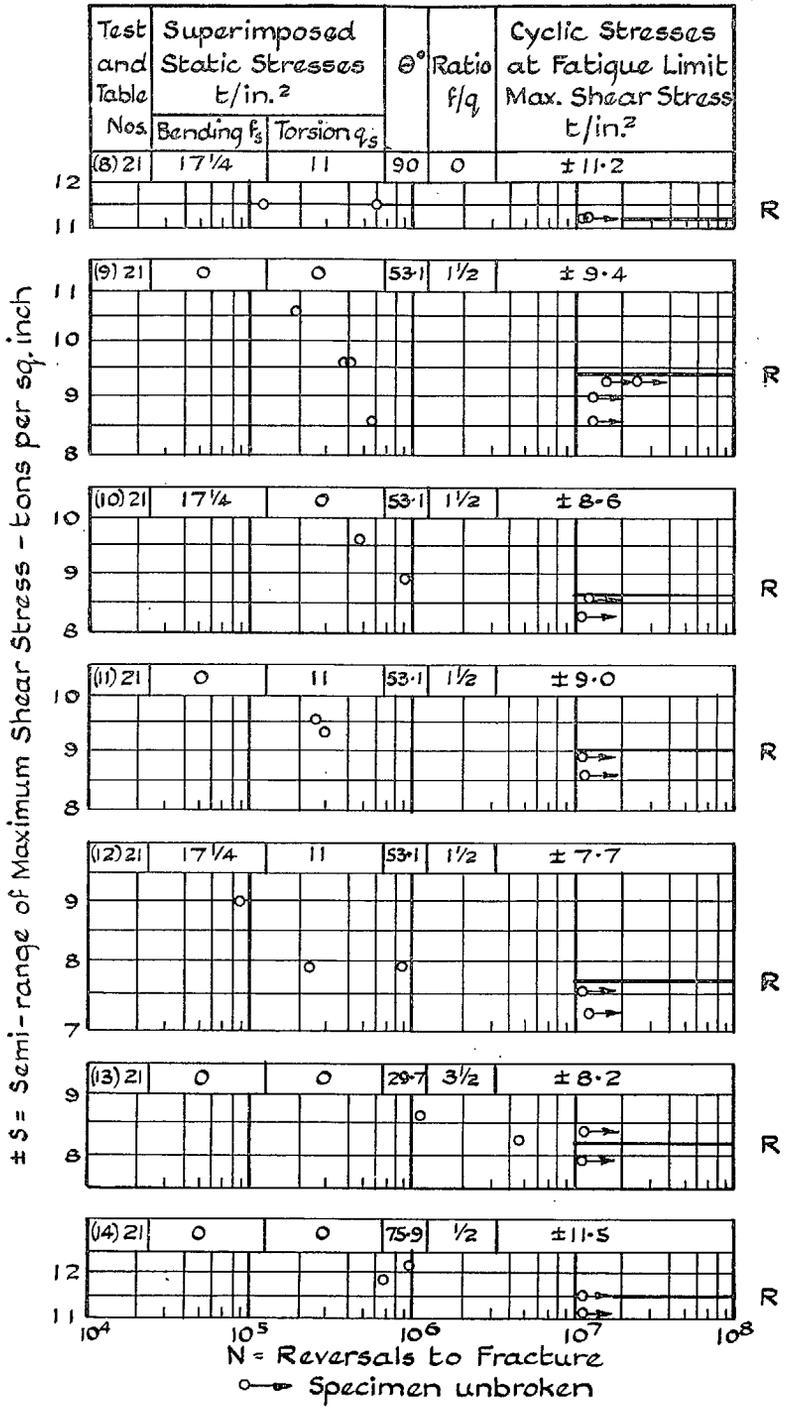

FIG. 73. *S/N* Diagrams. Hollow Specimens with Radial Drilled Hole. Tests (8) to (14)

These S/N curves call for no special remarks. With a few exceptions only, the test data are satisfactorily consistent for a complex heat-treated steel tested under combinations of stress of which several must have been critical in regard to elastic and fatigue failure.

On each specimen that failed by fatigue, careful measurements were made of the orientation of the cracks at their origins. Under pure bending stresses, the cracks were mainly transverse to the longitudinal specimen axis, while, under simple shearing stresses, longitudinal and helicoidal fractures were both encountered. But under the various systems of combined stress, the directions of the cracks showed such diversity and irregularity that no relation with the applied stressing system could be established. The measurements were, thus, quite inconclusive and are not recorded in this report.

The results of this group of tests are summarised in Table 22.

2. Tests on Hollow Specimens Having a Small Radial Oil-Hole

The S/N diagrams are reproduced as Figs. 72 and 73. The data, in general, plot much more consistently than those obtained in the tests made on the solid specimens. In each of tests (4) and (7), one result is inconsistent and could, perhaps justifiably, have been ignored: however, each has been retained. But in test (9), one result can clearly be neglected and this has been done.

The results of this group of tests are summarised in Table 23.

In Table 23, all stresses are expressed as nominal values, being calculated without reference to the radial hole, i.e. considering the specimen as of hollow cylindrical section without the drilled hole.

The orientations of the fatigue cracks were measured at their origins at the edges of the drilled holes. The recorded measurement is the included angle between the trace of the crack, at its origin, on the surface of the specimen and the trace of a transverse section of the specimen which also passes through the origin of the crack. The recorded orientations are somewhat inconsistent; their accurate measurement was rendered a little difficult by the radius at the edge of the drilled hole. The measured inclinations of the cracks at their origins are included in Table 23, where they are arranged in the sequence of decreasing values of cyclic maximum shear stress. In spite of the errors involved in these measurements, there is evident a very distinct tendency for these measurements to have an average value equal to $\frac{1}{2}\theta$. It will be shown in the discussion which follows that this value of $\frac{1}{2}\theta$ corresponds to the trace of the plane subjected to the greatest range of principal stress caused by the presence of the radial hole.

In the last column of Table 23 are recorded the uncorrected values of the 'Fatigue Strength Reduction Factor, K_f' where

$$K_f = \frac{\text{Fatigue limit of solid specimen}}{\text{Fatigue limit of hollow specimen with radial hole.}}$$

TABLE 23

SUMMARY OF RESULTS OF COMBINED STRESS FATIGUE TESTS ON HOLLOW SPECIMENS WITH RADIAL DRILLED HOLE (STEEL S.65A)

Test Reference No. (*see* Table 21)	Superimposed Static Stresses (Nominal) (t/in²)		Applied Cyclic Stresses					Assigned Reliability Index	Orientation of Fatigue Cracks (degrees)	Fatigue Strength Reduction Factor, K_f
			Value of θ	Dynamic Ratio	Fatigue Limits (Nominal), t/in²					
	Bending f_s	Torsion q_s	deg.	f/q	Range of direct stress due to bending, f	Range of Shear stress due to torsion, q	Range of Maximum Shear Stress, S			
(1)	0	0	0	∞ ($q = 0$)	±16·8	0	± 8·4	R	0, 11, 0	2·25
(2)	17½	0	0	∞ ($q = 0$)	±15·4	0	± 7·7	R	0, —2, 0	2·32
(3)	0	11	0	∞ ($q = 0$)	±16·8	0	± 8·4	R	—8, 3	2·12
(4)	17½	11	0	∞ ($q = 0$)	±15 to ±15·6	0	±7·5 to ±7·8	LR	13, 12, 7	2·3 to 2·4
(5)	0	0	90	0 ($f = 0$)	0	±11·7	±11·7	R	45, 45, 43, 15	2·05
(6)	17½	0	90	0 ($f = 0$)	0	±11·0	±11·0	R	—41, —44, —44, —42.	1·84
(7)	0	11	90	0 ($f = 0$)	0	±11 to ±11·5	±11 to ±11·5	LR	45, 45, 47.	1·9 to 2·0
(8)	17½	11	90	0 ($f = 0$)	0	±11·2	±11·2	R	32, 40	1·6 to 1·9
(9)	0	0	53·1	1½	±11·3	± 7·5	± 9·4	R	30, 25, 24, 24	2·23
(10)	17½	0	53·1	1½	±10·3₅	± 6·9	± 8·6	R	24, 17	2·42
(11)	0	11	53·1	1½	±10·8	± 7·2	± 9·0	R	38, 35	2·30
(12)	17½	11	53·1	1½	± 9·2₅	± 6·1₅	± 7·7	R	25, 25, 25	2·62
(13)	0	0	29·7	3½	±14·2₅	± 4·0₅	± 8·2	R	16, 15	2·49
(14)	0	0	75·9	½	± 5·6	±11·1₅	±11·5	R	38, 40	1·95

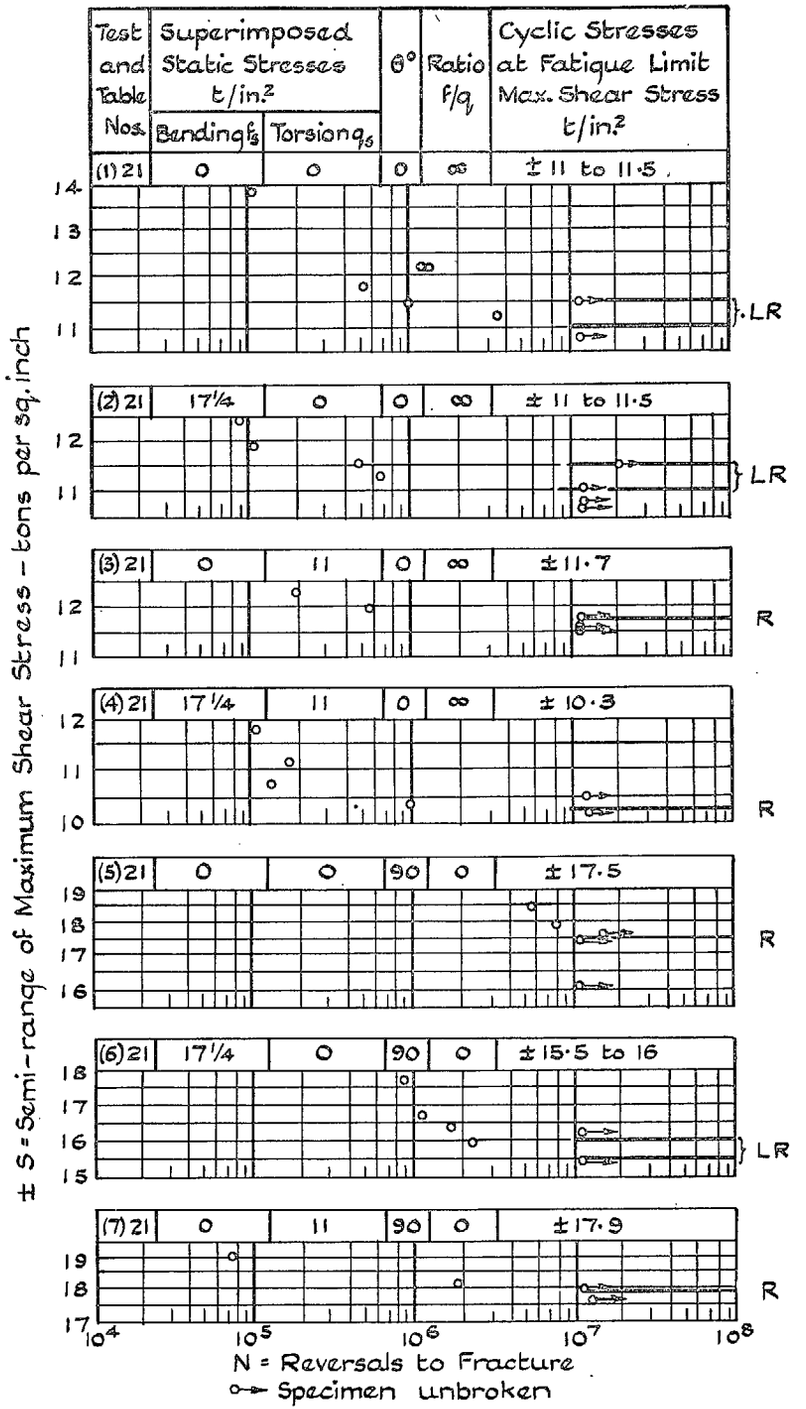

FIG. 74. *S/N* Diagrams. Hollow Specimens containing a Sharp Transition Fillet : Tests (1) to (7)

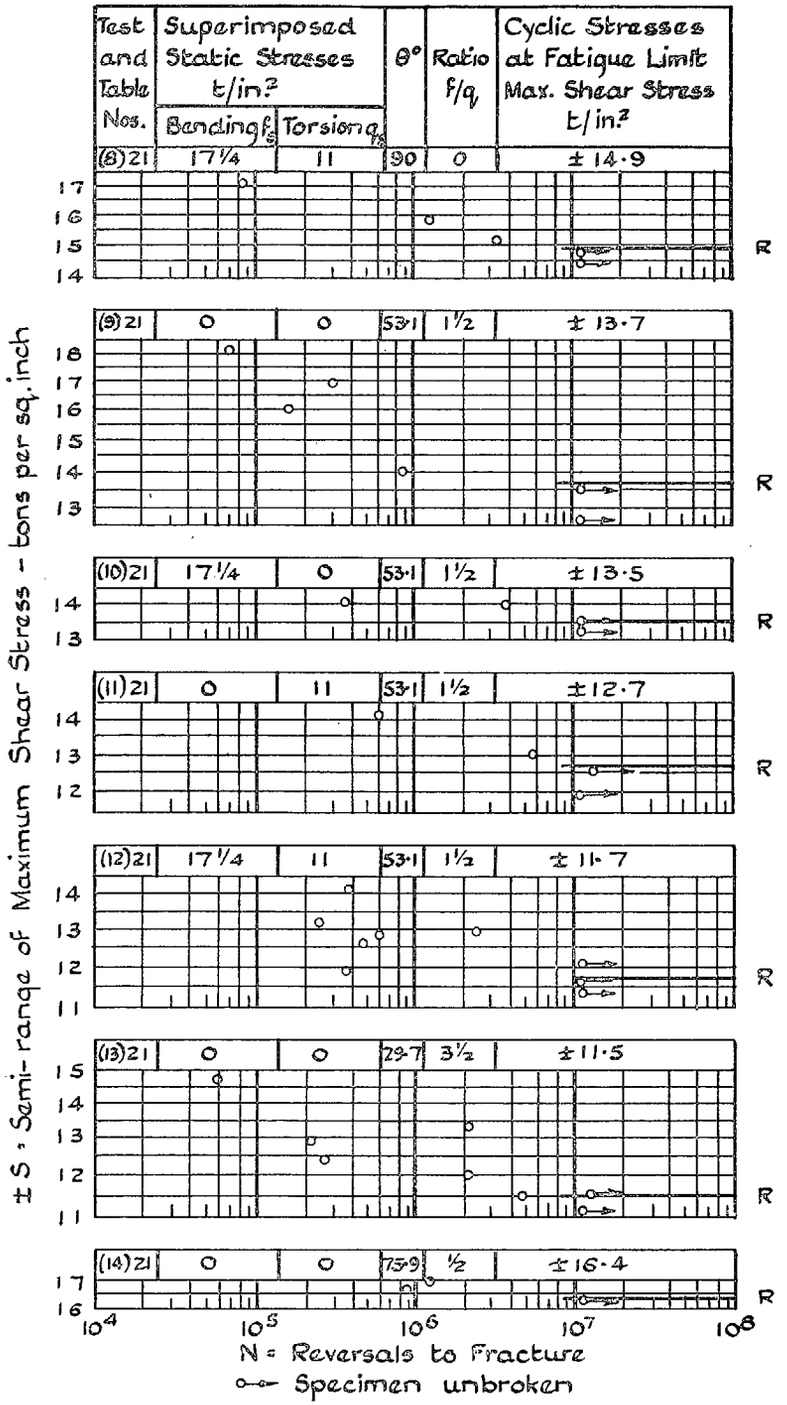

FIG. 75. *S/N* Diagrams. Hollow Specimens containing a Sharp Transition Fillet : Tests (8) to (14)

the appropriate value for the numerator being taken from Table 22. Both numerator and denominator represent the fatigue limit expressed in terms of Maximum Shear Stress and relate, therefore, only to the applied cyclic stresses, the nominal value of the applied static stresses being the same for each corresponding pair of solid specimens and specimen containing the 'stress - raiser.' The theoretical stress - concentration effect will be referred to in the discussion of the results.

3. Test on Hollow Specimens Containing a Sharp Transition Fillet

The S/N diagrams are reproduced as Figs. 74 and 75. In general, this group of tests has provided endurance data which are consistent and yield closely-defined fatigue limits. In a few cases, one test point is inconsistent but the fatigue limit is defined to within $\pm\frac{1}{2}$ t/in.^{2}, which is acceptable. Nearly all the specimens failed similarly: by a transverse crack situated at or very near to the junction of the fillet and the parallel central portion of the test piece.

The results of the tests are summarised in Table 24: all stated stresses are nominal, being calculated on the central cross-section of the specimen and neglecting the stress concentration effect due to the presence of the fillet. The values of the 'Fatigue Strength Reduction Factor, K_f' have, as before, been calculated using the cyclic fatigue limits expressed in terms of Maximum Shear Stress.

4. Tests on Hollow Splined-shaft Specimens

Fig. 76 relates to the preliminary reversed bending tests, already referred to in Section III, made to determine the relative fatigue strengths of the splined shafts when tested in the two principal alternative positions in respect to the plane of the applied bending moment. Although there is little, if any, real difference in fatigue strength, within the accuracy of the experiments, the apparently slightly lower strength is exhibited when the plane of maximum bending moment passes through the centres of an opposite pair of spline crests: all the remaining tests have been made with the specimens mounted in that position.

Figs. 77 and 78 show the S/N diagrams relating to the remaining tests on this form of specimen. In general, the test data plot regularly and consistently and the fatigue limits are defined within the limits of experimental accuracy.

The origins and directions of the fatigue cracks will be referred to in the later section when the stress concentration effects are discussed.

The results of this series of tests are summarised in Table 25: the stresses recorded are nominal values, calculated on the moduli of section at the minimum diameter as reported in Section III, which ignores any stress concentration effects due to the shape of the cross-section. The values of the 'Fatigue Strength Reduction Factor, K_f' are also stated in the table: as before, they are calculated using corresponding pairs of cyclic fatigue limits expressed in terms of Maximum Shear Stress.

TABLE 24

SUMMARY OF RESULTS OF COMBINED STRESS FATIGUE TESTS ON HOLLOW SPECIMENS CONTAINING A SHARP TRANSITION FILLET

$(r/D = 1/15)$

Test Reference No. (*see* Table 21)	Superimposed Static Stresses (Nominal) t/in^2		Applied Cyclic Stresses						
			Value of θ	Dynamic Ratio	Fatigue Limits (Nominal) t/in^2			Assigned Reliability Index	Fatigue Strength Reduction Factor, K_f
	Bending f_s	Torsion q_s	deg.	f/q	Range of Direct Stress due to bending, f	Range of Shear Stress due to torsion, q	Range of Maximum Shear Stress, S		
(1)	0	0	0	∞ ($q = 0$)	± 22 to ± 23	0	± 11 to $\pm 11{\cdot}5$	LR	1·65 to 1·72
(2)	$17\frac{1}{4}$	0	0	∞ ($q = 0$)	± 22 to ± 23	0	± 11 to $\pm 11{\cdot}5$	LR	1·55 to 1·63
(3)	0	11	0	∞ ($q = 0$)	$\pm 23{\cdot}4$	0	$\pm 11{\cdot}7$	R	1·52
(4)	$17\frac{1}{4}$	11	0	∞ ($q = 0$)	$\pm 20{\cdot}6$	0	$\pm 10{\cdot}3$	R	1·75
(5)	0	0	90	0 ($f = 0$)	0	$\pm 17{\cdot}5$	$\pm 17{\cdot}5$	R	1·37
(6)	$17\frac{1}{4}$	0	90	0 ($f = 0$)	0	$\pm 15{\cdot}5$ to ± 16	$\pm 15{\cdot}5$ to ± 16	LR	1·26 to 1·30
(7)	0	11	90	0 ($f = 0$)	0	$\pm 17{\cdot}9$	$\pm 17{\cdot}9$	R	1·20 to 1·26
(8)	$17\frac{1}{4}$	11	90	0 ($f = 0$)	0	$\pm 14{\cdot}9$	$\pm 14{\cdot}9$	R	1·23 to 1·41
(9)	0	0	53·1	$1\frac{1}{2}$	$\pm 16{\cdot}4_5$	$\pm 10{\cdot}9_6$	$\pm 13{\cdot}7$	R	1·53
(10)	$17\frac{1}{4}$	0	53·1	$1\frac{1}{2}$	$\pm 16{\cdot}2$	$\pm 10{\cdot}8$	$\pm 13{\cdot}5$	R	1·54
(11)	0	11	53·1	$1\frac{1}{2}$	$\pm 15{\cdot}2_5$	$\pm 10{\cdot}1_6$	$\pm 12{\cdot}7$	R	1·63
(12)	$17\frac{1}{4}$	11	53·1	$1\frac{1}{2}$	$\pm 14{\cdot}0_5$	$\pm 9{\cdot}3_5$	$\pm 11{\cdot}7$	R	1·73
(13)	0	0	29·7	$3\frac{1}{2}$	± 20	$\pm 5{\cdot}7$	$\pm 11{\cdot}5$	R	1·77
(14)	0	0	75·9	$\frac{1}{2}$	$\pm 8{\cdot}0$	$\pm 15{\cdot}9$	$\pm 16{\cdot}4$	R	1·37

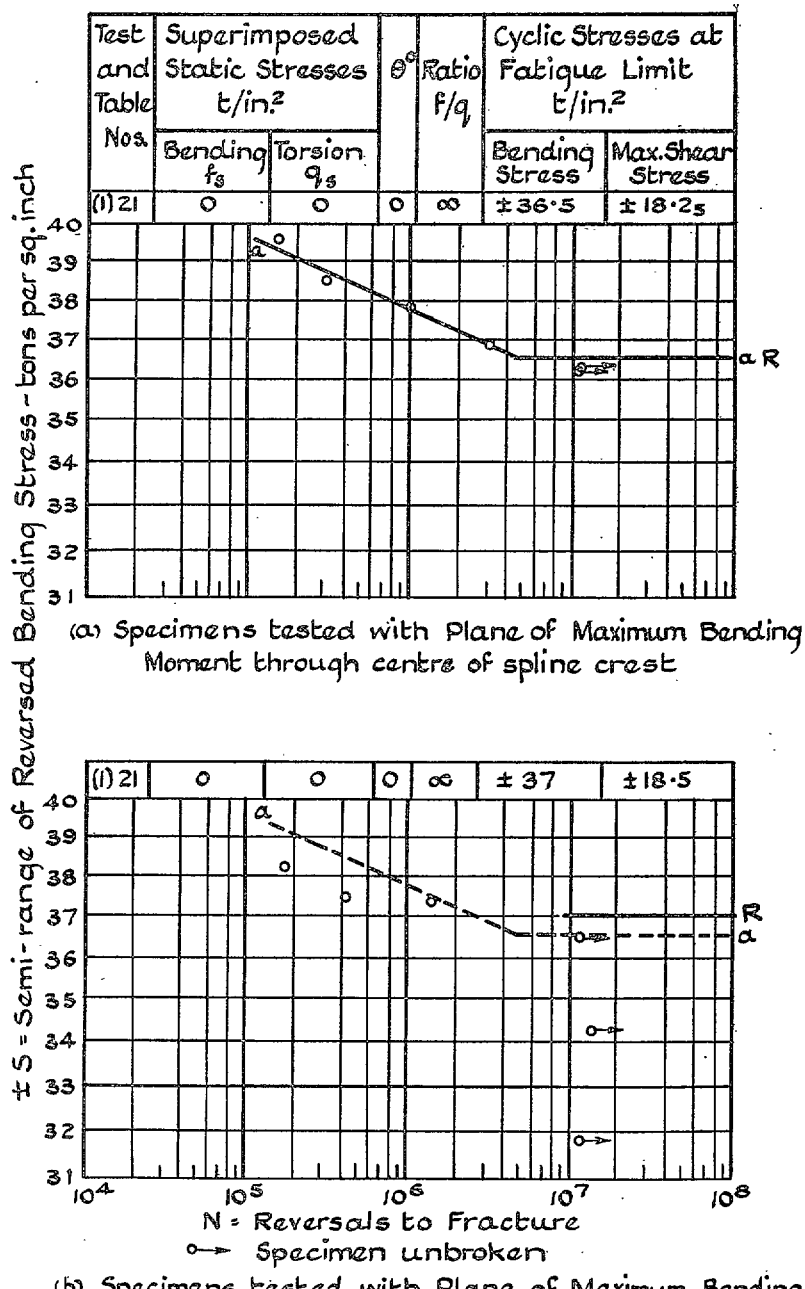

FIG. 76. *S/N* Diagrams. Hollow Splined-shaft Specimens. Test (1)

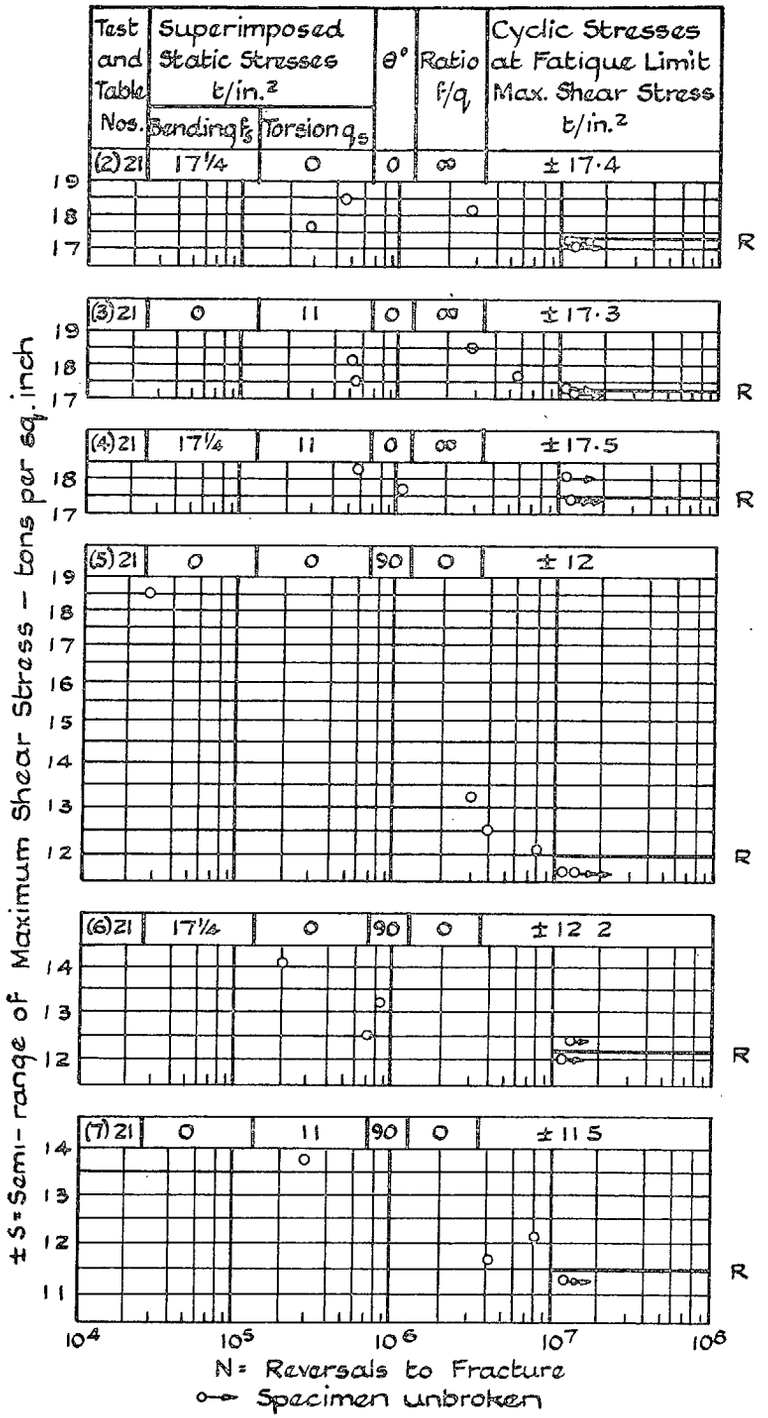

FIG. 77. *S/N* Diagrams. Hollow Splined-shaft Specimens. Tests (2) to (7)

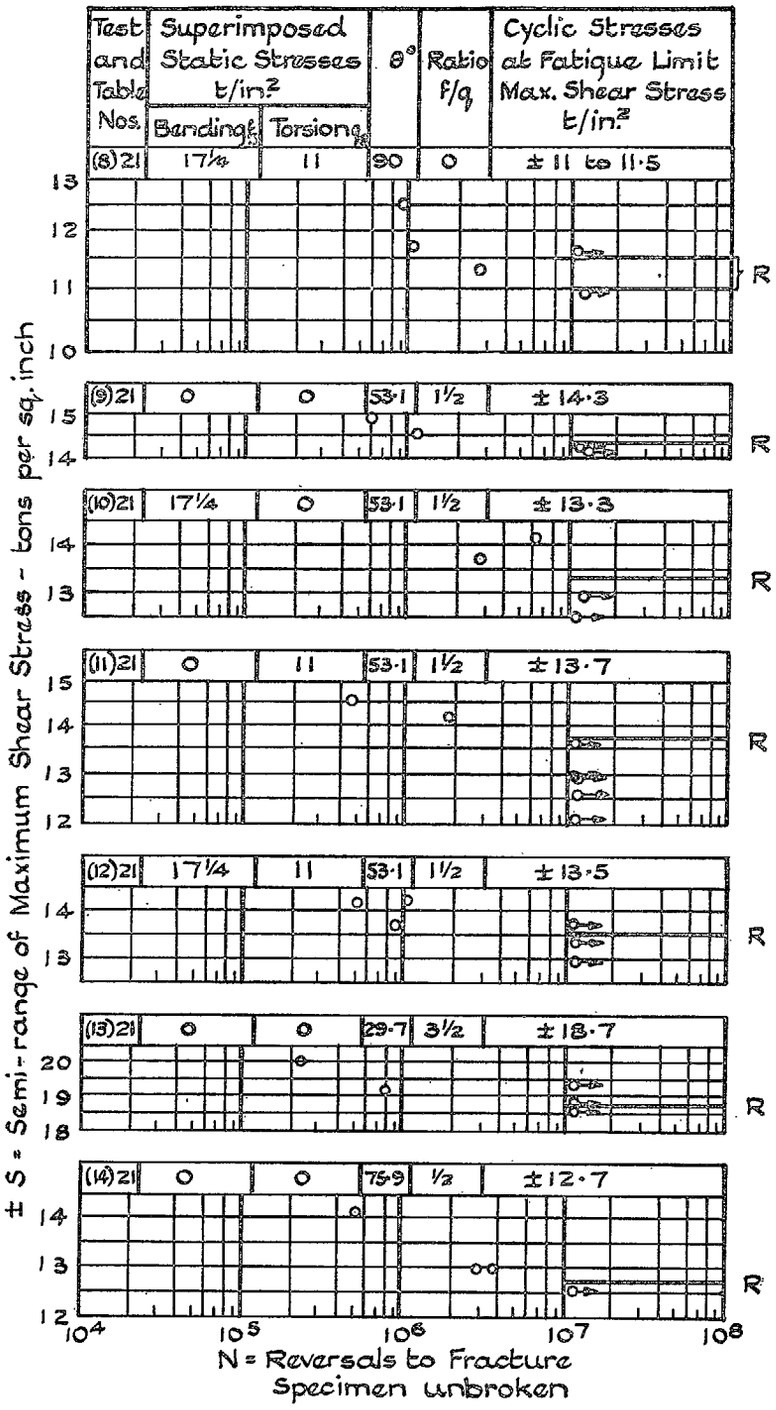

FIG. 78. *S/N* Diagrams. Hollow Splined-shaft Specimens. Tests (8) to (14)

TABLE 25

SUMMARY OF RESULTS OF C.S. FATIGUE TESTS MADE ON HOLLOW SPLINED-SHAFT SPECIMENS

Test Reference No. (*see* Table 21)	Superimposed Static Stresses (Nominal) t/in²		Applied Cyclic Stresses						
			Value of θ	Dynamic Ratio	Fatigue Limits (Nominal) t/in²			Assigned Reliability Index	Fatigue Strength Reduction Factor, K_f
	Bending f_s	Torsion q_s	deg.	f/q	Range of Direct Stress due to bending, f	Range of Shear Stress due to torsion, q	Range of Maximum Shear Stress, S		
(1)	0	0	0	∞ ($q = 0$)	$\pm 36{\cdot}5$	0	$\pm 18{\cdot}2_5$	R	1·04
(2)	$17\frac{1}{4}$	0	0	∞ ($q = 0$)	$\pm 34{\cdot}8$	0	$\pm 17{\cdot}4$	R	1·03
(3)	0	11	0	∞ ($q = 0$)	$\pm 34{\cdot}6$	0	$\pm 17{\cdot}3$	R	1·03
(4)	$17\frac{1}{4}$	11	0	∞ ($q = 0$)	$\pm 35{\cdot}0$	0	$\pm 17{\cdot}5$	R	1·03
(5)	0	0	90	0 ($f = 0$)	0	$\pm 12{\cdot}0$	$\pm 12{\cdot}0$	R	2·0
(6)	$17\frac{1}{4}$	0	90	0 ($f = 0$)	0	$\pm 12{\cdot}2$	$\pm 12{\cdot}2$	R	1·66
(7)	0	11	90	0 ($f = 0$)	0	$\pm 11{\cdot}5$	$\pm 11{\cdot}5$	R	1·86 to 1·96
(8)	$17\frac{1}{4}$	11	90	0 ($f = 0$)	0	± 11 to $\pm 11{\cdot}5$	± 11 to $\pm 11{\cdot}5$	R	1·67 to 1·83
(9)	0	0	53·1	$1\frac{1}{2}$	$\pm 17{\cdot}1_5$	$\pm 11{\cdot}4_5$	$\pm 14{\cdot}3$	R	1·47
(10)	$17\frac{1}{4}$	0	53·1	$1\frac{1}{2}$	$\pm 16{\cdot}0$	$\pm 10{\cdot}6_5$	$\pm 13{\cdot}3$	R	1·56
(11)	0	11	53·1	$1\frac{1}{2}$	$\pm 16{\cdot}4_5$	$\pm 10{\cdot}9_5$	$\pm 13{\cdot}7$	R	1·51
(12)	$17\frac{1}{4}$	11	53·1	$1\frac{1}{2}$	$\pm 16{\cdot}2$	$\pm 10{\cdot}8$	$\pm 13{\cdot}5$	R	1·50
(13)	0	0	29·7	$3\frac{1}{2}$	$\pm 32{\cdot}5$	$\pm 9{\cdot}2_5$	$\pm 18{\cdot}7$	R	1·09
(14)	0	0	75·9	$\frac{1}{2}$	$\pm 6{\cdot}2$	$\pm 12{\cdot}3$	$\pm 12{\cdot}7$	R	1·76

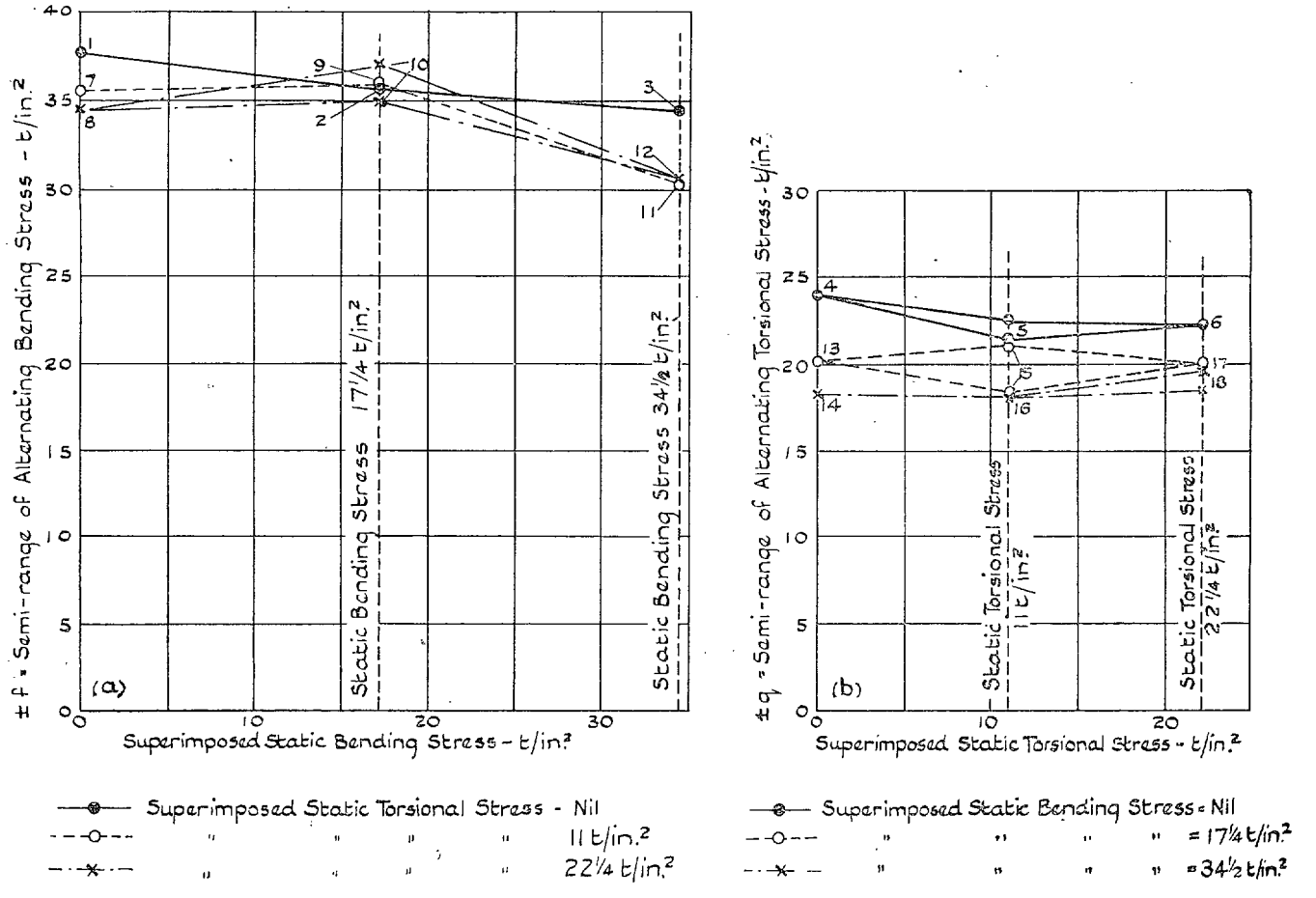

FIG. 79. The Effects of Superimposed Static Bending and Torsional Stresses, Singly and in Combination, on the Fatigue Limits under Reversed Cyclic Stresses : S.65 steel : solid plain specimens.

V. DISCUSSION OF RESULTS OF THE COMBINED STRESS FATIGUE TESTS

1. Solid Cylindrical Specimens

This group of experiments, made on a simple form of specimen free from sudden changes or discontinuities of section, should reveal, apart from any 'size effect' that may exist, the intrinsic characteristics of the S.65 steel under the applied combinations of static and fatigue stresses. The complete programme has been stated in Table 20; the experimental results are summarised in Table 22; any individual fatigue test will be completely identified by quoting the test reference number as stated in each of those tables.

(A) EFFECT OF SUPERIMPOSED STATIC STRESSES ON THE FATIGUE RANGE UNDER SIMPLE REVERSED STRESSES

All the test data are plotted to give the two diagrams forming Fig. 79. Fig. 79 (*a*) shows the effect, on the fatigue limit under simple reversed bending stresses, of superimposed static bending and/or static torsional stresses singly and in combination; Fig. 79 (*b*) shows the effect of similar imposed static stresses on the fatigue limit under simple reversed torsional stresses. Both diagrams are essentially of the M/R type (where M is the applied static stress system and R is the resulting safe range of cyclic stress), $R/2$ being plotted against M. In each diagram, the heavy line drawn through the data represented by the solid circles gives a curve which shows the effect on the fatigue range of superimposing a static stress of the same kind (bending or torsion); the lines joining the other sets of data points show the effect of the addition of a static stress of a dissimilar type.

(1) Effect of Superimposed Static Stress of Similar Type. In Fig. 79 (*a*), test numbers 1, 2 and 3 show the effect on the fatigue limit under reversed bending stresses ($\pm$ 37·8 t/in.^{2}) of superimposed static bending stresses of 17½ and 34½ t/in.^{2}; the maximum reduction effected—$\pm$ 3·3 t/in.^{2} on $\pm$ 37·8 or 8·7%—is small. Similarly, test numbers 4, 5 and 6 on Fig. 79 (*b*) show that the effect on the fatigue limit under simple reversed shearing stress ($\pm$ 24·0 t/in.^{2}) of superimposing static torsional stresses of 11 and 22¼ t/in.^{2} effects a maximum reduction of $\pm$ 2·0 t/in.^{2} on $\pm$ 24, or 8·3% only. Thus the effect of similar mean stress on the fatigue resistance under bending or torsional stresses of this steel is definite but quite small in amount. This is an important feature from the design aspect and in general accordance with other work on this subject to which brief reference may be made. Many reliable investigations have been made and it is established that the form of the M/R curve depends both on the material and on the kind of applied stressing. For example, the fatigue strength of ductile non-ferrous metals, especially light alloys and soft brasses, in general diminishes much more rapidly with increasing mean stress than does that of the steels. Also, in general, the reduction is much sharper under direct tensile stresses than when bending or torsional stresses are applied: this is, of course, to be expected as, in a ductile material having a normal yield/ultimate ratio, elasticity is exceeded and the actual cross-sectional area of the specimen is reduced under quite moderate values of tensile mean stress, whereas the specimen cross-section is practically unchanged under bending or torsional loading. Thus, the shape of the static load-extension diagram to fracture is a factor which enters into the result. Nevertheless, as far as engineering steels are concerned, the effect of mean stress on the fatigue strength is much less than is often assumed. Fig. 80 (*a*) relates to a series of comprehensive experiments carried out, by Gough and Wood[21], on a normalised mild steel, having an ultimate tensile strength of about 26½ t/in.^{2}, using cycles of direct stress. The ductility of this material is shown by the autographic tensile load/extension diagram of Fig. 80 (*b*). Six values of the fatigue limit were determined, covering from reversed direct stresses to that pulsating stress cycle of which the superior stress of the cycle was the smallest practicable amount less than the ultimate tensile strength of the material. The fatigue results are represented by the points A, B, C, D, E and F on Fig. 80 (*a*). With increasing values of tensile mean stress the specimens extended by amounts closely corresponding to the extension produced by a single static application of the maximum stress of the cycle: this is shown by the points A to F marked on the load/extension diagram of Fig. 80 (*b*), where each point records (*a*) the superior stress of each of the six fatigue ranges determined and (*b*) the percentage extension of the specimens which safely withstood 10^7 cycles of those stress ranges without fatigue failure. In Fig. 80 (*a*), the safe ranges of stress are nominal values, being calculated on the original unstrained cross-sectional areas of the specimens before test. The line ABCDE shows that, as the mean stress was increased from 0 to 16 t/in.^{2}, the safe range fell steadily from 24·6 ($\pm$ 12·3) t/in.^{2} to 19·8 (+ 6·2 to + 26) t/in.^{2}, a reduction of 19½% but surprisingly small in view of the severity of the applied stress and deformation conditions. The limiting stress condition is reached, of course, when the line xx is encountered; here, failure is determined by the maximum stress of the cycle reaching the ultimate tensile strength of the material; this limiting condition was closely approached in test E where the maximum stress of the cycle was 26 t/in.^{2} as against the tensile strength of about 26½ t/in.^{2}. That the boundary line xx really represents the limiting condition was brought out in a striking manner by the interesting and probably unique group of tests represented by the point F. By maintaining the superior stress of the cycle at 26½ t/in.^{2}, a safe range of 13·4 t/in.^{2} was successfully determined experimentally; four specimens safely withstood 10^7 cycles, but the slightest increase in either the maximum stress of the cycle or the applied range of stress caused the other specimens to fail at once by 'necking' and tensile static

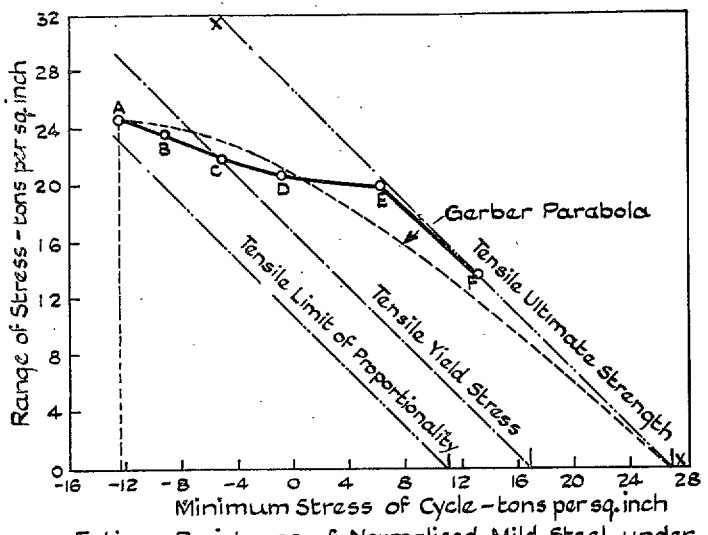

(a) Fatigue Resistance of Normalised Mild Steel under Cyclic Direct Stresses

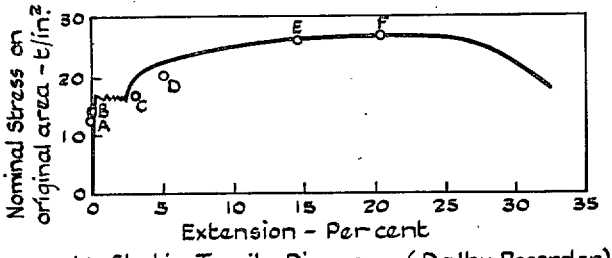

(b) Static Tensile Diagram (Dalby Recorder)

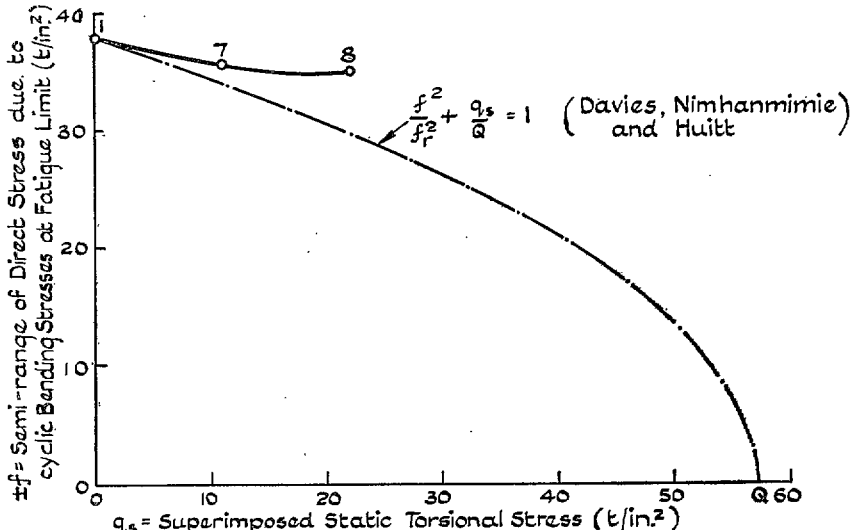

Note:- Q = Torsional Modulus of Rupture = 57·3 t/in.²

(c) Effect of Static Torsional Stress on Fatigue Limit under Reversed Bending Stresses (S65 Steel)

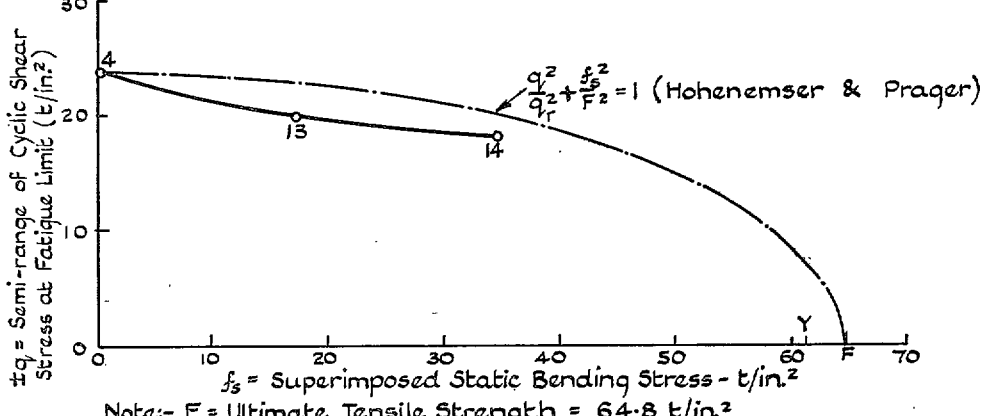

Note:- F = Ultimate Tensile Strength = 64·8 t/in.²
Y = Yield Point in Tension = 61·3 t/in.²

(d) Effect of Static Bending Stress on Fatigue Limit under Reversed Torsional Stresses (S. 65 Steel)

FIG. 80. Effect of Mean Stress (Mild Steel and S.65 Steel) and comparison with certain criteria.

fracture. This experiment is of very great interest in the present connection in considering what the action of static mean stress really is. Provided the conditions of the applied stress system are such that static failure is not produced by the maximum stress of the cycle (the sum of the static and half the cyclic component), any decrease in fatigue range is probably directly attributable to the damage caused to the crystalline structure by the deformation to which the specimen has been subjected by the maximum stress of the cycle; beyond this 'damage' effect, it appears reasonable to assume that the effect of mean stress, as such, is very small or of negligible amount. Therefore, if this view of fatigue—based on a comprehensive study of the subject—is sound, it would appear useless to expect any general form of M/R relation based on stress considerations alone, as the stress/strain deformation characteristics of the material also constitute an important factor. Materials would, therefore, be expected to exhibit quite different M/R relations, an expectation which is fully supported by the extensive test data recorded in the literature of the subject.

Reverting to the present tests, we are dealing with a material having a high yield/ultimate ratio, as shown by the following data taken from Table 3 :—

Tension Limit of Proportionality = 47·0 t/in.²
Yield Point .. .. = 61·3 t/in.² } Ratio
Ultimate Strength .. = 64·8 t/in.² } 94%

Torsion Limit of Proportionality = 31·4 t/in.²
Yield Point .. .. = 46·3 t/in.² } Ratio
Modulus of Rupture .. = 57·3 t/in.² } 81%

The applied stresses used in the present combined stress experiments are bending and torsion : under each type the deformations due to elastic conditions being exceeded will be small and the dimensions of specimen cross-section will not be appreciably affected. The effect on the fatigue limit of quite considerable superimposed mean stresses would, therefore, be expected also to be small and this is certainly borne out experimentally by the results of test numbers, 1, 2 and 3, also 4, 5 and 6.

(2) Effect of Superimposed Static Stress of Dis-similar Type.

In Fig. 79 (*a*), tests 1, 7 and 8 show the effect of imposing static torsional stresses of 11 and 22¼ t/in.² on to cycles of reversed bending stresses. The effect is small : a maximum reduction of ±2·8 t/in.² or 7·4% only. Davies, Nimhanmimie and Huitt* made some tests of this kind on 3% Ni. Steel, also a 3% Ni. Cr. Steel and suggested that their results, up to the point where failure occurred by static yielding, were represented by the empirical relation :—

$$\frac{f^2}{f_r^2} + \frac{q_s}{Q} = 1$$

where $\pm f$ is safe range of direct stress due to the cyclic bending stresses.
when q_s is the corresponding superimposed static torsional stress.
and $\pm f_s$ is fatigue range under reversed bending stresses only.
and Q is ultimate static torsional strength.

Fig. 80 (*c*) shows the above expression in relation to the results of the present tests 1, 7 and 8 ; these results do not conform to the suggested empirical formula.

In Fig. 79 (*b*), tests 4, 13 and 14 shows the effect of superimposing static bending stresses of 17¼ and 34½ t/in.² on to cycles of reversed shearing stresses. The fatigue limit is reduced quite appreciably from ±24 to a minimum of ±18·4 t/in.², a decrease of 23·4%, which is the maximum decrease produced by any combination of superimposed static stresses used in the present tests. These results are plotted in Fig. 80 (*d*). Hohenemser and Prager[3] have investigated the effect of static tensile stress superimposed on alternating torsional stresses ; the material used was a mild steel. Up to the point where yielding occurred, they found that the superimposed stress caused a drop in the torsional fatigue limit, according to the ellipse quadrant relation :—

$$\frac{q^2}{q_r^2} + \frac{f_s^2}{F^2} = 1$$

where $\pm q$ is fatigue range of cyclic shear stress
when f_s is superimposed static tensile stress
and F is ultimate tensile strength
and q_r is fatigue range under reversed shear stresses only.

The conditions of the present test are not quite comparable, as static bending stresses are imposed in place of the static direct stresses used by Hohenemser and Prager. As a matter of interest, however, an ellipse quadrant has been inserted in Fig. 80 (*d*), drawn through the point F corresponding to the tensile ultimate strength (the bending ultimate strength of the S.65 steel is not determinate). There is no reason to assume that the results of tests 4, 13 and 14 conform to such a quadrant relation.

In fact, the result of all four groups of tests
1, 2 and 3 (Fig. 79 (*a*))
4, 5 and 6 (Fig. 79 (*b*))
1, 7 and 8 (Fig. 80 (*c*))
4, 13 and 14 (Fig. 80 (*d*))
plot to a form very similar to that shown in Fig. 80 (*a*) ; this fact, coupled with the above discussion and a consideration of the various M/R tests reported by numerous other investigators, indicate that it would not be justifiable to attempt to associate the M/R relation with any general form of expression containing only stress terms.

* Discussion of paper by Gough and Pollard[9].

(3) Effect of Combinations of Superimposed Static Stresses of Dis-similar Kinds.

The effects of superimposing static bending and torsional stresses on to reversed bending, also reversed torsional stresses, are shown by the remaining data plotted on Figs. 79 (*a*) and (*b*).

In Fig. 79 (*a*), tests 9 and 10 show that adding torsional stresses of 11 and 22¼ t/in.² on to a static bending stress of 17¼ t/in.² produces an extremely small additional effect on the fatigue range under reversed bending stresses ; a greater effect results when these same torsional stresses are superimposed on a static bending stress of 34½ t/in.², as shown by tests 11 and 12. The most severe condition (bending of 34½ allied with torsion of 22¼ t/in.²) reduces the bending fatigue limit from ±37·8 to ±30·6 t/in.², or a total reduction of 19·1% only.

The effect of superimposing static bending and static torsional stresses on to the fatigue resistance under reversed shearing stresses is generally similar, as shown in Fig. 79 (*b*), by tests 15, 16, 17 and 18. The most severe conditions (bending of 34½ allied with torsion of 22¼ t/in.²) reduces the fatigue range from ±24 to, say, ±18½ t/in.², a maximum reduction of 23%.

Reviewing the results of all these experiments on the effect of superimposed static stress on the fatigue resistance of the steel, the data obtained are satisfactorily regular and consistent, and can reliably be used, by interpolation, to deduce the safe ranges of stress corresponding to any required intermediate values of static bending and/or torsional stresses between the limits investigated. This part of the combined stress field has, therefore, for design purposes been satisfactorily surveyed. The effect of the addition of a static mean stress, or a combination, is shown to be quite definite and regular but the amount of the reduction, caused even by static stresses which are quite high in relation to the ultimate strengths of the material, is relatively small. The effect of superimposing static bending stresses on cyclic torsional stresses is more damaging than that of static torsional stresses imposed on cyclic bending stresses.

(B) VARIOUS COMBINATIONS OF REVERSED BENDING AND REVERSED SHEARING STRESSES WITH A CONSTANT SYSTEM OF SUPERIMPOSED STATIC STRESS.

There are three principal series of such tests, in each of which the fatigue range has been determined under (*a*) reversed bending stresses, ±*f*, (*b*) reversed torsional

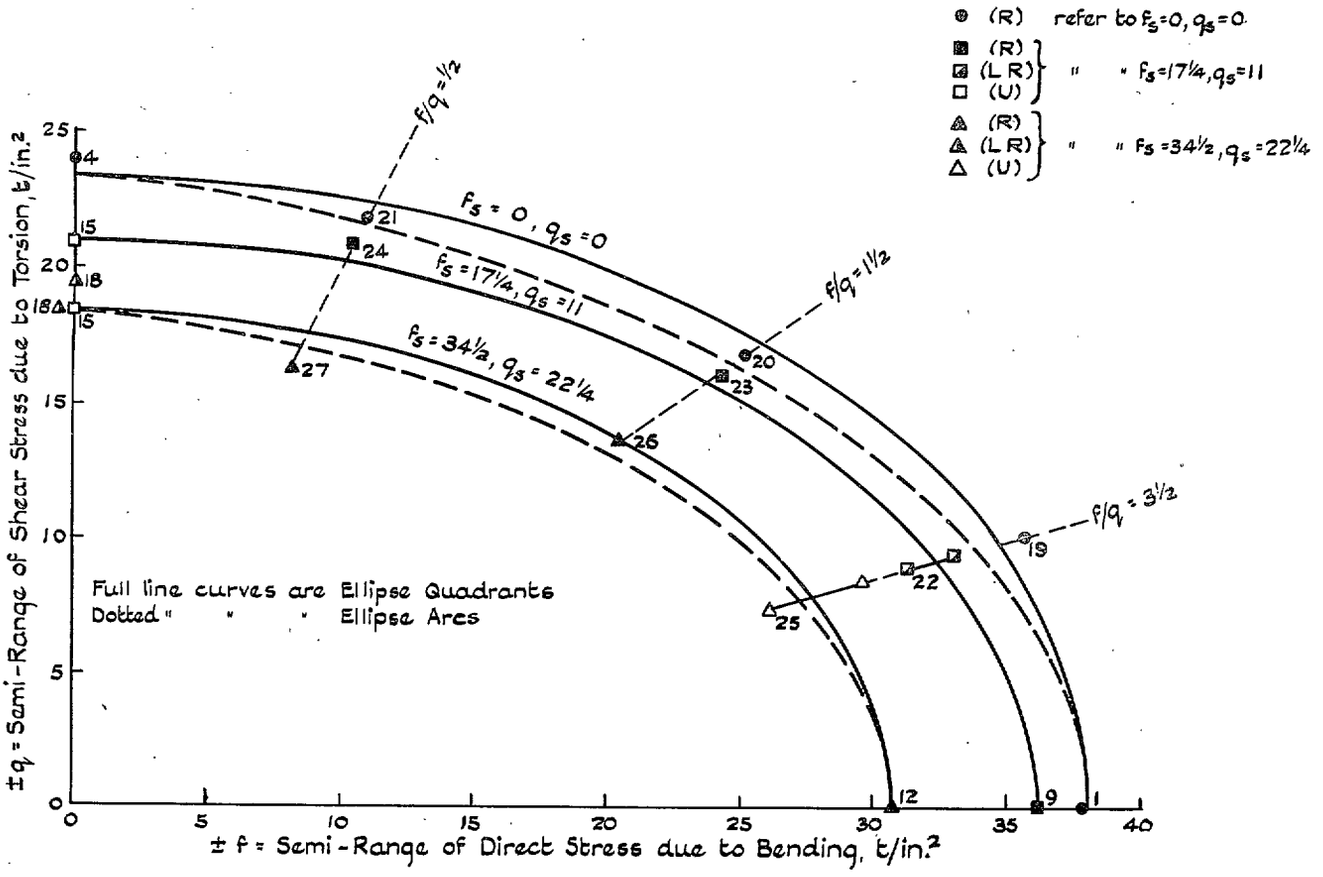

FIG. 81. Effect of Superimposed Static Stress on *f*/*q* Relation : Test Sections I, V and IX of Table 20 : Solid Plain Specimens.

stresses, $\pm q$, and, (*c*) three combinations of reversed bending and reversed shearing stresses, in the ratios of $f/q = 3\frac{1}{2}$, $1\frac{1}{2}$ and $\frac{1}{2}$. For each series, the selected superimposed static stress system was held constant throughout, thus :—

Series 1 :—$f_s = 0$, $q_s = 0$. (Square I, Table 20).

Series 2 :—$f_s = 17\frac{1}{4}$ t/in.^{2}, $q_s = 11$ t/in.^{2} (Square V, Table 20).

Series 3 :—$f_s = 34\frac{1}{2}$ t/in.^{2}, $q_s = 22\frac{1}{4}$ t/in.^{2} (Square IX, Table 20).

We have discussed the effect of these superimposed static stress systems on the ' end points,' where $f/q = \infty$ and 0; the effect of these static stress systems on the relation between the bending and shearing stress components—the f/q relation—can now be examined. Series 1, in which no static stress system is imposed, is, of course, exactly the same type of applied stress system as imposed in the No. 1 Type Combined Stress Machine employed in carrying out the complete series of tests reported in Part I of this investigation, where it was found that the f/q relation exhibited by solid specimens and hollow specimens, free from discontinuities of section, of twelve ductile steels was, in each case, an ellipse quadrant given by

$$\frac{f^2}{b^2} + \frac{q^2}{t^2} = 1$$

where $\pm b$ = fatigue limit (direct stress) under reversed bending stresses only ($f/q = \infty$)

where $\pm t$ = fatigue limit (shear stress) under reversed torsional stresses only ($f/q = 0$).

Reference to the *S/N* diagrams—Figs. 24 to 35 inclusive—of the present test shows that, as for reasons of economy, the number of specimens used to determine each fatigue limit was about the same, no greater accuracy can be attached to the ' end points ' (values of b and t) of each series, than to the intermediate points ($f/q = \frac{1}{2}$, $1\frac{1}{2}$ or $3\frac{1}{2}$). Therefore, in plotting the f/q relation, the curve has been drawn which provides the best fit, using the method of least squares, to the series of five points : based on previous experience, the two forms of curve which have been examined are the ellipse quadrant and the ellipse arc.

(*a*) Series 1 :—$f_s = 0 : q_s = 0$ (Square **I**, Table 20).

The reference numbers of the relevant tests are 4, 21, 20, 19 and 1, whose f/q components are plotted in Fig. 81 ; the best fitting ellipse quadrant passes through the slightly corrected ' end-values ' of $\pm q = 23{\cdot}4$ t/in.^{2} (Test 4) and $\pm f = 38{\cdot}0$ t/in.^{2} (Test 1). This curve represents closely the experimental data, thus confirming the conclusion drawn from the tests made in Part I on the No. 1. type of Combined Stress Machine, that, with solid or hollow specimens free from discontinuities, the f/q relation conforms closely to an ellipse quadrant. For comparison, the ellipse arc drawn through the same end-values is also shown on Fig. 81 : although the pair of curves are not widely separated, in this region where S_{90}/S_0 (corrected) $= 1{\cdot}23$*, the ellipse quadrant fits the data more closely.

* See Part I for discussion of the separation of equivalent curves of the two types as dependent on this ratio value.

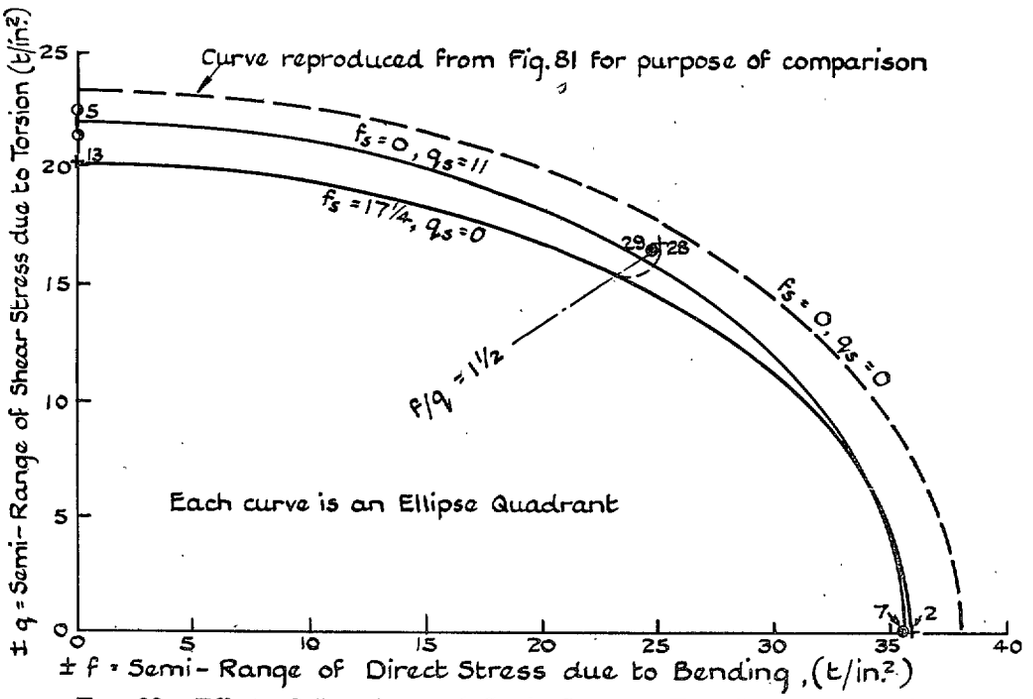

FIG. 82. Effect of Superimposed Static Stress : Test Sections **II** and **IV** of Table 20 : Solid Plain Specimens.

(*b*) Series 2 :—$f_s = 17\frac{1}{4}$, $q_s = 11$ (Square V, Table 20).

The reference numbers of the relevant tests are 15, 24, 23, 22, and 9 ; these are also plotted in Fig. 81, where the best fitting ellipse quadrant passes through the experimental end-value of test 9, $\pm f = 36{\cdot}0$ t/in.^{2} and the corrected value of $\pm q = 21{\cdot}0$ t/in.^{2} for the end-point 15. This ellipse quadrant represents the test data extremely closely, very much better than the ellipse arc (not shown on the diagram) drawn through the same end-points.

(*c*) Series 3 :—$f_s = 34\frac{1}{2}$, $q_s = 22\frac{1}{4}$ (Square IX, Table 20).

The reference numbers of the relevant tests are 18, 27, 26, 25 and 12. These data are plotted in Fig. 81, where the best fitting ellipse quadrant passes through the experimental value of test 12, $\pm f = 30{\cdot}6$ t/in.^{2}, and the lower of the bracketed values ($\pm$ 18·5/19·5) for test number 18, i.e. $\pm q = 18{\cdot}5$ t/in.^{2} Within the accuracy of the experimental data, the ellipse quadrant represents these data satisfactorily. The corresponding ellipse arc, drawn through the same end-points, is also shown on the diagram ; in this region, where $S_{90}/S_0 = 1{\cdot}20$, the pair of curves are very close to each other and either curve could, without serious error, be said to fit the somewhat irregular data. But, in view of the weight of accumulated evidence that the ductile steels conform much more closely to the ellipse quadrant when tested in the form of specimens free from discontinuities, it is justifiable to assume, in this case also, that the quadrant relation holds.

Thus, a most important further conclusion arises from these three series of tests. From the investigations reported in Part I, it emerged clearly that, when no superimposed static mean stress was operating, the f/q relation was satisfactorily represented by an ellipse quadrant. The present tests first confirm that conclusion but also show that, when considerable values of static bending and shearing stresses are operating, the f/q relation is still represented by an ellipse quadrant, the effect of the static stresses being merely to reduce the major and minor axes of the ellipse. Thus the general rule is indicated that, whatever the applied system of superimposed static stress, having determined experimentally the fatigue resistance to reversed bending stresses and reversed torsional stresses, the resistance to any combination of these reversed stresses can be simply calculated : this rule should be of considerable value for design purposes.

It is of interest to examine in this connection the data of the two remaining squares II and IV of Table 20 ; in each case, three fatigue-ranges only have been determined, affording insufficient data on which to base conclusions unless these are consistent with the results of the larger series of squares I, V and IX. The test data have been plotted to give Fig. 82.

(*d*) Series 4 :—$f_s = 17\frac{1}{4}$, $q_s = 0$ (Square II, Table 20).

(*e*) Series 5 :—$f_s = 0$, $q_s = 11$ (Square IV, Table 20).

In Series 4, the reference numbers of the relevant tests are 2, 28 and 13 : the ellipse quadrant shown on Fig. 82 has been drawn to pass through the experimental end

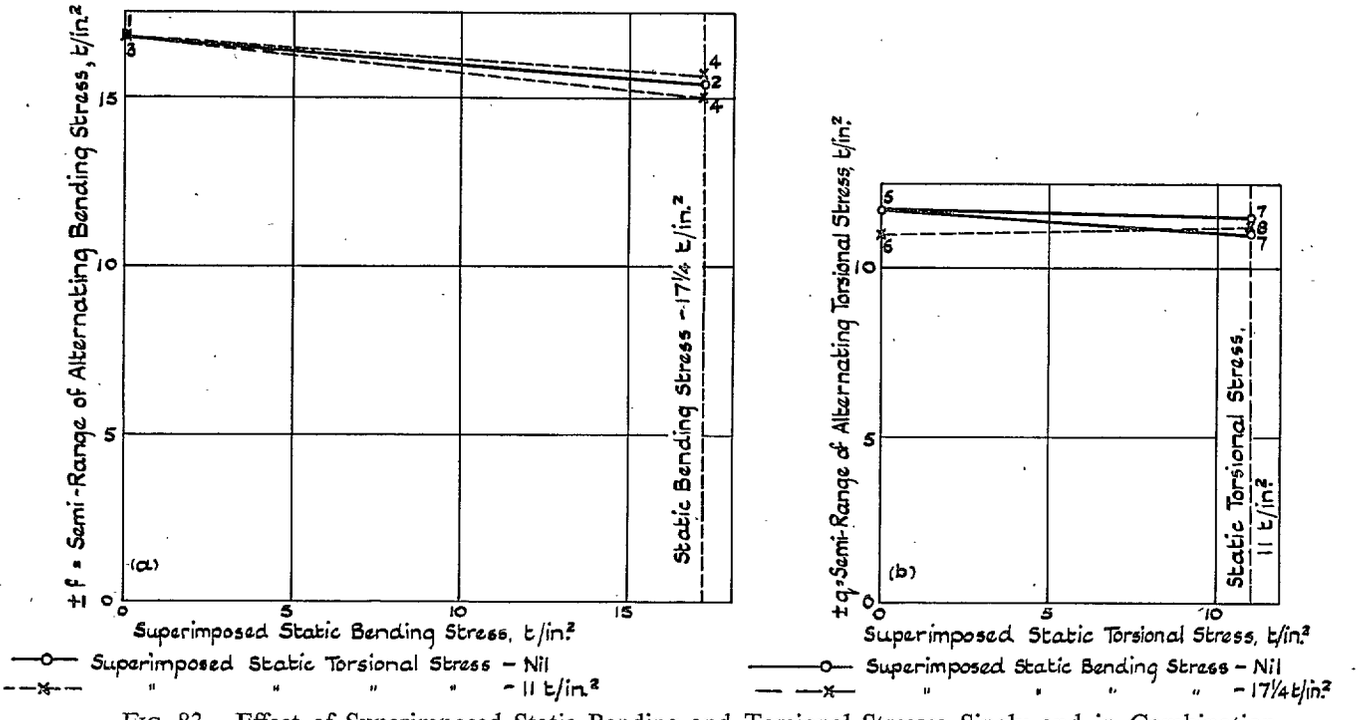

FIG. 83. Effect of Superimposed Static Bending and Torsional Stresses Singly and in Combination on the Fatigue Limits under Reversed Stresses : Hollow Specimens with radial Hole.

(92759) L 2

points (2 and 13) as no correction is justified. In Series 5, the reference numbers of the relevant tests are 7, 29 and 5: the corresponding ellipse quadrant has been similarly drawn to pass through the experimental end-point 7 and the average value, $\pm 21{\cdot}9_5$, of the bracketed values for test 5 ($\pm 21{\cdot}4/22{\cdot}5$). The intermediate test point, number 29, of Series 5 falls very close to the corresponding ellipse quadrant; test number 28, of Series 4, is distant from its corresponding ellipse quadrant by $\pm 1{\cdot}5$ t/in.^{2}, an error which does not greatly exceed the probable accuracy of any individual test point. In both cases, the ellipse quadrant affords a conservative estimate of the actual fatigue resistance. More data are desirable but, considered against the conclusions based on the more complete series plotted on Fig. 81, it is reasonable to assume that the results of Series 4 and 5 are consistent with those conclusions. Thus, the ellipse quadrant affords a satisfactory basis of design for the whole of the applied stress conditions represented by the nine squares of Table 20.

II. Hollow Specimens Having a Small Radial Oil Hole

The programme of tests is stated in Table 21; the results are summarised in Table 23: any individual fatigue test will be completely identified by quoting the test reference number as stated in each of those tables.

1. EFFECT OF SUPERIMPOSED STATIC STRESSES ON THE FATIGUE RANGE UNDER SIMPLE REVERSED STRESSES.

The results are plotted in Fig. 83.

Consider first Fig. 83 (*a*). The fatigue range under reversed bending stresses, $\pm 16{\cdot}8$ t/in.^{2} (test 1) is slightly reduced to $\pm 15{\cdot}4$ t/in.^{2} (test 2), or 8·3%, by superimposing a static bending stress of $17\frac{1}{4}$ t/in.^{2}. The further addition of a static torsional stress of 11 t/in.^{2} to each of these stress conditions (tests 3 and 4) produces no further effect. Fig. 83 (*b*) shows the effect of superimposed static stresses on the fatigue range under reversed shearing stress, $\pm 11{\cdot}7$ t/in.^{2} (test 5). The addition of a static torsional stress of 11 t/in.^{2} brings a slight reduction to $\pm 11/\pm 11{\cdot}5$ t/in.^{2} (test 7); a further addition of a static bending stress of $17\frac{1}{4}$ t/in.^{2} produces no appreciable further reduction, the recorded fatigue strength being $\pm 11{\cdot}2$ (test 8). The effect of adding static bending stress of $17\frac{1}{4}$ t/in.^{2} only reduces the reversed shearing value from $\pm 11{\cdot}7$ t/in.^{2} (test 5) to $\pm 11{\cdot}0$ t/in.^{2} (test 6), i.e. by 6%.

Thus, the effect of adding quite considerable static bending and/or torsional stresses is perceptible in some cases but is always small in amount.

2. THE STRESS CONCENTRATION EFFECT PRODUCED BY THE PRESENCE OF THE RADIAL HOLE

The experimental results of the two series of tests made, (*a*) on the solid cylindrical specimens, and (*b*) on the specimens containing the oil-hole, provide directly, for this material, the values of the Fatigue Strength Reduction Factor, K_f, where

$$K_f = \frac{\text{Fatigue strength of solid specimens}}{\text{Fatigue strength of hollow specimens containing oil-hole}}$$

The calculated values of K_f are listed in the last column of Table 23. For more convenient inspection and assessment, they are re-arranged in Table 26. It will be recalled that each K_f value was obtained by dividing the fatigue range obtained using solid specimens by the corresponding (i.e. exactly similar test conditions of θ, or f/q, and superimposed static mean stress) fatigue range obtained with hollow drilled specimens; as K_f is calculated from two quantities each of which is subject to experimental errors, small variations in material, etc., which may be cumulative, the values of K_f are themselves subject to error.

TABLE 26

FATIGUE STRENGTH REDUCTION FACTORS, K_f; HOLLOW SPECIMENS WITH RADIAL HOLE.

Superimposed Static Stress t/in^2		Values of K_f				
Bending f_s	Torsion q_s	$\theta=0°$	$\theta=29{\cdot}7°$	$\theta=53{\cdot}1°$	$\theta=75{\cdot}9°$	$\theta=90°$
0	0	2·25 (1)	2·49 (13)	2·23 (9)	1·95 (14)	2·05 (5)
$17\frac{1}{4}$	0	2·32 (2)	—	2·42 (10)	—	1·84 (6)
0	11	2·12 (3)	—	2·30 (11)	—	1·95 (7)
$17\frac{1}{4}$	11	2·35 (4)	—	2·62 (12)	—	1·75 (8)
Average Value		2·26		2·39		1·91

Note:—Figures in brackets are the test reference numbers.

Making due allowance for expected variations, these results suggest:—

(*a*) The value of K_f for reversed bending stresses is about 2·2, for reversed torsional stresses about 2·0 with, probably, a fairly regular change from one value to the other as the ratio of f/q diminishes.

(*b*) The value of K_f is determined primarily by the applied cyclic stresses and is not appreciably affected by the superimposition of the static bending and/or static torsional stresses.

Theoretical Stress Concentration Factors, K_t.

It is of interest to compare these purely experimental fatigue values with available data regarding the theoretical Stress Concentration Factor, K_t, where

$$K_t = \frac{\text{Maximum induced stress}}{\text{Nominal average stress}}$$

The stress system and the theoretical stress concentration factor produced by the presence of a circular hole have attracted much attention by many investigators, using the methods of mathematical analysis, photoelasticity and direct strain measurements. Many of the cases thus investigated are concerned only with thin plates subjected to simple stressing actions, but the results of some selected investigations are of considerable interest in the present connection.

In 1898, Kirsch[22] gave a solution for the stresses around a circular hole in a plate of infinite width, subjected to a uniform uniaxial tensile stress, f. At the boundary of the hole, two of the principal stresses vanish. The sole remaining stress, the third principal stress, which is the circumferential tensile stress, has the value

$$f(1 - 2\cos 2\alpha)$$

at that position, on the boundary of the hole, at which the radius passing through makes an angle α with the direction of the tensile stress, f. Thus, the maximum stress, equal to $3f$ (tensile) occurs at $\alpha = \pm \pi/2$, the minimum, equal to $-f$ (compressive), occurring at $\alpha = 0$ and π.

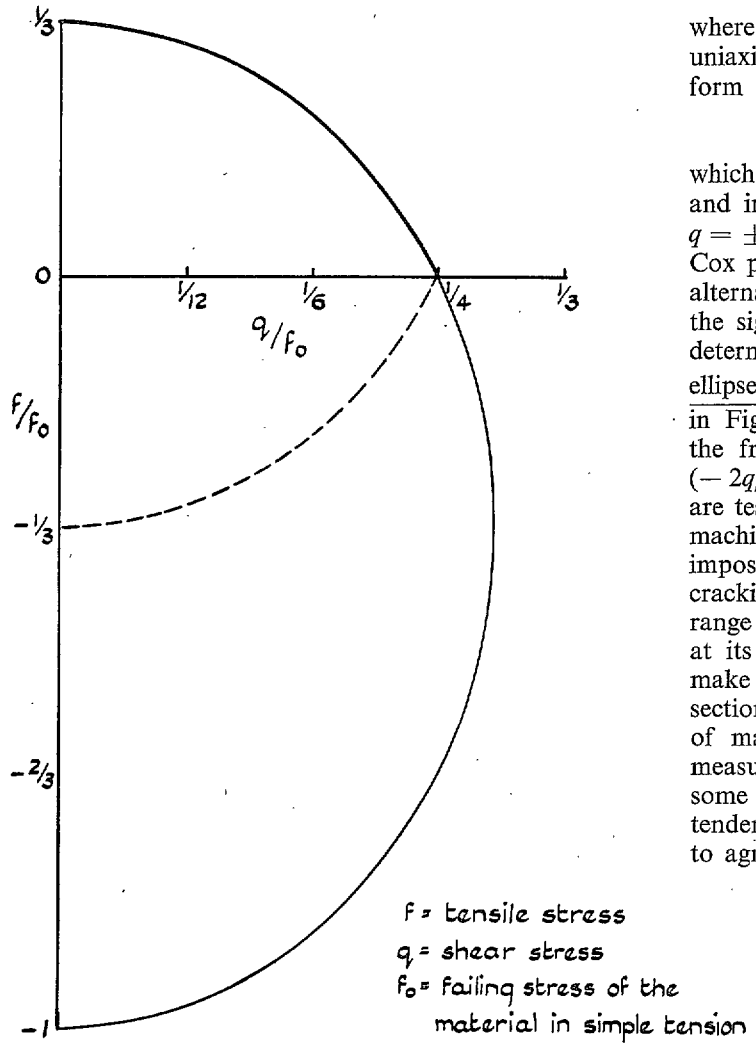

FIG. 84. Limiting Condition for Failure of a Plate Pierced by a Circular Hole under Combined Bending and Torsional Stresses (Cox).

Cox[23] in the course of a general investigation into the effect of elliptical holes has extended this case to that of combined direct stress and shear. The tensile stress due to a shear stress q on planes parallel and perpendicular to the same direction is $4q \sin 2\alpha$; the stress due to the combined tensile stress f and shear stress q is, therefore

$$f(1 - 2\cos 2\alpha) + 4q \sin 2\alpha$$

of which the maximum and minimum values are

$$f \pm 2(f^2 + 4q^2)^{1/2}$$

occurring at $\alpha = \frac{1}{2}\tan^{-1}(-2q/f)$ and at right-angles to this radius. The condition for failure is then

$$f + 2(f^2 + 4q^2)^{1/2} = f_0$$

where f_0 is the true failing stress of the material under uniaxial tension. This relation may be expressed in the form

$$16q^2 + 3(f + \tfrac{1}{3}f_0)^2 = \tfrac{4}{3}f_0^2 \quad .. \quad .. \quad .. \quad (1)$$

which is an ellipse, having its centre at $f = -\frac{1}{3}f_0$, $q = 0$ and intercepts on the axes at $f = \frac{1}{3}f_0$ and $-f_0$, and $q = \pm f_0/4$. The Cox ellipse is reproduced as Fig. 84. Cox points out that, when the applied stresses f and q alternate between equal positive and negative values, the signs of f and q are irrelevant and failure will be determined by the upper part of the curve, i.e. the ellipse arc contained by the rectangular axes, indicated in Fig. 84, by the full-line curve. The analysis gives the fracture plane as that denoted by :—$\alpha = \frac{1}{2}\tan^{-1}(-2q/f)$. Now, when specimens of circular cross-section are tested in the present combined stress fatigue-testing machines, the geometry of the machine and loading arm imposes the relation $f/q = 2\cot\theta$. Hence, if fatigue cracking were initiated on planes subjected to the greatest range of principal stress, the traces of the fatigue crack, at its origin, on the surface of the specimen, should make an angle of $\frac{1}{2}\theta$ with the trace of the transverse section of the specimen which passes through the point of maximum stress concentration. Reference to the measurements recorded in Table 23 shows that, although some inconsistencies exist, there is an unmistakable tendency for the orientation of the cracks, at their origin, to agree with $\frac{1}{2}\theta$ over the whole range of θ from 0 to 90 deg. and this applies irrespective of the type and amount of the superimposed static stresses. From this it can be inferred that (*a*) the propagation and the direction of fatigue cracking is determined by the maximum stress induced at the edge of the hole by the applied range of cyclic stressing and, inferentially, (*b*) the superimposed static stresses have little, if any, influence on the failure by fatigue.

In the Cox analysis, the deduced theoretical stress concentration factors apply only to the assumed conditions of an infinite plate or, correspondingly, a hole of infinitesimally small diameter. Investigations, by other authors, have established that, as the size of the hole increases in relation to the width of the plate or shaft diameter, the theoretical stress concentration factor decreases ; the factor values of $\frac{1}{3}f_0$ (bending) $\frac{1}{4}f_0$ (torsion) are, therefore, too high for direct comparison with the results of the fatigue tests.

Frocht[24], also Wahl and Beeuwkes[25], have determined, photoelastically, the stress-concentration factors for flat bars in tension, pierced by a transverse hole for a wide range of values of d/W where d is the diameter of the hole and W is the width of the plate. In the shaft specimens tested in the present research, the outside diameters of the specimen and the drilled hole were, respectively, 0·500 in. and 0·050 in. ($d/D = 0{\cdot}1$). For the flat bar where $d/W = 0{\cdot}1$, Frocht obtained a theoretical stress concentration factor of 2·7, while Wahl and Beeuwkes reported 2·72, their results thus being in extremely good agreement. These values relate to tensile (or bending) loading.

Peterson and Wahl[26] determined, by direct strain measurements, the stress-concentration factors present, in the three-dimensional case of shafts having transverse holes or transition fillets, and subjected to static bending forces. These tests were made on large shafts, of $7\frac{1}{4}$ in. diameter, the strains being measured using an accurate extensometer and a gauge length of 0·1 in. Various values of d/D were investigated. A slight extrapolation of Peterson and Wahl's experimental results yields a stress concentration factor of 2·26 for $d/D = 0{\cdot}1$ (present case) ; this value relates to the net area of the shaft, the hole being allowed for in the calculation. Reversed bending fatigue tests were then made on a number of steels by Peterson and Wahl on varying sizes of specimen, the maximum diameters of which were 2 in. and, in some cases, 3 in. In every case, a " size effect " was found, the stress concentration factor, for any series of tests in which d/D was held constant, increasing as D increased but tending towards an asymptotic value. They found that in some cases, the fatigue strength reduction factors approached closely to the static stress concentration factors as determined by strain measurements ; closer agreement was obtained with alloy steels and quenched carbon steels than with unquenched carbon steels. In a recent book, Frocht[27] reports photoelastic work on this three-dimensional case of a shaft, with oil hole or fillet, under bending stresses : the results are in remarkably good agreement with the strain

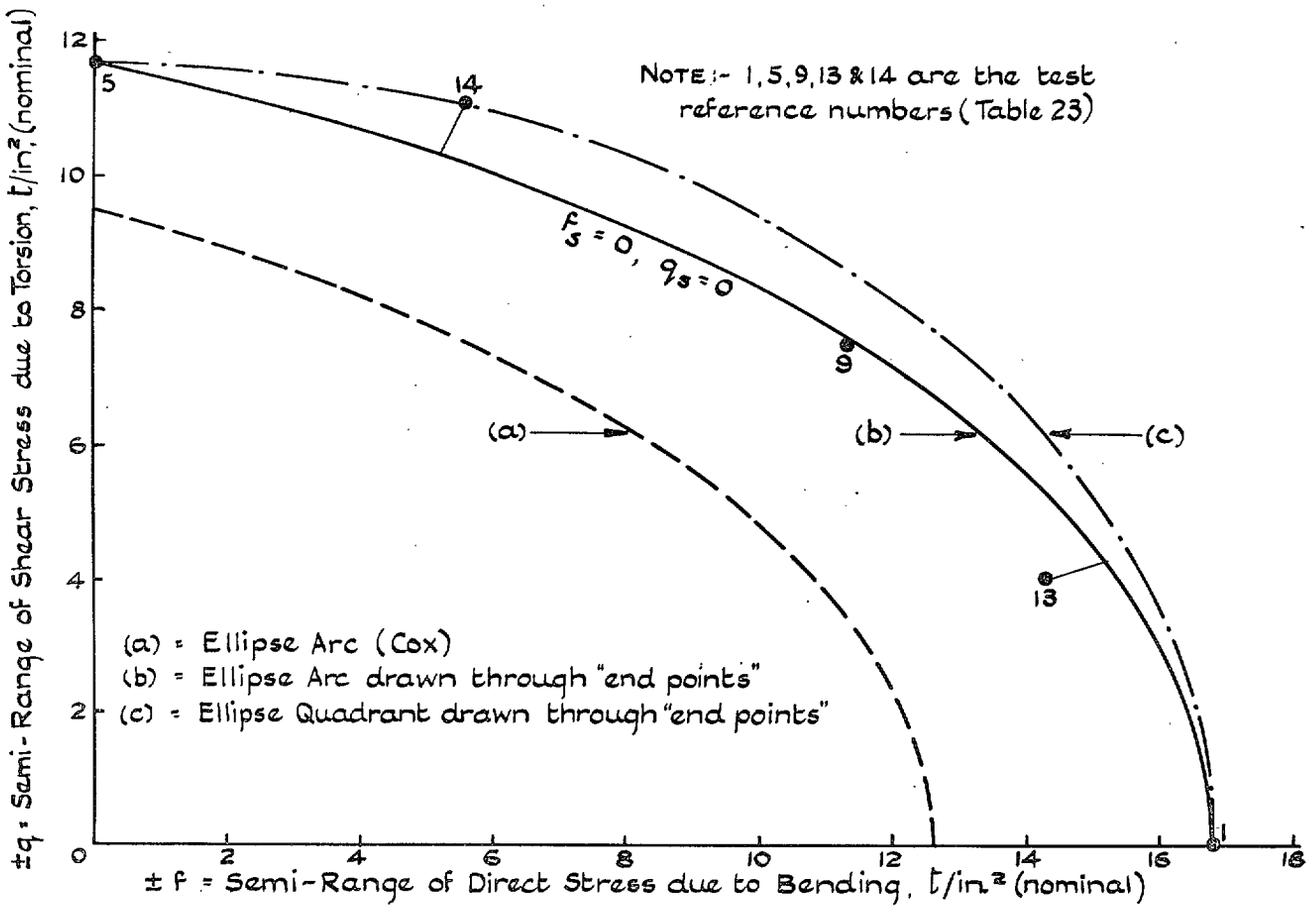

FIG. 85. *f/q* Relation : Hollow Specimens with Radial Hole.

measurements of Peterson and Wahl. Frocht shows, in general, that the stress concentration factors for the three-dimensional case are lower than those for the two-dimensional case, for the same value of d/D. For the drilled specimens used in the present experiments, it can, therefore, be assumed that the value of the stress concentration factor is about 2·26 when subjected to static bending stresses.

Thum and Kirmser[28], using the direct strain measurement method of Peterson and Wahl, have determined experimentally the stress concentration factors in a drilled shaft under static bending stresses and under static torsional stresses. In the case of bending, Thum and Kirmser obtained the value for K_t of about 2·1, when d/D equals 0·1, at the edge of the hole ; a slightly lower value than that of Peterson and Wahl (2·26). For the static torsional case, again when d/D equals 0·1, Thum and Kirmser obtained the value of 2·9 for the ratio f_0/q ; this ratio is the same as used by Cox and is not the torsional stress concentration factor as usually employed. These values of 2·1 (bending) and 2·9 (torsion) are, as with Peterson and Wahl's results, calculated on the net area of the shaft. To compare directly these results with the present fatigue results, which are calculated without reference to the loss of sectional area due to the hole, either the concentration factors or the fatigue results can be compensated : it is more convenient to adopt the former course.

The bending value is compensated by adding about 20%, giving comparison factors of 2·71 (Peterson and Wahl) and 2·52 (Thum and Kirmser) : the approximate compensation to the Thum and Kirmser torsion value is an addition of about 9%, giving the value of 3·16 for f_0/q.

The experimental values obtained for the fatigue ranges are :—

Solid Specimens ($f_s = 0$, $q_s = 0$)

(1) Reversed Bending Stresses = ±37·8 t/in.² (Test 1, Table 22).

(2) Reversed Torsional Stresses = ±24·0 t/in.² (Test 4, Table 22).

Pierced Specimens ($f_s = 0$, $q_s = 0$)

(3) Reversed Bending Stresses = ±16·8 t/in.² (Test 1, Table 23).

(4) Reversed Torsional Stresses = ±11·7 t/in.² (Test 5, Table 23).

For the fatigue strength of the drilled shafts under reversed bending stresses, the theoretical stress concentration factor obtained by Peterson and Wahl would predict a value $\left(\frac{37\cdot8}{2\cdot71}\right)$ of ±14 t/in.² and that of Thum and Kirmser, a value $\left(\frac{37\cdot8}{2\cdot52}\right)$ of ±15 t/in.², as against the experimental value of ±16·8 t/in.² ; differences of 16·7% and 10·7%, respectively. Applying the Thum and Kirmser theoretical value (compensated) for f_0/q, the calculated value of the fatigue range of the pierced

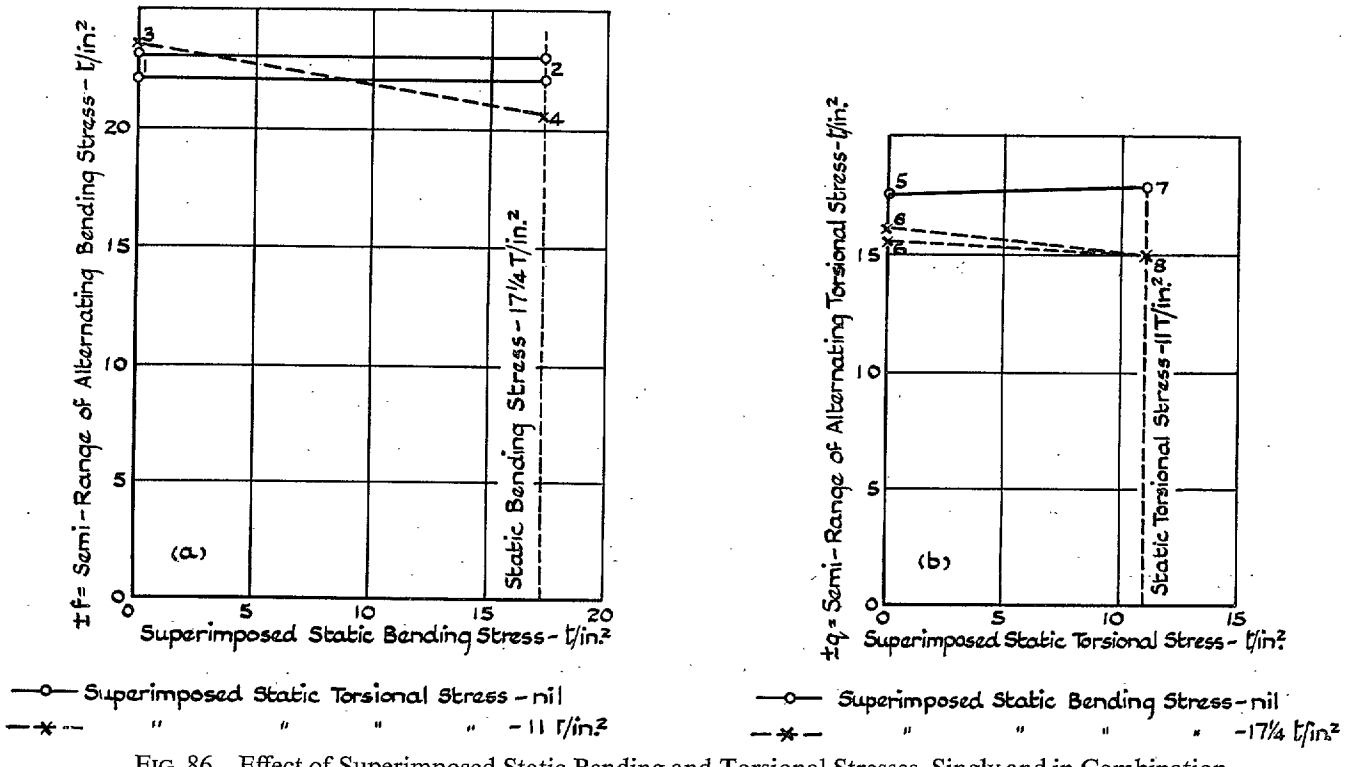

FIG. 86. Effect of Superimposed Static Bending and Torsional Stresses, Singly and in Combination, on the Fatigue Limits under Reversed Stresses : Hollow Specimens with Small Radius Fillet.

shafts under reversed torsional stresses becomes ± 12 t/in.^{2} $\left(\frac{37\cdot 8}{3\cdot 16}\right)$, as against the experimental value of $\pm 11\cdot 7$ t/in.^{2} ; a difference of $2\frac{1}{2}\%$ only.

It will be recalled that, in the specimens used in the present fatigue experiments, the intersection of the hole on the outside surface of the shaft is rounded off by a small radius (see Fig. 64B). It is very doubtful indeed if this radius has any appreciable strengthening effect : its value in practice is to remove burrs caused by machining, as such burrs might have an appreciable weakening effect under cyclic loading.

Thus, the presence of the drilled hole produces, in this alloy steel, a reduction in fatigue strength which, under reversed bending stresses, is somewhere between 10% and 16% less than the stress concentration effect deduced from static strain measurements while, under reversed torsional stresses, the full theoretical stress concentration effect is realised.

3. THE f/q RELATION

Referring to Table 23, the results of the series of five tests, in which no static stresses were superimposed, are plotted in Fig. 85. The " Cox " ellipse arc, representing the theoretical curve for an infinite plate, is shown on the diagram ; for the reasons previously explained, this curve is well below the experimental points. An ellipse arc, of the general empirical form as previously employed, passing through the " end points " ($f = 0$, $q = 0$) is also shown, together with the ellipse quadrant drawn through the same end points. Making allowance for the irregularity of results associated with this material, the ellipse arc provides a good fit for the data : the quadrant does not.

There remain for examination, the three series of tests in each of which static stresses were superimposed ; the test reference numbers, superimposed static stresses and fatigue ranges are as follows :—

A. $f_s = 17\frac{1}{4}$, $q_s = 0$. Test 2 ($f = \pm 15\cdot 4$, $q = 0$) ; test 10 ($f = \pm 10\cdot 3_5$, $q = \pm 6\cdot 9$) and test 6 ($f = 0$, $q = \pm 11$).

B. $f_s = 0$, $q_s = 11$. Test 3 ($f = \pm 16\cdot 8$, $q = 0$) ; test 11 ($f = \pm 10\cdot 8$, $q = \pm 7\cdot 2$) and test 7 ($f = 0$, $q = \pm 11/11\cdot 5$).

C. $f_s = 17\frac{1}{4}$, $q_s = 11$. Test 4 ($f = \pm 15/15\cdot 6$, $q = 0$) ; test 12 ($f = \pm 9\cdot 2_5$, $q = \pm 6\cdot 1_5$) and test 8 ($f = 0$, $q = \pm 11\cdot 2$).

As for each of the three series of data—A, B, or C—it is required to compare only the intermediate test result with the ellipse quadrant and ellipse arc passing through the corresponding pair of ' end-points ', it will be sufficient to compare the calculated ordinate of each curve, at the point corresponding to $\theta = 53\cdot 1$ deg., with the experimental value. For this purpose, it is convenient to express stresses in terms of the Range of Maximum Shear Stress, S at the fatigue limit ; the calculated values are obtained using the formulae (6) and (8) given in Section 5 of Part I of the paper. The results are as follows :—

Series	Test No.	Range of Maximum Shear Stress, S					
		Experimental		Ellipse Quadrant		Ellipse Arc	
		t/in^2	ratio	t/in^2	ratio	t/in^2	ratio
A	10	$\pm 8\cdot 6$	100	$\pm 9\cdot 38$	109	$\pm 8\cdot 47$	98·5
B	11	$\pm 9\cdot 0$	100	$\pm 9\cdot 92$	110	$\pm 9\cdot 35$	104
C	12	$\pm 7\cdot 7$	100	$\pm 9\cdot 42$	122	$\pm 8\cdot 76$	114

For each series, the ellipse quadrant value is considerably in excess of the experimental value. The ellipse arc gives values for series A and B which differ from the experimental values by $-1\frac{1}{2}\%$ and $+4\%$ only, amounts within the accuracy of the experiments. The ellipse arc value for series C is 14% in excess of the experimental value, a considerable error ; no conclusion can be drawn from this series. Recognising that more data are required to provide definite conclusions, the results of series A and B lend support to the conclusion drawn from the previous series (tests 1, 5, 9, 13 and 14, in which no static stresses were imposed) i.e. that in the presence of this type of discontinuity of section, the f/q relation is satisfactorily represented, for design purposes, by an ellipse arc and, further, that this relation may apply even when quite considerable static stresses are superimposed, the only effect of the latter being to depress slightly the values of the end-points through which the ellipse arc is drawn.

III. Hollow Specimens containing a Transition Fillet of Small Radius

The programme of tests is stated in Table 21 : the results are summarised in Table 24, in which all stress values quoted refer to nominal stresses, calculated in the usual manner on the parallel test portion (0·500 in. dia.) of the specimen and ignoring the stress concentration due to the presence of the fillet.

1. EFFECT OF SUPERIMPOSED STATIC STRESSES ON THE FATIGUE RANGE UNDER SIMPLE REVERSED STRESSES

The results are plotted in Fig. 86, to show, separately, the effect on the fatigue resistance to reversed bending stresses (Fig. 86 (*a*)) and reversed torsional stresses (Fig. 86 (*b*)).

Consider first Fig. 86 (*a*). The fatigue range under reversed bending stresses, $\pm 22/23$ t/in.^{2} (test 1), retains the same value (test 2) when a static bending stress of $17\frac{1}{4}$ t/in.^{2} is superimposed. The further addition of a static torsional stress of 11 t/in.^{2} (test 4) reduces the

fatigue range to $\pm$ 20·6 t/in.², i.e. by 8½%. The effect of superimposing a static torsional stress, only, of 11 t/in². (test 3) apparently raises slightly the reversed bending stress value to $\pm$ 23·4 t/in.², i.e. by 4%, but such an increase cannot be accepted as real, the apparent difference being probably due to slight variations in the material itself. Turning to Fig. 86 (*b*), the fatigue range under simple reversed torsional stresses is $\pm$ 17·5 t/in.² (test 5). The effect of superimposing a static torsional stress of 11 t/in.² is, apparently, to raise slightly the fatigue strength to $\pm$ 17·9 t/in.² (test 7); this difference is, also, probably unreal. The effect of superimposing a static bending stress of 17¼ t/in.² acting alone (test 6) reduces the safe range of stress to $\pm$ 15½/16 t/in.², i.e. by 10%: superimposing both the static bending stress of 17¼ t/in.² and a static torsional stress of 11 t/in.² (test 8) effects only a slight further reduction to $\pm$ 14·9 t/in.², or a total reduction of 14·9%.

This series of experiments shows, therefore, that the addition of a static mean stress of the same kind has little, if any, effect on the fatigue strength. Imposing a static torsional stress alone has no effect on the reversed bending fatigue limit: imposing a static bending stress effects a reduction of 10% in the reversed torsional fatigue limit. When the two types of static stress are applied simultaneously the total reductions in the fatigue limits under reversed bending and reversed torsional stresses are 8½% and 14·9% respectively.

2. THE STRESS CONCENTRATION EFFECT PRODUCED BY THE PRESENCE OF THE TRANSITION FILLET

The values of the Fatigue Strength Reduction Factor, K_f, are listed in the last column of Table 24. For more convenient inspection and assessment, they are rearranged in Table 27.

TABLE 27

FATIGUE STRENGTH REDUCTION FACTORS, K_f; HOLLOW SPECIMENS WITH SMALL FILLET

Superimposed Static Stress t/in²		Values of K_f				
Bending f_s	Torsion q_s	θ=0°	θ=29·7°	θ=53·1°	θ=75·9°	θ=90°
0	0	1·68 (1)	1·77 (13)	1·53 (9)	1·37 (14)	1·37 (5)
17¼	0	1·59 (2)	—	1·54 (10)	—	1·28 (6)
0	11	1·52 (3)	—	1·63 (11)	—	1·23 (7)
17¼	11	1·75 (4)	—	1·73 (12)	—	1·32 (8)
Average Value		1·63		1·61		1·30

Note.—Figures in brackets are the test reference numbers.

Making allowance for some irregularity in the data, the results suggest:—

(*a*) The value of K_f for reversed bending stresses is about $1{\cdot}6_5$, diminishing fairly regularly to a value of about $1{\cdot}3_5$ for reversed torsional stresses.

(*b*) The value of K_f is determined primarily by the applied cyclic stresses and is not appreciably affected by the superimposition of the static bending and/or static torsional stresses.

Theoretical Stress Concentration Factors, K_t

In the previous section dealing with drilled shafts, reference was made to the work of Peterson and Wahl[26] on the stress concentration factors present in the three-dimensional case of shafts having holes: the factors being determined by strain measurements on large shafts subjected to static bending forces. The same methods were employed for shafts having transition fillets. The values of K_t were determined, experimentally, for various values of r/d, where r is the radius of the transition fillet and d is the diameter of the parallel test portion of the shaft. Frocht[24] had previously determined, photo-elastically, the stress concentration factors, for a wide range of values of r/d, for the two-dimensional case of a flat bar and transition fillet; the results of Peterson and Wahl fall exactly on Frocht's curve. We may, therefore, take Frocht's value of the theoretical stress concentration factor, K_t, for the case of $r/d = 0{\cdot}066$, which relates to the present fatigue specimens ($r = 0{\cdot}033$ in., $d = 0{\cdot}500$ in.): Frocht's value is 2·10. The experimental fatigue strength reduction factor obtained in the present tests, for the case of reversed bending stresses (zero superimposed static stress) is 1·68 (see Table 27), giving $K_f/K_t = 80\%$, for the S.65 steel.

Jacobsen[29] has determined, by the electrical analogy method, the theoretical stress concentration effect produced by the fillet in a shaft subjected to static torsional stresses. He investigated a wide range of values of D/d, where D is the enlarged diameter of the shaft, and of r/d. For the shaft dimensions corresponding to the present combined stress fatigue specimens, Jacobsen obtains the value of 1·6 for K_t: this maximum stress concentration occurs not at the exact junction of the fillet with the smaller shaft diameter, but at a point slightly removed from that junction and within the fillet. The experimental fatigue strength reduction factor obtained under reversed torsional stresses (zero superimposed static stress), in the present tests, is 1·37 (see Table 27), giving

$$K_f/K_t = 85\tfrac{1}{2}\% \text{ for the S.65 steel.}$$

These comparisons show, therefore, that with this material, the actual reduction in fatigue strength of a shaft due to the presence of a sharp transition fillet is less than the theoretical stress concentration effect, both under reversed bending stresses and reversed torsional stresses; the values of the ratio, K_f/K_t,—80% and 85½% respectively—being very similar.

3. THE f/q RELATION

Taken from Table 24, the results of the series of five tests in which no static stresses were superimposed, are plotted in Fig. 87. Passing through the 'end points' (Tests 1 and 5), an ellipse quadrant, also an ellipse arc of the general empirical form previously employed, are shown on the diagram. Test 13 falls on the ellipse arc, tests 9 and 14 between the two curves. The ellipse arc provides the better fit to the experimental data and a safer guide to design and may be accepted as a satisfactory criterion.

There remain, for examination, the following three series of tests in each of which static stresses were superimposed :—

A. $f_s = 17\frac{1}{4}, q_s = 0$. Test 2 ($f = \pm 22/23, q = 0$); Test 10 ($f = \pm 16{\cdot}2, q = \pm 10{\cdot}8$) and Test 6 ($f = 0, q = \pm 15{\cdot}5/16$).

B. $f_s = 0, q_s = 11$. Test 3 ($f = \pm 23{\cdot}4, q = 0$); Test 11 ($f = \pm 15{\cdot}2_5, q = \pm 10{\cdot}1_5$) and Test 7 ($f = 0, q = \pm 17{\cdot}9$).

C. $f_s = 17\frac{1}{4}, q_s = 11$. Test 4 ($f = \pm 20{\cdot}6, q = 0$); Test 12 ($f = \pm 14{\cdot}0_5, q = \pm 9{\cdot}3_5$) and Test 8 ($f = 0, q = \pm 14{\cdot}9$).

As with the previous corresponding results of the specimens with a drilled hole, the experimental value of each intermediate test (Nos. 10, 11 and 12) will be compared, in terms of Range of Maximum Shear Stress, S, with the calculated value, at $\theta = 53{\cdot}1$ deg., of the ellipse quadrant and ellipse arc drawn through the appropriate pair of 'end points' (Nos. 2 and 6 ; 3 and 7 ; 4 and 8). The results are as follows :—

Series	Test No.	Range of Maximum Shear Stress, S					
		Experimental		Ellipse Quadrant		Ellipse Arc	
		t/in²	ratio	t/in²	ratio	t/in²	ratio
A	10	±13·5	100	±13·6	101	±12·7	94
B	11	±12·7	100	±14·7	116	±13·6	107
C	12	±11·7	100	±12·6	108	±11·4	97

The ellipse quadrant thus overestimates by 1%, 16% and 8%, respectively, for series A, B and C. The ellipse arc is in error by − 6%, + 7% and − 3%, none of which are serious. It may, therefore, be concluded that with this type of discontinuity—as with the drilled hole—the

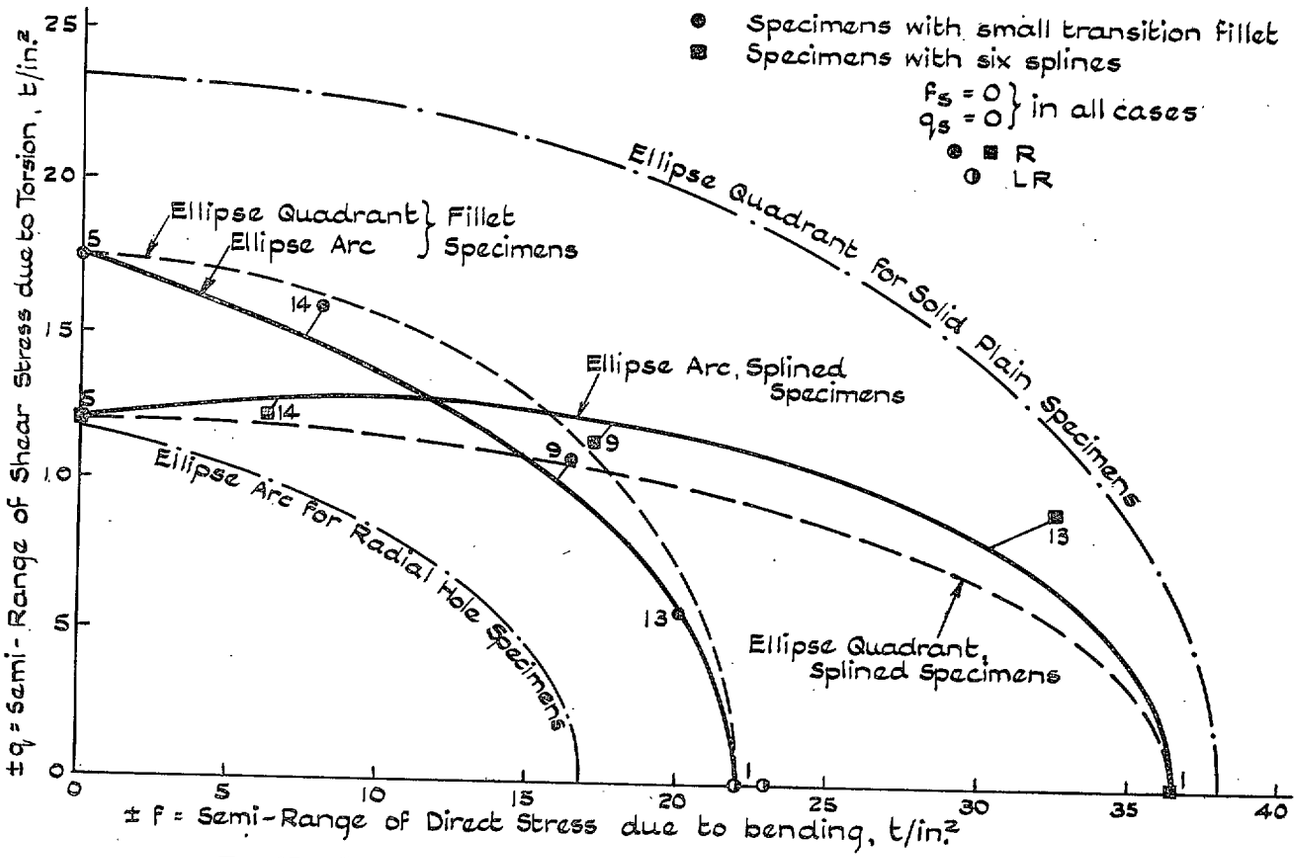

FIG. 87. f/q Relations. Hollow Specimens with Transition Fillet or Splines.

ellipse arc affords a satisfactory basis of design even when considerable static stresses are imposed.

IV. Hollow Splined-Shaft Specimens

The programme of tests is stated in Table 21 : the results are summarised in Table 25 ; any individual fatigue test will be completely identified by quoting the test reference number as stated in each of those tables.

1. EFFECT OF SUPERIMPOSED STATIC STRESSES ON THE FATIGUE RANGE UNDER SIMPLE REVERSED STRESSES.

The results are plotted in Fig. 88.

Fig. 88 (*a*) shows the effect of superimposing static stresses on cycles of reversed bending stress. The fatigue limit under simple reversed bending stresses, $\pm 36 \cdot 5$ t/in.^{2} (test 1) is only slightly reduced to $\pm 34 \cdot 8$ t/in.^{2} (test 2), by $4 \cdot 7\%$, by superimposing a static bending stress of $17\frac{1}{4}$ t/in.^{2} : the further addition of a static torsional stress of 11 t/in.^{2} produces no effect, the fatigue limit being $\pm 35 \cdot 0$ t/in.^{2} (test 4), which is the same value, within the accuracy of the experiment, as that produced by a static torsional stress of 11 t/in.^{2} acting alone, i.e. $\pm 34 \cdot 6$ t/in.^{2} (test 3). Fig. 88 (*b*) shows the effect of superimposing static stresses on cycles of reversed torsional stresses. The fatigue limit under simple reversed shearing stresses is ± 12 t/in.^{2} (test 5). If a static bending stress of $17\frac{1}{4}$ t/in.^{2} is superimposed, no effect is produced : the fatigue limit is $\pm 12 \cdot 2$ t/in.^{2} (test 6). The effect of superimposing a statical torsional stress of 11 t/in.^{2}, acting alone, reduces the reversed shearing value very slightly from ± 12 t/in.^{2} (test 5) to $\pm 11 \cdot 5$ t/in.^{2} (test 7), by $4 \cdot 2\%$, and the further addition of a static bending stress of $17\frac{1}{4}$ t/in.^{2} produces only a slight further reduction of 2%, to $\pm 11/11 \cdot 5$ t/in.^{2} (test 8).

Thus the effect of adding quite considerable static bending and/or torsional stresses is extremely small, and we have seen that this conclusion applies equally to the other forms of discontinuity examined, i.e. the drilled hole and the sharp transition fillet. The investigation shows, however, that the material is very sensitive to cyclic stresses when stress concentration is present ; this different response to static and cyclic stressing is of the greatest significance to design.

2. THE STRESS CONCENTRATION EFFECT PRODUCED BY THE PRESENCE OF THE SPLINES

A comparison of the results of the fatigue tests on the splined shafts with those obtained using solid cylindrical specimens provides, directly, for this material, the value of the Fatigue Strength Reduction Factor K_f, where

$$K_f = \frac{\text{Fatigue Strength of Solid Specimens}}{\text{Fatigue Strength of Hollow Splined-shafts}}$$

The calculated values of K_f are listed in Table 25, but they are more conveniently examined as re-arranged in Table 28.

TABLE 28

FATIGUE STRENGTH REDUCTION FACTORS, K_f ; HOLLOW SPLINED-SHAFT SPECIMENS

Superimposed Static Stress t/in^2		Values of K_f				
Bending f_s	Torsion q_s	$\theta=0°$	$\theta=29 \cdot 7°$	$\theta=53 \cdot 1°$	$\theta=75 \cdot 9°$	$\theta=90°$
0	0	1·04 (1)	1·09 (13)	1·47 (9)	1·76 (14)	2·0 (5)
$17\frac{1}{4}$	0	1·03 (2)	—	1·56 (10)	—	1·66 (6)
0	11	1·03 (3)	—	1·51 (11)	—	1·86/1·96 (7)
$17\frac{1}{4}$	11	1·03 (4)	—	1·50 (12)	—	1·67/1·83 (8)
Average Value		1·03		1·51		1·83

Note.—Figures in brackets are the test reference numbers.

Considering, first, the complete series of five tests—numbers 1, 13, 9, 14 and 5—in which no static stress was superimposed. Under reversed bending stresses (test 1), the value of K_f is very near to unity ; the spline crests all being parallel to the axis of the specimen, theoretically no stress concentration effect should be present and this is very nearly realised. Under reversed torsional stresses, the effect of the discontinuities of section is to halve the fatigue resistance. As the ratio of reversed torsional stresses/reversed bending stresses increases, the damage effect progressively increases.

The three groups of four results set out vertically in the table are very interesting because of the remarkable consistency in the values of K_f for any particular setting angle of the machine. This is particularly striking for the series $\theta = 0$ deg. and the series $\theta = 53 \cdot 1$ deg., where, in each case, the variation from the mean value is negligible. At $\theta = 90$ deg., a larger variation is shown which is probably due to slight irregularities in the material or in the shape of the splines, as indicated by the less clearly defined fatigue limits. The consistency of each group, tested under such widely differing conditions of superimposed static stress, is, of course, merely a restatement, in another form, of the previous conclusion ; that the nature and extent of the fatigue damage caused by the presence of a discontinuity, producing a stress concentration and subjected to cyclic stresses, is determined almost entirely by the range of stress, the mean stress of the cycle having little, if any, effect.

Theoretical Stress Concentration Factors, K_t. Under bending stresses, no stress concentration effect should exist ; we have seen that the experimental results obtained are in accordance with theory in this respect. Cox[30] has made an analytical study of the torsion of long

uniform shafts containing discontinuities of section, including the splined shaft. He finds that the stress concentration at the inner corner of a spline, representing as it does a sort of half-groove, is given, approximately, by $1 + \frac{1}{2}\,(d/r)^{1/2}$, where d is the depth of the spline and r is the average radius of curvature at its root. In the present case, the depth of the spline is 0·03315 in. and the root radius is 0·0075 in., giving the approximate value of $K_t = 2{\cdot}1$. The analysis relates to a long shaft free from restraint at its ends ; the end restraint which is definitely present in the specimens used in these tests may tend to reduce the value of K_t. The experimental values of K_f given in the last column of Table 28 vary between 1·66 and 2·0, with an average value of 1·83. Thus, a near approach to the full theoretical stress concentration effect is probably realised, with this material, in the case of a splined shaft subjected to cyclical torsional stresses.

Thus, from the stress concentration aspect, the splined shaft is of special interest when tested under the combined stress conditions used in this investigation. When subjected to reversed bending stresses ($\theta = 0$ deg.), no stress concentration is present ; under reversed torsional stresses, a marked stress concentration occurs tending to produce fatigue fracture at the inner corners of the splines and along their length. No theory is available to predict the type of fracture at intermediate values of θ deg., but the observed manner of actual fracture of the specimens is informative.

In the series of five tests made under zero static stress conditions (i.e. $f_s = 0$, $q_s = 0$), the fractures were all of the following distinct types. At $\theta = 0$ deg., where $q = 0$, the fracture commenced at the crest of a spline and propagated in a plane, with slight deviations, normal to the specimen axis : the crack reached and crossed the inner corner of the spline without any deviation in course. At $\theta = 29{\cdot}7$ deg. ($f/q = 3\frac{1}{2}$), exactly similar cracks always occurred ; the shear stress concentration was, clearly, still ineffective. At $\theta = 53{\cdot}1$ deg. ($f/q = 1\frac{1}{2}$), the cracks definitely started at the inner corner of the spline as a shear failure and followed its direction for a very short distance before turning into the direction of the trace of the plane normal to the axis of the specimen under the influence of the cyclic bending stresses. At $\theta = 75{\cdot}9$ deg. ($f/q = \frac{1}{2}$), the cracks again definitely started at the inner corner of the spline as a shear failure, followed its direction for a distance, longer than when $\theta = 53{\cdot}1$ deg., but still short in actual amount, before also turning into the normal direction. At $\theta = 90$ deg., under pure reversed shearing stresses, the behaviour was exactly similar to the two previous angle settings, but, even in this case, that portion of the crack originating at the inner spline corner and spreading along its length never measured more than 0·1 in. These observations bring out clearly, (i) the predominating and increasing influence of the shearing stress concentration at angles greater than $\theta = 29{\cdot}7$ deg. ($f/q = 3\frac{1}{2}$) and, (ii) the overriding influence of the cyclic bending stresses on the direction of the propagation of the crack. As will be seen (Fig. 87) the shape of the f/q curve is entirely consistent with these observations on the origin of the failures.

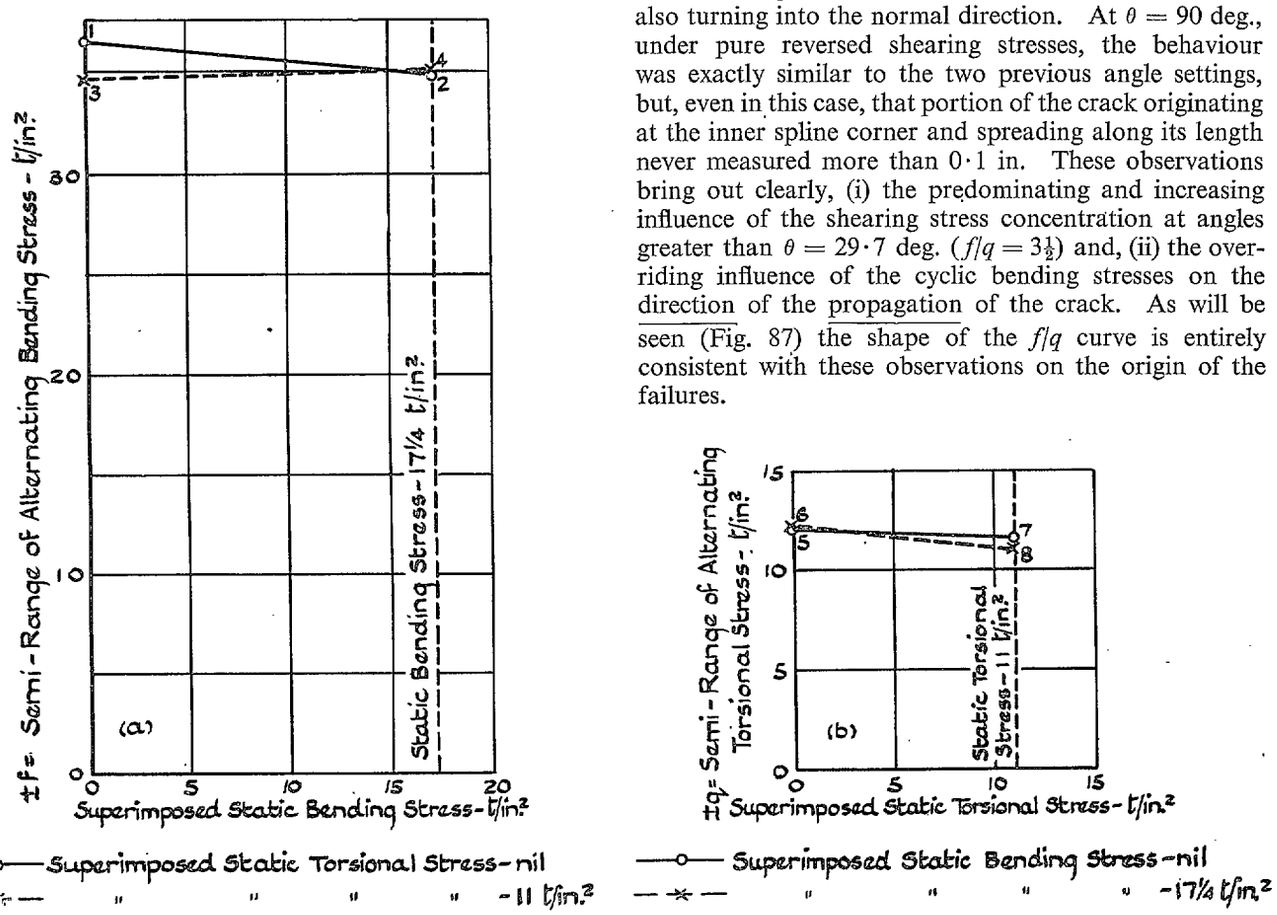

FIG. 88. Effect of Superimposed Static Bending and Torsional Stresses, Singly and in Combination, on the Fatigue Limits under Reversed Stresses : Hollow Specimens with six splines.

In the tests where superimposed static stresses were in operation—$f_s = 0, q_s = 11$; $f_s = 17\frac{1}{4}, q_s = 0$; $f_s = 17\frac{1}{4}$, $q_s = 11$—the point of origin and direction of propagation of the fatigue cracks, at $\theta = 0$, $53{\cdot}1$ and 90 deg., were exactly the same as described above. Clearly the static stresses had no perceptible effect on the method of cracking.

It may be worth mentioning that the fatigue strength of an assembly of a splined shaft with its mating member, in which the drive is transmitted from one component to the other, may be less than that of the splined shaft alone : the stress distribution in the two cases is quite different. This aspect of fatigue does not appear to have received the attention it merits. A few experiments made by Gough[31] on shafts containing a keyway, and on a keyed assembly, give an indication of the different behaviours that may occur.

3. THE f/q RELATION

Taken from Table 25, the results of the series of five tests, in which no static stresses were superimposed, are plotted in Fig. 87. Through the 'end-points' (tests 1 and 5), the corresponding ellipse quadrant and the ellipse arc have been drawn. Tests 14 and 9 both fall between the two curves and could be associated with either. But test 13 falls well outside the outer curve (the ellipse arc). Examination of the S/N curve (Fig. 78) shows no reason to suppose that the recorded value of the safe range is in error and the result is accepted. But it is very significant that, as we have seen, the study of the fractures clearly indicated that the stress concentration effect of the spline corner was not effective at this value of f/q. Thus, the interesting conclusion is reached that, with this type of discontinuity, the f/q relation is a discontinuous curve, changing from the ellipse quadrant (as for a specimen of circular section free from discontinuities producing stress concentrations) at the value of f/q where fracture commences to occur at the corner of the spline, the remaining points fitting the ellipse arc. The ellipse arc is clearly a better fit to the series of results as a whole than the ellipse quadrant and the former can be accepted as the criterion affording a safe design basis, being thus in agreement with the other series of tests—on grooves, oil holes and sharp fillets—in which stress concentration effects were present due to discontinuities of section.

It remains only to examine the following three series of tests in each of which static stresses were superimposed:—

A. $f_s = 17\frac{1}{4}, q_s = 0$. Test 2 ($f = \pm 34{\cdot}8$, $q = 0$) ; Test 10 ($f = \pm 16{\cdot}0$, $q = \pm 10{\cdot}6_5$) and Test 6 ($f = 0$, $q = \pm 12{\cdot}2$).

B. $f_s = 0$, $q_s = 11$. Test 3 ($f = \pm 34{\cdot}6$, $q = 0$) ; Test 11 ($f = \pm 16{\cdot}4_5$, $q \pm = 10{\cdot}9_5$) and Test 7 ($f = 0$, $q = \pm 11{\cdot}5$).

C. $f_s = 17\frac{1}{4}, q_s = 11$. Test 4 ($f = \pm 35{\cdot}0$, $q = 0$) ; Test 12 ($f = \pm 16{\cdot}2$, $q = \pm 10{\cdot}8$) and Test 8 ($f = 0$, $q = \pm 11/11{\cdot}5$).

As with the corresponding results of the specimens having a drilled hole or a sharp fillet, the experimental value of each intermediate test (Nos. 10, 11 and 12) will be compared, in terms of Range of Maximum Shear Stress, S, with the calculated value, at $\theta = 53{\cdot}1$ deg., of the ellipse quadrant and ellipse arc drawn through the appropriate pair of 'end-points' (Nos. 2 and 6 ; 3 and 7 ; 4 and 8).

The results are as follows :—

Series	Test No.	Range of Maximum Shear Stress, S					
		Experimental		Ellipse Quadrant		Ellipse Arc	
		t/in²	ratio	t/in²	ratio	t/in²	ratio
A	10	±13·3	100	±13·5	102	±14·9	112
B	11	±13·7	100	±12·9	94	±14·4	105
C	12	±13·5	100	±12·7	94	±14·3	106

Thus, test 10 falls on the ellipse quadrant and is removed from the ellipse arc by 12% of the experimental value, while tests 11 and 12 each fall midway between the two curves and, within the experimental accuracy of the determinations of about 5%, could be assigned to either curve. Series B and C are, therefore, in line with the corresponding tests on the drilled hole and sharp fillet and the conclusion that the ellipse arc affords a satisfactory basis of design even when considerable static stresses are imposed. Series A supports the ellipse quadrant as the criterion ; as this solitary exception rests upon the accuracy of one fatigue determination only, its importance must not be exaggerated.

GLOSSARY OF ABBREVIATIONS

C	Carbon
Cr	Chromium
Ni	Nickel
Mo	Molybdenum
Va	Vanadium
W	Tungsten
H. and T.	Hardened and tempered
O.H.	Oil hardened
O.H. and T.	Oil hardened and tempered
O.Q. and T.	Oil quenched and tempered
N.P.L.	National Physical Laboratory
U.T.S.	Ultimate tensile stress
B.H.N.	Brinell hardness number
B.S.I.	British Standards Institution
F.Lt.	Fatigue limit

CONVERSION FACTORS (British to Metric System)

1 foot	ft. =	30·480 centimetres
1 pound weight	lb. =	0·453 59 kilogramme
1 ton weight	t =	1016·0 kilogrammes
1 ton per square inch	t/in.^{2} =	157·43 kilogrammes per square centimetre

To convert British to Metric units, multiply by the conversion factor.

REFERENCES

No.	*Author*	*Title, etc.*
1.	Ono, A.	Fatigue of Steel under Combined Bending and Torsion. *Kyushu Imper. Univ. Memoirs Eng. Coll.*, Vol. II, No. 2. 1921.
2.	Lea and Budgeon ..	Combined Torsional and Repeated Bending Stresses. *Engineering*, 1926. Vol. 122, p. 242.
3.	Hohenemser, K. and Prager, W.	The Problem of Fatigue Strength under Complex Stresses. *Metallwirtschaft* XII, 24. June, 1933.
4.	Stanton, T. E. and Batson, R. G.	On the Fatigue Resistance of Mild Steel under various conditions of Stress Distributions. *British Association Report, Newcastle.* 1916. p. 288.
5.	Peterson, R. E. ..	Stress - Concentration Phenomena in Fatigue of Metals. *Trans. A.S.M.E.* 1933. Vol. 55.
6.	Peterson, R. E. ..	Model Testing as applied to Strength of Materials. *Trans. A.S.M.E.*, Vol. 55. 1933.

No.	*Author*	*Title, etc.*
7.	Mailander, R. and Bauersfeld, W.	Influence of Size and Shape of Specimens on the Fatigue Strength of Steel in Torsion. *Tech. Mitt. Krupp*, Vol. 2. December, 1934.
8.	Horger, O. J. ..	Effect of Surface Rolling on the Fatigue Strength of Steel. *Trans. A.S.M.E.*, Vol. 57. 1935.
9.	Gough, H. J. and Pollard, H. V.	The Strength of Metals under Combined Alternating Stresses. *Proc. Inst. Mech. E.* November, 1935.
10.	Gough, H. J. and Pollard, H. V.	The Effect of Specimen Form on the Resistance of Metals to Combined Alternating Stresses. *Proc. Inst. Mech. E.* December, 1936.
11.	Gough, H. J. and Pollard, H. V.	Properties of some materials for Cast Crankshafts, with Special Reference to Combined Stresses. *Proc. Inst. Auto. Engrs.*, Vol. 31. 1937.
12.	Frith, P. H.	Fatigue Tests on Crankshaft Steels. *Jour. I. & S. Institute.* 1948.
13.	Hatfield, W. S. ..	Study of a Ni. Cr. Mo. Va. Steel Ingot. *8th Report on the Heterogeneity of Steel Ingots. Special Report No. 25, Section V, Iron and Steel Institute.* 1939.
14.	Gough, H. J. and Tapsell, H. J.	Some Comparative Fatigue Tests in Special Relation to the Impressed Conditions of Test. *Aero. Res. Ctee., Reports and Memoranda*, No. 1012. 1925/1926.
15.	Smith, H. E. and Cox, H. L.	Determination of the Elastic Moduli of a Mild and a Medium Steel. *Aero. Res. Ctee., Reports and Memoranda* No. 1138. 1927.
16.	Jenkin, C. F. ..	Report on Materials of Construction used in Aircraft and Aircraft Engines. *H.M. Stationery Office, London.* 1920.
17.	Inglis, C. E.	Stresses in a Plate due to the Presence of Cracks and Sharp Corners. *Trans. Inst. Nav. Arch.*, Pt. I. 1913.
18.	Guest, J. J.	Recent Research on Combined Stress. *Journ. Inst. Auto. Engrs.*, Vol. IX, No. 3. December, 1940.
19.	Gough, H. J. ..	Fatigue of Metals. *Scott Greenwood. London.* 1924.
20.	Southwell, E. V. and Gough, H. J.	On the Concentration of Stress in the Neighbourhood of a Small Spherical Flaw and on the Propagation of Fatigue Fractures in 'Statistically Isotropic' Materials. *Phil. Mag.*, Vol. 1. January, 1926.
21.	Gough, H. J. and Wood, W. A.	Deformation and Fracture of Mild Steel under Cyclic Stresses in relation to Crystalline Structure. *Proc. Inst. Mech. Engrs.* March, 1939.
22.	Kirsch, G.	Theory of Flaws. *Zeitschrift des Vereines deutscher Ingenieur*, Vol. 42. January/June, 1898.
23.	Cox, H. L.	The Effect of Holes on the Strength of Materials under Complex Stress Systems. (*In course of publication.*)
24.	Frocht, M. M. ..	Factors of Stress Concentration Photoelastically determined. *Trans. A.S.M.E.*, Vol. 57. 1935.
25.	Wahl, A. M. and Beeuwkes, R.	Stress Concentrations produced by Holes and Notches. *Trans. A.S.M.E.*, Vol. 56. 1934.
26.	Peterson, R. E. and Wahl, A. M.	Two- and Three-Dimensional Cases of Stress Concentration and Comparison with Fatigue Tests. *Trans. A.S.M.E.*, Vol. 58. 1936.
27.	Frocht, M. M. ..	Photoelasticity. *Chapman and Hall.* 1948.
28.	Thum, A. and Kirmser, W.	Superimposed Alternating Stresses. *V.D.I.*, Vol. 419. 1943.
29.	Jacobsen, L. S. ..	Torsional Stresses in Shafts having Grooves or Fillets. *Trans. A.S.M.E.*, Vol. 57. 1935.
30.	Cox, H. L.	Stress Concentration in Twisted Shafts. (*In course of publication.*)
31.	Gough, H. J. ..	The Effect of Keyways upon the Strength and Stiffness of Shafts subjected to Torsional Stresses. *Aero. Res. Ctee., Reports and Memoranda* No. 864. 1925.

(92759) Wt. 13/806 K.5 11/51 Hw.

PRINTED IN GREAT BRITAIN

Publications of the Aeronautical Research Council

ANNUAL TECHNICAL REPORTS OF THE AERONAUTICAL RESEARCH COUNCIL (BOUND VOLUMES)—

1934–35 Vol. I. Aerodynamics. *Out of print.*
Vol. II. Seaplanes, Structures, Engines, Materials, etc. 40*s.* (40*s.* 8*d.*)

1935–36 Vol. I. Aerodynamics. 30*s.* (30*s.* 7*d.*)
Vol. II. Structures, Flutter, Engines, Seaplanes, etc. 30*s.* (30*s.* 7*d.*)

1936 Vol. I. Aerodynamics General, Performance, Airscrews, Flutter and Spinning. 40*s.* (40*s.* 9*d.*)
Vol. II. Stability and Control, Structures, Seaplanes, Engines, etc. 50*s.* (50*s.* 10*d.*)

1937 Vol. I. Aerodynamics General, Performance, Airscrews, Flutter and Spinning. 40*s.* (40*s.* 10*d.*)
Vol. II. Stability and Control, Structures, Seaplanes, Engines, etc. 60*s.* **(61*s.*)**

1938 Vol. I. Aerodynamics General, Performance, Airscrews. 50*s.* (51*s.*)
Vol. II. Stability and Control, Flutter, Structures, Seaplanes, Wind Tunnels, Materials. 30*s.* (30*s.* 9*d.*)

1939 Vol. I. Aerodynamics General, Performance, Airscrews, Engines. 50*s.* (50*s.* 11*d.*)
Vol. II. Stability and Control, Flutter and Vibration, Instruments, Structures, Seaplanes, etc. 63*s.* (64*s.* 2*d.*)

1940 Aero and Hydrodynamics, Aerofoils, Airscrews, Engines, Flutter, Icing, Stability and Control, Structures, and a miscellaneous section. 50*s.* (51*s.*)

Certain other reports proper to the 1940 *volume will subsequently be included in a separate volume.*

ANNUAL REPORTS OF THE AERONAUTICAL RESEARCH COUNCIL—

1933–34	1*s.* 6*d.* (1*s.* 8*d.*)
1934–35	1*s.* 6*d.* (1*s.* 8*d.*)
April 1, 1935 to December 31, 1936.	4*s.* (4*s.* 4*d.*)
1937	2*s.* (2*s.* 2*d.*)
1938	1*s.* 6*d.* (1*s.* 8*d.*)
1939–48	3*s.* (3*s.* 2*d.*)

INDEX TO ALL REPORTS AND MEMORANDA PUBLISHED IN THE ANNUAL TECHNICAL REPORTS, AND SEPARATELY—

April, 1950	R. & M. No. 2600.	2*s.* 6*d.* (2*s.* 7½*d.*)

INDEXES TO THE TECHNICAL REPORTS OF THE AERONAUTICAL RESEARCH COUNCIL—

December 1, 1936 — June 30, 1939.	R. & M. No. 1850.	1*s.* 3*d.* (1*s.* 4½*d.*)
July 1, 1939 — June 30, 1945.	R. & M. No. 1950.	1*s.* (1*s.* 1½*d.*)
July 1, 1945 — June 30, 1946.	R. & M. No. 2050.	1*s.* (1*s.* 1½*d.*)
July 1, 1946 — December 31, 1946.	R. & M. No. 2150.	1*s.* 3*d.* (1*s.* 4½*d.*)
January 1, 1947 — June 30, 1947.	R. & M. No. 2250.	1*s.* 3*d.* (1*s.* 4½*d.*)

Prices in brackets include postage.

Obtainable from

HIS MAJESTY'S STATIONERY OFFICE

York House, Kingsway, LONDON, W.C.2 — 429 Oxford Street, LONDON, W.1
P.O. Box 569, LONDON, S.E.1
13a Castle Street, EDINBURGH, 2 — 1 St. Andrew's Crescent, CARDIFF
39 King Street, MANCHESTER, 2 — Tower Lane, BRISTOL, 1
2 Edmund Street, BIRMINGHAM, 3 — 80 Chichester Street, BELFAST

or through any bookseller.